

USAARL Report No. 2003-07

Analysis of Head Motion in Rotary-Wing Flight Using Various Helmet-Mounted Display Configurations (Part I. Azimuth)

By Ryan J. Rostad, Clarence E. Rash, Joshua K. Briley, John C. Mora, and John S. Crowley



Aircrew Health and Performance Division
and
Aircrew Protection Division

April 2003

Approved for public release, distribution unlimited.

U
S
A
A
R
L

U.S. Army
Aeromedical Research
Laboratory

Notice

Qualified requesters

Qualified requesters may obtain copies from the Defense Technical Information Center (DTIC), Cameron Station, Alexandria, Virginia 223 14. Orders will be expedited if placed through the librarian or other person designated to request documents from DTIC.

Change of address

Organizations receiving reports from the U.S. Army Aeromedical Research Laboratory on automatic mailing lists should confirm correct address when corresponding about laboratory reports.

Disposition

Destroy this document when it is no longer needed. Do not return it to the originator.

Disclaimer

The views, opinions, and/or findings contained in this report are those of the author(s) and should not be construed as an official Department of the Army position, policy, or decision, unless so designated by other official documentation. Citation of trade names in this report does not constitute an official Department of the Army endorsement or approval of the use of such commercial items.

REPORT DOCUMENTATION PAGE				Form Approved OMB No. 0704-0188	
1a. REPORT SECURITY CLASSIFICATION Unclassified		1b. RESTRICTIVE MARKINGS			
2a. SECURITY CLASSIFICATION		3. DISTRIBUTION / AVAILABILITY OF REPORT Approved for public release, distribution unlimited			
2b. DECLASSIFICATION / DOWNGRADING					
4. PERFORMING ORGANIZATION REPORT NUMBER(S) USAARL Report No. 2003-07		5. MONITORING ORGANIZATION REPORT NUMBER(S)			
6a. NAME OF PERFORMING ORGANIZATION U.S. Army Aeromedical Research Laboratory		6b. OFFICE SYMBOL (If MCMR-UAD	7a. NAME OF MONITORING ORGANIZATION U.S. Army Medical Research and Materiel Command		
6c. ADDRESS (City, State, and ZIP Code) P.O. Box 620577 Fort Rucker, AL 36362-0577		7b. ADDRESS (City, State, and ZIP Code) 504 Scott Street Fort Detrick, MD 21702-5012			
8a. NAME OF FUNDING / SPONSORING ORGANIZATION		8b. OFFICE SYMBOL (If	9. PROCUREMENT INSTRUMENT IDENTIFICATION NUMBER		
8c. ADDRESS (City, State, and ZIP Code)		10. SOURCE OF FUNDING NUMBERS			
		PROGRAM ELEMENT NO. 622787	PROJECT NO. 879	TASK NO. P	WORK UNIT ACCESSION NO. DA336445
11. TITLE (Include Security Classification) (U) Analysis of head motion in rotary-wing flight using various helmet-mounted display configurations (Part I. - Azimuth)					
12. PERSONAL AUTHOR(S) Ryan J. Rostad, Clarence E. Rash, Joshua K. Briley, John C. Mora, John S. Crowley					
13a. TYPE OF REPORT Final		13b. TIME COVERED FROM TO	14. DATE OF REPORT (Year, Month, Day) 2003 April		15. PAGE COUNT 172
16. SUPPLEMENTAL NOTATION					
17. COSATI CODES			18. SUBJECT TERMS (Continue on reverse if necessary and identify by block number) helmet-mounted display (HMD), head motion, head position, head velocity		
FIELD	GROUP	SUB-GROUP			
23	02				
19. ABSTRACT (Continue on reverse if necessary and identify by block number) In spite of an immense increase in interest in helmet-mounted displays (HMDs) over the past two decades, there have been few studies on head motion while using HMDs in operational flight. Rotary-wing flights conducted using a number of HMD configurations have resulted in a head position database that will be useful in filling this void. Azimuth head position data have been analyzed for a slalom flight maneuver for four visual environments: good visual environment (daytime, unaided), night vision goggles, HMD with thermal imagery, and HMD with thermal imagery and symbology. The major thread throughout these analyses was that the pilots exhibited greatest head motion for the NVG environment. The two HMD configurations (TIO and RWS) were very similar in exhibited head motion, not indicating any significant differences between the TIO FLIR imagery alone and the RWS FLIR imagery plus symbology. Based on this analysis of the head azimuth position data, it is concluded that the interquartile range IQR (or some other IQR) dispersion statistic (continued on next page)					
20. DISTRIBUTION / AVAILABILITY OF <input checked="" type="checkbox"/> UNCLASSIFIED/UNLIMITED <input type="checkbox"/> SAME AS RPT. <input type="checkbox"/> DTIC USERS			21. ABSTRACT SECURITY CLASSIFICATION Unclassified		
22a. NAME OF RESPONSIBLE INDIVIDUAL Supervisor, Science Information Center		22b. TELEPHONE (Include Area) (334) 255-6907		22c. OFFICE SYMBOL MCMR-UAX-GI	

19. Abstract (continued):

is a good discriminator between the head position distributions for the four visual environments. For all subjects, the IQR for the night vision goggle visual environment was larger than for the other three visual environments. Likewise, the IQR for good visual environment was always the second largest. The IQR values for thermal imaging only and rotary wing symbology, the most closely related visual environments, vie for third and fourth ranking.

Table of contents

	<u>Page</u>
Introduction.....	1
Background	2
Experimental design.....	10
Instrumentation	11
Subjects	15
Visual environments	15
Flight maneuvers.....	15
Final overall trial design	18
Database	18
Data analysis	21
Data preparation.....	21
Data analysis methods.....	22
Position analyses	22
Rate analyses.....	42
Graphical Comparison.....	59
Discussion.....	62
Summary.....	64
Position analysis.....	64
Rate analyses.....	65
Conclusions	68
References.....	69
Appendix A. Discussion on analyzing distribution.....	72

Table of contents (continued)

	<u>Page</u>
Appendix B. Azimuth position distributions	80
Appendix C. Graphical rationale for combining head motion data across LOA and run type	93
Appendix D. Summary tables of azimuth position distributions by visual environments.....	95
Appendix E. Azimuth position box plots.....	100
Appendix F. Azimuth position quantile curves for all subjects and visual environments.....	108
Appendix G. Azimuth reversal summary tables	116
Appendix H. Azimuth excursion distributions	121
Appendix I. Azimuth excursion summary tables.....	134
Appendix J. Azimuth excursion box-plots.....	139
Appendix K. Azimuth velocity distributions	147
Appendix L. Azimuth velocity summary tables for combined distributions	160
Appendix M. Azimuth velocity box-plots	165

List of figures

1. Head azimuth angle histograms for a single pilot for the bob-up maneuver	4
2. Head elevation angle histograms for a single pilot for the bob-up maneuver	4
3. Frequency histogram for azimuth position	6
4. Frequency histograms for elevation position.....	6
5. Frequency histogram for azimuth velocity	7
6. Frequency histogram for elevation velocity	7
7. Percent relative cumulative frequency versus azimuth velocity.....	9
8. Percent relative cumulative frequency versus elevation velocity.....	9
9. The DERA Lynx research helicopter outfitted with custom amber-tinted panels	11

Table of contents (continued)
List of figures (continued)

	<u>Page</u>
10. Flight helmet with 53-degree FOV HMD.....	13
11. The SDVE system.....	14
12. Representative flight path for slalom flight maneuver	17
13. Screen capture of sample head motion data file	20
14. Definition of cycle used in analysis to equalize the slalom maneuver	21
15. Graphical overlay of head motion data on slalom flight path for a sample GVE run for subject #2	23
16. Azimuth position histogram for subject #2, GVE run in Figure 15 above	23
17. Combined histograms for subject #1	28
18. Combined histograms for subject #2	29
19. Combined histograms for subject #3	30
20. Combined histograms for subject #4	31
21. Combined azimuth position box-plots for subject #1	36
22. Combined azimuth position box-plots for subject #2	36
23. Combined azimuth position box-plots for subject #3	37
24. Combined azimuth position box-plots for subject #4	37
25. Combined azimuth position quantile curves for subject #1	39
26. Combined azimuth position quantile curves for subject #2	39
27. Combined azimuth position quantile curves for subject #3	40
28. Combined azimuth position quantile curves for subject #4	40
29. Reversal standard deviation charts showing +1and –1 standard deviation and means by subjects by visual environments	43

Table of contents (continued)
List of figures (continued)

	<u>Page</u>
30. Subject #1 combined excursion histograms by flight type with cumulative frequency curve	46
31. Subject #2 combined excursion histograms by flight type with cumulative frequency curve	47
32. Subject #3 combined excursion histograms by flight type with cumulative frequency curve	48
33. Subject #4 combined excursion histograms by flight type with cumulative frequency curve	49
34. Overall excursion histogram for all subjects, for all visual environments	49
35. Combined velocity histograms for subject #1	53
36. Combined velocity histograms for subject #2	54
37. Combined velocity histograms for subject #3	55
38. Combined velocity histograms for subject #4	56
39. Overall velocity histogram for all subjects, for all visual environments	57
40. Combined azimuth velocity box-plots for subject #1	60
41. Combined azimuth velocity box-plots for subject #2	60
42. Combined azimuth velocity box-plots for subject #3	61
43. Combined azimuth velocity box-plots for subject #4	61
44. Frequency histogram for current study GVE azimuth position combined for all subjects.....	67
45. Frequency histogram for current study GVE azimuth velocity combined for all subjects.....	67

List of tables

1. Reported anatomical and biomechanical head motion ranges.....	3
--	---

Table of contents (continued)

List of tables (continued)

	<u>Page</u>
2. Azimuth and elevation position summary statistics.....	8
3. Azimuth and elevation velocity summary statistics.....	8
4. Slalom tolerances	17
5. Summary of head motion database	19
6. Summary of files for slalom head tracking analysis by subject.....	20
7. Combined azimuth position summary by subject and visual environment	33
8. Comparison of IQR, range and standard deviation.....	41
9. Spearman rank-correlation coefficients for IQR, range and standard deviation.....	42
10. Spearman rank-correlation coefficients for skewness and kurtosis	42
11. Mean reversal rates	43
12. Spearman ranking correlation	44
13. Cumulative excursion percentile values	44
14. Combined azimuth velocity summary by subject and visual environment	58
15. Spearman rank-correlation coefficients for velocity mean and median	62
16. Spearman rank-correlation coefficients for velocity standard deviation and IQR	62

Introduction

From the mid to late 1990s, the Defence Evaluation and Research Agency (DERA), Farnborough, United Kingdom, conducted a rotary-wing (helicopter) research effort known as the Day/Night All Weather (D/NAW) program. The principal aim of this program was to enable safe tactical helicopter flight in severely limited visibility. The major focus of the program was advanced helmet- or head-mounted display (HMD) technologies and the associated symbology design issues (Crowley, 1998).

HMDs are devices or systems that present the pilot(s) with pilotage imagery, flight information, and/or fire control (weaponry) imagery and symbology (Rash, 1999). They are, by definition, head- or helmet-mounted systems. Melzer and Moffitt (1997) describe an HMD as minimally consisting of “an image source and collimating optics in a head mount.” Rash (2000) expands this description to include a visual coupling system which performs the function of slaving head and/or eye positions and motions to one or more aircraft systems. Examples of rotary-wing HMDs include the U. S. Army’s fielded Integrated Helmet and Display Sighting System (IHADSS) used on the AH-64 Apache attack helicopter and the under-development Helmet Integrated Display and Sight System (HIDSS) to be used on the RAH-66 Comanche helicopter.

From March to September 1997, under the auspices of the D/NAW program, a series of flights was flown to establish baseline flight performance for future HMD performance comparisons. These flights consisted of several flight path maneuvers (e.g., slalom, rapid egress, side-step, etc) and visual environments, defined by the mode of visual information presentation (i.e., unaided day, using night vision goggles (NVGs), and using two HMD configurations). For safety considerations, all flights except with NVGs were conducted during the day.

As an aside to the normal flight performance parameters measured during the flights, head azimuth, elevation, and roll position data also were collected, not as part of the experimental design but as standard practice. This paper reports the analysis of the azimuth data for the slalom maneuver. (Elevation and roll data analyses will be presented in future reports.)

The availability of this head position data is advantageous for two reasons. First, extremely limited operational head position data have been presented in the literature. And, very little of this has been collected in the operational flight environment using HMDs. Second, for the same flights for which head position data are presented here, measures of motion sickness symptoms, pre and postflight, were made. In order to test the hypothesis that motion sickness symptoms may be correlated with differences in head motion attributed to the different visual environments (or conversely, head motion is affected by the onset of motion sickness symptoms due to different visual environments), it is necessary to be able to describe the different visual environment head position distributions using a set of parameters (e.g., central moments).

Background

A major operational characteristic of HMDs is their capability to allow the pilot to control external imaging sensors and weapons via head movement. This head slaving capability is achieved through the use of head trackers of various technologies, e.g., mechanical, electro-optical, magnetic, ultrasonic, etc. Most recently, magnetic systems have been the most widely used head tracking technology and are considered to be relatively mature for use in the aviation environment (Borah, 1998). The performance of a head tracking system (sometimes referred to as a visually coupled system [VCS]) is determined by a number of parameters, which include motion box size, pointing angle accuracy, pointing angle resolution, update rate, and jitter. Specifications for these parameters usually are affected by the aircraft platform (fixedwing and rotary-wing). A more detailed discussion of tracking performance parameters can be found in Kocian and Task (1995).

Prior to the fielding of the AH-64 IHADSS, limited research had been conducted to measure the ability of the head (to include neck and shoulder muscles) to be used as an aiming/tracking system. These studies include Nicholson (1965), who investigated the feasibility of using the head as a means of aiming a weapons systems; Haywood (1975) and Polhemus (1976) who attempted to ascertain performance characteristics of specific sighting systems; and Verona, Johnson, and Jones (1979) who investigated the influences of target speed, helmet suspension types, and helmet weighting parameters on head aiming/tracking.

The immense popularity of helmet-mounted displays has since produced only a relatively small increase in studies investigating visually coupled systems. Most of these studies have looked at the performance of head (or eye) tracking technologies (Borah, 1989; Robinson and Wetzel, 1989; and Cameron et al., 1995) or head motion prediction (Azuma and Bishop, 1995; Curtis and Sowizral, 1994). However, there has been very limited data collected and made available on head position and velocity within the operational flight environment. In addition, a literature search produced only two studies that included head motion data during operational flights using HMDs.

Several anatomical and biomechanical studies have reported values for range of head motion for azimuth (rotation), elevation (flexion and extension) and roll (tilt or lateral bending). The reported ranges of these values, as well as for peak velocity and acceleration, are presented in Table 1. Note that only a few of the cited studies indicated clearly as to whether or not neck and shoulder participation was included in the reported values. Caution must be taken when reviewing the values for head motion in Table 1. These values, based on laboratory anatomical and biomechanical measures, would most likely be reduced in an operational cockpit where seat, restraint system and cockpit design present physical obstructions and other limits to allowable ranges of motion. In addition, it has been shown that head motion is reduced by inertial loading such as that induced by the increased head supported weight of HMDs (Gauthier, Martin and Stark, 1986), and the increased neck muscle loading associated with the use of HMDs increases

fatigue which may indirectly reduce the frequency and range of head motion (Phillips and Petrofsky, 1983).

Table 1.
Reported anatomical and biomechanical head motion ranges.

	Allen and Webb (1983)	Zangemeister and Stark (1981)	Sherk (1989)	Glanville and Kreezer (1937); Hertzberg (1972)	Durlach and Mavor (1995)
Azimuth (rotation)	-90° to 90° Note A.	---	Avg of 128° from right to left	-80° to 80°	---
Elevation (total)	-10° to 25° Note B.	---	---	-60° to 60°	---
-flexion only	---	---	54°-74°	---	---
-extension only	---	---	39°-93°	---	---
Roll (tilt)	---	---	Avg of 59° from right to left	-40° to 40°	---
Peak Velocity -azimuth	---	48°/sec for 5° head movement 352°/sec for 60° head movement	---	---	600°/sec
-elevation	---	---	---	---	300°/sec
Peak acceleration	---	551°/sec ² for 5° head movement 3300°/sec ² for 60° head movement	---	---	---

Note A. Values include neck participation.

Note B. Values do not include neck participation.

As stated previously, the studies summarized in Table 1 do not represent a description of head motion values as would be encountered in actual flight scenarios. Only two studies could be found which collected and present head motion data during actual flight conditions. Szoboszlai et al. (1995) investigated the effect of field of view (FOV) restriction on rotary-wing pilot workload and performance in an instrumented NAH-1S Cobra. In this study, pilots executed seven flight maneuvers adapted from the U.S. Army Aeronautical Design Standard (ADS) 33D (U.S. Army Aviation and Troop Command, 1994). The flight maneuvers were slalom, acceleration/deceleration, hover, bob-up/turn/bob-down, hovering turn, pirouette, and precision landing. These maneuvers were executed in the daytime under good visual conditions with no precipitation. Cockpit instruments were covered in order to force the pilot to rely on the outside scene cues. Trials were flown for six FOV configurations ranging from 20 degrees to 100

degrees in 20-degree increments and for an unrestricted (natural) FOV condition. One of the performance parameters measured was time spent at specific azimuth and elevation positions. Figures 1 and 2 show the resulting histograms of the azimuth and elevation angle, respectively, of the head position for a typical pilot during one of the bob-up

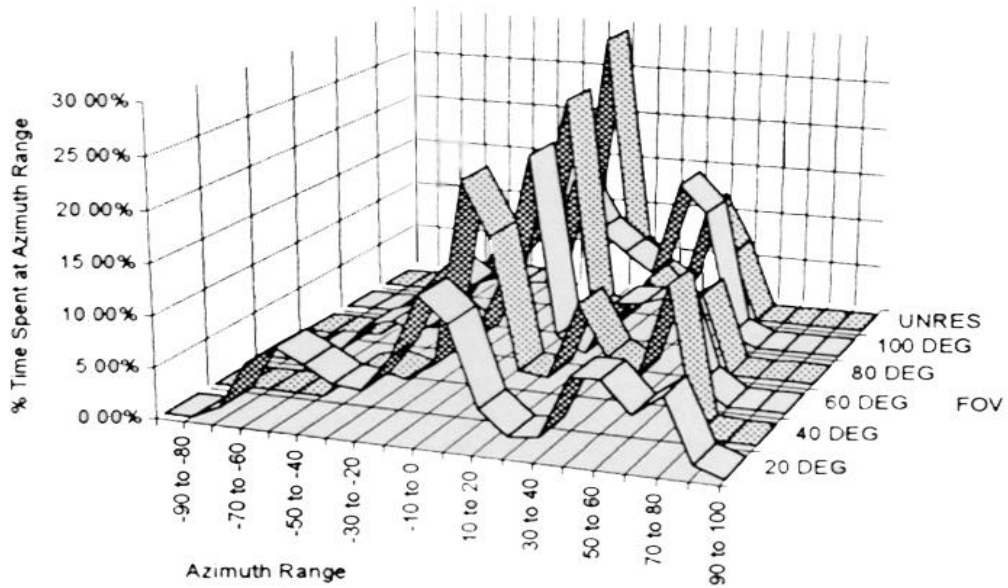


Figure 1. Head azimuth angle histograms for a single pilot for the bob-up maneuver (Szoboszlay et al., 1995).

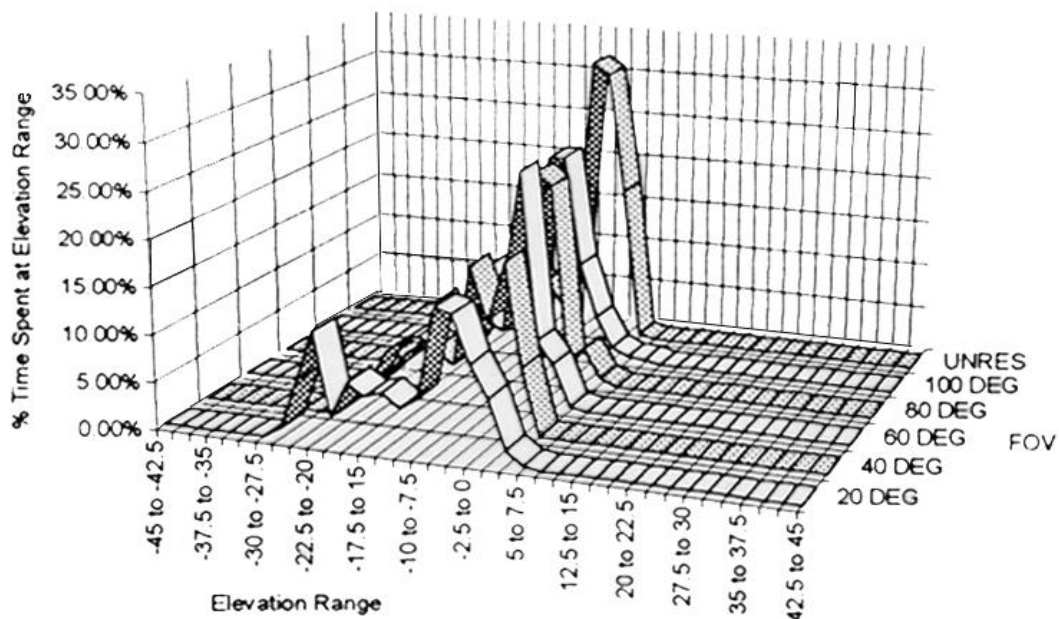


Figure 2. Head elevation angle histograms for a single pilot for the bob-up maneuver. (Szoboszlay et al., 1995).

maneuvers. The azimuth histograms (Figure 1) show a trend if FOV was reduced, the pilot's right gazing angle also increased. The elevation histograms (Figure 2) show a similar increase in head motion as the horizontal FOV was decreased.

Perhaps, the most pertinent study to this current paper was conducted by Verona et al. (1986), where head motion data were collected from six pilots as each flew a modified UH-1M Huey helicopter over a circular 15-mile contour course. (Data from one of the six pilots (#2) were not incorporated in the analysis due to loss of boresight.) All of the pilots were rated in the UH-1M aircraft, and pilot #4 was an Army MEDEVAC pilot with previous search and rescue experience. The pilots also were required to visually search for an "enemy" aircraft, which could appear anywhere, while flying the contour course. A head tracking system was used to measure the pilot's head motion. The system provided coverage of $\pm 180^\circ$ azimuth and -90° to $+30^\circ$ elevation with 0.5° accuracy. The head tracking data were collected over two flights of 25-minute duration per pilot with head position samples taken every 40 milliseconds (ms). All of the flights and data acquisitions were conducted on the same day. Of the five remaining pilots, three flew in the morning and two flew in the afternoon. They were not told that head motion was the focus of the study; instead, they were advised that they were assessing a new helmet fit. The subject pilots sat in the left seat of the aircraft.

The first and last 3 minutes were not used in the analysis, which consisted of constructing position and velocity frequency histograms for azimuth and elevation from the head tracking line-of-sight data. The azimuth and elevation position histograms collapsed across the remaining five subjects are presented in Figures 3 and 4, respectively. Figures 5 and 6 show the corresponding velocity histograms. The summary statistics for mean, median, standard deviation, skewness and kurtosis, collapsed across the five pilots for azimuth and elevation position, are presented in Table 2. Summary statistics for azimuth and elevation velocities are presented in Table 3. Percent relative cumulative frequency curves for azimuth and elevation velocities are presented in Figures 7 and 8, respectively.

The positive means and medians for azimuth position in the top section of Table 2 indicated that the pilots were looking slightly to the right, toward the center of the aircraft, most of the time. (Note: 0° is directly in front of the left-seated pilot, not at the center of the aircraft.) The large standard deviations were interpreted as meaning the pilots exhibited considerable variability with respect to head position (line of sight) while performing the search task. Figure 3, the azimuth position histogram, showed a slight peak at -75° corresponding to the center of the aircraft door window. The range was -90° to $+90^\circ$. The elevation position data and statistics, Figure 4 and bottom of Table 2, showed a range of -65° to $+30^\circ$. The major peak occurred at -1° . The small hump at -40° corresponds to the position of the chin transparency in the lower front of the aircraft. The pilots spent 95 percent of their time between -14° and $+14^\circ$; the pilots' heads remained essentially level. The standard deviations for elevation were not as large as for azimuth,

as would be expected since elevation range of motion is more limited. The negative medians indicated the pilots were looking down more often than they were looking up.

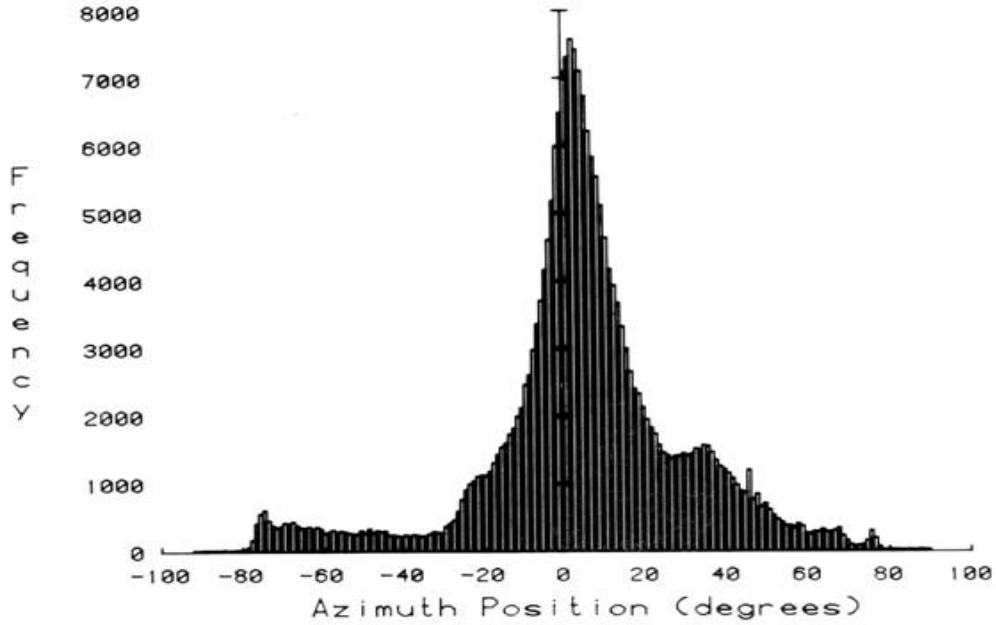


Figure 3. Frequency histogram for azimuth position (Verona et al., 1986).

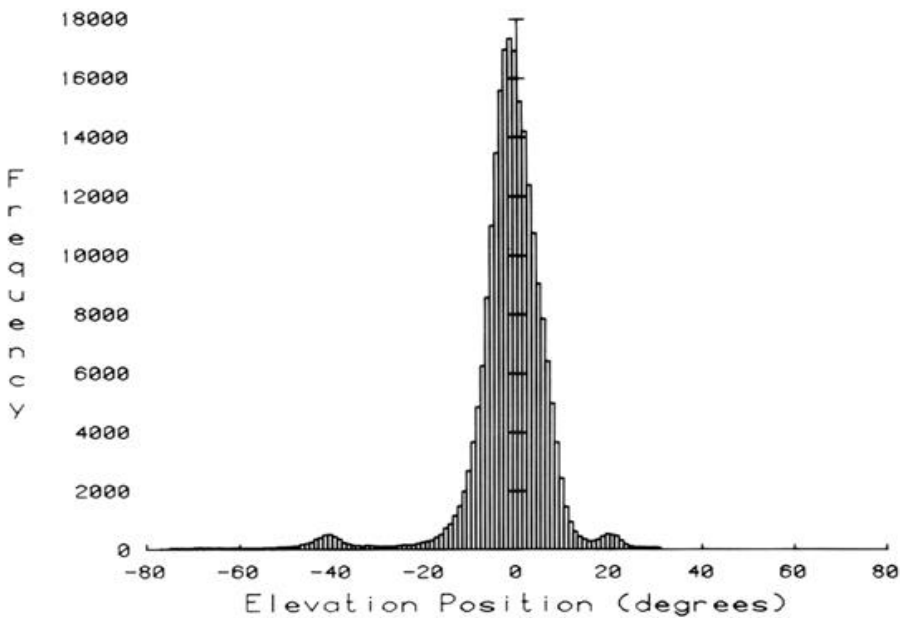


Figure 4. Frequency histograms for elevation position (Verona et al., 1986).

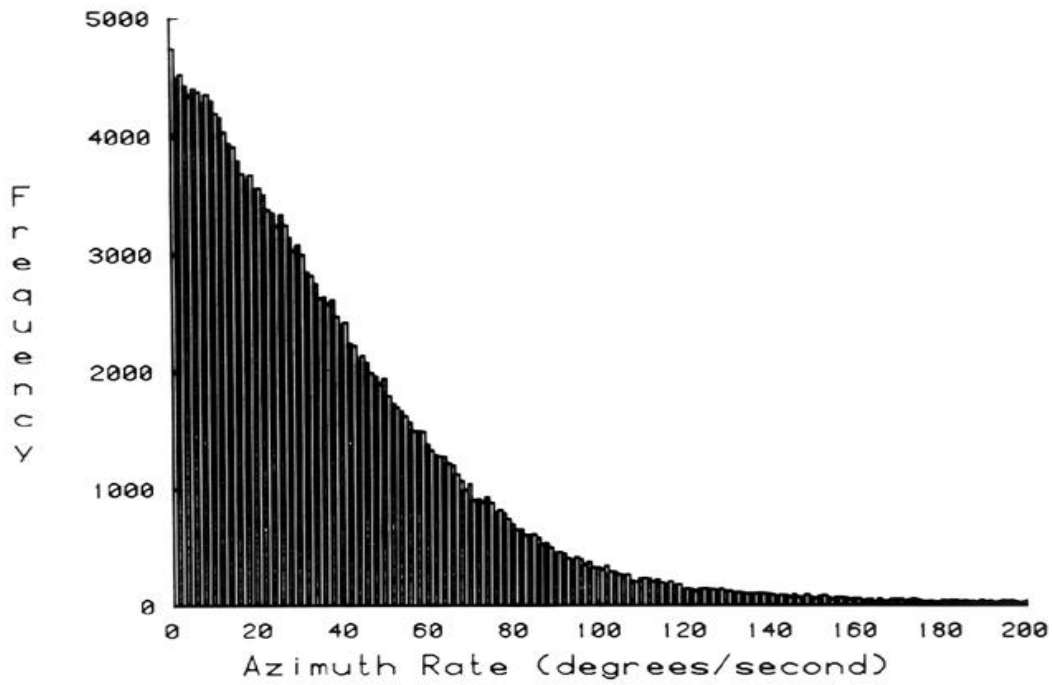


Figure 5. Frequency histogram for azimuth velocity (Verona et al., 1986).

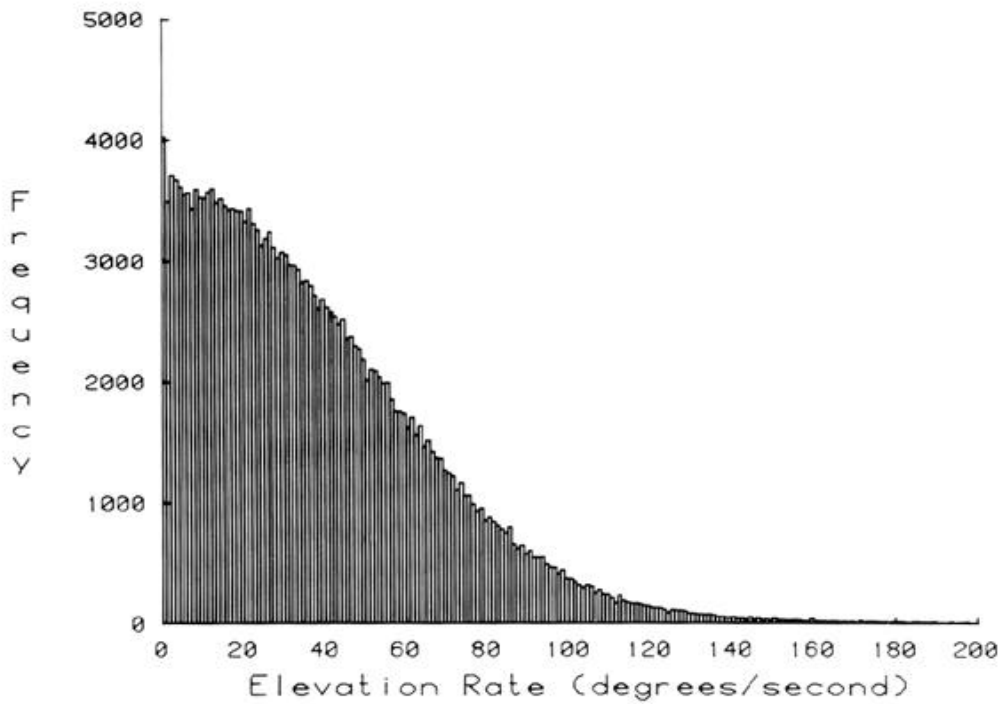


Figure 6. Frequency histogram for elevation velocity (Verona et al., 1986).

Table 2.
Azimuth and elevation position summary statistics.

Subject	Mean	Median	S.D.	Skewness	Kurtosis
Azimuth position					
1	50.5	3.23	19.62	-0.11	2.21
3	5.98	6.11	18.03	-0.37	2.57
4	3.63	3.63	33.85	-0.36	0.12
5	1.90	3.23	25.00	-0.74	2.04
6	5.17	4.20	24.90	-0.57	1.94
All 5 subjects	4.35	4.43	24.77	-0.52	1.93
Elevation position					
1	-3.73	-3.14	3.85	0.40	8.96
3	-3.03	-2.27	6.26	-2.64	20.00
4	-6.39	-3.24	12.31	-1.62	3.55
5	-2.32	0.47	7.25	-2.32	24.31
6	3.13	4.41	6.86	-3.67	26.32
All 5 subjects	-2.09	-1.08	8.46	-2.25	11.79

Table 3.
Azimuth and elevation velocity summary statistics.

Subject	Mean	Median	S.D.	Skewness	Kurtosis
Azimuth velocity					
1	33.50	26.53	29.50	1.61	3.65
3	33.54	27.16	28.71	1.53	3.40
4	37.44	26.85	36.81	1.73	3.26
5	40.58	33.49	33.46	1.39	2.45
6	35.60	27.69	32.18	1.64	3.43
All 5 subjects	35.97	28.16	32.23	1.63	3.45
Elevation velocity					
1	36.23	30.91	28.10	1.11	1.52
3	37.08	32.10	28.11	0.99	1.07
4	35.78	29.71	29.57	1.45	2.96
5	43.69	38.73	32.15	1.04	1.37
6	37.16	32.08	28.81	1.19	1.98
All 5 subjects	37.93	32.50	29.46	1.17	1.81

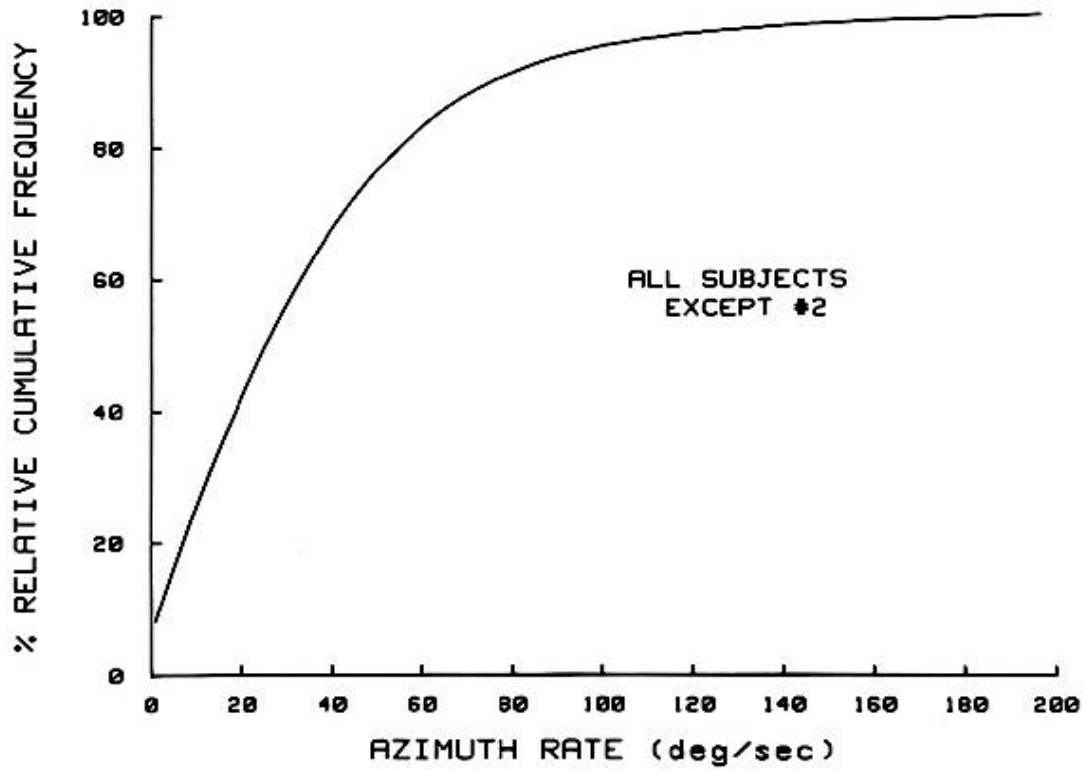


Figure 7. Percent relative cumulative frequency versus azimuth velocity (Verona et al.,1986).

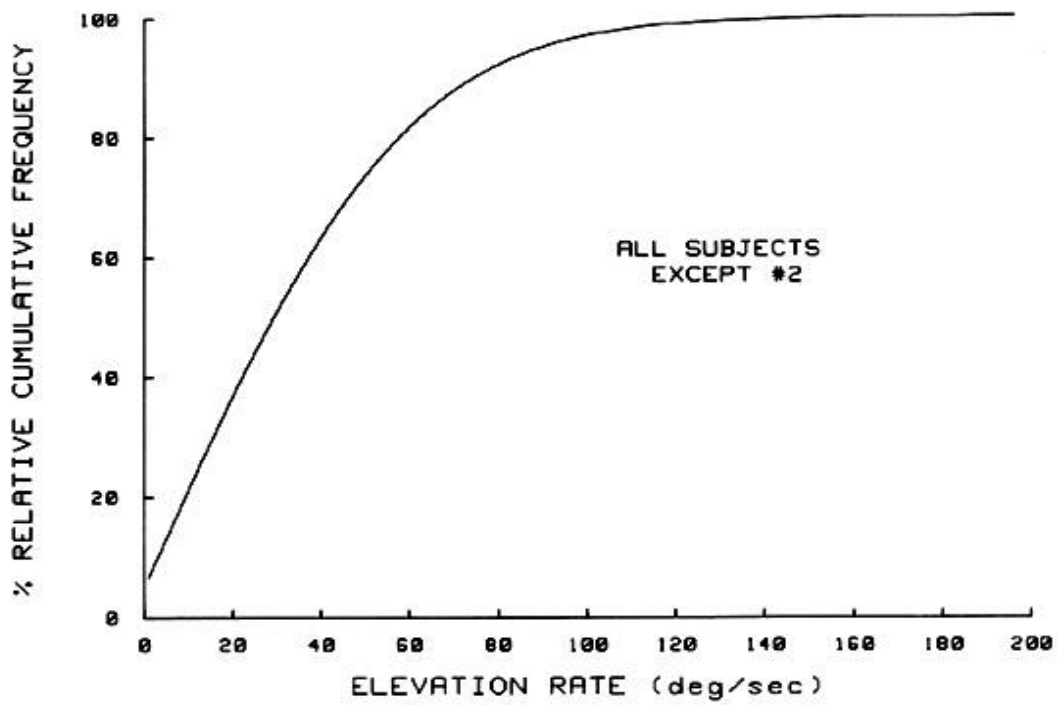


Figure 8. Percent relative cumulative frequency versus elevation velocity (Verona et al.,1986).

The summary of statistics for azimuth and elevation velocities is presented in Table 3. The small medians indicated that the velocity distribution was weighted heavily toward the lower values. The variability between subjects was greater than the variability within subjects, underlining the role of individual differences in search dynamics. There was greater variability in the elevation velocity data (bottom of Table 3). The within-subject variability in the median ranged from approximately 1°/sec to 11°/sec, and between-subject differences in the median for all the pilots combined ranged from approximately 0°/sec to 9°/sec. In addition, the medians were again smaller than the means, indicating more data points at the lower velocities.

The relative cumulative frequency curves of the velocity data (Figures 7 and 8) indicated that 50 percent of the azimuth and elevation velocities were less than or equal to 32°/sec. The curves also showed that 90 percent of both the azimuth and elevation velocities were less than or equal to 80°/sec. As an aside, approximately 97 percent of the azimuth velocities and 98 percent of the elevation velocities were equal to or less than 120°/sec, the maximum slew rate of the thermal imaging system selected for the AH-64 Apache helicopter.

In a summary of Verona et al. (1986), it was found that the concentration of azimuth and elevation head positions indicated that the pilots looked primarily forward, even though the flight scenario required a large range of head movements for the search task. In addition, this study supported a maximum slew rate of 120°/sec.

The current study presented herein attempts to expand the small database of head position and velocity values for actual flight scenarios while wearing HMDs.

Experimental design

The original overall study design for the D/NAW flights consisted of six flight maneuvers, two levels of aggressiveness (LOAs) and four visual conditions. Each of these factors is described in detail in the sections below. A full flight trial was limited to approximately 90 minutes in duration. A flight was defined as consisting of a varying numbers of “runs” where a “run” was the completion of the full set of all six maneuvers at a given LOA by a single pilot for one of the four visual conditions. The original study design called for each flight to consist of a combination of practice, intermediate and full test runs. It should be noted that the subject pilots were already familiar with the flight area. Practice runs were primarily flown for the purpose of familiarization with the various visual environments. In practice runs, all maneuvers were performed in succession. Intermediate runs varied by the fact that at the end of each maneuver the pilot landed the aircraft and completed a questionnaire on situational awareness. Full runs were identical to practice runs, with the obvious exception of flight performance data collection. Head tracking data were collected on all flights.

Instrumentation

Aircraft

All flights were in a Lynx ZD285 helicopter (Figure 9), which is a standard Lynk AH Mk 7 airframe with Gem Mk 205 engines but modified to exclude infrared suppressors, missile mounts, or other role equipment. The automatic flight control system (AFCS) was switched on during all flights to improve aircraft handling. The AFCS provided pitch, roll and yaw rate damping; and pitch and roll attitude hold. The Lynx ZD285 also was modified to incorporate a VCS, a Military Standard 1553B avionics architecture, navigation systems, and instrumentation.

The aircraft was configured for two experimenters seated in the rear cabin, an evaluated pilot, who served as a subject, in the front left seat, and a safety pilot in the front right seat. A system operator occupied the right cabin seat and was concerned mainly with operation and monitoring of the experimental systems. The flight test engineer in the left rear seat provided sortie direction and recorded subjective data. The instrument panel was modified to provide the safety pilot with ready access to all normal cockpit instruments. The subject pilot was provided with a cut-down panel providing primary flight instruments only.

An additional aircraft modification was the outfitting of all forward cockpit windows (but not overhead windows) with custom amber-tinted panels. The purpose of this modification was to allow the day-use, simulated HMD visual environment.



Figure 9. The DERA Lynx research helicopter outfitted with custom amber-tinted panels.

Visually Coupled System (VCS)

The VCS was comprised of a direct current (DC) electromagnetic head positioning system (HPS) with a transmitter affixed to the airframe close to the subject pilot's head with a sensor attached to his helmet. The HPS provided six degrees of freedom (DOF) output over a large range of head movements. A pair of boresight reticule units was associated with the HPS and permitted the subject pilot to align the system at start-up. HPS signals were processed and used to drive a nose-mounted turreted platform. The platform could be directed to the HPS line of sight over a range of $\pm 120^\circ$ azimuth and $+30^\circ$ to -90° elevation at a maximum rate of $110^\circ/\text{sec}$. The platform also carried a thermal imager derived from the Class II Thermal Imaging Common Module (TICM II) with a FOV of 55° horizontal by 37° vertical, producing a raster output in a 625 line/50 Hz format. A Radstone symbol generator was used to produce symbology.

The HPS sampled head position approximately every 5 ms. However, to reduce the volume of the data for storage and analysis, the available head position data files were transformed to 100 ms (0.1 sec)-samples.

Helmet-mounted display (HMD)

The aircraft was equipped with an HMD, manufactured by GEC, which used 625 line/50 Hz miniature (1-inch diameter) monochrome cathode ray tubes (CRTs) as image sources (Figure 10). The optical train provided a fully overlapped 53° horizontal by 37° vertical FOV. Although capable of binocular operation, the HMD was driven by a single video channel in a biocular mode (same image in both eyes). The HMD could display symbology only (not used in this study), thermal imaging only (TIO), or combined thermal imaging and symbology. The HMD helmet was heavy and had a forward center of gravity (comparable to the Night Vision Goggle (NVG) system). A single size helmet shell was used, incorporating a variety of fitting techniques including personalized foam pads, standard foam pads, a thermal-plastic liner or a combination of all three. The HMD could be adjusted for focus and interpupillary distance. However, the minimum interpupillary distance corresponded to approximately the 50th percentile male and was marginal for some subject pilots. Contrast and brightness controls were adjustable by the subject pilot. The HMD imagery was relatively dim and could not be seen easily under daylight conditions. For safety reasons flights in this study were conducted only under daylight conditions. For this combination of reasons, a modification to the HMD was necessary.



Figure 10. Flight helmet with 53-degree FOV HMD.

Simulated degraded visual environment (SDVE)

The daytime study flight requirement created several problems:

- The HMD imagery was difficult to see against the bright daytime sky.
- The flat surfaces of the HMD combiner optics resulted in numerous reflections that distracted and disoriented the pilot.
- The daytime visual environment was full of visual cues that were absent during night flight.

Therefore, to be able to use the HMD during the required daytime flights, a novel hood assembly referred to as a SDVE was developed (Crowley, 1998). The SDVE consisted of a full HMD hood assembly and a blue filter that was complementary to the amber screens already in place over all cockpit transparencies except the overhead panels. The combination of the amber and blue filters prevented exterior viewing by the subject pilot. The hood assembly consisted of a tailored fire-retardant black cloth hood worn over the pilot's helmeted head (Figure 11). The hood wrapped around the top and front of the helmet and was secured in the rear with hook and pile fasteners. Light could be completely prevented from entering the hood interior by gathering the drape material about the neck. The hood weighed 1.56 pounds (0.71 kg), with some of the weight being borne by the shoulders. To assist air exchange for the purpose of improving comfort, ventilation was provided using an off-the-shelf nuclear-biological-chemical ventilator.

The subject pilot could not see anything directly outside the aircraft but was able to view his arms, the controls, most of the instrument panel, and the left side cockpit structure when looking ahead. The instrument panel was heavily tinted and darkened due to a dark blue filter. This made it so that pilots could not read any numbers on the gauges, but could make out the main needle on the bigger gauges.



Figure 11. SDVE system.

Night Vision Goggles (NVGs)

A single pair of Fenn NG600 (Gen III) NVGs was used for all flights. The Fenn NG600 was 3rd GEN and had a 47° circular FOV. The NVGs were checked for serviceability before each flight using Night Vision Cased Test Equipment, Type ETS85FP, in accordance with standard servicing instructions.

Subjects

Severe limitations on manpower resources for subject pilots and safety pilots, combined with additional logistical problems, resulted in only four subject pilots, but no single subject flew every combination of factors. All four subject pilots were male. Ages were 31, 33, 34 and 37 with 1500, 1830, 2000 and 2700 flight hours, respectively.

Visual environments

The study employed four types of visual environments. These environments were:

- Good visual environment (GVE)
- Night Vision Goggles (NVG)
- Thermal imaging only (TIO)
- Rotary-wing symbology (RWS)

GVE flight was conducted in a normal daytime environment only when “good visibility” was available. These flights served as a baseline to document a reference level of functional quality performance.

NVG flights were flown in a night time environment using the Fenn NG600 night vision goggle system. A mean ambient light level of 10 milliLux was the target illumination level. However, any illumination within the range 5-50 milliLux was deemed acceptable. Along with the GVE flights, these flights also were used to develop a baseline for evaluating the VCS.

TIO flights were flown in a daytime environment using the SDVE hood and amber filter windscreen systems. Under the SDVE, the subject pilots were presented with thermal imagery only on the 53° HMD. No symbology was presented.

RWS flights were flown in a daytime environment using the SDVE hood and amber filter windscreen systems. Under the SDVE, the subject pilots were presented with thermal imagery and symbology on the 53° HMD.

Flight maneuvers

Flights were flown during the period mid-March to late-September 1997. The subjects flew a total of six maneuvers: Slalom, curved approach, hovering (spot) turns, rapid egress, bob-up/down, and sidestep. The focus for this analysis is on the slalom maneuver due to its more consistent flight pattern and easily defined flight cycle. The analyses of the other five maneuvers are deferred to future analyses.

All six maneuvers were performed successively in each run starting with the slalom and ending with the sidestep maneuver. Under ideal conditions, the maneuvers would be randomly presented. However, this counterbalancing design was not possible because the VCS was not available during the first two months of planned flights.

All flights were conducted during daytime hours with the exception of the NVG flights. Flights occurred in the region of southern England known as the Salisbury Plain training area at a location known as Haxton Down, approximately 6.6 miles (11 kilometers) north of the Boscombe Down airfield. All flights approached the test area by originating from the Boscombe Down airfield via a set route flown by the safety pilot at 90 knots indicated air speed (KIAS) at 200 feet above ground level (AGL), descending to 50 feet AGL on approach to the course. The safety pilot aligned the aircraft over the track and handed the controls over to the subject pilot at an appropriate ground speed, at 50 feet AGL, and at a point at least 200 m (650 feet) prior to the first slalom turn. Ground speed at release was to be approximately 30 knots for low LOA and 40 knots for moderate LOA.

There were two LOA: Low and moderate. Low LOA consisted of the use of up to a thirty-degree angle of bank (AOB), as required, and a moderate speed (> 0 knots, but 30 knots desired) to achieve an unhurried progression through the course. Pedal-assisted skidding turns were acceptable. There were no time constraints. The moderate LOA intended to exploit the full VCS flight envelope as far as possible and to target 30-degree AOB in all turns with up to 45-degree transients (at safety pilot discretion). Speed was adjusted to achieve rapid progression through the course with an appropriate turn radius (>0 knots, 40 knots desired). Pedal-assisted skidding turns were again acceptable. The required slalom course maneuver completion time was less than 90 seconds.

The slalom segment of the test course consisted of a South to North transit through the Haxton Down area at nap of the earth (NOE) heights and speeds. At Haxton Down, a convenient group of South-North oriented woods labeled Woods One through Four (with "gates" between woods), with intervening East-West avenues, provided a serpentine (slalom) course, which was developed into a variant of the ADS-33 slalom mission task elements (MTEs). The MTEs started at a ground speed appropriate to the LOA and ended at any suitable exit speed. The directions of the progressive course turns were: Right, followed by two left turns, two more right turns, and ending with two left turns (Figure 12). Ground track was maintained as close as possible (but not less than 5 meters) from N-S edges of woods, and as close as possible to centerlines of E-W avenues.

The flight tolerances for the slalom segment of the test flights, in general, were derived from those of ADS-33. The ADS-33 slalom MTEs are representative of actual tactical flight because they incorporate real obstacles, irregular turns and rectilinear phases. The modified ADS-33 tolerances used for the slalom segment of this study are presented in Table 4.

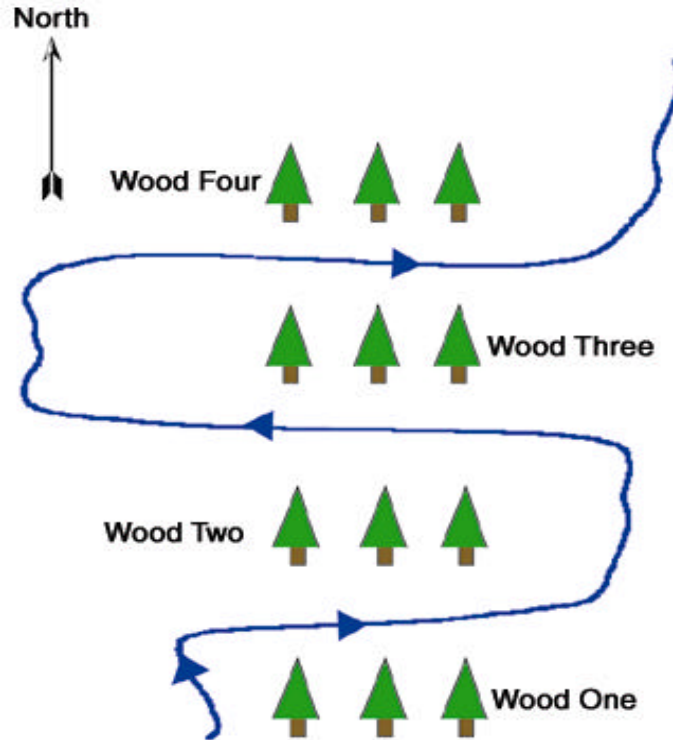


Figure 12. Representative flight path for slalom flight maneuver.

Table 4.
Slalom tolerances.

Over track, 50 feet AGL			Desired	Acceptable
Low LOA – 30 knots ground speed	<30° angle of bank; No time limit	Track	Within 20 meters	Within 30 meters
		Gate position	±5 meters	±10 meters
Moderate LOA – 40 knots ground speed	40° angle of bank transients	Height	+10 to 5 ft	+20 to -10 ft
		Speed	>20 knots	>0 knots

Note: 1) LOA – Level of aggressiveness. 2) AGL – Above ground level

The desired performance tolerance was to maintain datum height within -5 and +10 feet throughout, pass through gates within ±5 meters, and keep S-N flight path within twenty meters of edges of woods. It was not satisfactory to reduce ground speed below 20 knots at any stage. Adequate performance was a datum height maintained within -10 and +20 feet throughout, pass through gates at ±10 meters, and keep S-N flight path within 30 meters of edges of woods. It was not acceptable to stop the aircraft completely at any stage.

Six performance objectives were defined for the study: 1) Ability to maneuver with respect to ground features in NOE flight in the degraded visual environments (NVGs and HMDs) , 2) Ability to maintain spatial awareness and obstacle clearance during a complex multi-axis maneuver, 3) Check for undesirable display dynamics when performing maneuvers representative of moderate aggressiveness NOE flight, 4) Ability to control height during turning flight, 5) Ability to adjust airspeed to maintain a ground track defined by obstacles, and 6) Ability to control sideslip in turns at moderate airspeed.

Final overall trial design

Field experiments play havoc with even the best-designed study. As described above, two factors that impacted the study were the severe limitation on the availability of subject pilots and the late delivery of the VCS, which eliminated the ability to counterbalance. In general, the number of flights required by the experimental design of (two levels of aggressiveness) X (six maneuvers) X (four visual environments) far exceeded the allotted schedule time, available number of pilots, and logistical resources of the study. In addition, and having specific impact on the analysis presented herein, head motion data for some flights, either full or partial, were not collected due to head tracking system failure or flight interruption. As a consequence, the head tracking data files made available for this analysis were a subset of the original study design. And, as noted previously, only data files for the slalom maneuver were used in this analysis.

Database

The provided head motion database consisted of 628 files. The files were divided into 33 subdirectories, where each subdirectory contained the files for a given flight. A flight was defined as consisting of a varying numbers of “runs” where a “run” was the completion of the full set of all six maneuvers at a given LOA by a single pilot for one of the four visual conditions. A given file in the database contained data pertaining to a single subject for one combination of LOA, flight maneuver, visual environment, and type of run (practice, intermediate or full). A summary of the provided database is presented in Table 5. Note there were 107 files for the slalom maneuver.

This analysis focused on head motion for the slalom maneuver. Of the 107 files provided in the database, four were eliminated from the analysis due to missing or corrupted data. This left 103 files. These files are presented in Table 6 by subject, visual environment, LOA, and run type.

Table 5.
Summary of head motion database.

File overview									
Visual environment	LOA	Run type	Slalom	Curved approach	Spot turn	Rapid egress	Bob-up/down	Side step	Total
GVE	Low	Practice	4	4	4	4	4	4	24
		Intermediate	8	8	8	8	8	8	48
		Full	4	4	4	4	4	4	24
	Moderate	Practice	7	7	7	7	7	7	42
		Intermediate	14	14	14	14	14	14	84
		Full	7	7	7	7	7	7	42
NVG	Low	Practice	3	3	5	4	4	3	22
		Intermediate	4	4	4	4	4	4	24
		Full	4	5	4	3	3	4	23
	Moderate	Practice	6	6	6	6	6	6	36
		Intermediate	9	9	9	9	9	9	54
		Full	5	6	6	6	6	6	35
TIO	Low	Practice	5	5	4	4	5	4	27
		Intermediate	6	6	4	5	6	4	31
		Full	3	3	3	3	3	3	18
	Moderate	Practice	0	0	0	0	0	0	0
		Intermediate	0	0	0	0	0	0	0
		Full	0	0	0	0	0	0	0
RWS	Low	Practice	3	2	2	1	3	1	12
		Intermediate	5	5	3	3	5	3	24
		Full	1	1	1	1	1	1	6
	Moderate	Practice	2	2	2	2	2	2	12
		Intermediate	6	6	6	6	5	5	34
		Full	1	1	1	1	1	1	6
Total			107	108	104	102	107	100	628

The file structure for a sample slalom maneuver file is presented in Figure 13. The column headings (left to right) are: Time, head azimuth, head elevation, head roll, X-ground speed, Y-ground speed, Z-speed, inertial navigation unit (INU) ground speed, and differential global positioning system (DGPS) latitude and longitude. Time is expressed in 0.1-second intervals. Head azimuth, elevation and roll positions are expressed in degrees. Ground speeds (not used in analysis) are expressed in knots. Latitude and longitude values are expressed in global positioning system (GPS) units.

Table 6.
Summary of files for slalom head tracking analysis by subject.

		GVE		NVG		TIO		RWS		Total
		Low	Moderate	Low	Moderate	Low	Moderate	Low	Moderate	
#1	P	1	2	0	2	1	0	1	0	7
	I	2	4	1	2	2	0	2	0	13
	F	1	2	1	1	0	0	0	0	5
#2	P	1	1	1	0	1	0	1	1	6
	I	2	2	1	3	2	0	2	2	14
	F	1	1	1	0	1	0	0	0	4
#3	P	1	2	1	2	2	0	0	1	9
	I	2	4	1	2	1	0	1	4	15
	F	1	2	1	2	2	0	1	1	10
#4	P	0	2	1	2					5
	I	2	4	1	2					9
	F	1	2	1	2					6
Total		15	28	11	20	12	0	8	9	103

Notes. Visual environments: GVE- Good visual environment, NVG- Night Vision Goggle, TIO- Thermal imaging only, RWS- Rotary-wing Symbology
 Level of aggressiveness: Low, Moderate
 Flight type: P- Practice, I- Intermediate, F- Full

G19 = 3.0507											
	A	B	C	D	E	F	G	H	I	J	K
1	Flight	BLGYE01E	Manoeuvre	SLALOM	Run_No	47	Tape_name	HEIM/D4/01/97			
2	time	HEADAZIN	HEADELE	HEADROL	XGNDSP	YGNDSP	ZSPEED	INUGround	DGPSLAT	DGPSLONG	IT(SKIDS)
3	10:25.1	14.9337	-12.5195	6.7201	12.0421	-0.6911	3.5858				
4	10:25.2	17.2049	-14.98	5.7107	12.0499	-0.7391	3.6824				
5	10:25.3	17.2721	-16.2977	4.7851	12.0178	-0.8545	3.437				
6	10:25.4	17.5472	-14.0863	5.8773	11.9798	-0.8451	3.8333				
7	10:25.5	20.4979	-14.376	5.4262	12.0063	-0.8904	3.7454				
8	10:25.6	20.5331	-13.9935	5.4656	11.9601	-0.8852	3.8663				
9	10:25.7	22.4382	-14.202	3.9351	11.9889	-0.8931	3.7567				
10	10:25.8	21.1423	-12.9494	5.1315	11.9812	-0.8824	3.8251				
11	10:25.9	22.8266	-12.8276	4.2701	11.9872	-0.8143	3.9389				
12	10:26.0	21.7222	-13.9368	3.5921	11.9953	-0.8055	3.7952				
13	10:26.1	20.1733	-13.1986	3.6975	11.9844	-0.7344	3.8121		5762978	-115803	
14	10:26.2	21.9857	-12.5544	4.3703	12.0193	-0.7248	3.6685		5762980	-115803	
15	10:26.3	19.7578	-12.5505	5.1981	12.0138	-0.7263	3.7054		5762981	-115803	
16	10:26.4	20.0262	-11.6324	4.4567	12.0291	-0.6601	3.6417		5762982	-115803	
17	10:26.5	18.821	-13.3912	3.2039	12.0655	-0.7189	3.3922		5762983	-115803	
18	10:26.6	17.2932	-13.4656	4.9062	12.0771	-0.6895	3.371		5762984	-115803	
19	10:26.7	15.781	-14.4208	5.3989	12.1432	-0.734	3.0507	23.0152	5762986	-115803	
20	10:26.8	14.3969	-14.9357	7.0074	12.1431	-0.6756	3.031	23.0589	5762987	-115803	
21	10:26.9	15.7159	-15.6634	5.5106	12.1675	-0.6145	2.8917	23.1026	5762988	-115803	
22	10:27.0	15.7427	-16.2001	6.1139	12.2012	-0.5967	2.6962	23.1464	5762989	-115803	
23	10:27.1	16.3383	-15.3457	6.0131	12.2309	-0.5492	2.7873	23.1901	5762991	-115803	
24	10:27.2	18.2963	-14.0763	5.4058	12.2611	-0.5373	2.6426	23.2339	5762992	-115803	
25	10:27.3	22.1005	-16.14	3.9914	12.2433	-0.5468	2.5791	23.2776	5762993	-115803	
26	10:27.4	22.8571	-15.5719	3.8499	12.2706	-0.4924	2.6034	23.3214	5762994	-115803	
27	10:27.5	23.6826	-16.3704	3.6325	12.2685	-0.4767	2.6187	23.3651	5762995	-115803	
28	10:27.6	23.6404	-15.6048	5.027	12.2667	-0.4628	2.7301	23.4089	5762997	-115803	
29	10:27.7	21.07	-16.2873	4.8467	12.3134	-0.4797	2.4158	23.4461	5762998	-115803	

Figure 13. Screen capture of sample head motion data file.

Data analysis

The question to be answered by this analysis is: Are the distributions for head motion position (and velocity) different for the four visual environments? The head motion data files under analysis herein for the slalom maneuver are time series of head azimuth position values (elevation and roll data to be analyzed in future reports) for four different visual environments, confounded by two levels of aggressiveness and three run types. In addition to analyses of position data, transformations on these data included construction of velocity, reversal and excursion distributions. Briefly, a reversal was defined as a change in head motion direction (e.g., turning from looking right to looking left) and an excursion was defined as the change in angular position between two reversal points.

Data preparation

The slalom files consisted of data collected for a flight pattern flown over a set course running north and south with the turns going east and west (Figure 12). In order to be able to compare across subjects and visual conditions, it was decided to equalize across files by using data over a defined section within the slalom maneuver. This section, referred to as a cycle, was defined as shown in Figure 14. A cycle consisted of two right hand turns and two left hand turns. We also wanted to include a small portion before and after the turns in order to capture pilot head movements during preparation for and recovery from turns. In order to do this consistently, the means of the minimum and the maximum values of the longitude both prior and following the four turns were calculated. The point where the longitude exceeded the mean before the first right hand turn was used as the start point of the cycle. Where the longitude fell below the mean after the last left hand turn was used as the end point of the cycle. The cycle times for the slalom maneuver ranged from approximately 42 to 120 seconds. For a given visual environment, times for runs of moderate LOA were obviously shorter than for runs of low LOA, and run times for GVE runs were shorter than the other visual environments for both low and moderate LOAs.

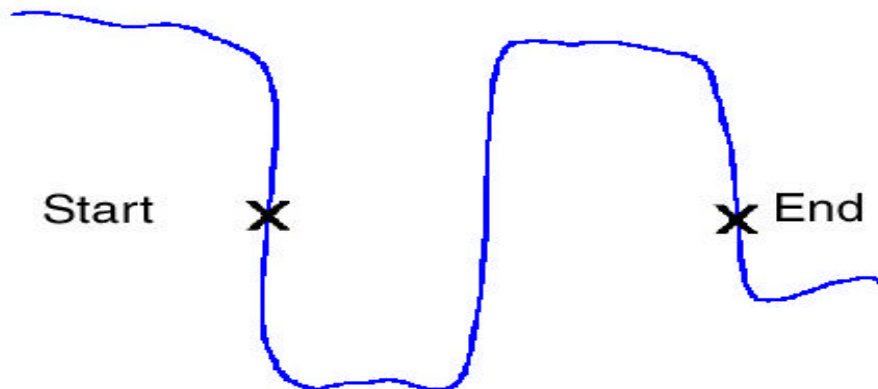


Figure 14. Definition of cycle used in analysis to equalize the slalom maneuver. Once a cycle was defined for each file, the data were smoothed using a three-point moving average routine in preparation for analysis.

Data analysis methods

Multiple approaches were used to answer the research question. The first approach was to transform all of the position time series data into histograms that represented position distributions. Then, the distribution moments (and additional distribution statistics) were calculated for each distribution. The second approach was to construct graphical representations of the distributions in the form of box-plots and quantile curves. Another approach was to use a Chi-square analysis to attempt direct comparisons of distributions.

A distribution can be fully defined by four moments: Mean, variance (or standard deviation), skewness, and kurtosis. However, it is useful to calculate additional distribution statistics (e.g., minimum, maximum, median, interquartile range (IQR), etc.). Graphical methods, e.g., box-plots, quantile curves, etc., also can be employed to provide rough quantitative descriptions of distributions.

Distributions are generally compared by performing standard parametric statistical tests involving means. However, the head motion distributions analyzed herein are multimodal and deviate significantly from normality. In cases of departure from normality, distribution-free approaches should be adopted, e.g., chi-square method.

Chi-square analysis can be used to compare goodness-of-fit between two or more frequency distributions. In this analysis, the chi-square statistic is a summation of adjusted differences between the two or more distributions for each allowable distribution value.

A more thorough discussion of these approaches is provided in Appendix A.

Position analyses

Before beginning the analyses, it may be instructive to investigate a sample data file. Figure 15 is a graphical overlay of azimuth head motion data for a slalom flight path for subject #2 for a GVE run. The solid line represents the flight path, with one cycle of two left and two right turns demarcated. The associated azimuth position histogram for this run over the defined cycle is presented in Figure 16. This representative distribution shows a maximum left-looking (negative) angle of approximately 68° and a maximum right-looking (positive) angle of approximately 56° . Calculation of the various additional statistics will fully define this distribution.

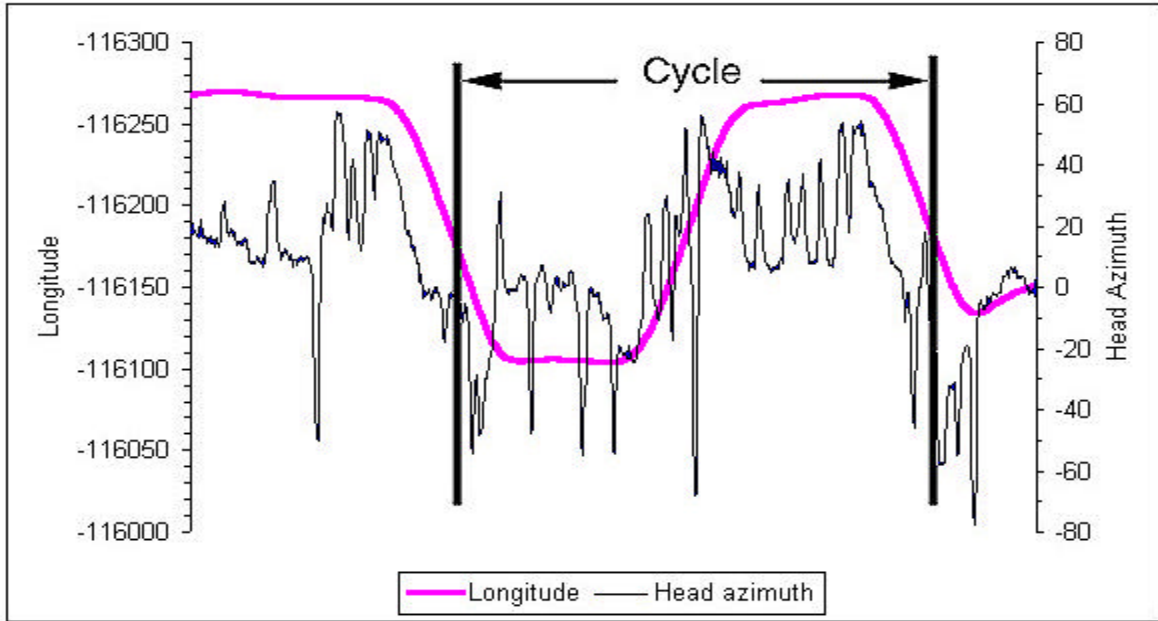


Figure 15. Graphical overlay of head motion data on slalom flight path for a sample GVE run for subject #2.

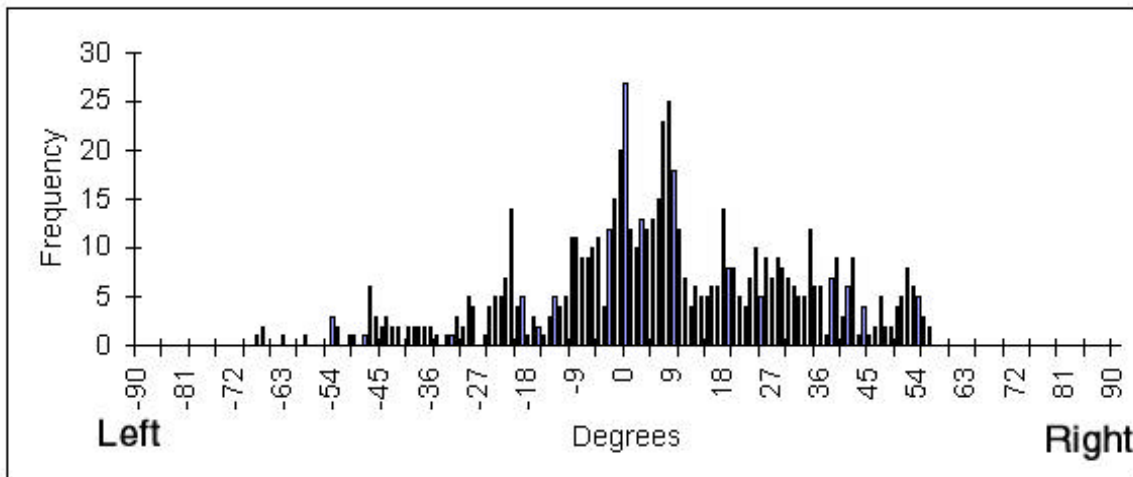


Figure 16. Azimuth position histogram for subject #2, GVE run in Figure 15 above.

Position distribution histograms

The use of histograms to represent the position distributions is a fundamental technique to allow an overall appreciation of head motion. The histograms presented herein use 1-degree intervals. From Table 6 it can be determined that for the combinations of four subjects, four visual environments and two LOAs, there are 103 azimuth position

distributions available for analysis. The resulting position histograms are presented in Appendix B. Subject #1 has a total of 25 histograms that represent the various combinations of LOA, run type and visual environment; subject #2 has 24 histograms; subject #3 has 34 histograms; and subject #4 has 20 histograms. See Table 6.

Individual position distributions

These individual distributions are worth examining for general characteristics and trends for each subject and visual condition. Such an examination yields the following:

Subject #1. The individual GVE head position distributions for subject #1 (Figure B-1, Appendix B) present the following characteristics: a) The typical range of motion is 115° (from -60° to $+55^\circ$), b) all run distributions show a central mode located near 0° , c) there appears to be a secondary mode located at $+45^\circ$, d) there is a no presence of outliers, e) the data indicate a greater time spent looking to the right, and f) the most extreme left looking angle is consistently greater than the right looking angle.

NVG head position distributions for subject #1 (Figure B-2, Appendix B) present the following characteristics: a) The central mode is much less defined than for GVE and is located at approximately 0° , b) the range is between approximately -65° to $+60^\circ$ (125°), c) the majority of runs show presence of a secondary mode at $+45^\circ$, d) there are no data outliers, and e) some of the runs weakly indicate less defined modes at -35° and -50° .

TIO head position distributions for subject #1 (Figure B-3, Appendix B) present the following characteristics: a) There are well defined central modes, slightly positive of 0° , b) in general, the range is -60° to $+60^\circ$ (120°), but with one run -65° to $+70^\circ$ (135°), and c) there is strong evidence for a secondary mode near $+45^\circ$.

RWS head position distributions for subject #1 (Figure B-4, Appendix B) present the following characteristics: a) There are well defined central peaks, just slightly positive to zero, b) the range is approximately -60° to $+55^\circ$ (115°), and c) a well defined secondary mode is at $+45^\circ$.

Subject #2. The GVE head position distributions for subject #2 (Figure B-5, Appendix B) present the following characteristics: a) There appears to be greater variability than for subject #1, b) several runs fail to show a distinct central mode (flatter), c) there is an approximate range of -65° to $+65^\circ$ (130°) and d) distributions show an occasional outlier value near $+70^\circ$.

NVG head position distributions for subject #2 (Figure B-6, Appendix B) present the following characteristics: a) Most runs show slightly better defined central modes than for GVE condition, but several runs still are relatively flat, b) the

range is approximately -75° to $+65^\circ$ (140°), c) the secondary mode is present near $+45$ degrees, but generally not well-defined, and d) there are no outliers.

TIO head position distributions for subject #2 (Figure B-7, Appendix B) present the following characteristics: a) There are better defined central modes than for GVE or NVG conditions, b) the ranges are quite variable with -55° to $+50^\circ$ (105°) as smallest and -68° to $+63^\circ$ ($\sim 130^\circ$) as largest, and c) the secondary mode generally is present.

RWS head position distributions for subject #2 (Figure B-8, Appendix B) present the following characteristics: a) Central modes are well-defined but much narrower and significantly shifted towards the negative (or left), b) secondary modes near 40° , c) five out of six runs show secondary mode at approximately $+15^\circ$, d) approximately a range of -70° to $+60^\circ$ (130°), and e) no outliers.

Subject #3. The GVE head position distributions for subject #3 (Figure B-9, Appendix B) present the following characteristics: a) The central modes are almost nonexistent, b) the secondary modes at 45° are somewhat evident, and c) the ranges are very limited, typically -35° to 60° (95°), as compared to other subjects and are somewhat truncated on the left side for all runs.

NVG head position distributions for subject #3 (Figure B-10, Appendix B) present the following characteristics: a) the central mode is very weak defined in all runs, b) the secondary modes are evident at 45° to 60° , and c) the ranges are significantly greater than for GVE, generally -60° to $+70^\circ$ (130°).

TIO head position distributions for subject #3 (Figure B-11, Appendix B) present the following characteristics: a) The range is typically $+60^\circ$ to the right and -50° to -65° to the left (110° - 125°), b) the central mode is more distinctive than for GVE and NVG and is displaced slightly negative from zero, and c) the secondary mode is present somewhere around 10° to 15° .

RWS head position distributions for subject #3 (Figure B-12, Appendix B) present the following characteristics: a) There are the greatest number of RWS runs (8), b) the range is considerably variable with an upper range value of approximately $+50^\circ$ degrees but with a lower range value of from -45° to -65° (95° - 115°), c) a central (but always prominent) mode slightly shifted to the negative, d) a primary mode is at $+15^\circ$, and e) there is weak evidence of secondary mode at $+45^\circ$.

Subject #4. The GVE head position distributions for subject #4 (Figure B-13, Appendix B) present the following characteristics: a) The range was extremely variable, with a lower range value from -30° to -55° and an upper value from $+40^\circ$ to $+50^\circ$,

b) the central mode is slightly displaced to the left, and c) a secondary mode is at +15°.

NVG head position distributions for subject #4 (Figure B-14, Appendix B) present the following characteristics: a) The range is expanded compared to GVE environment but variable with a lower range value varying from -50° to -65° and an upper range value varying from +60° to +70°, b) a central mode is weakly present in most runs, and c) a secondary mode is located between 45° and 50°.

Note: Head position data for subject #4 were not available for TIO and RWS visual environments.

Combined distributions

This rather large aggregate of histograms makes it difficult to compare head motion across visual environments. To overcome this problem, the authors contend that distribution comparisons can be based on combined distributions that are total data sets formed by combining data from all runs for a given visual environment. These combined distributions are not based on the average of individual runs but rather the summation of individual runs.

It is obvious that the distribution of head positions during rotary-wing flight was influenced by many factors. Even for a single individual, a considerable level of variability in head position was to be expected across flights, even if all quantifiable conditions were equal. The variability in the data under analysis herein was most assuredly increased further by the added confounds of LOAs and run types.

Faced with the large amount of data and the obvious variability, the authors propose the following argument. It is suggested that the influence of the LOA and run type confounds contributes to, but does not define, the general shape and characteristics of the head motion distribution for a given visual environment. Looking at the two LOAs, they differed in the study design by a speed difference of 10 knots (target speeds of 30 knots and 40 knots for low and moderate LOAs, respectively). However, as presented in Table 4, any forward speed was allowable. Three run types were possible: Practice, intermediate, and full. Practice runs were primarily flown for the purpose of familiarization with the various visual environments. In practice runs, all maneuvers were performed in succession. Intermediate runs varied by the fact that at the end of each maneuver the pilot landed the aircraft and completed a questionnaire on situational awareness. Full runs were identical to practice runs, with the obvious exception of flight performance data collection. An additional factor that would influence the head motion distributions is that the four subjects were very experienced test pilots and were familiar with the flight area and the flight maneuvers.

Therefore, the approach adopted by the authors was to perform analyses upon the combined data distributions. This argument is supported further by a graphical technique of successive additions of run distributions. In this technique an arbitrary distribution for

a given visual environment is selected. A second distribution for the same visual environment is combined to the first to create a new distribution representative of the first two. Then, additional distributions are added until a final distribution is built which consists of all of the position data for the selected visual environment. As these intermediate combination distributions are created, culminating in the final combined distribution, the authors argue that a general trend in the shape of the distribution can be seen. The authors contend that comparisons of head motion across visual environments between subjects can be made based on these combined distributions. An illustration of this argument for GVE runs for subject #2 is presented in Appendix C. In this example, six GVE runs with various LOA and run type are successively combined to form a single combined distribution histogram. As the individual runs are combined, a defined shape becomes readily apparent and is maintained.

Accepting the above argument, Figures 17-20 present the combined position distributions by subject and visual environment. Note that head position data for subject #4 were available for only two visual environments, GVE and NVG. As with the individual distributions, these combined distributions can be examined visually for general characteristics and trends, which should generally be similar to those found for the individual distributions. The following observations are made:

Subject #1. The combined GVE head position distribution for subject #1 (Figure 17) present the following characteristics: a) There is a central mode at approximately 0° , b) there is a secondary mode located at approximately $+45^\circ$, c) there are two weakly defined modes at -35° and -50° , and d) the range is approximately -65° to $+65^\circ$ (130°).

The combined NVG head position distribution for subject #1 (Figure 17) present the following characteristics: a) There is a not as well defined central mode as for GVE environment, b) the secondary mode seen at 45° for the GVE environment is present but not as obvious, and c) the range is approximately -65° to $+60^\circ$ (125°).

The combined TIO head position distribution for subject #1 (Figure 17) present the following characteristics: a) There is a well-defined central mode (slightly positive of 0°), b) a secondary mode is at $+45^\circ$, and c) there is a range of approximately -65° to $+60^\circ$ (125°) with an outlier near -70° .

The combined RWS head position distribution for subject #1 (Figure 17) present the following characteristics: a) There is a well-defined central mode, b) a well-defined secondary mode at $+45^\circ$, and c) there is a range of approximately -60° to $+60^\circ$ (120°).

Subject #2. The combined GVE head position distribution for subject #2 (Figure 18) present the following characteristics: a) An ill-defined central mode is shown, b) a lesser secondary mode is at $+45^\circ$, c) there is a preponderance of positive positions, and d) the range is approx -70° to $+65^\circ$ (135°).

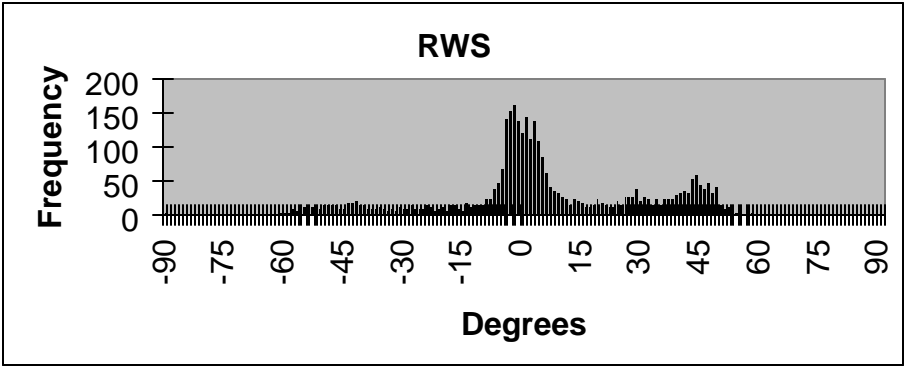
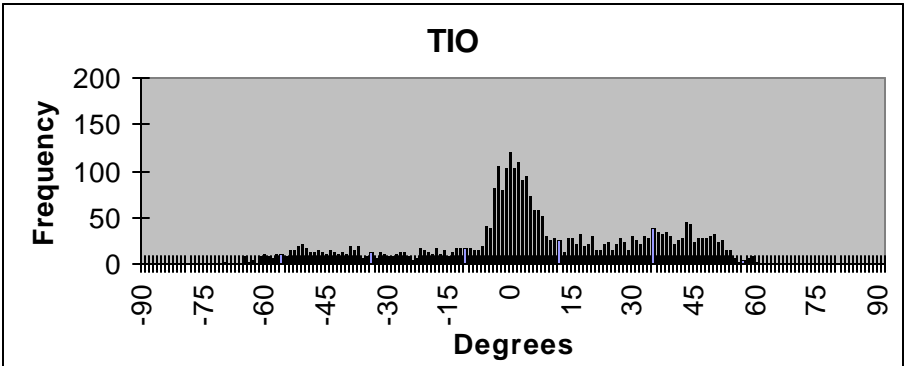
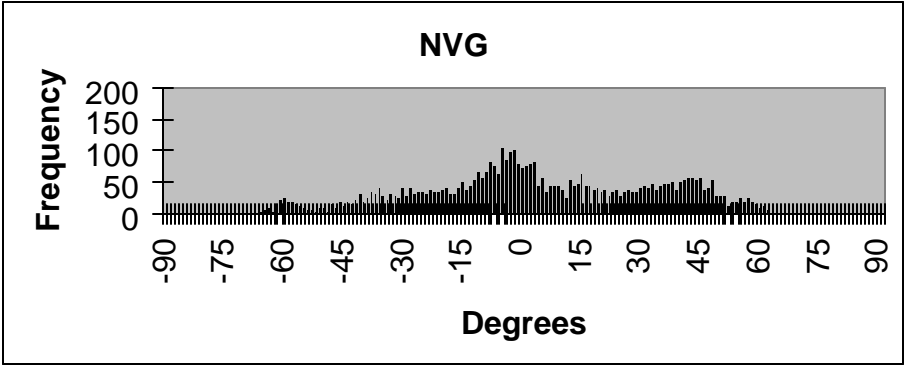
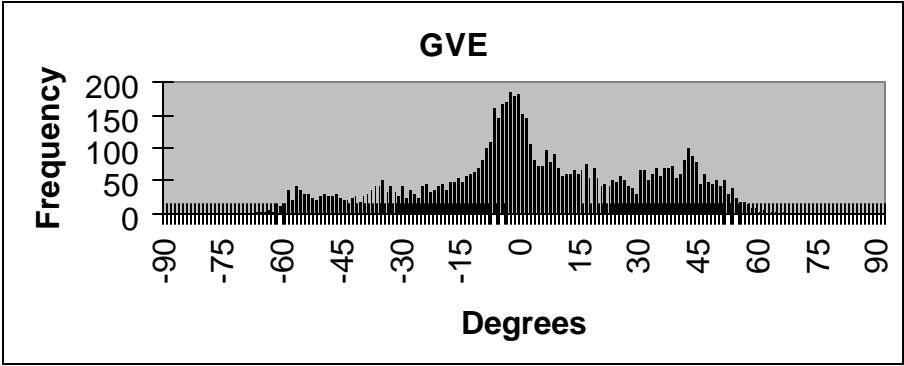


Figure 17. Combined position histograms for subject #1.

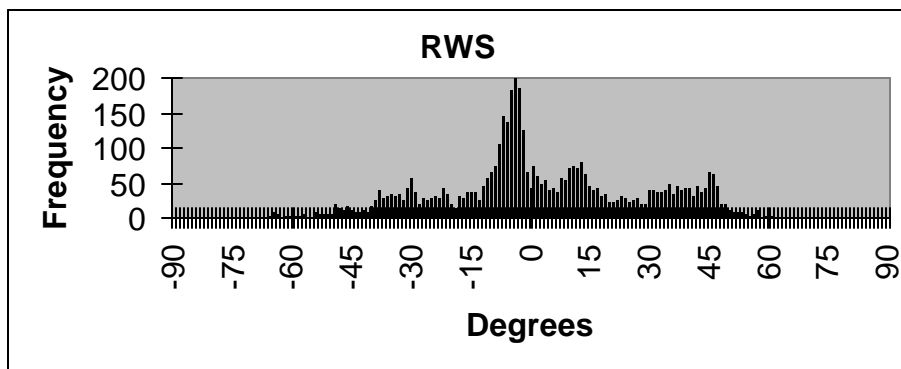
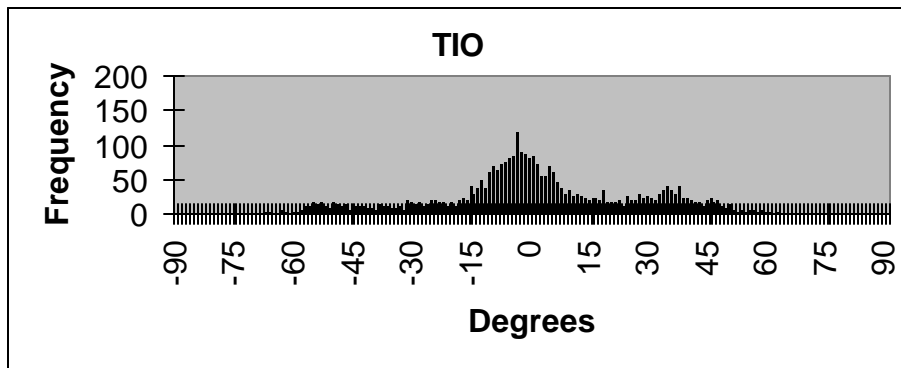
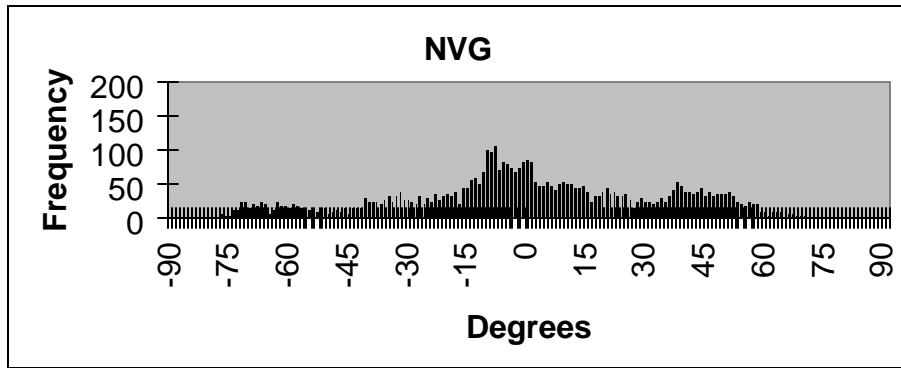
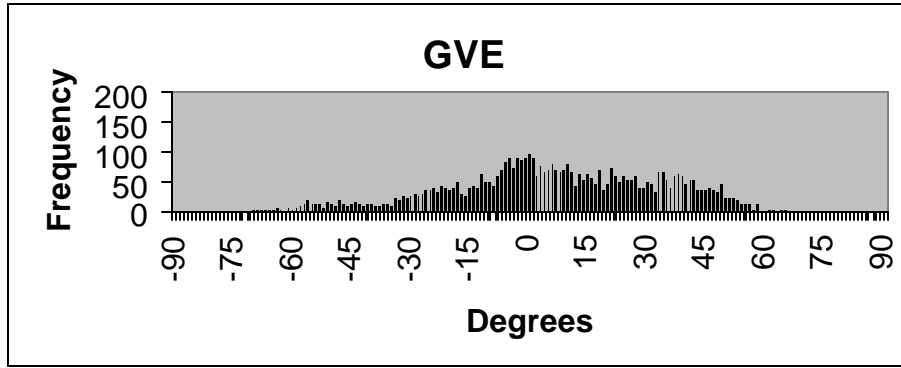


Figure 18. Combined position histograms for subject #2.

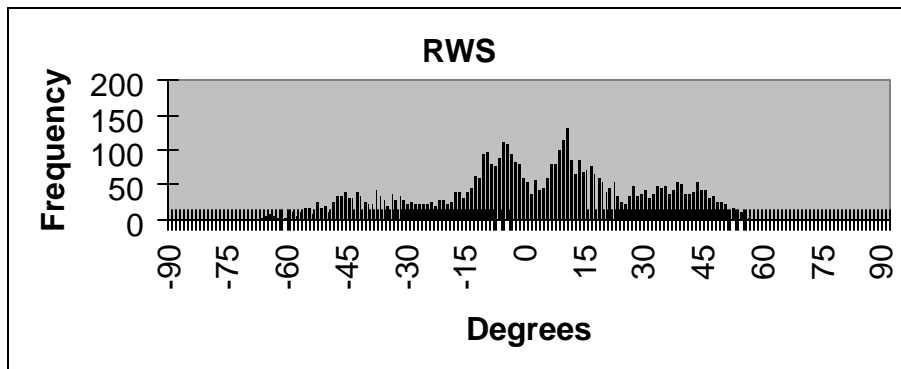
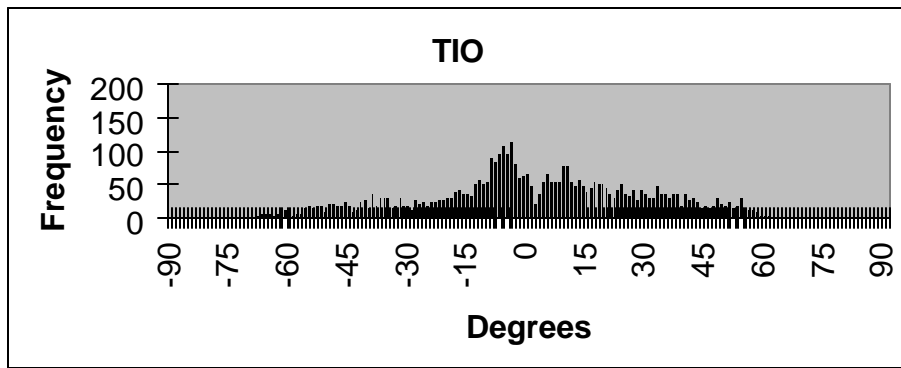
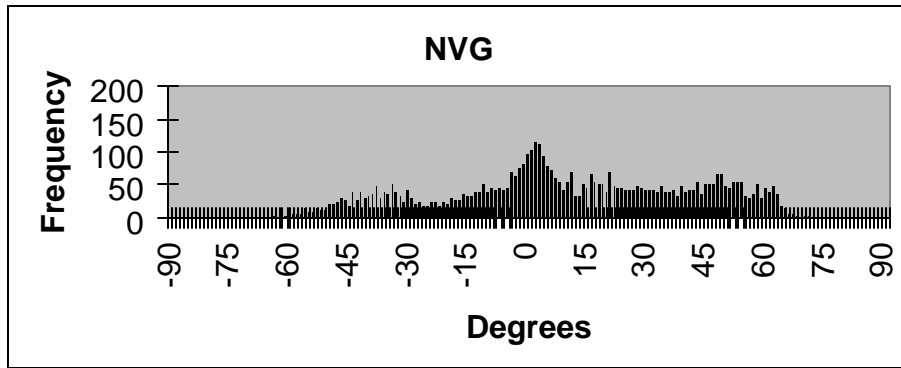
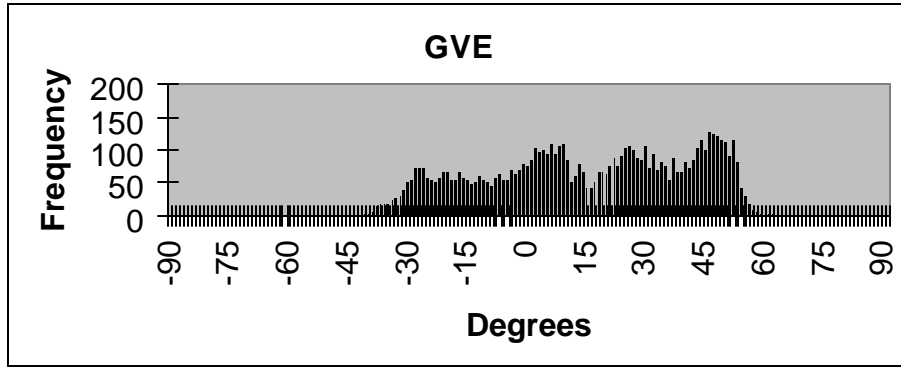


Figure 19. Combined position histograms for subject #3.

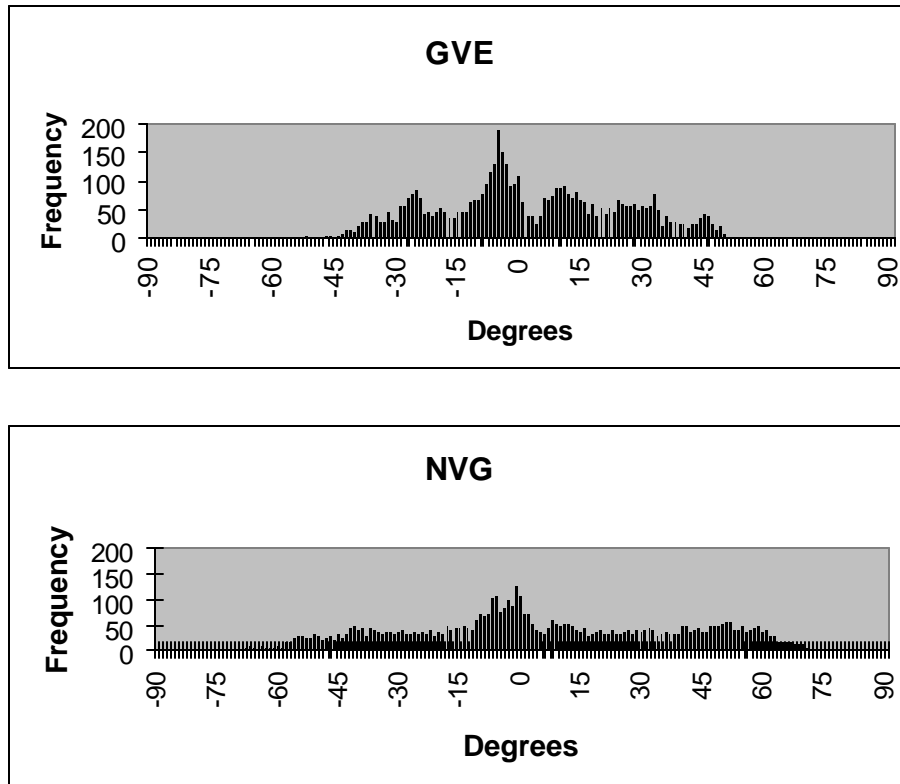


Figure 20. Combined position histograms for subject #4.

The combined NVG head position distribution for subject #2 (Figure 18) present the following characteristics: a) There are relatively flat, ill-defined central and secondary modes and b) a larger range of approximately -75° to $+70^{\circ}$ (140°).

The combined TIO head position distribution for subject #2 (Figure 18) present the following characteristics: a) There is a well-defined central mode, slightly negative (left) of 0° , b) a secondary mode at $+40^{\circ}$, and c) an approximate range of -70° to $+65^{\circ}$ (135°).

The combined RWS head position distribution for subject #2 (Figure 18) present the following characteristics: a) There is a well-defined central mode at approximately -5° , b) a range of approximately -65° to $+60^{\circ}$ (125°), and c) two secondary modes at $+10^{\circ}$ and from 35° to 45° .

Subject #3. The combined GVE head position distribution for subject #3 (Figure 19) present the following characteristics: a) The range is approximately from -40° to $+60^{\circ}$ (100°), b) the central mode is prominent at approximately $+10^{\circ}$ but not predominate, and c) additional prominent modes are at $+30^{\circ}$ and 45° .

The combined NVG head position distribution for subject #3 (Figure 19) present the following characteristics: a) The central mode is present but weak, b) there is a relatively flat distribution, and c) the range is from -60° to 70° (130°).

The combined TIO head position distribution for subject #3 (Figure 19) present the following characteristics: a) The central mode is present but weak, b) there is a relatively flat distribution, c) a weak secondary mode at +15°, and d) the range is approximately -65° to +60° (125°).

The combined RWS head position distribution for subject #3 (Figure 19) present the following characteristics: a) The range is from -65° to +55° (120°) and b) the modes are -45°, -5°, +15° and +45°.

Subject #4. The combined GVE head position distribution for subject #4 (Figure 20) present the following characteristics: a) A central mode is present but not dominate, b) there is possible evidence of secondary modes, and c) the range is approximately -55° to +50° (105°).

The combined NVG head position distribution for subject #4 (Figure 20) present the following characteristics: a) There is a weak central mode at 0°, b) a very flat distribution both left and right of center, and c) a range of approximately -70° to +75° (145°).

Note: Head position data for subject #4 were not available for TIO and RWS visual environments.

Moments and additional distribution statistics

While distribution shape provides a basic understanding of the ongoing head motion, the semi-quantitative nature of distribution histograms does not allow for comprehensive comparison. For this reason, distributions often are described or defined by the distribution's moments. There are four such moments: First (mean), second (variance or standard deviation), third (skewness), and fourth (kurtosis). It is also useful to calculate additional distribution statistics, e.g., minimum, maximum, median, etc.

Summary individual and combined distribution moments and statistics tables for all subjects, grouped by visual environment, are provided in Appendix D. However, following the previous arguments that comparisons can be based on the combined distributions, a summary of distribution moments and statistics by subject and visual environment for the combined distributions only is presented in Table 7. Examination of Appendix D and Table 7 lead to the identification of a number of characteristics and trends:

Subject #1. The summary GVE head position distribution statistics for subject #1 present the following characteristics: a) A combined minimum and maximum of -67.6° and +65.7°, respectively, indicate a balanced overall range about the center point, b) a combined median of -1.8°, c) a low skewness value (-0.1) indicates a lack of outliers, and d) 50% of combined position values lie between -12.1° and +24.9°.

The combined NVG head position distribution statistics for subject #1 present the following characteristics: a) The extreme left-looking values consistently are greater than the extreme right-looking values with a combined range of -66.9° to $+61.5^{\circ}$, b) the combined median is $+1.0^{\circ}$, c) a low skewness value (-0.1) indicates a lack of outliers, and d) 50% of the combined position values lie between -15.3° and $+28.3^{\circ}$, the largest of the 4 visual environments.

Table 7.

Combined azimuth position summary by subject and visual environment.
(Time expressed in seconds; Other dimensional statistics expressed in degrees)

Subject	Visual Environment	Mean Time	Min	Max	Mean	Median	S.D.	IQR	Skew	Kurt
1	GVE	57.6	-67.6	65.7	0.4	-1.8	28.8	-12.1 to 24.9	-0.1	-0.6
1	NVG	66.7	-66.9	61.5	3.5	1.0	30.4	-15.3 to 28.3	-0.1	-0.7
1	TIO	105.3	-72.2	61.1	5.0	2.8	28.2	-5.2 to 27.0	-0.4	-0.2
1	RWS	109.4	-61.4	57.8	5.4	1.4	25.0	-4.3 to 24.5	-0.2	-0.0
2	GVE	60.5	-70.5	64.5	6.3	6.0	26.3	-9.7 to 26.4	-0.3	-0.3
2	NVG	75.3	-77.9	69.6	-0.3	-1.6	32.1	-18.2 to 22.3	-0.2	-0.4
2	TIO	80.2	-67.9	63.3	1.2	-1.0	25.5	-10.9 to 17.7	-0.1	-0.1
2	RWS	77.6	-66.3	61.1	2.0	-2.6	25.1	-10.9 to 18.2	0.0	-0.4
3	GVE	56.5	-41.2	61.1	14.5	16.2	25.5	-5.0 to 37.0	-0.2	-1.1
3	NVG	58.3	-64.6	70.6	10.0	11.0	32.7	-14.6 to 38.7	-0.2	-1.0
3	TIO	82.8	-68.4	60.3	1.3	-0.1	27.1	-13.4 to 20.1	-0.2	-0.4
3	RWS	62.2	-67.7	55.3	1.1	2.7	26.8	-13.7 to 19.0	-0.2	-0.5
4	GVE	52.9	-57.0	51.2	1.6	-1.0	22.1	-12.9 to 17.9	0.1	-0.7
4	NVG	60.8	-68.6	72.0	4.7	0.3	33.6	-18.6 to 32.7	0.0	-0.9
4	TIO	None								
4	RWS	None								

The combined TIO head position distribution statistics for subject #1 present the following characteristics: a) The combined median shifted to right ($+2.8^{\circ}$), b) a greater negative skewness (-0.4) reflects the few values in the -70° position, and c) 50% of the combined position values lie between -5.2° and $+27.0^{\circ}$.

The combined RWS head position distribution statistics for subject #1 present the following characteristics: a) A Combined median of $+1.4^{\circ}$, b) a balanced combined overall range of -61.4° to $+57.8^{\circ}$, and c) 50% of the combined position values lie between -4.3° and $+24.5^{\circ}$.

When these four visual environments characteristics are studied in comparison for subject #1, the following observations can be made: a) The medians are positive, except GVE, b) the NVG has the largest IQR (43.6°), c) the RWS has the smallest range (119.2°) and IQR (28.8°), d) the most extreme left position is -72.2° for TIO, e) the most extreme right position is $+65.7^{\circ}$ for GVE, f) the TIO has the highest skewness, g) all kurtosis values are negative with NVG highest, and h) the NVG has the largest standard deviation.

Subject #2. The summary, GVE head position distribution statistics for subject #2 present the following characteristics: a) there is an usually right-shifted median at $+6^\circ$ and b) 50% of the combined position values lie between -9.7° and $+26.4^\circ$.

The combined NVG head position distribution statistics for subject #2 present the following characteristics: a) A total combined range of -77.9° to $+69.6^\circ$ (147.5°), 12.5° larger than for GVE, b) a median of $+1.6^\circ$, and c) 50% of the combined position values lie between -18.2° and $+22.3^\circ$, the largest of the 4 visual environments.

The combined TIO head position distribution statistics for subject #2 present the following characteristics: a) A total combined range of -67.7° to $+63.3^\circ$ (131.0°), b) a slightly negative combined median of -1.0° , and c) 50% of the combined position values lie between -10.9° and $+17.7^\circ$.

The combined RWS head position distribution statistics for subject #2 present the following characteristics: a) Combined median is shifted slightly to left at -2.6° and b) 50% of combined position values lie between -10.9° and $+18.2^\circ$.

When these four visual environments characteristics are studied in comparison for subject #2, the following observations can be made: a) The medians are negative, except GVE, b) the NVG has the largest IQR (40.5°) and range (147.5°), c) the NVG has the most extreme left (-77.9°) position, d) the most extreme right position is TIO (80.2°), e) the TIO and RWS have similar range and IQR values, f) the TIO has the lowest skewness, g) all skewness values are negative, and h) the NVG has the largest standard deviation.

Subject #3. The summary, GVE head position distribution statistics for subject #3 present the following characteristics: a) A most pronounced median value of 16.2° (to the right), b) an overall range of -41.2° to $+61.1^\circ$ which favors positions to the right, and an IQR (-5.0° to $+37.0^\circ$) which also favors positions looking to the right.

The combined NVG head position distribution statistics for subject #3 present the following characteristics: a) An unbalanced range (-64.6° to $+70.6^\circ$) to a lesser degree than GVE but still favoring positions to the right, b) the largest standard deviation, 32.7° , and c) the largest IQR of -14.6° to $+38.7^\circ$.

The combined TIO head position distribution statistics for subject #3 present the following characteristics: a) A total combined range of -68.4° to $+60.3$ (128.7°) which favors positions to the left, b) an almost directly centered median at -0.1° , and c) 50% of the position combined values lie between -13.4° and $+20.1^\circ$.

The combined RWS head position distribution statistics for subject #3 present the following characteristics: a) A combined median value of $+2.7^\circ$ (slightly to the

right), b) a combined range of -67.7° to $+55.3$ (123.0°), and c) 50% of the position values lie between -13.7° and $+19.0^\circ$.

When these four visual environments characteristics are studied in comparison for subject #3, the following observations can be made: a) The medians are strongly positive, except for TIO (-0.1), b) the NVG has the largest IQR (53.3°) and range (135.2°), c) the TIO and RWS have similar range and IQR values, d) the NVG and GVE have highest kurtosis values, e) all skewness values are the same, f) the GVE has the smallest range (102.3°), and g) the NVG has the largest standard deviation.

Subject #4. The summary GVE head position distribution statistics for subject #4 present the following characteristics: a) There is a nearly centered median of -1.0° , b) the combined overall range is -57.0° to $+51.2^\circ$ (108.2°), and c) 50% of the combined position values lie between -12.9° and $+17.9^\circ$.

The combined NVG head position distribution statistics for subject #4 present the following characteristics: a) There is a directly centered median at $+0.3^\circ$, b) the combined overall range is -68.6° to $+72.0^\circ$ (140.6°), and c) 50% of the combined position values lie between -18.6° and $+32.7^\circ$.

When these two visual environments characteristics are studied in comparison for subject #4, the following observations can be made: a) The NVG has greater range (140.6°) and IQR (51.3°), b) the NVG has the most extreme left (-68.6°) and right (72.0°) positions, c) the kurtosis values are both negative, and d) the NVG has the largest standard deviation.

Note: Head position data for subject #4 were not available for TIO and RWS visual environments.

Graphical comparisons

While considerable information is available in Table 7 and several pages have been spent enumerating and comparing the distribution characteristics presented in Table 7, distributions are often better understood through graphical techniques. In addition, the shapes of the head position distributions under analysis generally appear to deviate from normality and are asymmetrical, which speaks against conventional parametric analysis. When this is the case, graphical techniques such as box-plots and quantile curves can provide excellent methods of comparing distributions. See Appendix A for further discussion of these techniques.

The box-plot technique provides a visual summary of a data set by emphasizing a select set of statistic values, e.g., median, quartiles, and IQR. Box-plots for combined azimuth position distributions for all subjects are presented in Figures 21-24. Individual box-plots for all subjects by visual environment are presented in Appendix E.

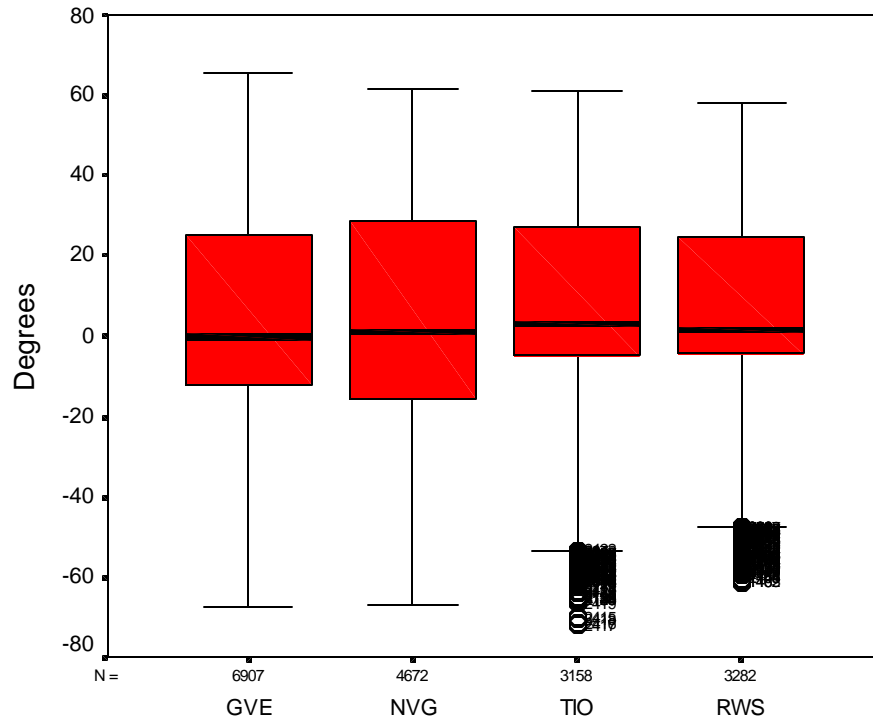


Figure 21. Combined azimuth position box-plots for subject #1.

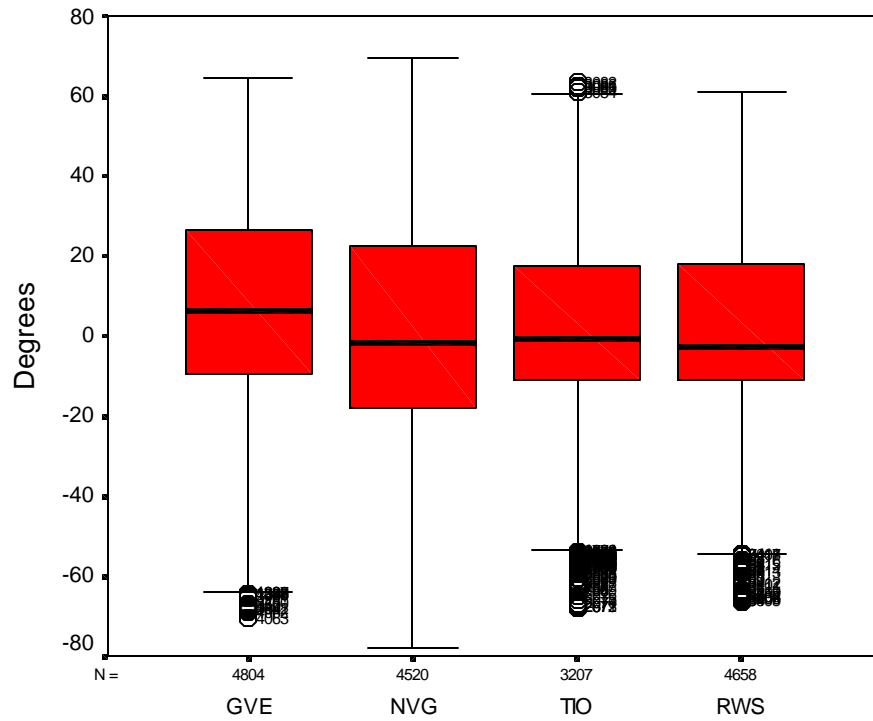


Figure 22. Combined azimuth position box-plots for subject #2.

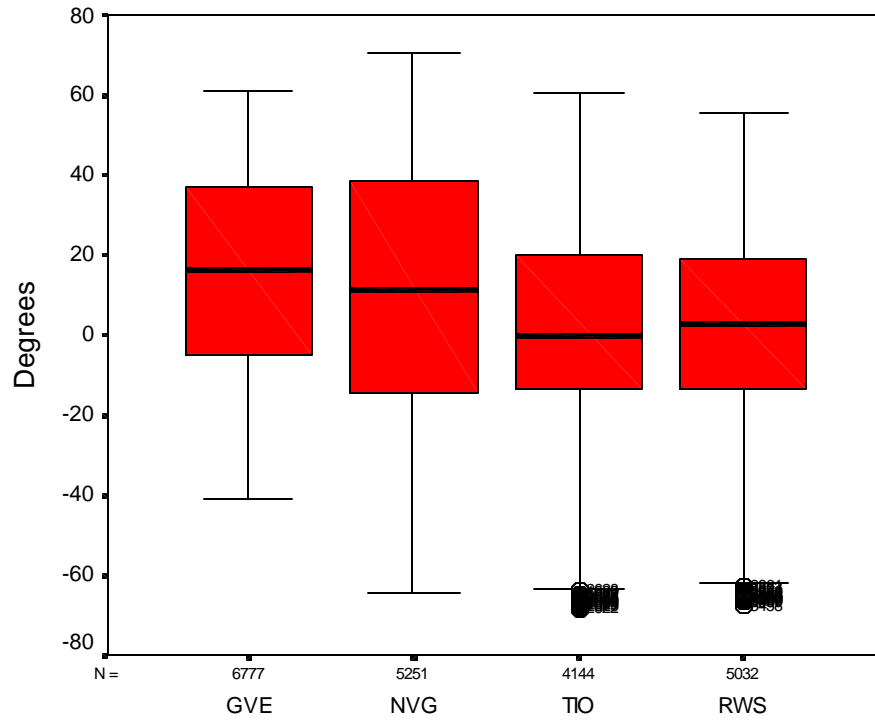


Figure 23. Combined azimuth position box-plots for subject #3.

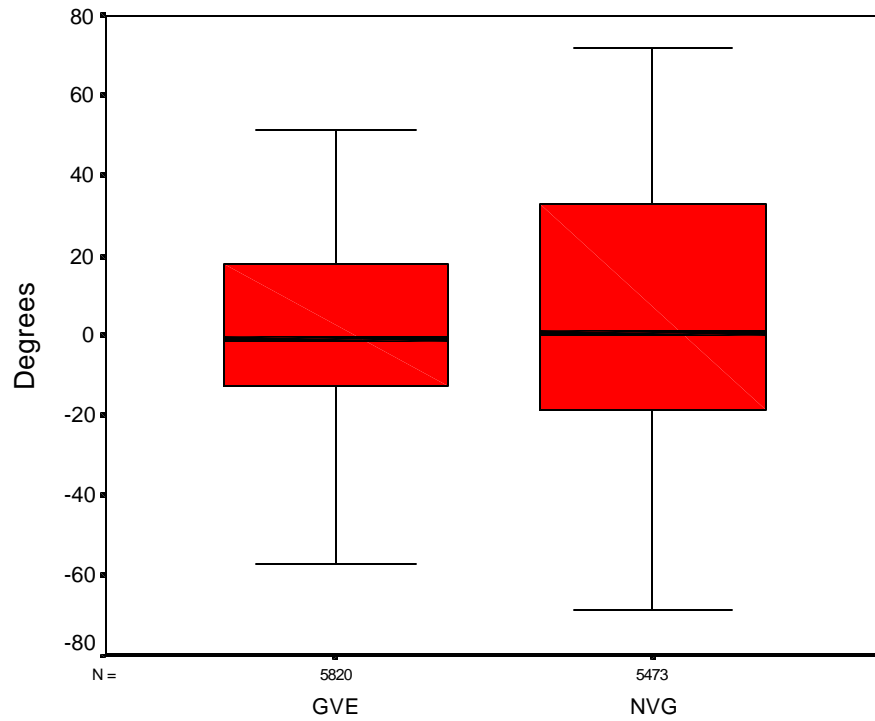


Figure 24. Combined azimuth position box-plots for subject #4.

From the box-plots for subject #1 in Figure 21, the following characteristics and trends can be construed: a) The NVG has the largest IQR, b) the medians are relatively the same, c) the 3rd quartiles consistently have a larger range than the 2nd quartiles, d) the TIO and RWS are most similar in shape, and e) the TIO and RWS have outlier values at extreme left.

From the box-plots for subject #2 in Figure 22, the following characteristics and trends can be construed: a) The NVG has the largest range and IQR, b) the GVE median is more positive (right shifted), c) the TIO and RWS are most similar in shape, and d) the 3rd quartiles are consistently larger in range than the 2nd quartiles.

From the box-plots for subject #3 in Figure 23, the following characteristics and trends can be construed: a) The NVG has the largest range and IQR, b) all the medians are positive (right shifted), c) the TIO and RWS are most similar in shape, and d) the TIO and RWS have outlier values at extreme left.

From the box-plots for subject #4 in Figure 24, the following characteristics and trends can be construed: a) The NVG range and IQR are greater, b) the medians are relatively equal, and c) the 3rd quartiles consistently have larger range than the 2nd quartiles.

An alternative graphical technique, the quantile curve, is better than the box-plot in comparing fine differences in distribution shapes, especially the presence of extreme values and dominant modes. The upper and lower ends of quantile curves terminate at the minimum and maximum data values. The slopes of quantile curves in the vicinity of the ends indicate the presence or not of outliers (values greatly smaller or larger than the majority of the data set); steep slopes indicate outliers. The vertical shift from zero at the 50-percentile point indicates the value and direction of the median. The slope of the quantile curve in the central region is an indication of the standard deviation and IQR of the data. Quantile curves for combined azimuth position distributions by subject are presented in Figures 25-28. Individual quantile curves for all subjects by visual environment are presented in Appendix F.

In general, many of the distribution characteristics that can be derived from the quantile curves in Figures 25-28 have already been listed above. However, these curves do offer additional information.

The quantile curves of subject #1 for the four visual environments are presented in Figure 25. The following characteristics and trends can be construed: a) the GVE has the most extreme right value, b) the TIO has the most extreme left value, c) the RWS has the smallest 1st and 2nd quartile range, d) the medians are all fairly similar with that of TIO being most positive, e) the NVG has the steeper slope near the center, indicating the less dominant (flatter) central mode, and f) the steepness of the RWS curve between the position values of approximately -65° to -5° indicates the very low frequency of head positions in this range.

The quantile curves of subject #2 for the four visual environments are presented in Figure 26. The following characteristics and trends can be construed: a) The NVG has the most extreme left and right values, b) the medians are negative, except for the GVE (strongly positive), c) The GVE has the most uniform distribution, d) there are strong central modes, except for the GVE, and e) the NVG has the largest 1st quartile range.

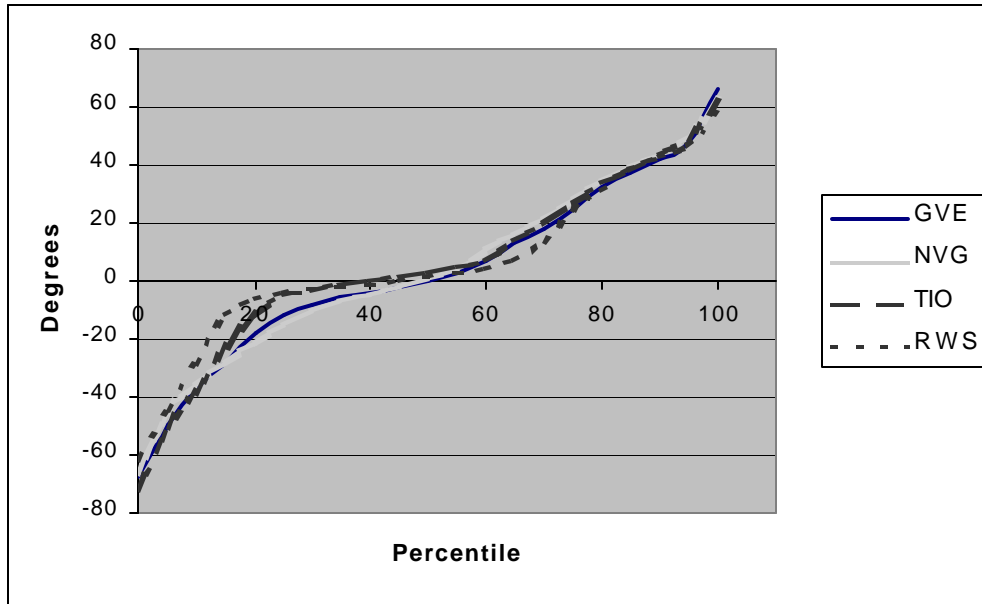


Figure 25. Combined azimuth position quantile curves for subject #1.

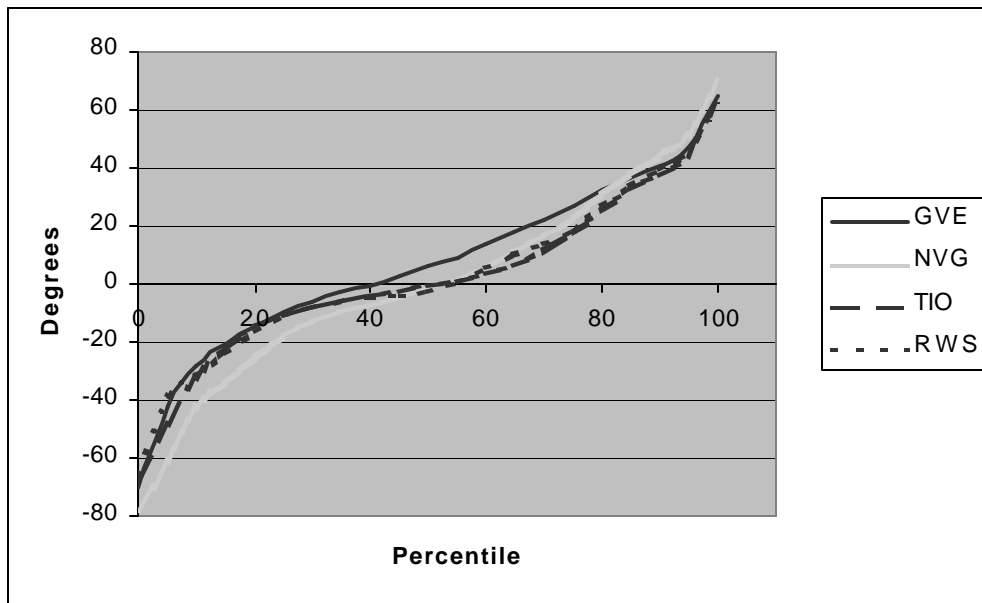


Figure 26. Combined azimuth position quantile curves for subject #2.

The quantile curves of subject #3 for the four visual environments are presented in Figure 27. The following characteristics and trends can be construed: a) the GVE has smallest range, b) the NVG has the largest range and the most extreme right value, c) the TIO and RWS are very similar in shape, d) there are weak central modes, and e) the GVE and NVG medians are very positive (shifted towards right), with GVE being the largest.

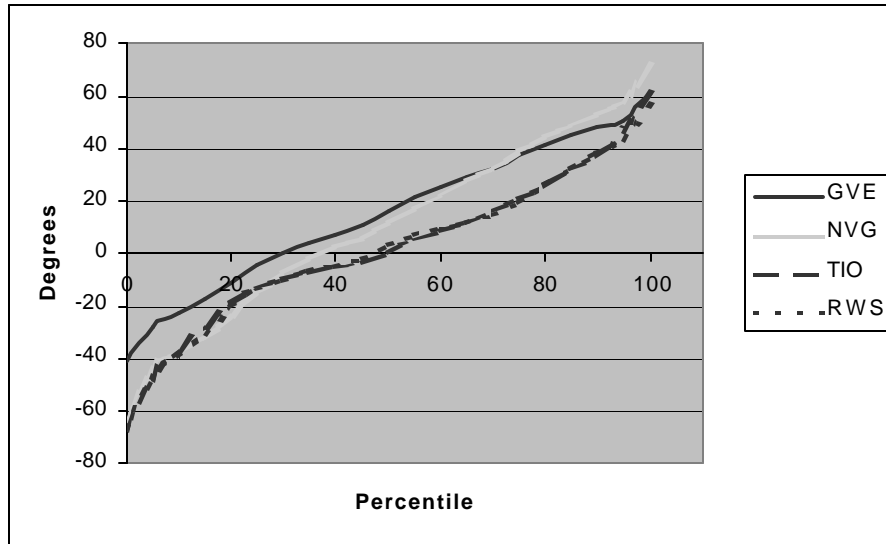


Figure 27. Combined azimuth position quantile curves for subject #3.

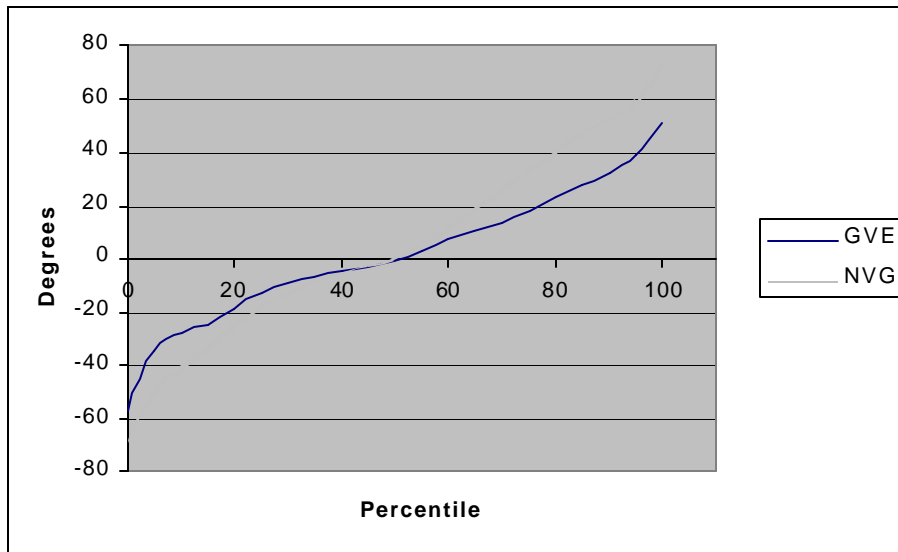


Figure 28. Combined azimuth position quantile curves for subject #4.

The quantile curves of subject #4 for the two visual environments are presented in Figure 28. The following characteristics and trends can be construed: a) The medians are

very similar, b) the NVG has more extreme right and left values, c) the NVG has larger range and IQR, d) the NVG has larger 2nd and 3rd quartile ranges, and the 3rd quartile range is larger than the 2nd quartile.

Chi-square analysis

The comparison of distributions is generally accomplished using a Chi-square goodness of fit test. However, when this test was applied to all pair-wise combinations of the combined head position distributions for the four visual conditions within each subject, all of the combinations were found to be significantly different from each other. This finding was not surprising since the argument previously presented for comparing combined distributions rather than individual distributions pointed out the often considerable differences between the specific characteristics of individual head position distributions even for the same subject performing the same maneuver with same visual environment. For this reason, the validity of using the Chi-square statistic to test for differences in the combined distributed was compromised.

Because the chi-square statistic could not be used to meaningfully test for differences between combined head position distributions, another approach was investigated. In the analysis of the histograms, the distribution moments, and the graphical plots, a common trend was noticed. In each analysis, there seemed to be a strong indication that the spread of the head positions for the four visual environments exhibited a common rank order. To investigate this, Table 8 was constructed to allow comparison of various spread statistics, which included the IQR, the range and the standard deviation.

Table 8.
Comparison of IQR, range and standard deviation.
(expressed in degrees, ranks within subject given in ())

Subject	Visual environment	IQR	Range	S.D.
1	GVE	37.0 (2)	133.3 (1.5)	28.8 (2)
1	NVG	43.6 (1)	128.4 (3)	30.4 (1)
1	TIO	32.2 (3)	133.3 (1.5)	28.2 (3)
1	RWS	28.8 (4)	119.2 (4)	25.0 (4)
2	GVE	36.1 (2)	135.0 (2)	26.3 (2)
2	NVG	40.5 (1)	147.5 (1)	32.1 (1)
2	TIO	28.6 (4)	131.2 (3)	25.5 (3)
2	RWS	29.1 (3)	127.4 (4)	25.1 (4)
3	GVE	42.0 (2)	102.3 (4)	25.5 (4)
3	NVG	53.3 (1)	135.2 (1)	32.7 (1)
3	TIO	33.5 (3)	128.7 (2)	27.1 (2)
3	RWS	32.7 (4)	123.0 (3)	26.8 (3)
4	GVE	30.8 (2)	108.2 (2)	22.1 (2)
4	NVG	51.3 (1)	140.6 (1)	33.6 (1)

Table 9.
Spearman rank-correlation coefficients for IQR, range and standard deviation.

IQR					Range					S.D.				
	#1	#2	#3	#4		#1	#2	#3	#4		#1	#2	#3	#4
#1		+0.80	+1	+1	#1		+0.35	-0.15	-1	#1		+1	+0.40	+1
#2			+0.80	+1	#2			+0.40	+1	#2			+0.40	+1
#3				+1	#3				+1	#3				+1
#4					#4					#4				

Table 10.
Spearman rank-correlation coefficients for skewness and kurtosis.

Skewness					Kurtosis				
	#1	#2	#3	#4		#1	#2	#3	#4
#1		-0.65	0.35	+0.50	#1		+0.55	+0.60	+1
#2			+0.50	-1	#2			+0.35	+1
#3				+0.50	#3				-1
#4					#4				

While remembering that correlation coefficients involving subject #4 should be given less weight because only GVE and NVG data were available, the Spearman rank-correlation tests showed a strong association between IQR and visual environment (Table 9). In addition, there was some evidence, although much less strong, for a similar association for range, standard deviation and kurtosis (Tables 9 and 10). Restated, in general, dispersion statistics, primarily the IQR, appeared to be the best characteristics for discriminating between visual environments.

Rate analyses

Up to this point all of the characteristics of head motion that have been investigated have related to position. It may easily be argued that more valuable information regarding head motion can be obtained from investigating the frequencies, magnitudes and rates (velocities) of change in head position. Three possible new characteristics for investigation are reversals, excursions, and head velocities. Reversals, which measure frequency of head movement, are defined as the number of times that the pilot changes movement from one direction to the other during the cycle. Excursions (magnitudes) are a measurement of the angular distance that the pilot's head travels in degrees between reversals, and velocities are a measure of the rate of speed in which the pilot moves his head during excursions.

Reversals

The first temporal characteristic is based on the number of times the pilot reverses head movement from one direction to the other, e.g., reversing from moving towards the right to moving towards the left. To account for the differences in run times, a reversal rate was adopted and was expressed as the number of reversals per minute. Tables G-1 to G-

4 in Appendix G present the number of reversals and reversal rates for each run for all subjects by visual environment. Mean reversal rates were calculated and are presented in Table 11 with rank orders within subjects provided in parenthesis. These mean reversal rates are plotted with ± 1 standard deviation bars in Figure 29.

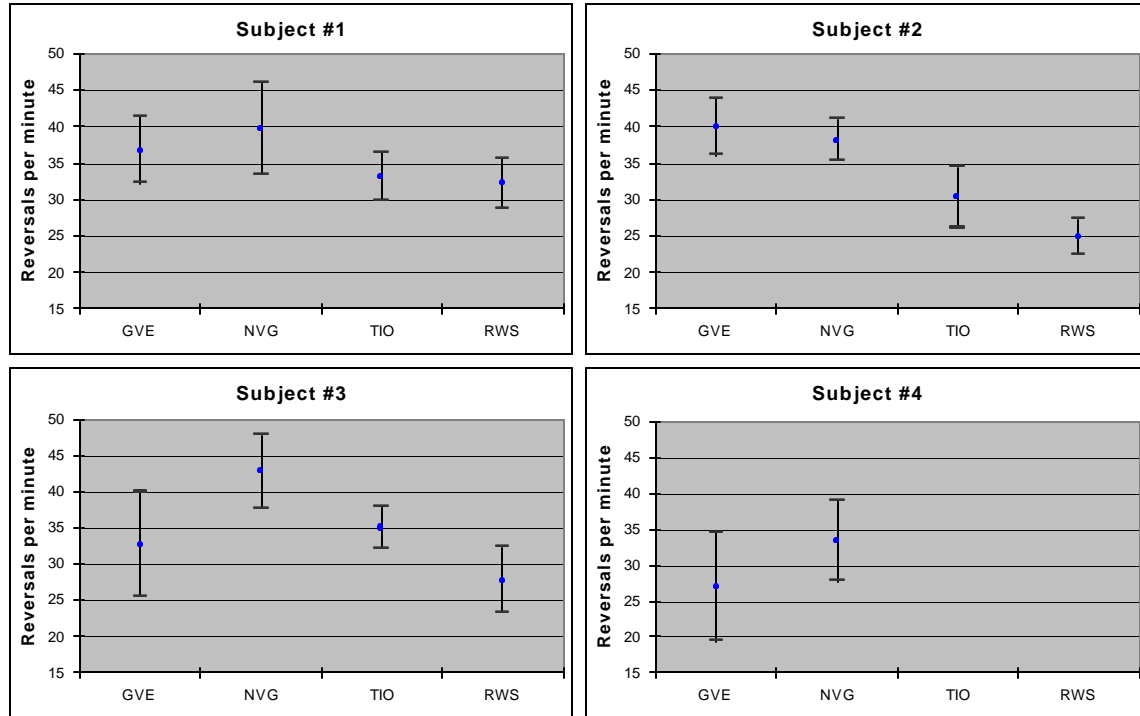


Figure 29. Reversal standard deviation charts showing +1 and -1 standard deviation and means by subject, by visual environment.

An examination of Figure 29 shows considerable variability in the mean reversal rates between visual environments for all of the subjects. As with the measures of dispersion, ranking of these rates appears to be the only meaningful analysis. For three of the four subjects, mean reversal rates for the GVE and NVG visual environments were ranked first and second, respectively. For the three subjects for which TIO and RWS data were present, these mean reversal rates were similar in value and less than those rates for GVE and NVG. The RWS mean reversal rate was always ranked 4th.

Table 11.
Mean reversal rates.

	Subject #1	Subject #2	Subject #3	Subject #4
GVE	35.6(2)	39.0(1)	31.7(3)	25.7(2)
NVG	38.7(1)	37.3(2)	41.7(1)	32.3(1)
TIO	32.9(3)	29.6(3)	34.3(2)	N/A
RWS	31.6(4)	24.0(4)	26.8(4)	N/A

Note: Means expressed in reversals per minute.

As with the measures of dispersion, the Spearman rank-correlation was used to test correlation between subjects (Table 12). Due to the variation across subjects and the lack of sample size, mean reversal rate is, at best, only a weak indicator of the difference in head motion within the four different visual environments.

Table 12.
Spearman ranking correlation.

Reversal Rates				
	#1	#2	#3	#4
#1		+0.8	+1	+1
#2			+0.4	-1
#3				+1
#4				

Excursions

The second temporal characteristic investigated was excursions. An excursion is defined as the distance the pilot moved his head between reversals expressed in degrees. Distribution histograms for excursion values for individual runs for each subject and visual environment are presented in Appendix H. Combined histograms overlaid with cumulative frequency curves are shown in Fig. 30-33. Excursion values representing the 25th-, 50th-, 95th-, and 99th-percentile points are presented in Table 13 for the combined excursion distributions. Tables summarizing the azimuth excursion data by subject and visual environment are presented in Appendix I. Box-plots are presented in Appendix J.

Examining the histograms, box-plots and tables, the following observations or features were noted. First, the distributions of excursions values varied greatly even for individual runs for a given subject and visual condition. Second, across all subjects and visual environments, the smallest and largest head excursions recorded were 0.01° and 121.4°, respectively. Excursions of greater than 100° were confined to the GVE and NVG visual environments. For all subjects across all visual conditions, 95% of the excursions were 83° or less in size. Third, the first and second quartile ranges for the RWS visual environment were very small compared to the third and fourth quartiles. From Table 13, the 25th-percentile values were 3° for each of the three subjects having RWS runs; the 50th-percentile values were 16°, 6°, and 9°, respectively. The most reasonable explanation for this abundance of small excursions is that the pilot was relying heavily on the added symbology provided by the RWS condition and made fewer moderate to large angular head movements.

Overall, with the one exception of an increased frequency of small head movements associated with the RWS visual environment, examination of the distribution of the head excursions provided no definitive differences between the four visual environments. The distribution shapes were not well defined for any visual environment.

Table 13.
Cumulative excursion percentile values.

Subject	Flight Environment	25%	50%	95%	99%
Subject #1	GVE	9	26	64	100
	NVG	14	28	57	71
	TIO	9	35	67	94
	RWS	3	16	56	66
Subject #2	GVE	10	27	83	109
	NVG	16	37	77	104
	TIO	7	16	54	71
	RWS	3	6	49	81
Subject #3	GVE	9	21	49	81
	NVG	15	27	62	101
	TIO	8	17	53	75
	RWS	3	9	57	93
Subject #4	GVE	3	8	46	79
	NVG	8	26	61	77
	TIO	None			
	RWS				

Note: All values expressed in degrees.

In an attempt to obtain an overall sense of the range of excursions exhibited by all of the pilots, for all of the visual environments, a histogram of excursion size combining across all runs was constructed (Figure 34). This overall distribution has the following statistics: Mean of 25.2°, median of 22.0°, standard deviation of 20.8°, and IQR of 32.1°. An overlaid cumulative frequency curve indicates 50% of all excursions were 22° or less. The 95% and 99% excursion values were 62° and 93°, respectively. The largest (maximum) excursion exhibited by any pilot during any run was 122°.

Velocity

Biomechanical and physiological data (Zangemeister and Stark, 1981; Durluch and Mavor, 1995) support unloaded head velocity values as high as 600°/sec. Larger peak velocity values are associated with increasing size of head motion excursions. It is very likely that when the head is supporting additional weights of HMDs, peak velocity values would be less.

For these analyses, all velocity values were expressed as positive in value. There was no attempt to separate velocities of motions to the left from motions to the right. Velocity values were calculated from the time-sequenced azimuth position data using an algorithm based on the central derivative (Bloch, 2000). The algorithm calculated the instantaneous velocities at the middle of a moving three-point interval of the time-sequenced data. Velocities at the initial and final data points were not calculated. An inspection of the resulting velocities verified there were no artifacts introduced by the derivative process.

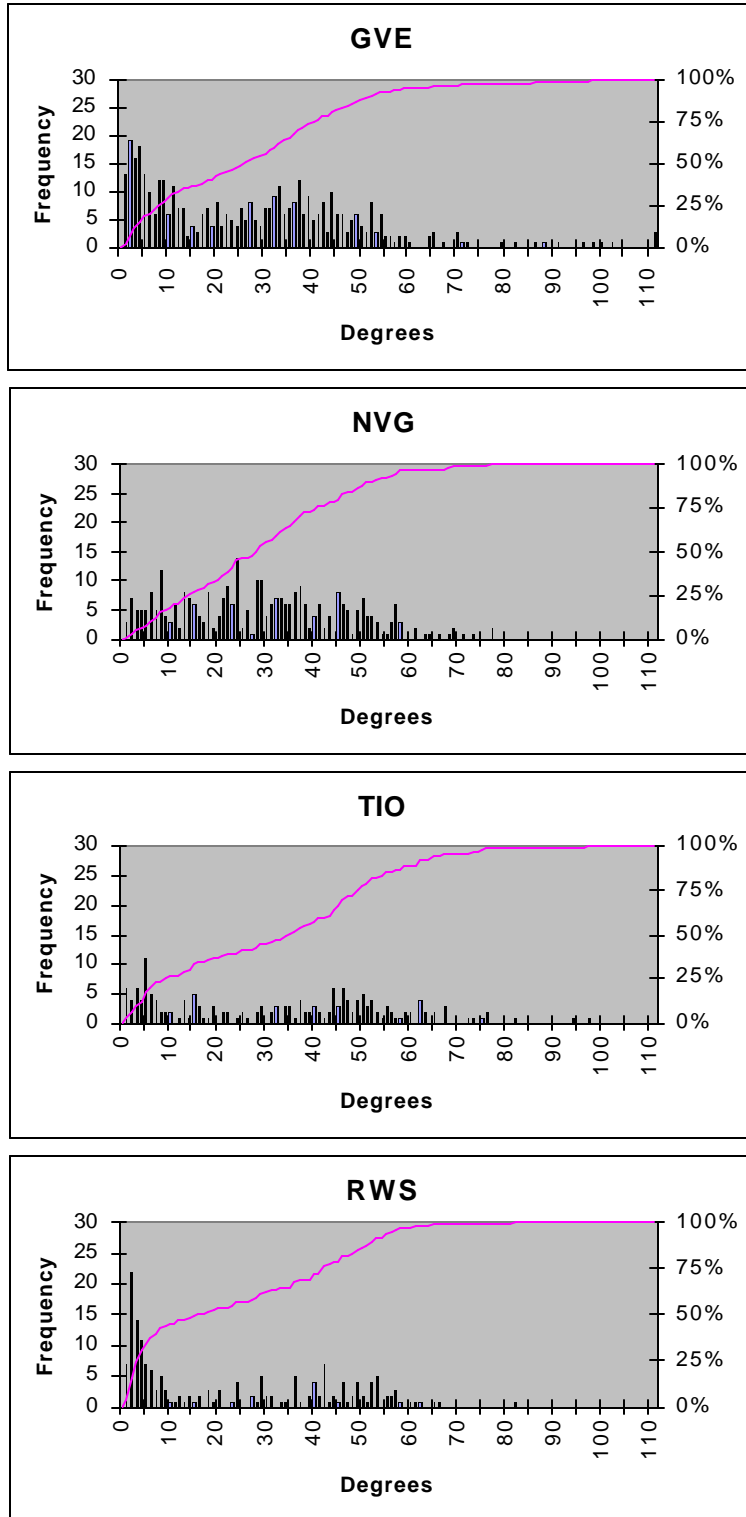


Figure 30. Subject #1 combined excursion histograms by flight type with cumulative frequency curve.

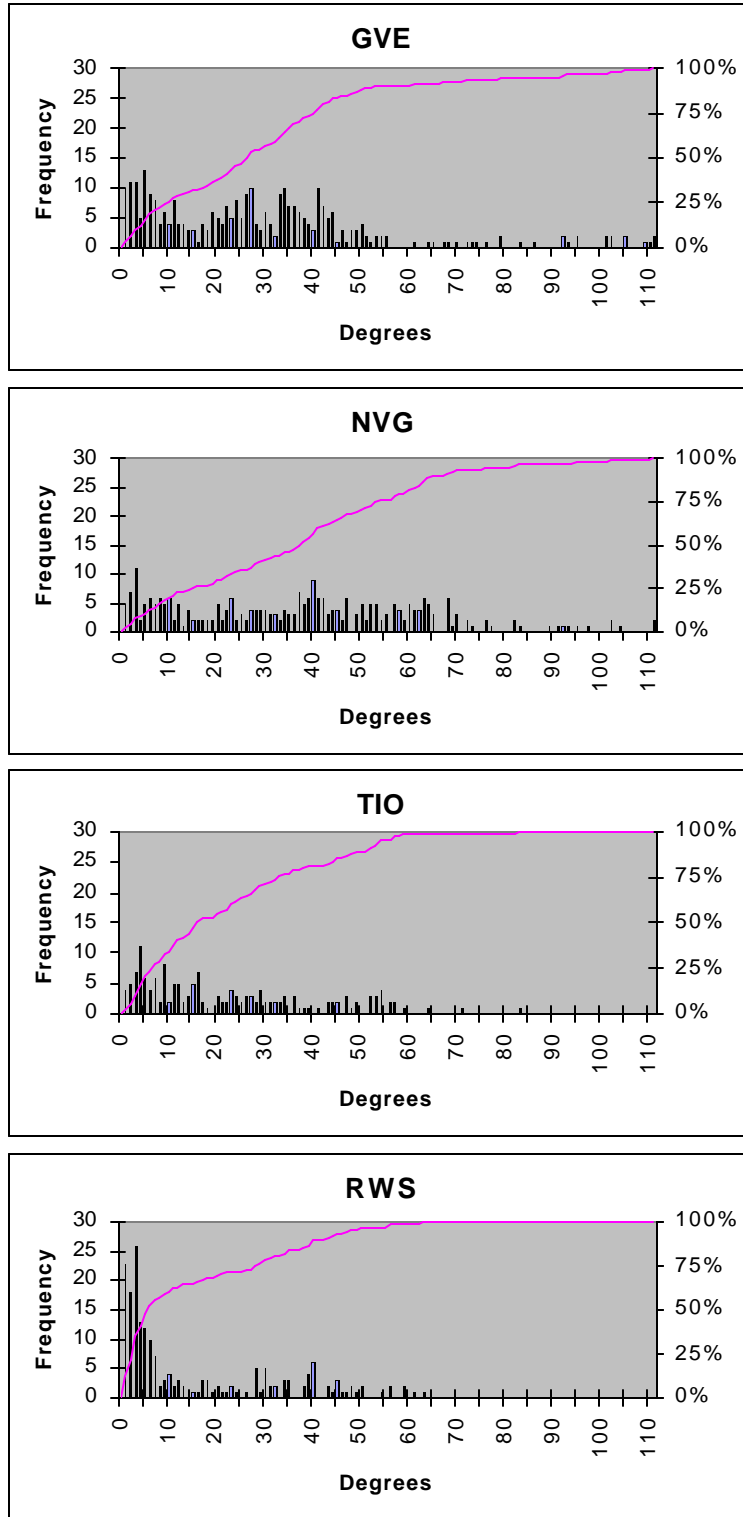


Figure 31. Subject #2 combined excursion histograms by flight type with cumulative frequency curve.

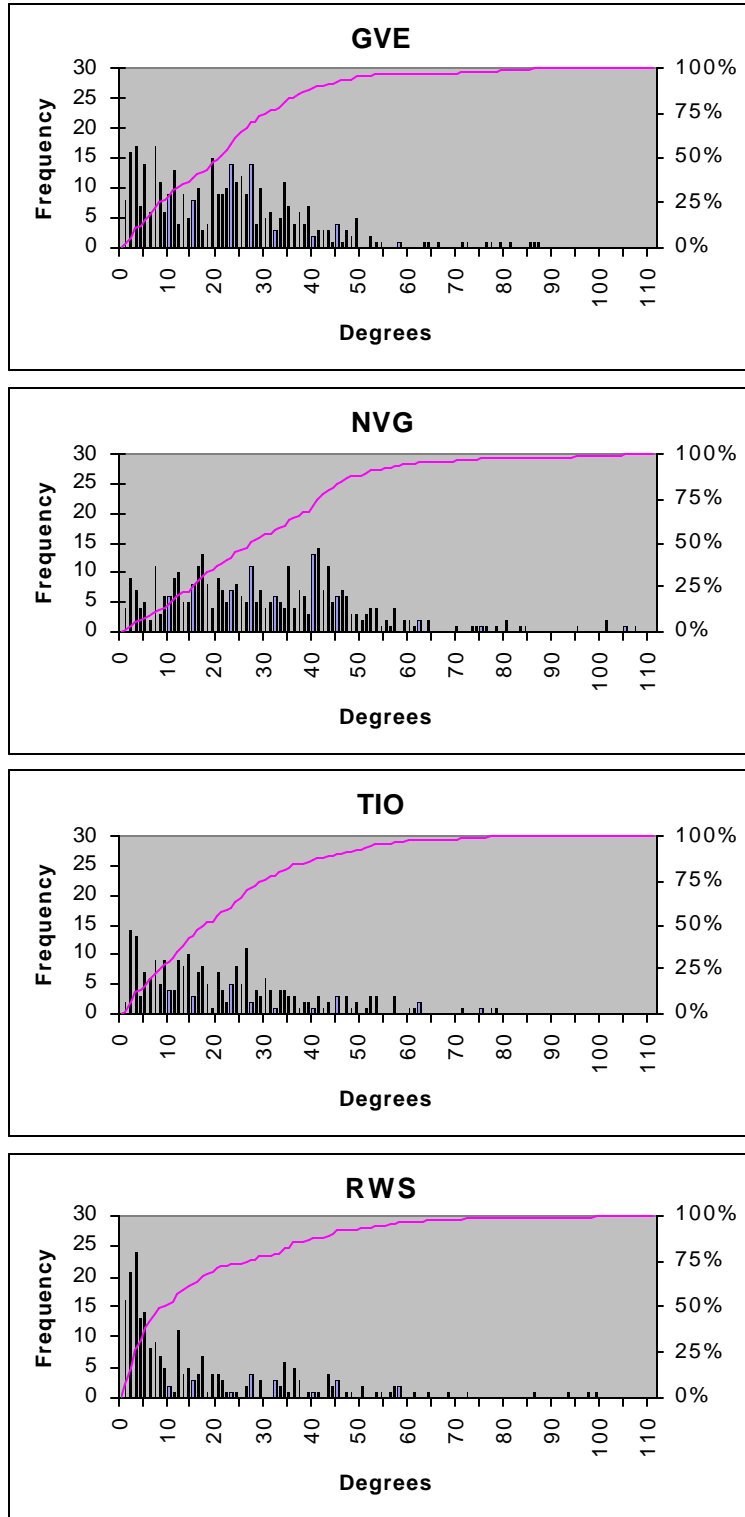


Figure 32. Subject #3 combined excursion histograms by flight type with cumulative frequency curve.

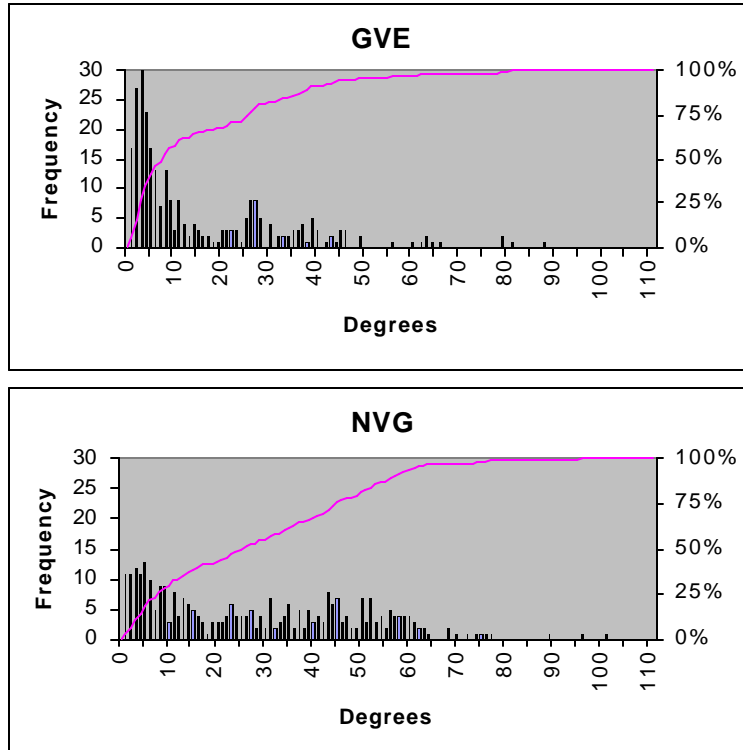


Figure 33. Subject #4 combined excursion histograms by flight type with cumulative frequency curve.

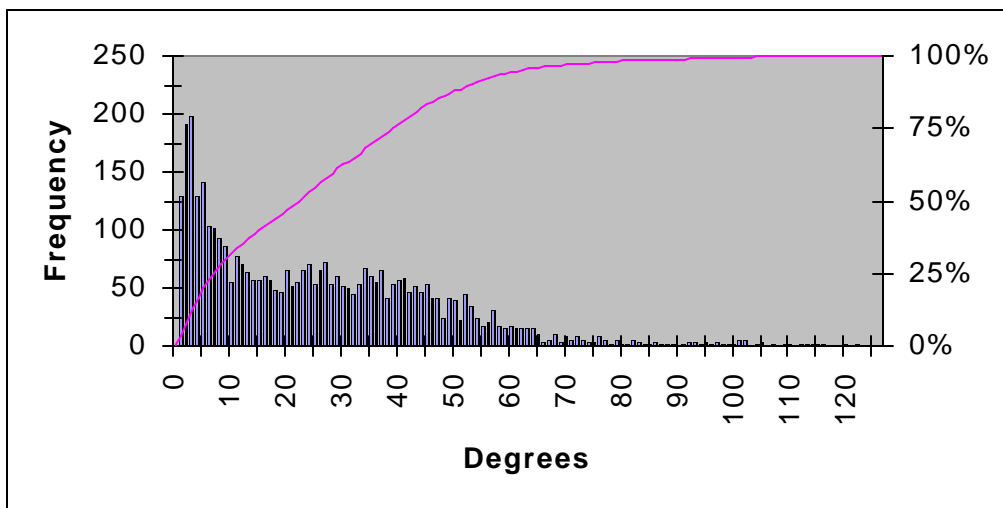


Figure 34. Overall excursion histogram for all subjects, for all visual environments.

Velocity distribution histograms

As with head position data, the use of histograms to represent the velocity distributions is a fundamental technique in the understanding of head motion. The histograms presented herein use 1-degree per sec ($^{\circ}/\text{sec}$) intervals. As with the position data, for the combinations of four subjects, four visual environments and two LOAs, there were 103 azimuth velocity distributions available for analysis. (See Table 6.)

Individual velocity distributions. Subject #1 has a total of 25 velocity histograms that represent the various combinations of LOA, run type and visual environment; subject #2 has 24 histograms; subject #3 has 34 histograms; and subject #4 has 20 histograms. The resulting individual velocity histograms, with cumulative frequency curves overlaid, are presented in Appendix K. Examining these individual histograms for general characteristics and trends for each subject and visual condition yields the following:

Subject #1. The individual GVE head position distributions for subject #1 (Figure K-1) present the following characteristics: a) Cumulative frequency curves become asymptotic at velocities equal to or greater than $110^{\circ}/\text{sec}$, and b) the beginning slopes of the cumulative frequency curves have a gradual rise implying that the frequency of the low velocity values are spread out over a larger range.

NVG head velocity distributions for subject #1 (Figure K-2) present the following characteristics: a) Cumulative frequency curves become asymptotic at velocities equal to or less than $100^{\circ}/\text{sec}$, and b) the beginning slopes of the cumulative frequency curves are even more gradual than for the GVE visual condition.

TIO head velocity distributions for subject #1 (Figure K-3) present the following characteristics: a) Cumulative frequency curves become asymptotic at velocities equal to or less than $20^{\circ}/\text{sec}$, and b) the beginning slopes of the cumulative frequency curves are much steeper than for the GVE and NVG visual conditions.

RWS head velocity distributions for subject #1 (Figure K-4) present the following characteristics: a) Cumulative frequency curves become asymptotic at velocities between $80-90^{\circ}/\text{sec}$, and b) the beginning slopes of the cumulative frequency curves are steeper than for the GVE and NVG visual conditions but not as steep as the TIO visual environment.

Subject #2. The GVE head velocity distributions for subject #2 (Figure K-5) present the following characteristics: a) Cumulative frequency curves become asymptotic at velocities equal to or greater than $110^{\circ}/\text{sec}$, and b) the beginning slopes of the cumulative frequency curves have a gradual rise implying that the frequency of the low velocity values are spread out over a larger range.

NVG head velocity distributions for subject #2 (Figure K-6) present the following characteristics: a) Cumulative frequency curves are not consistent and become

asymptotic at velocities between 95-140°/sec, and b) the beginning slopes of the cumulative frequency curves are not quite as gradual as the GVE visual condition.

TIO head velocity distributions for subject #2 (Figure K-7) present the following characteristics: a) Cumulative frequency curves are not consistent and become asymptotic at velocities between 55-105°/sec, and b) the beginning slopes of the cumulative frequency curves are steeper than the GVE and NVG visual conditions.

RWS head velocity distributions for subject #2 (Figure K-8) present the following characteristics: a) Cumulative frequency curves become asymptotic at velocities between 55-85°/sec, and b) the beginning slopes of the cumulative frequency curves are steeper than for the GVE, NVG, and TIO visual conditions with sharp transitions to a very gradual slope.

Subject #3. The GVE head velocity distributions for subject #3 (Figure K-9) present the following characteristics: a) Cumulative frequency curves are not consistent and become asymptotic at velocities between 50-95°/sec, and b) the beginning slopes of the cumulative frequency curves have a gradual rise implying that the frequency of the low velocity values are spread out over a larger range.

NVG head velocity distributions for subject #3 (Figure K-10) present the following characteristics: a) Cumulative frequency curves become asymptotic at velocities equal to or greater than 100°/sec, and b) the beginning slopes of the cumulative frequency curves are even more gradual than for the GVE visual condition.

TIO head velocity distributions for subject #3 (Figure K-11) present the following characteristics: a) Cumulative frequency curves become asymptotic at velocities equal to or less than 75°/sec, and b) the beginning slopes of the cumulative frequency curves are similar to the GVE curves, but are steeper than for NVG visual condition.

RWS head position distributions for subject #3 (Figure K-12) present the following characteristics: a) Cumulative frequency curves become asymptotic at velocities, on average, about 40-45°/sec with a few as high as 65°/sec, and b) the cumulative frequency curves have a steeper climb than for the subjects other three flight conditions.

Subject #4. The GVE head velocity distributions for subject #4 (Figure K-13) present the following characteristics: a) Cumulative frequency curves are not consistent and become asymptotic at velocities between 35-90°/sec, and b) the beginning slopes of the cumulative frequency curves have moderate steepness indicating a high frequency of lower velocities.

NVG head velocity distributions for subject #4 (Figure K-14) present the following characteristics: a) Cumulative frequency curves become asymptotic at velocities of 80°/sec or less except for a few as high as 120°/sec, and b) the beginning slopes of the cumulative frequency curves are more gradual than for the GVE visual condition.

Note: Head position data for subject #4 were not available for TIO and RWS visual environments.

Combined velocity histograms. As with the position data, it is argued that combined velocity histograms are more useful in understanding the general (average) nature of head velocities present in the shalom course flown in this study. Figures 35-38 present the combined velocity distributions by subject and visual environment. Note that head velocity data for subject #4 were available for only two visual environments, GVE and NVG. As with the individual distributions, these combined distributions can be examined visually for general characteristics and trends. The following observations are made:

Subject #1. The combined GVE head velocity distribution for subject #1 (Figure 35) present the following characteristics: a) The cumulative frequency curve becomes asymptotic near 135°/sec, and b) the 50-percent velocity value is 12°/sec.

The combined NVG head velocity distribution for subject #1(Figure 35) shows: a) The cumulative frequency curve becomes asymptotic at around 145°/sec, and b) the 50-percent velocity value is 14°/sec.

The combined TIO head velocity distribution for subject #1(Figure 35) shows: a) The cumulative frequency curve becomes asymptotic near 20°/sec, and b) the 50-percent velocity value is 3°/sec.

The combined RWS head velocity distribution for subject #1 (Figure 35) shows: a) the cumulative frequency curve becomes asymptotic near 110°/sec, b) the 50-percent velocity value is 6°/sec.

Subject #2. The combined GVE head velocity distribution for subject #2 (Figure 36) present the following characteristics: a) The cumulative frequency curve becomes asymptotic near 170°/sec, and b) the 50-percent velocity value is 12°/sec.

The combined NVG head velocity distribution for subject #2 (Figure 36) present the following characteristics: a) The cumulative frequency curve become asymptotic near 150°/sec, and b) the 50-percent velocity value is 13°/sec.

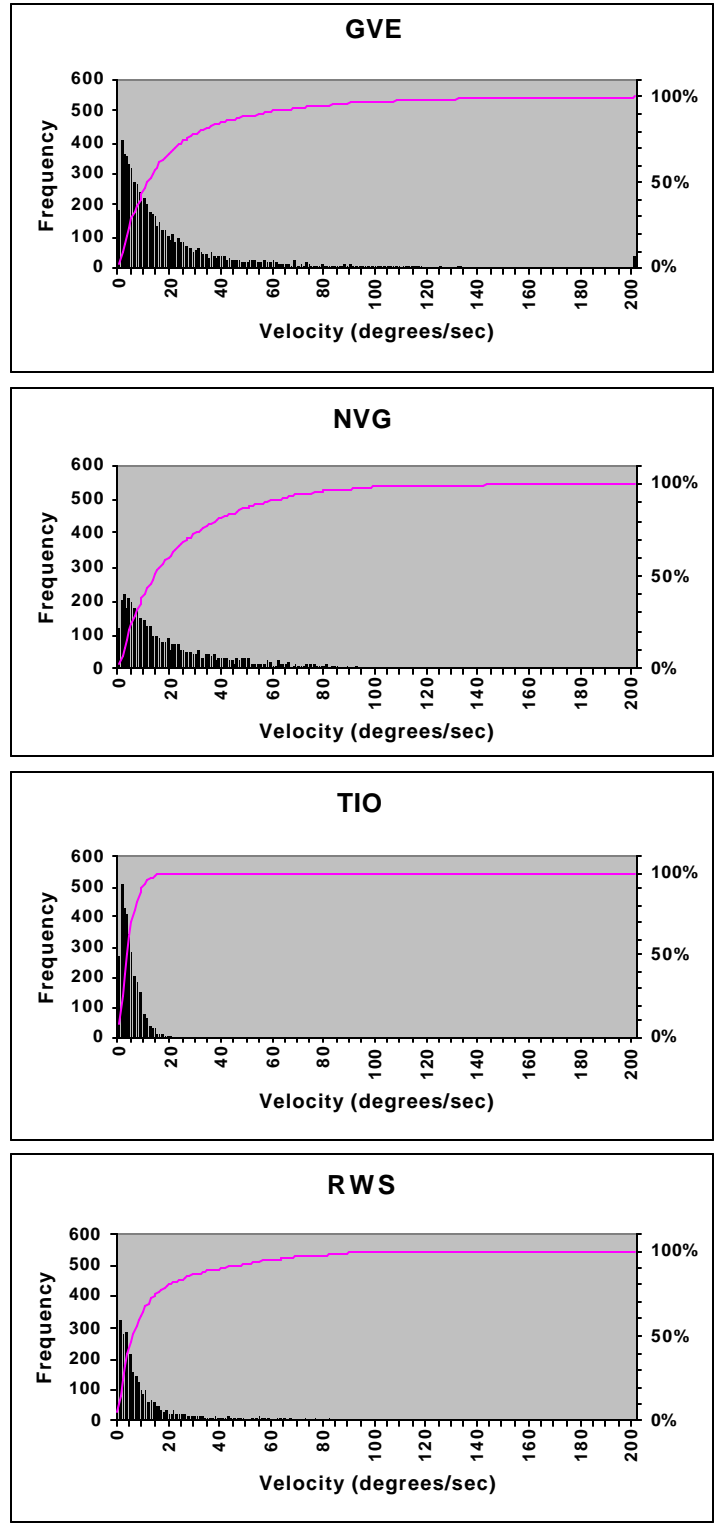


Figure 35. Combined velocity histograms for subject #1.

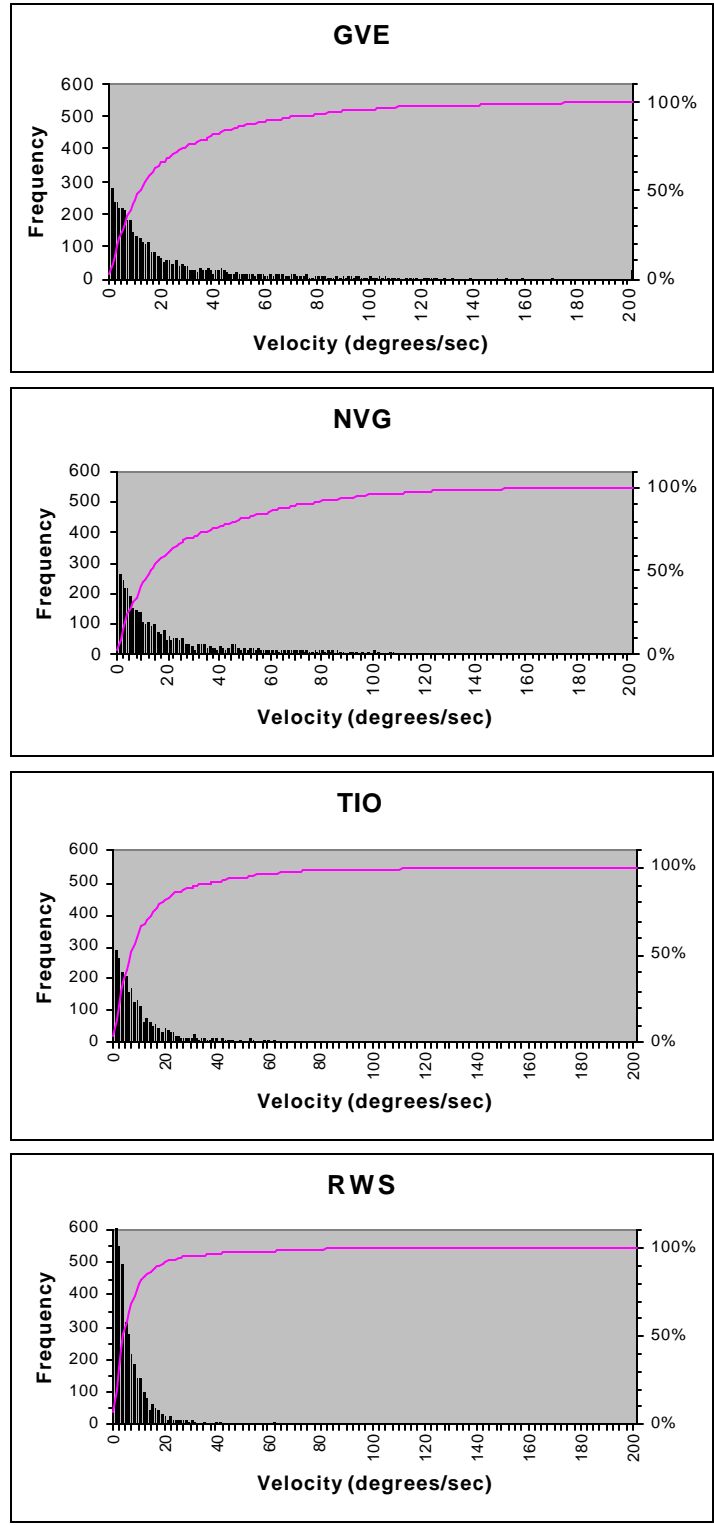


Figure 36. Combined velocity histograms for subject #2.

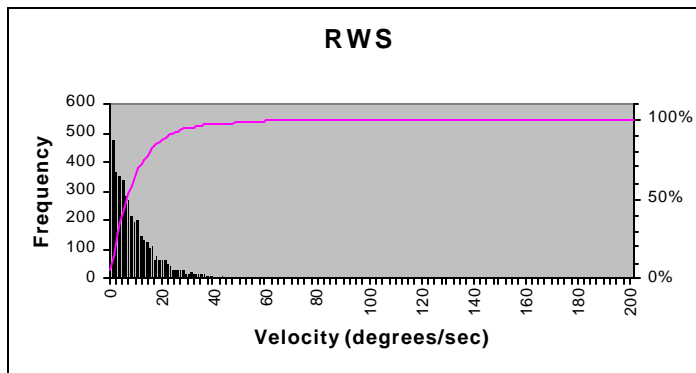
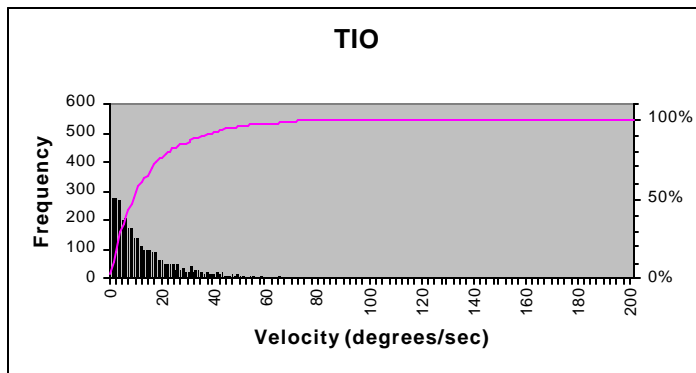
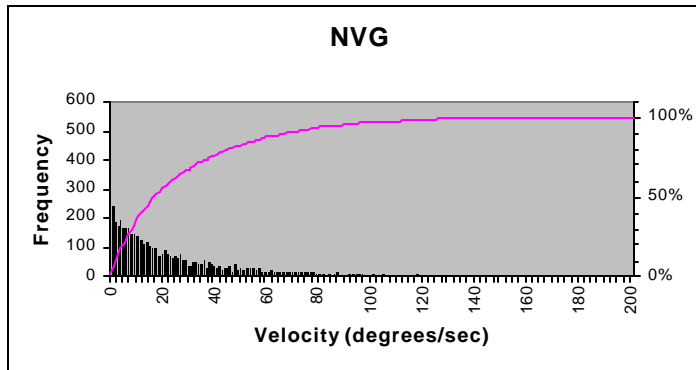
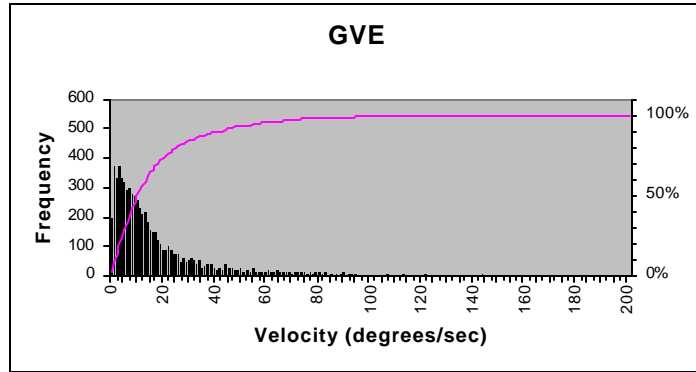


Figure 37. Combined velocity histograms for subject #3.

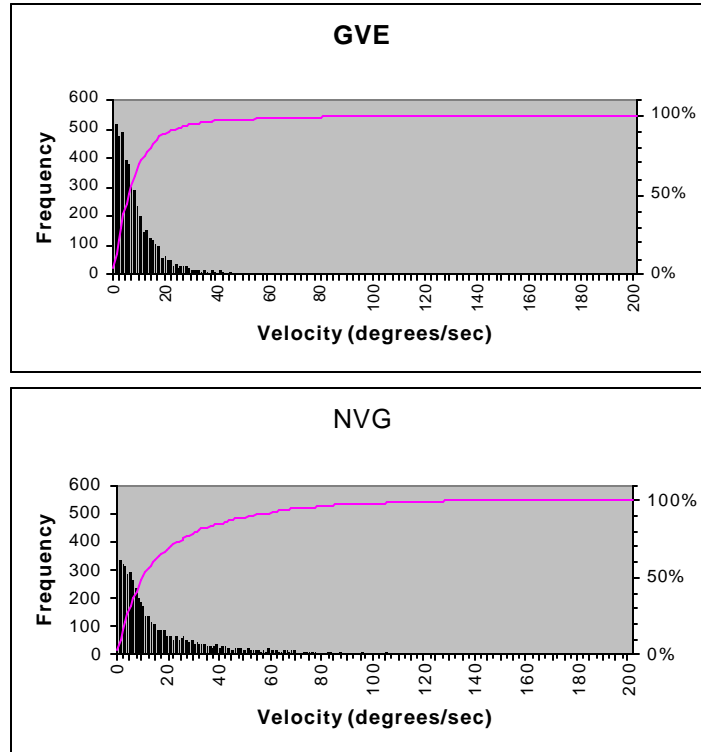


Figure 38. Combined velocity histograms for subject #4.

The combined TIO head velocity distribution for subject #2 (Figure 36) shows: a) The cumulative frequency curve becomes asymptotic near $110^{\circ}/\text{sec}$, and b) the 50-percent velocity value is $7^{\circ}/\text{sec}$.

The combined RWS head velocity distribution for subject #2 (Figure 36) shows: a) The cumulative frequency curve becomes asymptotic near $80^{\circ}/\text{sec}$, and b) the 50-percent velocity value is $4^{\circ}/\text{sec}$.

Subject #3. The combined GVE head velocity distribution for subject #3 (Figure 37) present the following characteristics: a) The cumulative frequency curve becomes asymptotic near $90^{\circ}/\text{sec}$, and b) the 50-percent velocity value is $11^{\circ}/\text{sec}$.

The combined NVG head velocity distribution for subject #3 (Figure 37) present the following characteristics: a) The cumulative frequency curve becomes asymptotic near $180^{\circ}/\text{sec}$, and b) the 50-percent velocity value is $17^{\circ}/\text{sec}$.

The combined TIO head velocity distribution for subject #3 (Figure 37) shows: a) The cumulative frequency curve becomes asymptotic near $110^{\circ}/\text{sec}$, and b) the 50-percent velocity value is $9^{\circ}/\text{sec}$.

The combined RWS head velocity distribution for subject #3 (Figure 37) shows: a) The cumulative frequency curve asymptotic near 105°/sec, and b) the 50-percent velocity value is 7°/sec.

Subject #4. The combined GVE head velocity distribution for subject #4 (Figure 38) present the following characteristics: a) The cumulative frequency becomes asymptotic at around 175°/sec, and b) the 50-percent velocity value is 6°/sec.

The combined NVG head velocity distribution for subject #4(Figure 38) present the following characteristics: a) The cumulative frequency curve becomes asymptotic at around 125°/sec, and b) the 50-percent velocity value is 10°/sec.

When the above observations are examined across subjects, the 50-percent velocity values range from 11-17 °/sec for the GVE and NVG visual conditions, and 3-10°/sec for the TIO and RWS visual conditions. In general, the asymptotic velocity values are greater for the GVE and NVG visual conditions, and the 50-percent velocities for the two HMD visual conditions (TIO and RWS) are approximately half of those values for the GVE an NVG velocities.

As with excursions, it was useful to construct a histogram that represents all velocities exhibited by all pilots during all runs (Figure 39). This overall distribution has the following statistics: Mean of 17°/sec, median of 9°/sec, standard deviation of 24°/sec, and IQR of 17°/sec. An overlaid cumulative frequency curve indicates that 50% of all velocities were 9°/sec or less. The 95% and 99% velocity values were 66°/sec and 121°/sec, respectively. The largest (maximum) velocity exhibited by any pilot during any run was 362°/sec.

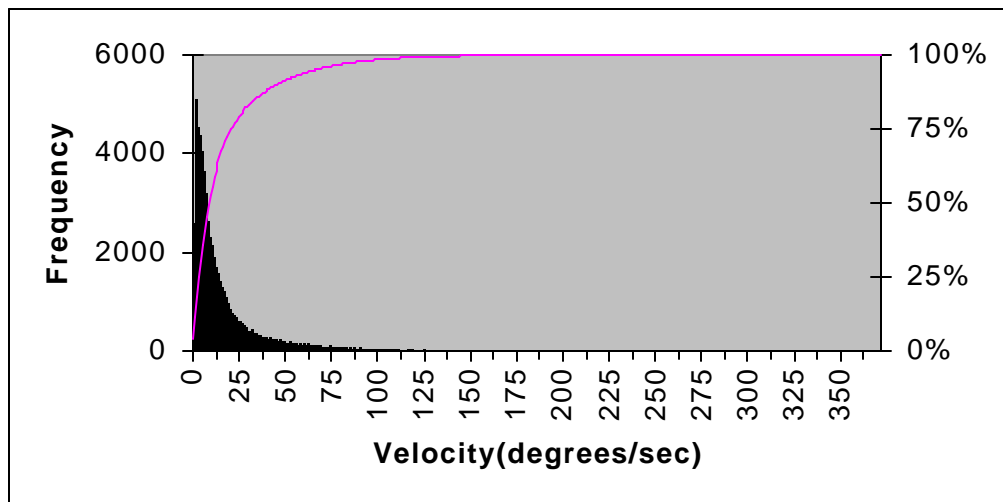


Figure 39. Overall velocity histogram for all subjects, for all visual environments.

Velocity distribution statistics

While distribution shape provides a basic understanding of the ongoing head motion, the semi-quantitative nature of distribution histograms does not allow for comprehensive comparison. For this reason, distributions often are described further by the distribution's moments and other additional statistics. For the velocity distributions presented herein, the maximum, mean, median, standard deviation, and IQR have been calculated.

Summary individual and combined distribution moments and statistics tables for all subjects, grouped by visual environment, are provided in Appendix I. However, following the previous arguments that comparisons can be based on the combined distributions, a summary of the calculated distribution moments and statistics by subject and visual environment for the combined distributions only is presented in Table 14. Provided in parentheses beside each value is the within subject rank of that value for the selected statistic.

Table 14.

Combined azimuth velocity summary by subject and visual environment.

Time expressed in seconds; other dimensional statistics expressed in °/sec, ranks within subject given in ().

Subject	Visual Environment	Time	Max	Mean	Median	S.D.	IQR
1	GVE	690.6	350	21.8(2)	12(2)	30.5(1)	5 to 26(2)
1	NVG	467.2	194	23.0(1)	14(1)	24.8(2)	6 to 32(1)
1	TIO	315.8	45	4.3(4)	3(4)	3.9(4)	2 to 6(4)
1	RWS	328.2	141	14.3(3)	6(3)	20.3(3)	3 to 16(3)
2	GVE	480.4	362	24.8(2)	12(2)	34.4(1)	5 to 30(2)
2	NVG	452.0	205	26.5(1)	13(1)	31.9(2)	5 to 37(1)
2	TIO	320.7	113	13.0(3)	7(3)	16.6(3)	3 to 16(3)
2	RWS	465.8	143	8.4(4)	4(4)	13.3(4)	2 to 9(4)
3	GVE	677.7	191	17.3(2)	11(2)	19.8(2)	5 to 22(2)
3	NVG	525.1	247	27.3(1)	17(1)	28.8(1)	7 to 38(1)
3	TIO	414.4	127	16.0(3)	9(3)	16.0(3)	4 to 19(3)
3	RWS	497.8	116	11.8(4)	7(4)	10.3(4)	3 to 14(4)
4	GVE	582.0	215	10.5(2)	6(2)	15.3(2)	3 to 12(2)
4	NVG	557.3	175	19.7(1)	10(1)	24.2(1)	4 to 26(1)
4	TIO	None					
4	RWS	None					

An examination of Appendix I and Table 14 lead to the identification of a number of characteristics and trends. For all subjects, the mean and median velocity values and the IQR range of velocity values were greatest for the NVG visual environment. The GVE visual condition have the second greatest values for these statistics. In general, the GVE and NVG visual conditions exhibited higher standard deviation values than the TIO and

RWS visual conditions. With the exception of subject #3, the GVE condition exhibited higher maximum velocity values. However, these maximum velocities ranged greatly from 191°/sec to 362°/sec.

Graphical comparison

Graphical comparisons are based on a 5-number summary box-plot employed in the SPSS for Windows™ statistical software. The box-plot technique provides a visual summary of a data set by emphasizing a select set of statistic values, e.g., median, quartiles, and IQR. Box-plots for combined azimuth velocity distributions for all subjects are presented in Figures 40-43. Individual box-plots for all subjects by visual environment are presented in Appendix M. It should also be noted that extreme values have been removed to provide a less cluttered graphical representation.

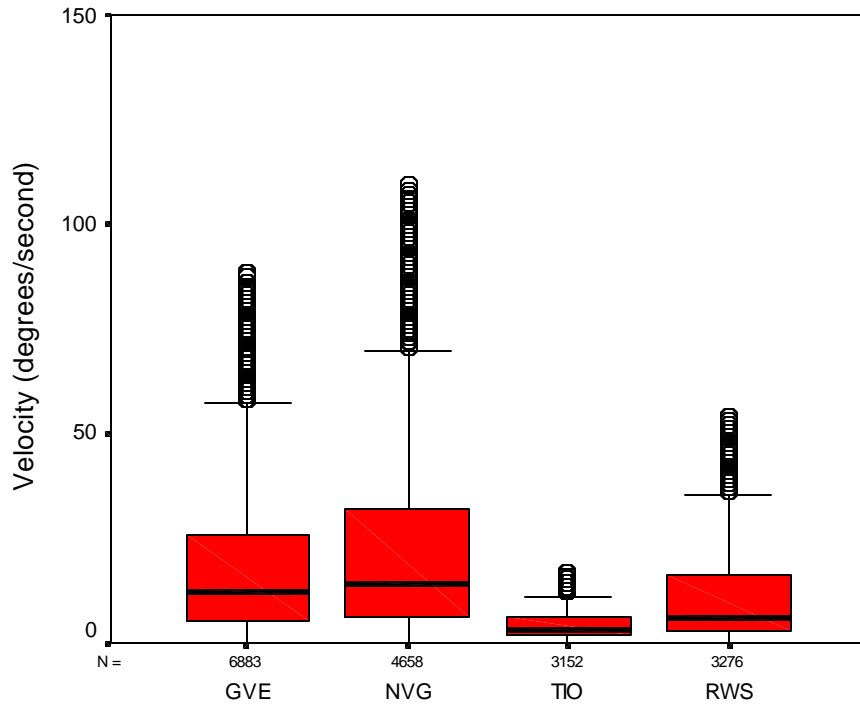
From the box-plots for subject #1 in Figure 40, the following characteristics and trends can be observed: a) The GVE and NVG box-plots have similar 1st and 2nd quartiles and medians, but there is an increase in the 3rd and 4th quartile ranges for the NVG visual condition, b) all TIO quartiles are greatly reduced in range in comparison to all of the other visual environments, and c) the RWS quartiles are smaller than those of GVE and NVG but are larger than TIO.

From the box-plots for subject #2 in Figure 41, the following characteristics and trends can be observed: a) GVE and NVG again have similar 1st and 2nd quartiles and medians, and NVG still has the larger 3rd and 4th quartiles and b) the TIO combined box-plot has a larger quartile range and median than RWS.

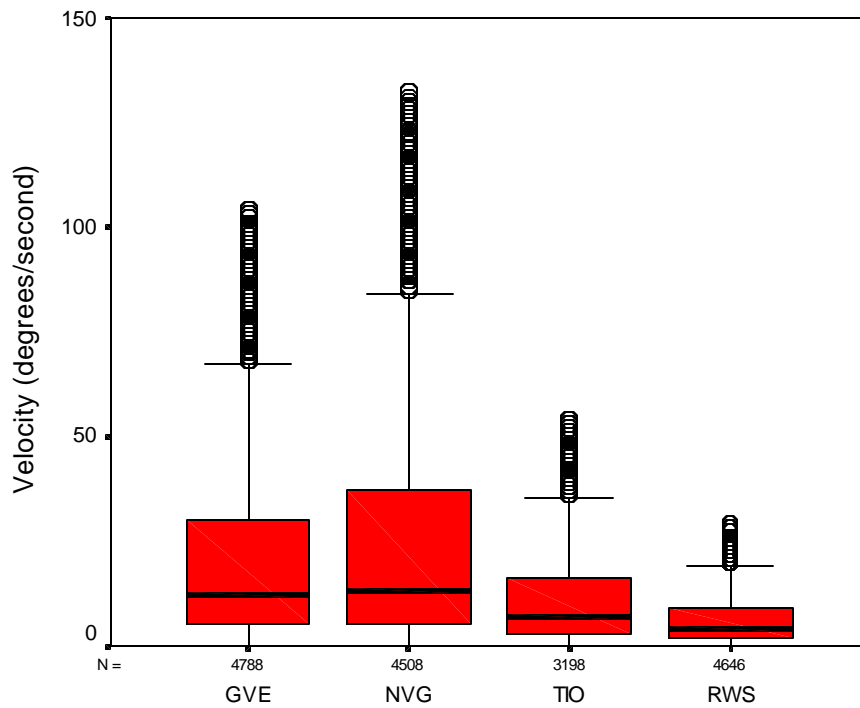
From the box-plots for subject #3 in Figure 42, the following characteristics and trends can be construed: a) NVG has the largest quartile ranges of all visual conditions and b) RWS has decreased quartile ranges and median when compared the other visual environments.

From the box-plots for subject #4 in Figure 43, the following characteristics and trends can be construed: a) NVG has the larger quartile ranges and median as compared to GVE.

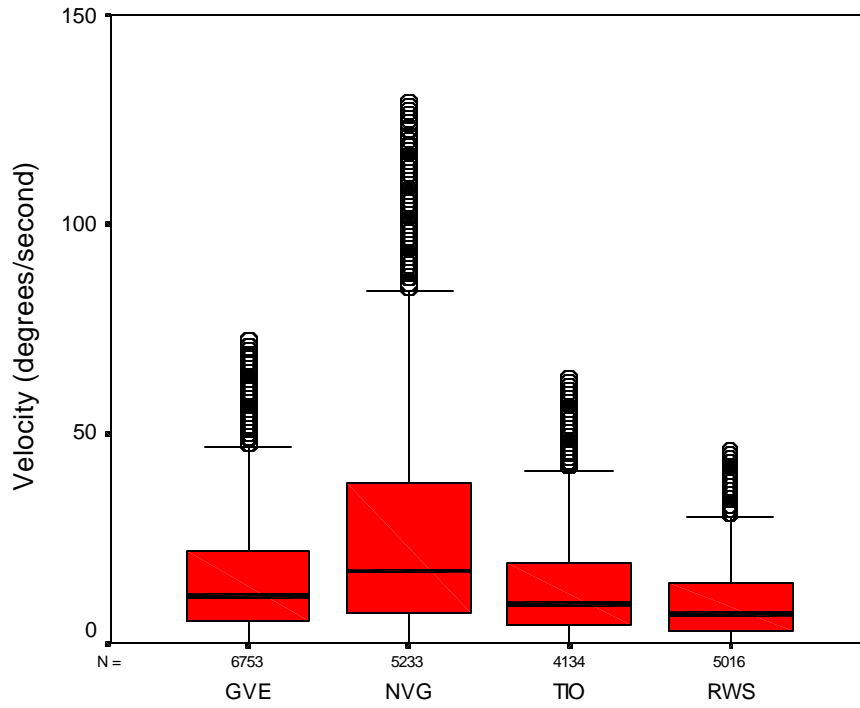
Across subjects, the NVG visual condition has the greatest velocity range, the greatest IQR, and the highest median velocity values. Box-plots for GVE and NVG show similarities, as do those for TIO and RWS. As first identified in the combined distribution histograms, lower velocity values are more frequent, causing the quartile ranges (1st - 4th) to increase.



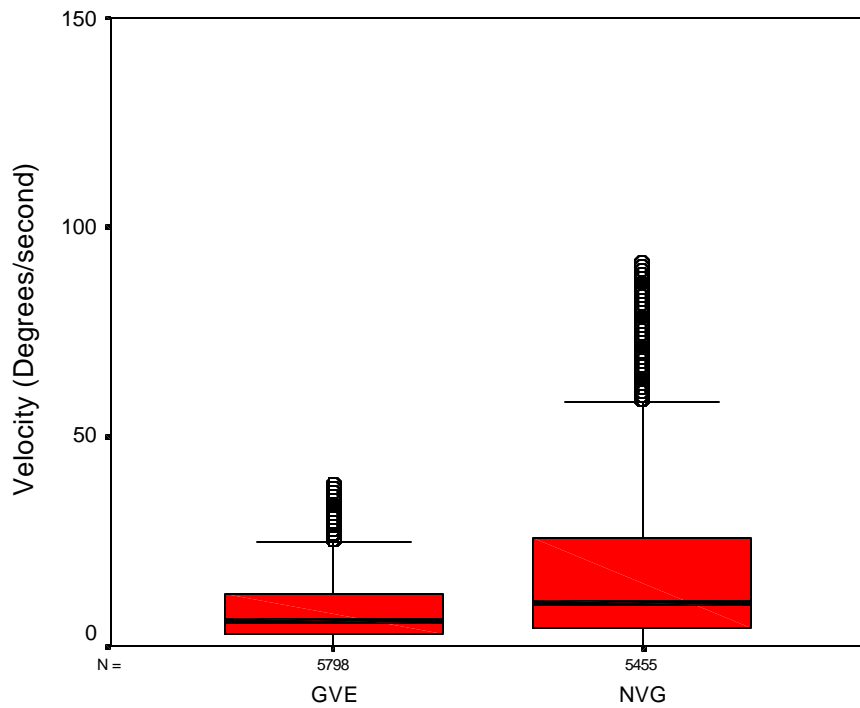
*Note: Extreme values are excluded to allow for better visual representation.
 Figure 40. Combined azimuth velocity box-plots for subject #1.



*Note: Extreme values are excluded to allow for better visual representation.
 Figure 41. Combined azimuth velocity box-plots for subject #2.



*Note: Extreme values are excluded to allow for better visual representation.
 Figure 42. Combined azimuth velocity box-plots for subject #3.



*Note: Extreme values are excluded to allow for better visual representation.
 Figure 43. Combined azimuth velocity box-plots for subject #4.

To investigate the trend in ranking amongst the various velocity statistics, Tables 15 and 16 present the Spearman rank-correlation coefficients for two measures of central tendency, mean and median, and two measures of dispersion, standard deviation and IQR. While remembering that correlation coefficients involving subject #4 should be given less weight because only GVE and NVG data were available, the Spearman rank-correlation tests showed a strong association between the visual environment and the mean, median and IQR. The association was much less strong for the standard deviation statistic.

Table 15.
Spearman rank-correlation coefficients for velocity mean and median.

Mean					Median				
	#1	#2	#3	#4		#1	#2	#3	#4
#1		+0.80	+0.80	+1	#1		+0.80	+0.80	+1
#2			+1	+1	#2			+1	+1
#3				+1	#3				+1
#4					#4				

Table 16.
Spearman rank-correlation coefficients for velocity standard deviation and IQR.

S.D.					IQR				
	#1	#2	#3	#4		#1	#2	#3	#4
#1		+0.80	+0.60	+1	#1		+0.80	+0.80	+1
#2			+0.80	-1	#2			+1	+1
#3				+1	#3				+1
#4					#4				

Discussion

Verona et al. (1986) identified two major factors that influence head motion characteristics in rotary-wing flight. The first factor is aircraft configuration, which encompasses crewstation design, seating configuration (tandem vs. side-by-side), seat adjustment (fore/aft and up/down), and transparency (window) locations. The second factor is the flight task/environment, which encompasses the flight maneuver, terrain/route familiarity, and threat level. The introduction of HMDs (to include NVGs) into the cockpit with their reduced FOVs is an additional element of the flight task/environment factor.

For the data analyzed herein, the aircraft had side-by-side seating and the subject was in the left seat; 0° was associated with the direction directly in front of subject (not along the centerline of the aircraft): The two-part forward transparency subtended an angle of approximately -40° (left) to +60° (right) with respect to the subject (depending on seat adjustment) with a narrow (~4°) obstructing center rail at approximately +20° with respect to the subject pilot: The right forward transparency subtended an angle between approximately +25° to +60°: There were two side-door windows subtending approximately -75° to -40° on the left and +65° to +80° on the right (but blocked by the

safety pilot) (See Figure 9): The flight course was well known to the subject, and overall, the slalom maneuver task was relatively benign.

Considering the preceding discussion, several characteristics of the resulting head motion for the data herein might be predicted. First, the slalom maneuver over a familiar course with a zero threat level was not a very demanding flight task requiring large head movements. Except for standard safety reasons, the subject might be expected to look primarily forward. However, it would be expected that the use of HMDs would result in an increase in the range of head motion in an attempt to compensate for the reduced HMD FOV. Another predicted characteristic is the effect of the subject being seated in the left seat of a side-by-side aircraft with the added vision blockage by the right-seated pilot (for GVE and NVG). The subject had the advantage of (unmeasured) eye movement out of the left side, but was required to rely on head motion to view right due to presence of safety pilot.

The impact on head motion due to the reduced FOVs for NVG, TIO and RWS visual environments is worth exploring further. When the 47° NVGs were worn, the pilot was required to exercise a head movement in order to see an object more than approximately 24° to the left or right of his current line of sight. For the 53° HMD used for TIO and RWS, additional head movement must have occurred in order for the pilot to see an object more than approximately 27° from his current line of sight. For unaided, daytime flight (GVE), the human eye has an instantaneous monocular FOV of roughly 120° (V) by 150° (H). When both eyes are considered, the overall binocular FOV measures approximately 120° (V) by 200° (H) (Zucherman, 1954). Humans have the option of both eye and head rotation to assist in viewing. However, in a static scenario, it is generally accepted that humans will use eye movements to view objects up to approximately 15° beyond the current line of sight direction, beyond which head movement will occur (Bahill, Adler and Stark, 1975). It would be reasonable to predict that between the NVG, TIO and RWS HMD visual environments, that NVG, with the smallest instantaneous FOV, would have the greatest extent of head motion. When GVE is considered, the 15° value must not be interpreted as a value beyond which one "must" invoke head movement. While NVG, TIO and RWS visual environments force head movements to look beyond their respective FOVs, GVE allows for peripheral vision and head/eye combination movements, precluding forced head movement in many situations. As a result, speculation on head movement for GVE is difficult. In fact, it is more logical to use head motion in the GVE visual environment as a baseline to which head motion in the NVG, TIO, and RWS visual environments are compared.

The GVE visual environment provides the greatest FOV, that of the human visual system, with only small losses due to the presence of the subjects flight helmet. The NVG visual environment results in the additional head supported weight of the NVG system, produces a forward offset center of gravity (CG), and reduces the FOV to 47°. These factors are opposite in their anticipated impact on head motion. The additional head-supported weight and CG offset would be expected to reduce both range of head positions and velocities through the impact of fatigue and moment of inertia. The two HMD visual environments, TIO and RWS, also are influenced by additional head-

supported weight and offset CG. The FOV for these two environments, at 53°, is reduced with respect to the GVE environment but slightly larger than the 47° NVG environment. Head motion for these two environments is further affected by the inherent delays associated with the head tracking system and the sensor/turret gimbal.

One final factor, and initial driver for this study, is the possible influence of motion sickness on head motion. The actual HMD design used in this study had look-under, look-around capability. However, this capability was offset by the use of the SDVE system, restricting external visual input to that solely provided by the FLIR imagery (and symbology for RWS). This produced a near full-immersion system that has been linked to the phenomenon of “cybersickness.” Cybersickness is similar to simulator sickness in that the symptoms of motion sickness (e.g., nausea, sweating, pallor, etc.) can result from lack of correlation between visual and vestibular sensory inputs. Of course, in this study both inputs were present. However, imagery presented by HMDs has a measurable delay in its presentation due to lag times and update rates. This may manifest itself as cybersickness (Melzer and Moffitt, 1997; Rash (Ed.), 1999).

Summary

Position analyses

With regard to head position data, one of the first findings concerned the variability of the data within and between subjects. While the combined distributions were emphasized, an examination of each of the individual 103 position distributions revealed considerable variability, both within and between subjects. This is why the Chi-square analysis above was not very meaningful. This analysis, which compared the distributions for the four visual environments within each subject, found all of the position distributions to be statistically different from each other. This was an expected result and, while certainly true, should not be assigned any useful importance.

What was found to be meaningful is the ranked relationship of the dispersion statistics for the four visual environments, particularly for the IQR. For all subjects, the IQR for NVG was larger than for the other three visual environments. Likewise, the IQR for GVE was always the second largest. The IQR values for TIO and RWS, the most closely related visual environments, vie for third and fourth ranking. Based on this finding, the IQR appears to be the most valuable statistic for comparing head position distributions.

Several additional, but less significant, characteristics and trends in the head position data were identified:

- A strong central mode was generally present. This was an expected finding since pilots, like the operator of any other vehicle, tend to look in the direction of movement.
- The means and medians support the usually strong central direction mode.

- All kurtosis values are negative, between 0.0 and -1.1, implying the distributions deviate, to a degree, from normality.
- There were no extreme position values for any distribution. This was not surprising, since the threat level was insignificant.
- Range and standard deviation were not as strong a discriminator for the distributions as the IQR statistic since they are more easily influenced by the maximum values (left and right).
- The consistent presence of a secondary mode at 45° correlated highly with the location of the center of the right forward transparency. Less understandable was the presence of this mode for TIO and RWS distributions, since the visual sensor for these visual environments was located on the nose of the aircraft and was unaffected by the obstruction of the center and side rails.
- The spread of the second quartile (left side) (Figures 21-24) was consistently smaller than for the third quartile (right side). This may have been a result of the subject's position in the left seat of the side-by-side seating allowing the use of eye movement and peripheral vision on the left side, in contrast to the obstructed view on the right side due to the safety pilot in the right seat.
- Outliers were present on the left (negative) side for the TIO and RWS visual environments.

Rate analyses

With regard to rate of change in head position across the four visual environments, three parameters were investigated: reversal rates, excursion distributions, and velocities. Reversal rates, which attempted to quantify the number of times pilots reversed head motion direction, failed to show significant differences between the visual environments. However, in general, there was a trend for higher reversal rates in the GVE and NVG (non-HMD) visual environments; and, the RWS mean reversal rate was always the least.

Excursions were used as an additional measure of the angular rotation of the head by the pilots between reversal points, expressed in degrees. Histograms of excursion sizes showed angular movements as large as 122°. However, none of the distribution histograms, for any of the pilots, for any of the visual environments, showed any high degree of similarities. While some pilots had relatively large frequencies of smaller head excursions (<10°), other pilots had higher frequencies of moderate-sized head excursions (typically 20° to 40°). The only consistent, although weak, trend in the excursion distributions was that the NVG excursions were more evenly distributed across the range of excursion values. An analysis of all excursions collapsed across all runs, indicated that 50% of all excursions were less than 22° in size; 95% were less than 62°.

Velocities exhibited for the four visual environments showed greater differences than the other two rate parameters. Velocities were consistently greater for the NVG environment. This was true for the mean, median, and IQR velocity statistics. The values of these statistics also, in general, were much higher for the GVE and NVG

environments than for the two non-HMD environments (TIO and RWS). For three of the four subjects, the largest velocity values were exhibited during GVE runs.

An analysis of all velocity values collapsed across all runs, indicated that 50% of all velocities were less than $9^\circ/\text{sec}$; 95% were less than $66^\circ/\text{sec}$. The largest velocity exhibited by any pilot during any run was $362^\circ/\text{sec}$.

The Spearman rank-correlation tests showed a strong association between the visual environment and the mean, median and IQR. Therefore, either of these statistics could be used for discriminating between visual environments.

As a final part of the summary, it is worthwhile to compare the results of this current investigation of head motion with the previous Verona et al. study (1986). This comparison, while valid only for the GVE environment, would be based on the only other head motion database available that represents operational, military, rotary-wing flight. In Verona et al. (1986), 6 male U.S. Army aviators flew a modified UH-1M Huey helicopter over a circular 15-mile contour course while wearing a prototype AH-64 Apache helmet, which allowed measurement of head position. In both studies, the aircraft had side-by-side seating with the subject pilot in the left seat. The most significant difference between the two studies was the level of aggression. In the study reported herein, the subjects were flying a well-known flight pattern in a no-threat environment. In Verona et al. (1986), subjects were instructed to look for a threat aircraft that would appear somewhere in their FOV during the flight.

For Verona et al. (1986) study, the combined azimuth position and velocity histograms have been presented previously in Figures 3 and 5, respectively; azimuth position and velocity summary statistics were presented in Tables 2 and 3, respectively.

To facilitate a comparison between the two studies, Figures 44 and 45 present GVE azimuth position and velocity histograms, respectively, for combined for all subjects, for the current study. Due to the less demanding nature of the flights in the current study, it is reasonable to expect less extreme head positions and lower velocities.

In Verona et al. (1986), the combined head positions ranged from approximately -93° (left) to $+90^\circ$ (right), for a range of 183° , and exhibited a positive mean and median. In the current study, the combined head positions were significantly reduced in comparison, ranging from approximately -71° (left) to $+66^\circ$ (right), for a range of 137° , also with the overall mean and median positive but not as high in value (Figure 44). Further comparison of the shapes of the combined azimuth position histograms in Figures 3 and 44 shows several similarities. These include a clustering of head positions near 0° azimuth (directly in front of the pilot) and the presence of secondary mode(s) - near 35° for the Verona et al. (1986) data and (weakly) at 25° and 45° for the current data. It is speculated that the modes are associated with obstructions presented by windscreen posts.

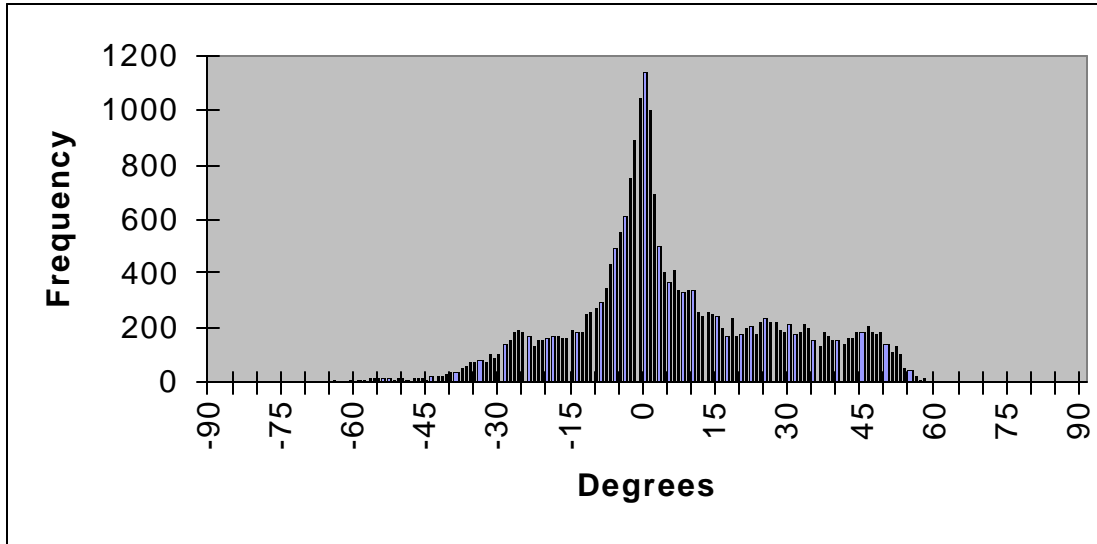


Figure 44. Frequency histogram for current study GVE azimuth position combined for all subjects.

For velocity comparison, Verona et al. (1986) (Figure 5) found that 50% of the combined azimuth velocities were less than $32.5^{\circ}/\text{sec}$; 90% were less than $80^{\circ}/\text{sec}$; and, while no maximum velocity was reported, the cumulative frequency curve (Figure 7) became asymptotic at $200^{\circ}/\text{sec}$. In the current study (Figure 45), the median (50%) velocity for GVE was significantly slower at $9^{\circ}/\text{sec}$; 90% were less than $45^{\circ}/\text{sec}$; and becomes asymptotic at $125^{\circ}/\text{sec}$ with a maximum velocity of $362^{\circ}/\text{sec}$. As was expected, all compared velocity figures-of-merit were lower for the current study with the less demanding flight profiles.

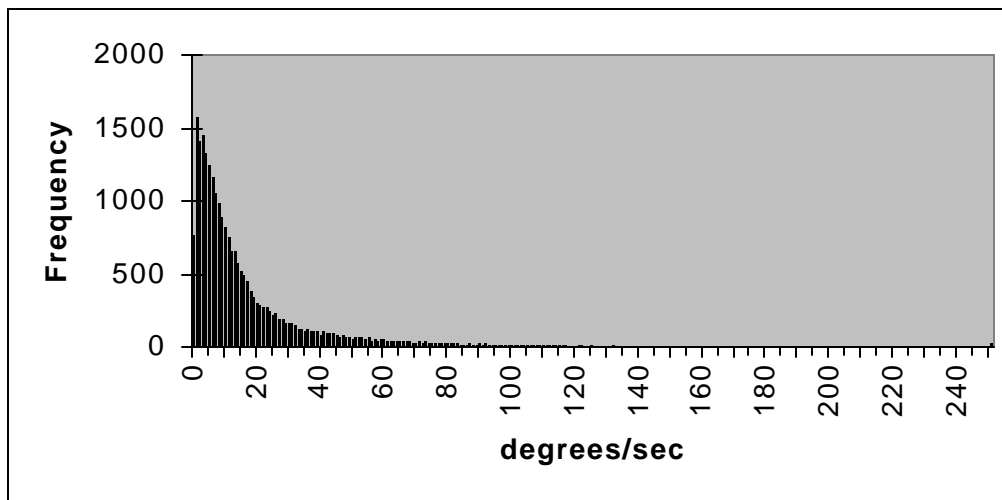


Figure 45. Frequency histogram for current study GVE azimuth velocity combined for all subjects.

Conclusions

This investigation had two objectives. The first was to expand the understanding of the head motion of (Army) pilots in an operational rotary-wing environment, especially while wearing various HMD configurations. The second objective was to identify which characteristics of head motion position and velocity data could be used to differentiate between head motion distributions (e.g., different visual flight environments).

The first objective was met via the construction of frequency histograms for the measured head positions, excursions, and velocities for four different visual flight conditions, i.e., GVE, NVG, TIO, and RWS. These distributions were defined by the calculation of their moments (i.e., mean, standard deviation, skewness, and kurtosis) as well as additional statistics (e.g., minimum, maximum, median, IQR, etc).

The position distributions showed strong, but expected, central modes indicating considerable time spent looking forward. While head position distributions were not identical in shape across visual environments, there was considerable equality in the ranges of head position. When all position distributions were combined, the overall extreme position values were -71° (left) and $+66^{\circ}$ (right) for a total range of 137° . When the spread of head position values was examined by visual environment, the NVG environment produced the greatest IQR for each subject, followed by the GVE environment.

The maximum velocity exhibited by any pilot for any visual environment was $362^{\circ}/\text{sec}$. For all velocity distributions combined, 50% of all velocities were $9^{\circ}/\text{sec}$ or less; 90% were $45^{\circ}/\text{sec}$ or less; and over 99% of all velocities were less than $125^{\circ}/\text{sec}$. When velocity distributions were compared by visual environment, the NVG environment consistently produced the largest mean and median velocities and the greatest spread in velocities, as measured by the IQR.

The major thread throughout these analyses was that the pilots exhibited greatest head motion for the NVG environment. The two HMD configurations (TIO and RWS) were very similar in exhibited head motion, not indicating any significant differences between the TIO FLIR imagery alone and the RWS FLIR imagery plus symbology.

The second objective was achieved by the finding of the IQR as the most valid statistic for differentiating between head position distributions; and, the finding of the mean, median, and IQR as the most valid statistics for differentiating between head velocity distributions.

References

- Allen, J. H., and Webb, R. C. 1983. Helmet mounted display feasibility model. Orlando, FL: Naval Training Equipment Center. NAVTRAEQUIPCEN IH-338.
- Azuma, R., and Bishop, G. 1995. A frequency-domain analysis of head-motion prediction. Computer Graphics Proceedings, SIGGRAPH 95, Los Angeles, CA, August 6-11 401-408.
- Bahill, A. T., Adler, D., and Stark, L. 1975. Most naturally occurring human saccades have magnitudes of 15 degrees or less. Investigative Ophthalmology, June, Vol. 14/6, 468-469.
- Bloch, S. C. 2000. Excel for engineers and scientists. New York: John Wiley and Sons. 69-74.
- Borah, J. 1989. Helmet mounted eye tracking for virtual panoramic display systems. Vol. II: Eye tracker specification and design approach. Wright Patterson Air Force Base, OH: Armstrong Aerospace Medical Research Laboratory. AAMRL-TR-89-019.
- Borah, J. 1998. Technology and application of head based control. Proceedings of Research and Technology Organization, Lecture Series 215, Alternative Control Technologies: Human Factors Issues, RTO-EN-3, 6-1 to 6-12.
- Cameron, A. A., Trythall, S., and Barton, A. M. 1995. Helmet trackers – The future. Helmet- and Head-Mounted Displays and Symbology Design Requirements II, Proceedings of SPIE, Vol. 2465, 281-295.
- Crowley, J. S. 1998. Simulating a degraded visual environment in the Lynx helicopter. Farnborough: DERA. DERA Report No. DERA/CHS/PP5/CR9780005/1.0.
- Curtis, W., and Sowizral, H. 1994. A note on dynamics of human head motions and on predictive filtering of head-set orientations. SPIE Proceedings: Telemanipulator and telepresence technologies, vol. 2351. Boston, MA. 23-58.
- Durlach, N. J. and Mavor, A. S. 1995. Virtual reality scientific and technological challenges. Washington D.C., National Academy Press 188-204.
- Glanville, A. D., and Kreezer, G. 1937. The maximum amplitude and velocity of joint movements in normal male human adults. Human Biology, 9: 197
- Gauthier, G. M., Martin, B. J., and Stark, L. W. 1986. Adapted head- and eye-movement responses to head inertia. Aviation, Space, and Environmental Medicine. 57:336-42.
- Hays, W. L. 1963. Statistics for psychologists. NY: Holt, Rinhart and Winston.

- Haywood, W. J., Jr. 1975. Advanced helmet mounted sight study program. Bedford, MA: Raytheon Co. AMRL-TR-73-10.
- Hertzberg, H. T. E. 1972. Human anthropology. In VanCott, H. P. and Kinkade, R. G. (Eds). Human engineering guide to equipment design. Washington D.C.: American Institutes for Research.
- Kocian, D. F., and Task, H. L. 1995 “Visually coupled systems hardware and the human interface” In Barfield, W., and Furness, T. A., (Eds) Virtual environments and advanced interface design. New York: Oxford University Press.
- Melzer, J. E., and Moffitt, K. 1997. Head mounted displays: Designing for the user. New York: McGraw Hill.
- Nicholson, R. M. 1965. The feasibility of a helmet-mounted sight as a controlled device. Minneapolis, MN: Honeywell Inc. HD-55B-53.
- Phillips, C. A., and Petrofsky, J. S. 1983. Neck muscle loading and fatigue: Systematic variation of headgear weight center-of-gravity. Aviation, space, and environmental medicine. 54(10):901-905.
- Polhemus, W. L. 1976. An advanced helmet mounted sight (AHMS) system, November 71 – April 73. Burlington, VT: Polhemus Navigation Sciences, Inc. AMRL-TR-73-47.
- Rash, C. E. Editor. 1999. Helmet-mounted display: Design issues for rotary-wing aircraft. Fort Rucker, AL: U. S. Army Aeromedical Research Laboratory.
- Robinson, R. M. , and Wetzel, P. A. 1989. Eye tracker development in the fiber optic helmet mounted display. Helmet-Mounted Displays, Proceedings of SPIE Vol. 1116, 102-108.
- Sherk, H. H. 1989. Physiology and biomechanics. In H. H. Sherk, E. J. Dunn, F. J. Eismont, J. W. Fielding, D. M. Long, K. Ono, L. Penning, R. Raynor (Eds.), The Cervical Spine. Philadelphia, PA: J. B. Lippincott.
- Szoboszlay, Z., Haworth, L., Reynolds, T., Lee, A. 1995. “Effect of field-of-view restriction on rotorcraft workload and performance – Preliminary results,” in Helmet and Head-Mounted Displays and Symbology Design Requirements II, Ronald Lewandowski, Wendall Stephens, Loran A. Haworth, Editors, Proc. SPIE 2465, pp.142-153.
- U.S. Army Aviation Troop Command. 1994. “Aeronautical design standard, handling qualities requirements for military rotor craft,” ADS-33D.

Verona, R.W., Johnson, J. C., and Jones, H. 1979. Head aiming/tracking accuracy in a helicopter environment. Ft. Rucker, AL: U.S. Army Aeromedical Research Laboratory. USAARL Report No. 79-9.

Verona, R.W., Rash C. E., Holt, W. R., and Crosley, J. K. 1986. Head movements during contour flight. Ft. Rucker, AL: U.S. Army Aeromedical Research Laboratory. USAARL Report No. 87-1.

Zangemeister, W. H., and Stark, L. 1981. Active head rotations and eye-head coordination. Annals of New York Academy of Sciences. 374:541-59.

Zuckerman, J. 1954. Perimetry. Philadelphia: Lippincott.

Appendix A.

Discussion on analyzing distributions.

Introduction

The data sets reported herein for head motion position and velocities consist of distributions of numerical values. There are a number of methods used to analyze such data distributions. The first method employs graphical techniques. Common graphical techniques include frequency histograms and cumulative frequency curves. A second method is the calculation of various summary characteristics, which commonly consist of the mean (average value), median (middle value), mode (most frequently occurring value) and variance (or standard deviation). A more strict mathematical treatment defines a set of summary characteristics called the “moments” of the distribution. There are four such moments: First (mean), second (variance), third (related to skewness), and fourth (related to kurtosis). The use of this entire set of moments ordinarily will fully define a distribution (Hays, 1963). Once the distributions are fully described graphically and mathematically, they can be compared by various statistical “goodness of fit” techniques such as the Chi-square test.

Graphical techniques

When the data set consists of a large number of values, it is common to organize them into a frequency table. The range of the data set is calculated and divided into a number of classes usually of equal size having upper and lower boundaries. The values within the data set are then placed in the appropriate class and then tabulated. See example in Table A-1.

Table A-1.
Example of frequency table.

Class	Data values	Frequency
1-25	3, 15, 21, 11, ...	11
26-50	45, 32, 26, 31, ...	20
51-75	67, 53, 73, 61, ...	28
76-100	99, 79, 83, 86, ...	35
101-125	105, 124, 115, ...	39
126-150	131, 145, 128, ...	27
151-175	174, 165, 155, ...	19
176-200	199, 179, 195, ...	13
201-225	223, 205, 220, ...	8

A frequency histogram results when the class frequencies are graphed as a vertical bar chart. The bars are commonly graphed centered on the class midpoints. See Figure A-1.

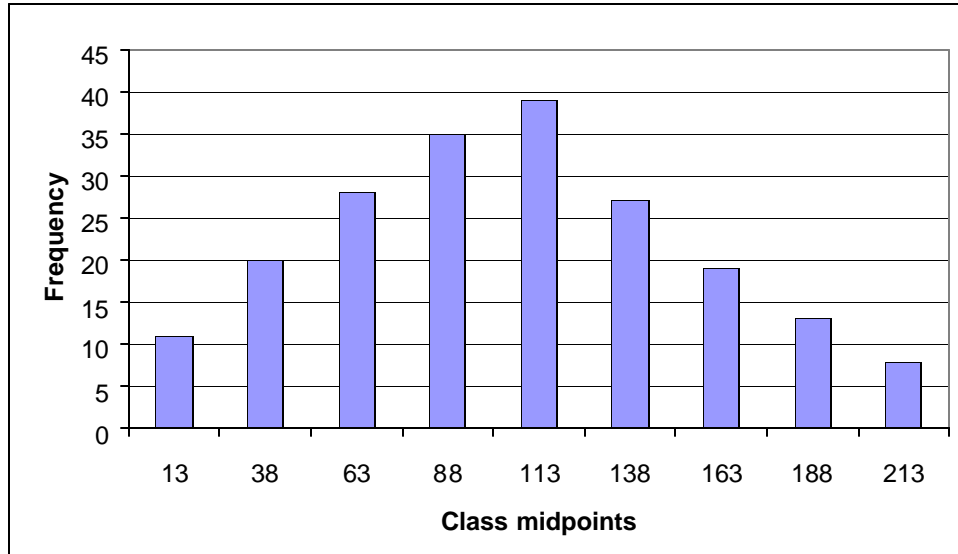


Figure A-1. Example of frequency histogram.

A second graphical method requires two additional columns being added to the frequency table above. The first extra column presents the cumulative frequency total for all preceding classes. The second column provides the cumulative percentage of data values in the preceding classes. By definition, the final cumulative frequency must equal the total number of data values, and the final cumulative percentage must equal 100. See Table A-2, where a data set of 200 values is assumed.

Table A-2.
Example of cumulative frequency table.

Class	Data values	Frequency	Cumulative frequency	Cumulative percentage
1-25	3, 15, 21, 11, 25, ...	11	11	6 %
26-50	45, 32, 26, 31, ...	20	31	16 %
51-75	67, 53, 73, 61, 55, ...	28	59	30 %
76-100	99, 79, 83, 86, 77, ...	35	94	47 %
101-125	105, 124, 115, ...	39	133	66 %
126-150	131, 145, 128, ...	27	160	80 %
151-175	174, 165, 155, ...	19	179	90 %
176-200	199, 179, 195, ...	13	192	96 %
201-225	223, 205, 220, ...	8	200	100 %

A cumulative frequency (or percentage) polygon results when the cumulative frequency of percentage values are graphed against the class midpoints (or upper boundary limits). If the polygon is smoothed, then a curve often referred to as an *ogive* is produced. See Figure A-2.

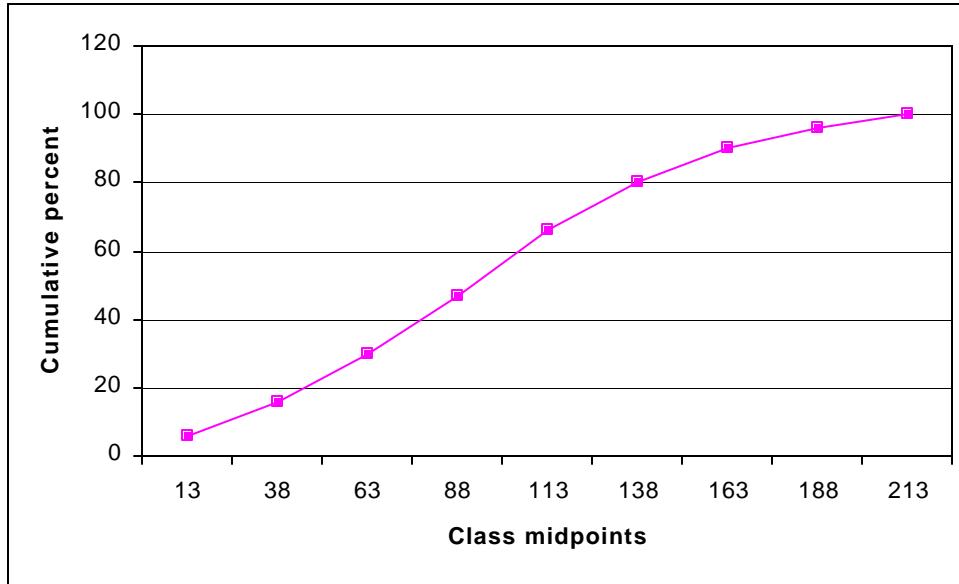


Figure A-2. Example of cumulative percentage curve.

A useful alternative to the cumulative percentage curve can be derived if the axes are reversed (Figure A-3). This modified curve is called a *quantile curve*. The upper and lower ends of quantile curves terminate at the minimum and maximum data values. The slopes of the quantile curve in the vicinity of the ends indicate the presence or not of outliers (values greatly smaller or larger than the majority of the data set); steep slopes indicate outliers. The vertical shift from zero at the 50-percentile point indicates the value and direction of the median.

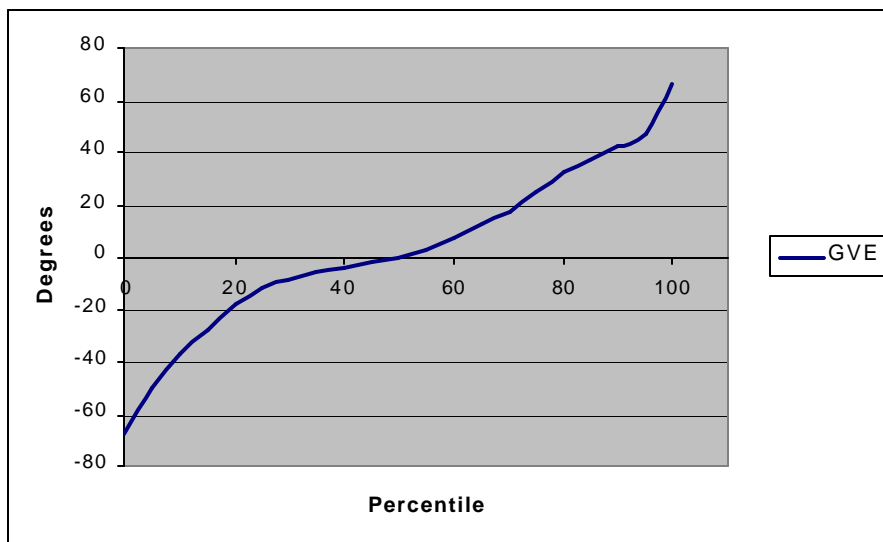


Figure A-3. Example of quantile curve.

A final useful graphical technique is the box plot (or box and whiskers) presentation. Several versions of boxplots are possible. The version used in this paper is based on a 5-number summary employed in the SPSS for WindowsTM statistical software. These numbers are: the smallest value that is not an outlier, the first, second (median) and third quartiles, and the largest value that is not an outlier. The first, second and third quartiles are defined as the 25th, 50th and 75th percentile values, respectively. SPSS for windows modifies the standard boxplot technique in several ways. First, values which fall between 1.5 and 3 box-lengths from either the first or third quartiles are called *outliers* and are designated in the graph using the “o” symbol. Values which are beyond 3 box-lengths are called *extremes* and are designated by the “*” symbol. The box-length is equivalent to the interquartile range (IQR) of the data set. See Figure A-4.

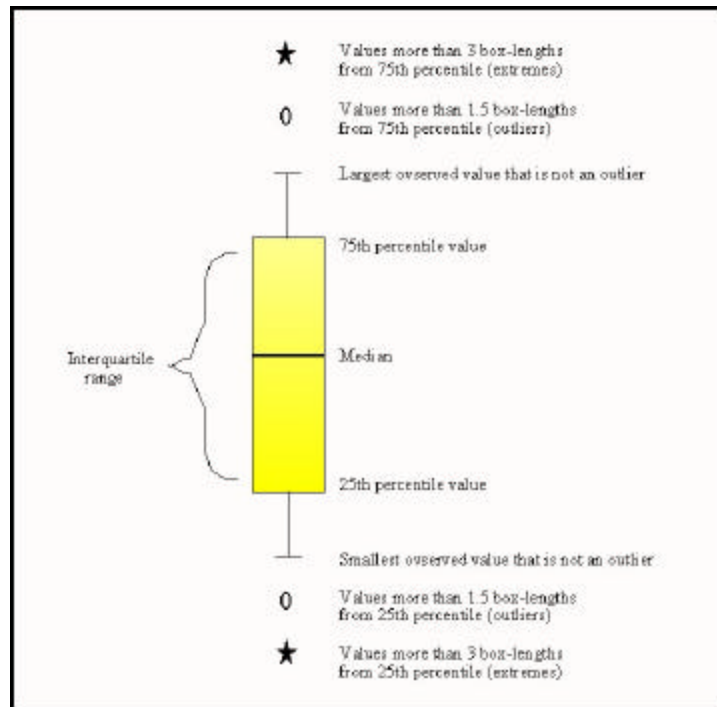


Figure A-4. Example of a box plot.

Moments of a distribution

A distribution can be fully defined by a set of characteristics known as the “moments” of the distribution. There are four such moments. The first moment of a distribution is called the mean. The mean is one measure of central tendency. Other measures of central tendency are the median and the mode. The mean can be thought of as a fulcrum point of the distribution values. The value of the mean is weighted by each value of the distribution. The mean calculated for the head motion data herein is the arithmetic mean and is defined by the formula:

$$\text{Mean} = \frac{\sum_i x_i}{n}$$

Where, “ x_i ” is each value in the distribution of “ n ” values.

Note: The mean value calculated above is the first moment about the origin. Moments can be calculated about the mean, also, and then are called central moments. This approach is used for the second, third and fourth moments which follow. If the first moment was calculated about the mean, its value would by definition always be zero.

The second central moment is a measure of dispersion and is called the variance (s^2). Variance is a measure of spread or dispersion within the data. The square root of the variance is the standard deviation(s). Herein, the variance is calculated using the formula:

$$s^2 = \frac{n \sum_i x_i^2 - \left(\sum_i x_i \right)^2}{n(n-1)}$$

Where, “ x_i ” is each value in the distribution of “ n ” values.

Skewness is a function of the third central moment of a distribution and is a measure of the distribution’s symmetry, or how the values are distributed about the mean. Conversely, skewness is the degree of asymmetry of a distribution. If the distribution has a longer tail less than the maximum (to the left), the function has negative skewness. Otherwise, it has positive skewness. A skewness value of zero implies a perfectly symmetrical distribution (the left half of the distribution is a mirror image of the right half). For a positively skewed distribution, the mean is greater than the median, which in turn, is greater than the mode. See Figure A-5. Several types of skewness are defined. The values reported herein were calculated using the following formula:

$$\text{Skewness} = \frac{(n-1)}{(n-1)(n-2)} \sum_i \left(\frac{x_i - \bar{x}}{s} \right)^3$$

Where, “ x_i ” is each value in the distribution of “ n ” values having a standard deviation of “ s ” and mean of “ \bar{x} .”

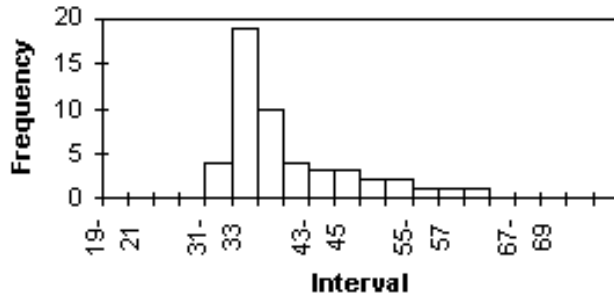


Figure A-5. Example of a positively skewed distribution.

Kurtosis is the fourth central moment of a distribution and is a measure of the “peakedness” of non-normality of a distribution. Positive kurtosis indicates a relatively peaked distribution. Negative kurtosis indicates a relatively flat distribution. Several mathematical expressions for kurtosis are used. The one used in this paper is that used by Microsoft EXCEL™ :

$$\text{Kurtosis} = \frac{n(n+1)}{(n-1)(n-2)(n-3)} \sum_i \left(\frac{x_i - \bar{x}}{s} \right)^4 - \frac{3(n-1)^2}{(n-2)(n-3)}$$

Where, “ x_i ” is each value in the distribution of “ n ” values having a standard deviation of “ s ” and mean of “ \bar{x} .”

Chi-square comparison of distributions

Two or more multinomial distributions can be compared using the Chi-square test. Assume the three elementary school children age groups (distributions) given in Table A-3. The ages in all three groups range from 6 to 11. The values which the age variable can take on are: 6, 7, 8, 9, 10 and 11.

Table A-3.
Example school children age distributions.

Group 1	6, 6, 6, 8, 9, 9, 10, 10, 10, 10, 11, 11
Group 2	6, 6, 7, 7, 8, 8, 8, 9, 9, 9, 10, 10, 11
Group 3	6, 6, 7, 7, 7, 8, 8, 8, 9, 9, 9, 10, 10, 11

The first step in the Chi-square analysis is to establish the following contingency table (Table A-4). The data values are recorded as frequencies of occurrence. Frequencies are

totalled in columns and rows. The values in parentheses are called expected values and are calculated by dividing the product of the associated row and column totals by the grand total (right lower cell).

Table A-4.
Contingency table for school children age data.

	6	7	8	9	10	11	Totals
Group 1	3 (2.1)	0 (1.5)	1 (2.0)	2 (2.3)	4 (2.9)	2 (1.2)	12
Group 2	2 (2.4)	2 (1.7)	3 (2.4)	3 (2.7)	3 (3.4)	1 (1.4)	14
Group 3	2 (2.6)	3 (1.8)	3 (2.6)	3 (2.9)	3 (3.7)	1 (1.5)	15
Totals	7	5	7	8	10	4	41

The Chi-square test statistic is defined as:

$$c^2 = \sum_{i=1}^n \sum_{j=1}^k \frac{(o_{ij} - e_{ij})^2}{e_{ij}}$$

Where, “n” is the number of distributions, “k” is the number of values the distribution variable can take, o_{ij} is the observed frequency of a value, and e_{ij} is the expected frequency of that value.

For the distributions in Tables A-3 and A-4, the Chi-square statistic calculates to a value of 5.14 for the comparison. The number of degrees of freedom $(n-1)(k-1)$ for this test is 10.

In this paper, the one-tailed probability of the chi-square distribution is calculated using the CHIDIST function used by Microsoft EXCEL™. For the above example with 10 degrees of freedom and a chi-square statistic value of 5.14, the CHIDIST function returns a probability of 0.88, which is interpreted loosely as there being an 88% probability the age distributions are the same.

Appendix B.

Azimuth position distributions.

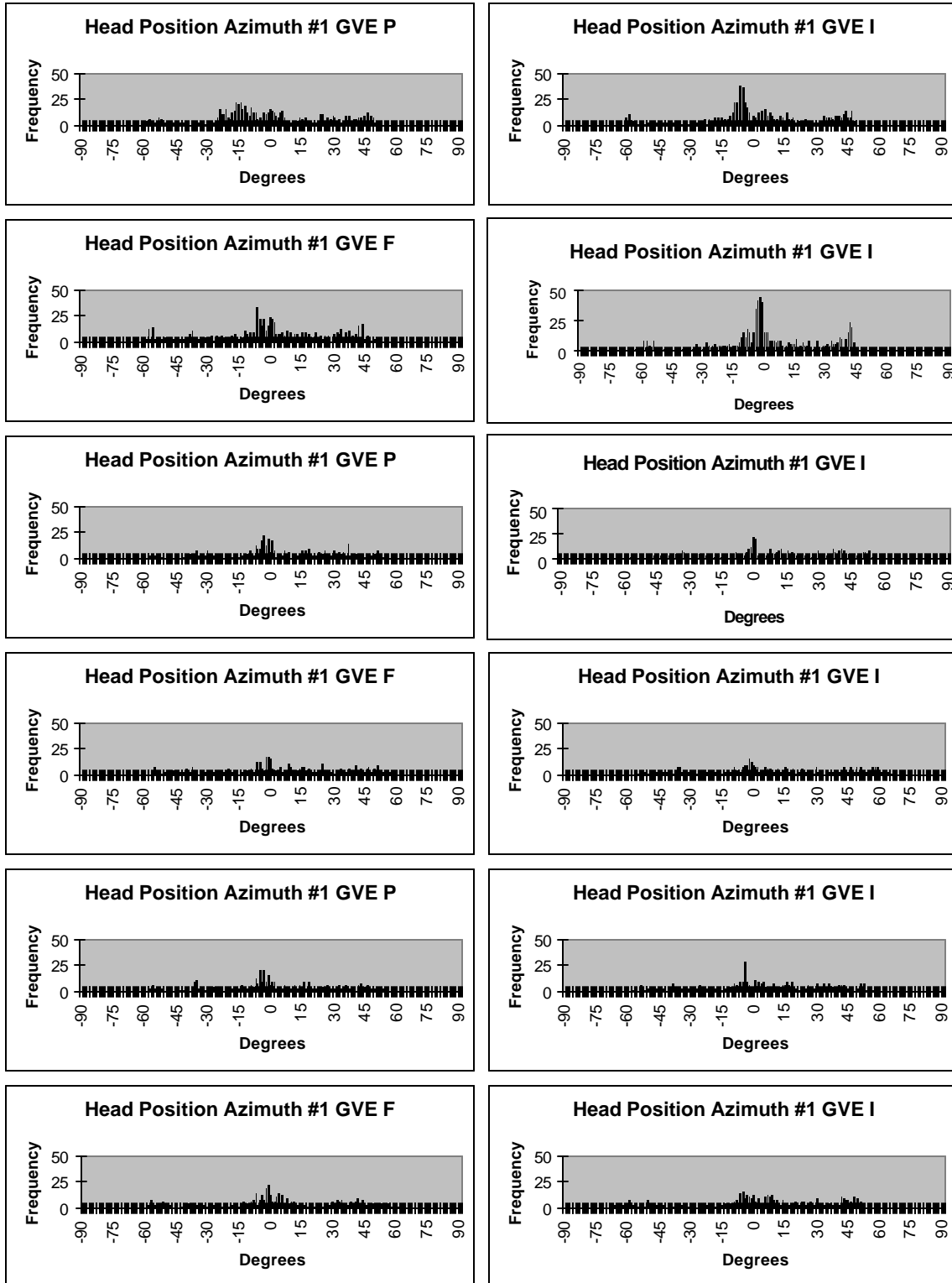


Figure B-1. Subject #1 GVE head position data.

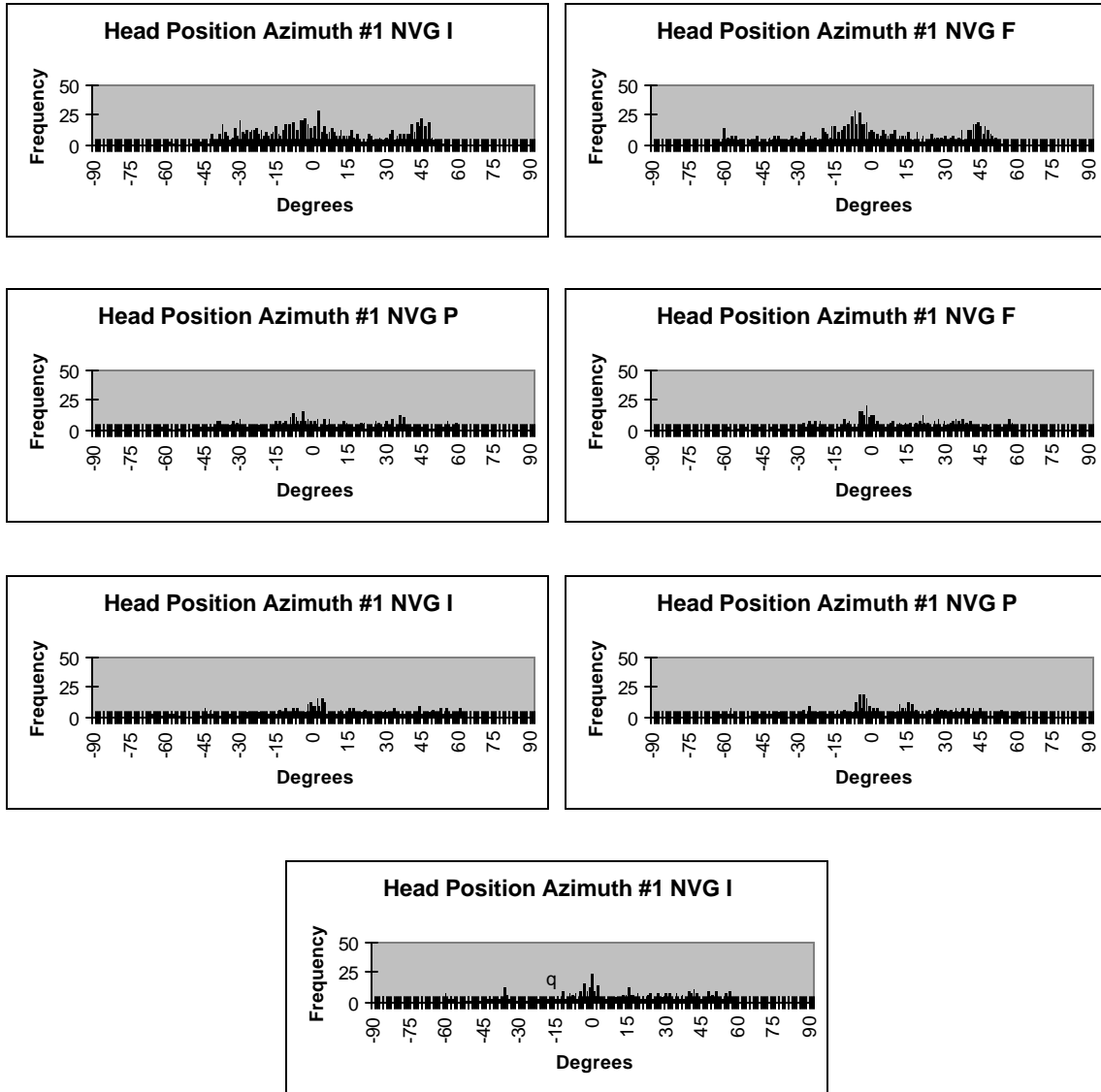


Figure B-2. Subject #1 NVG head position data.

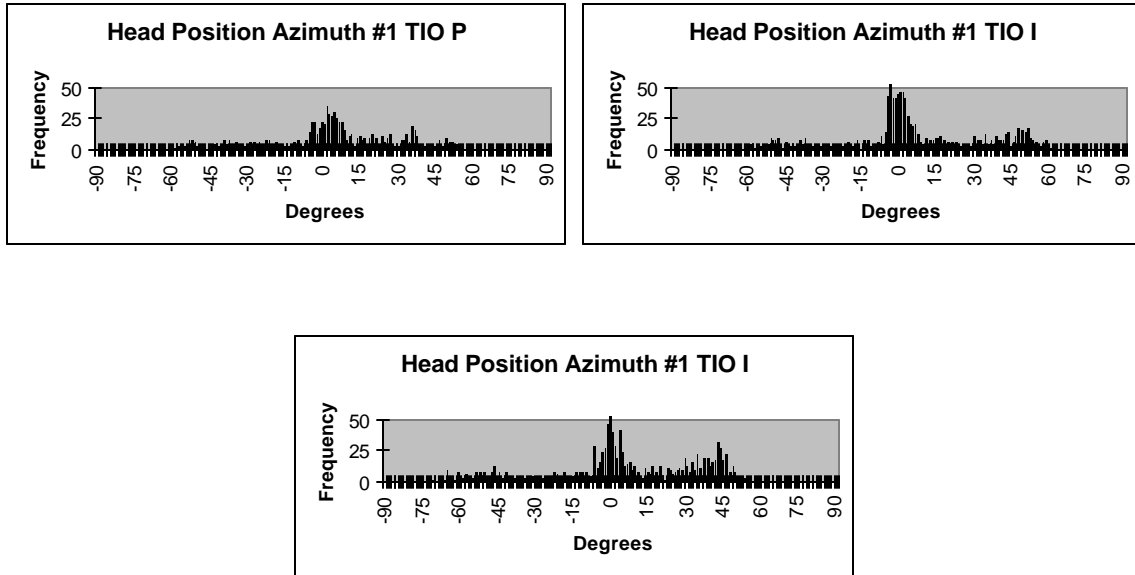


Figure B-3. Subject #1 TIO head position data.

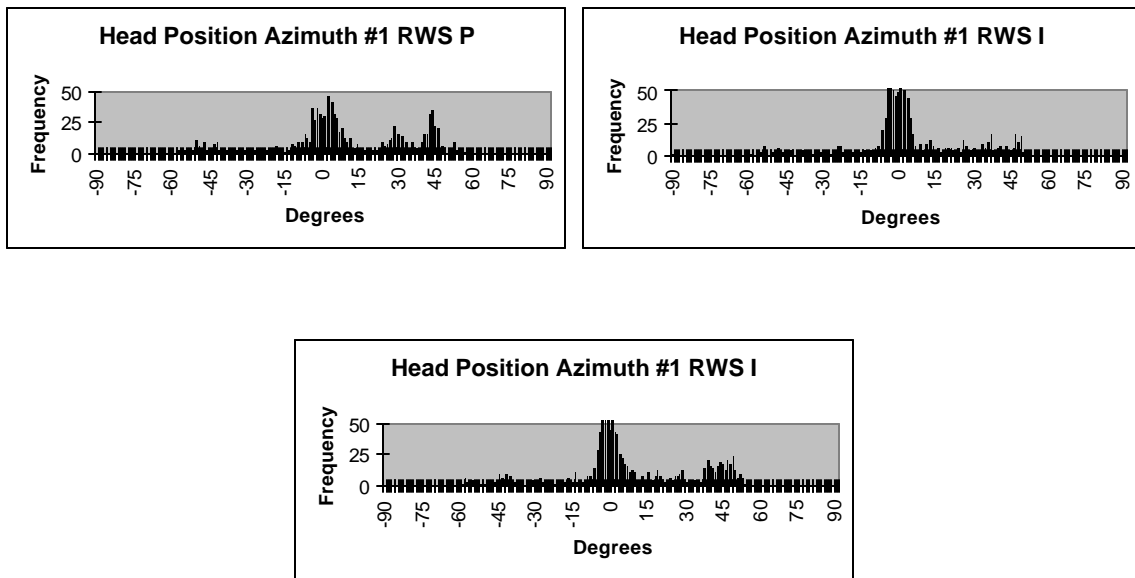


Figure B-4. Subject #1 RWS head position data.

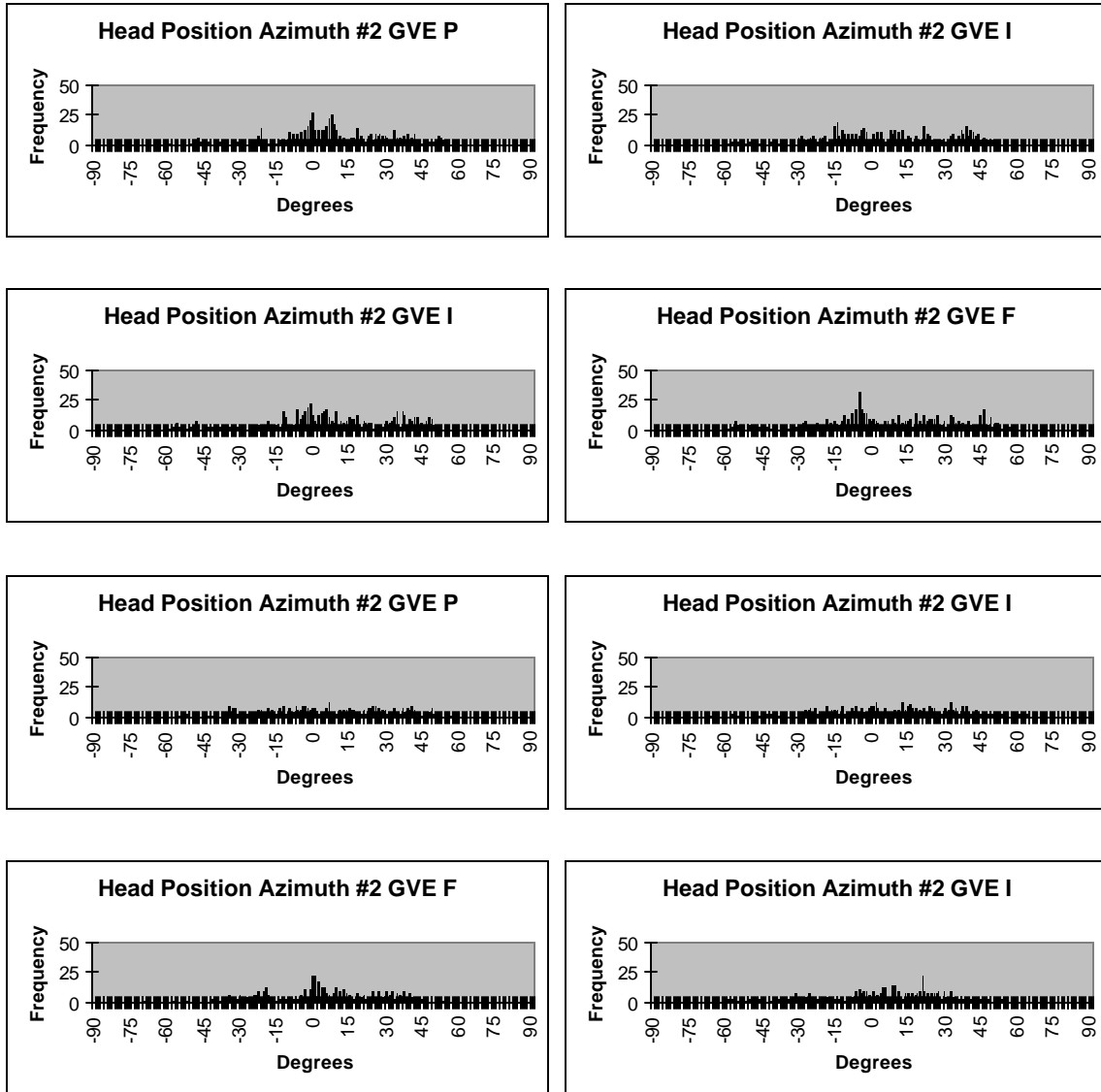


Figure B-5. Subject #2 GVE head position data.

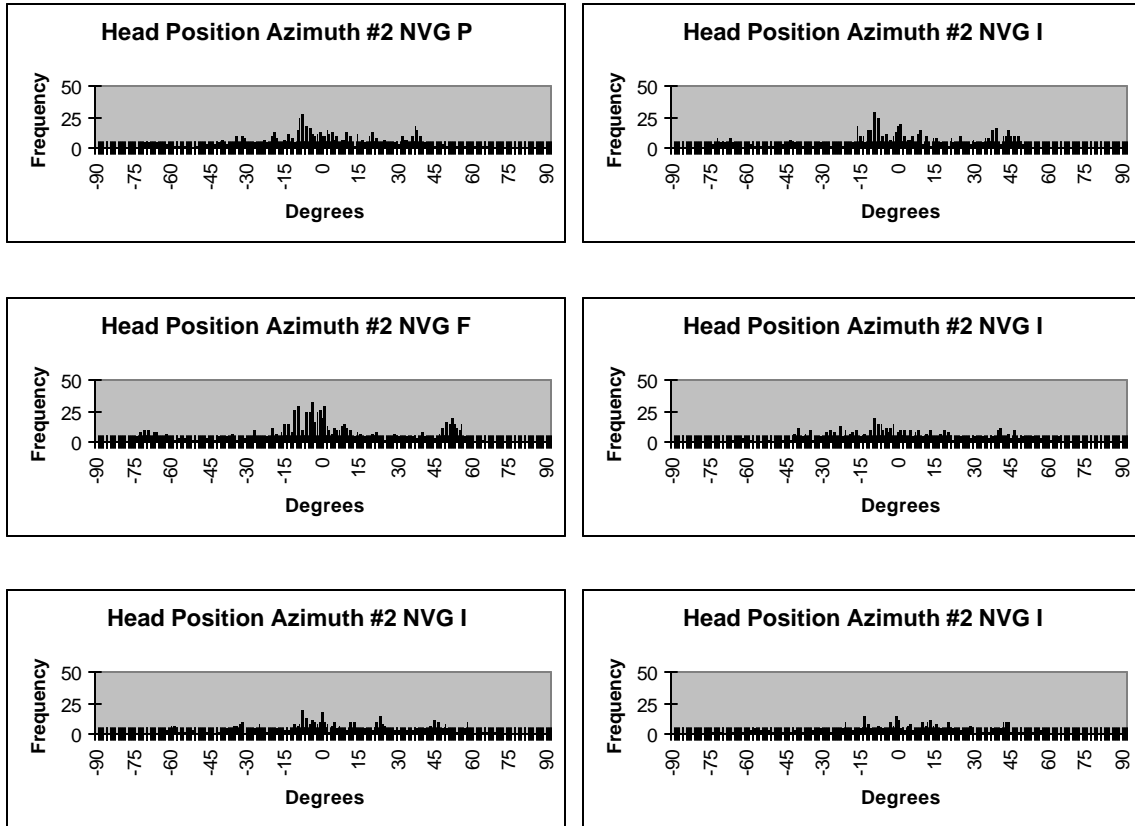


Figure B-6. Subject #2 NVG head position data.

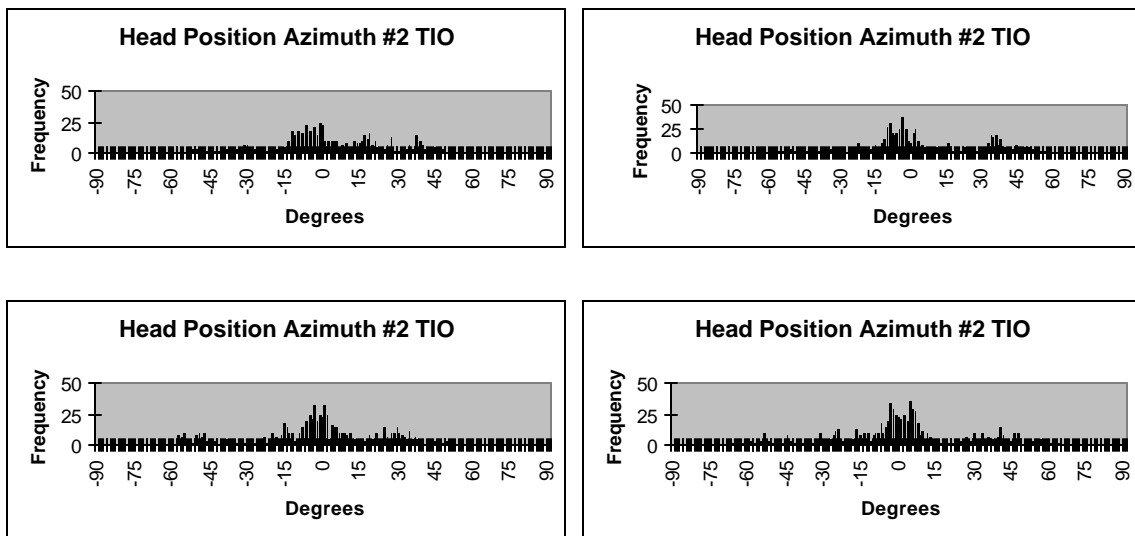


Figure B-7. Subject #2 TIO head position data.

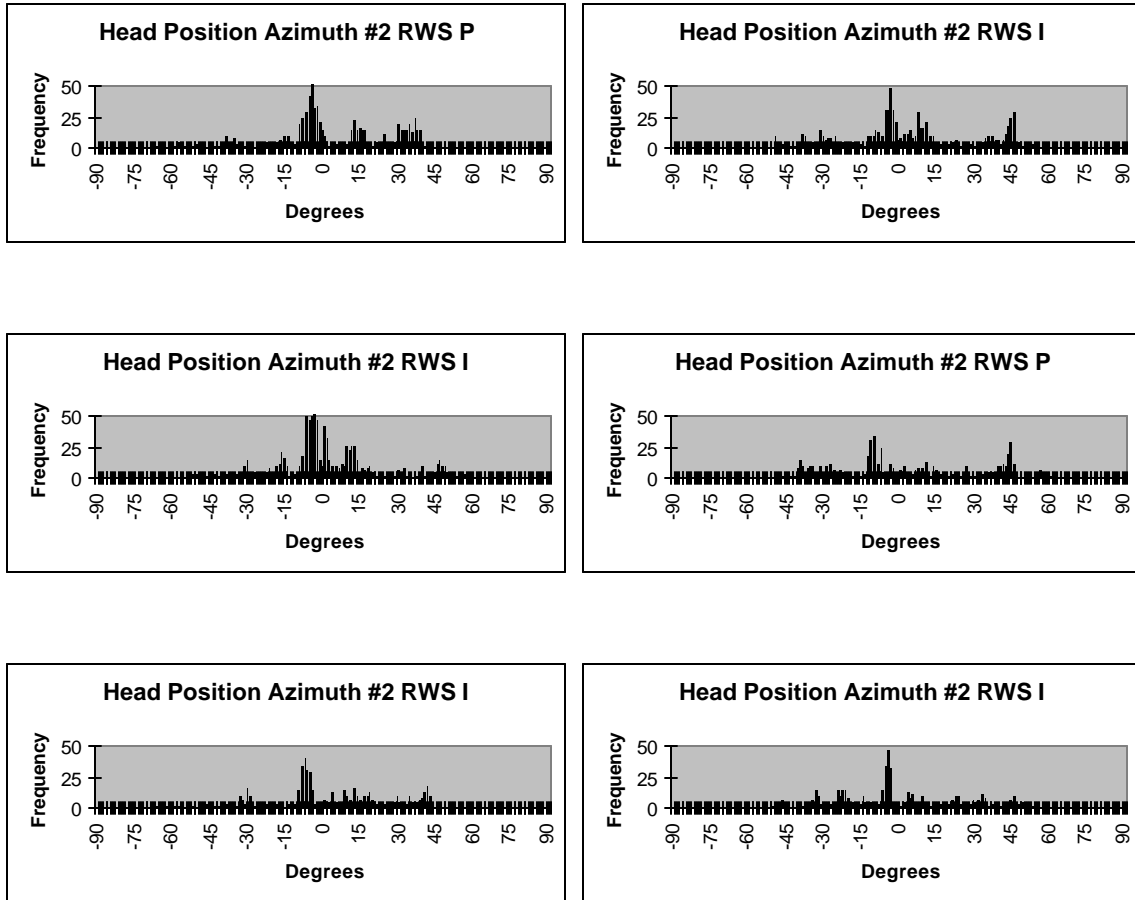


Figure B-8. Subject #2 RWS head position data.

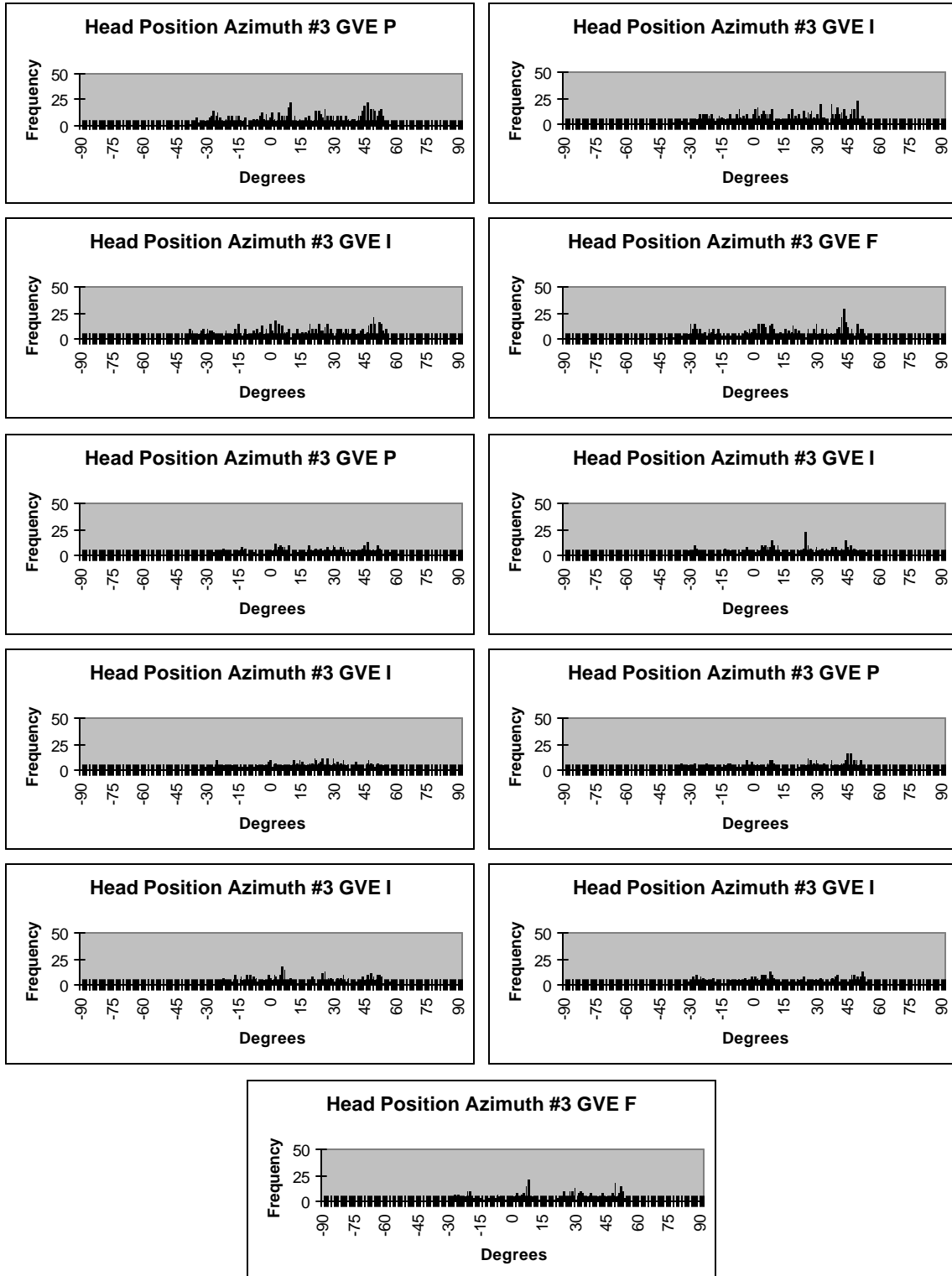


Figure B-9. Subject #3 GVE head position data.

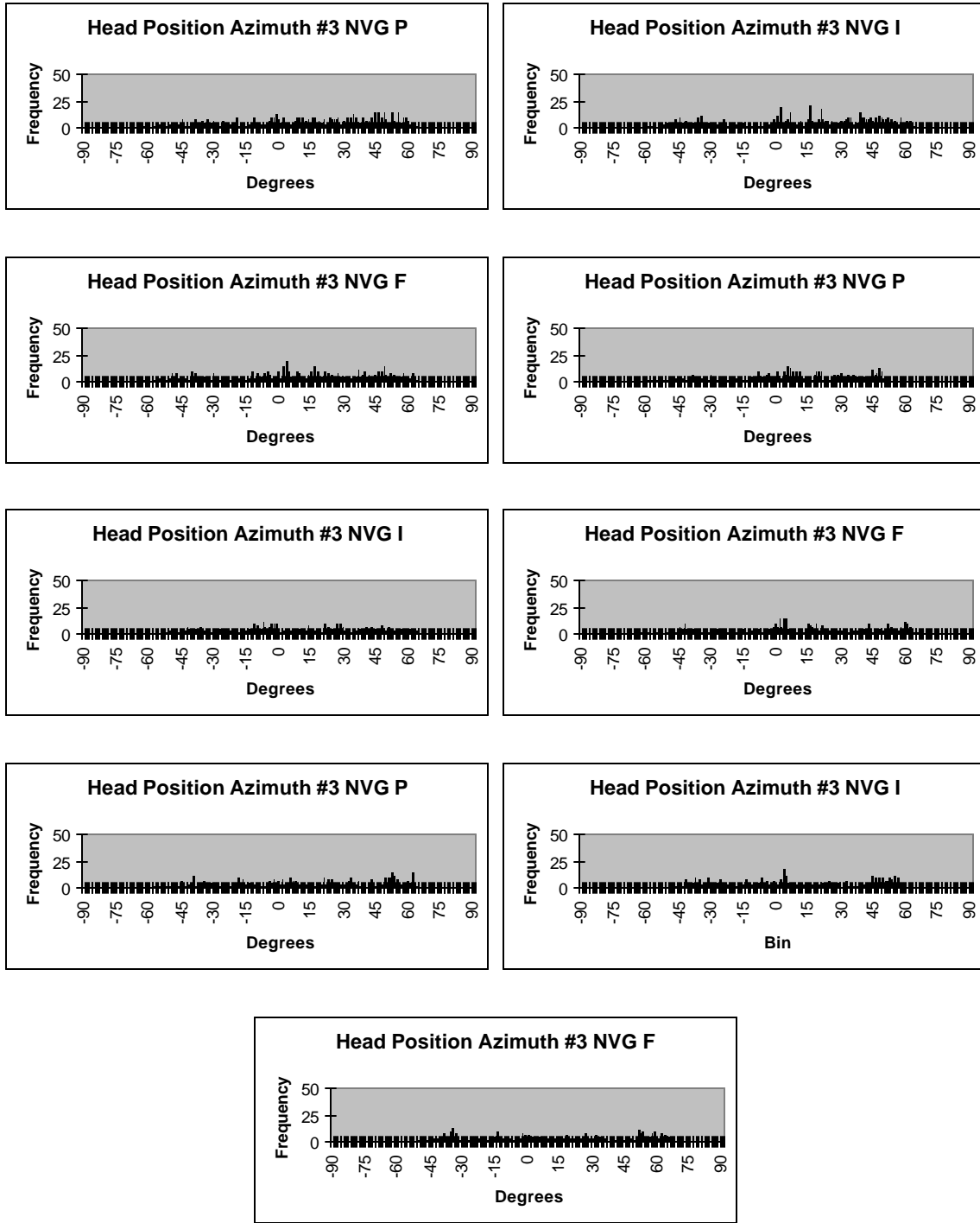


Figure B-10. Subject #3 NVG head position data.

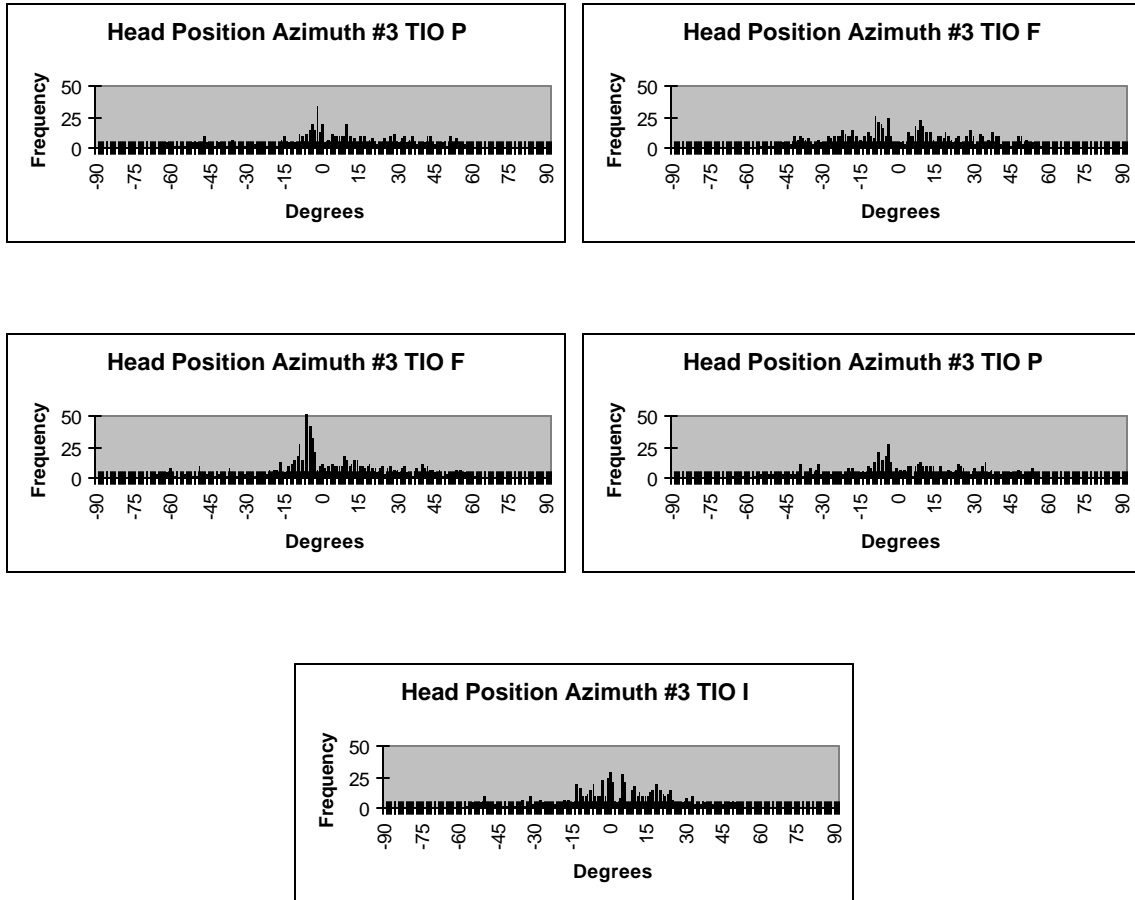


Figure B-11. Subject #3 TIO head position data.

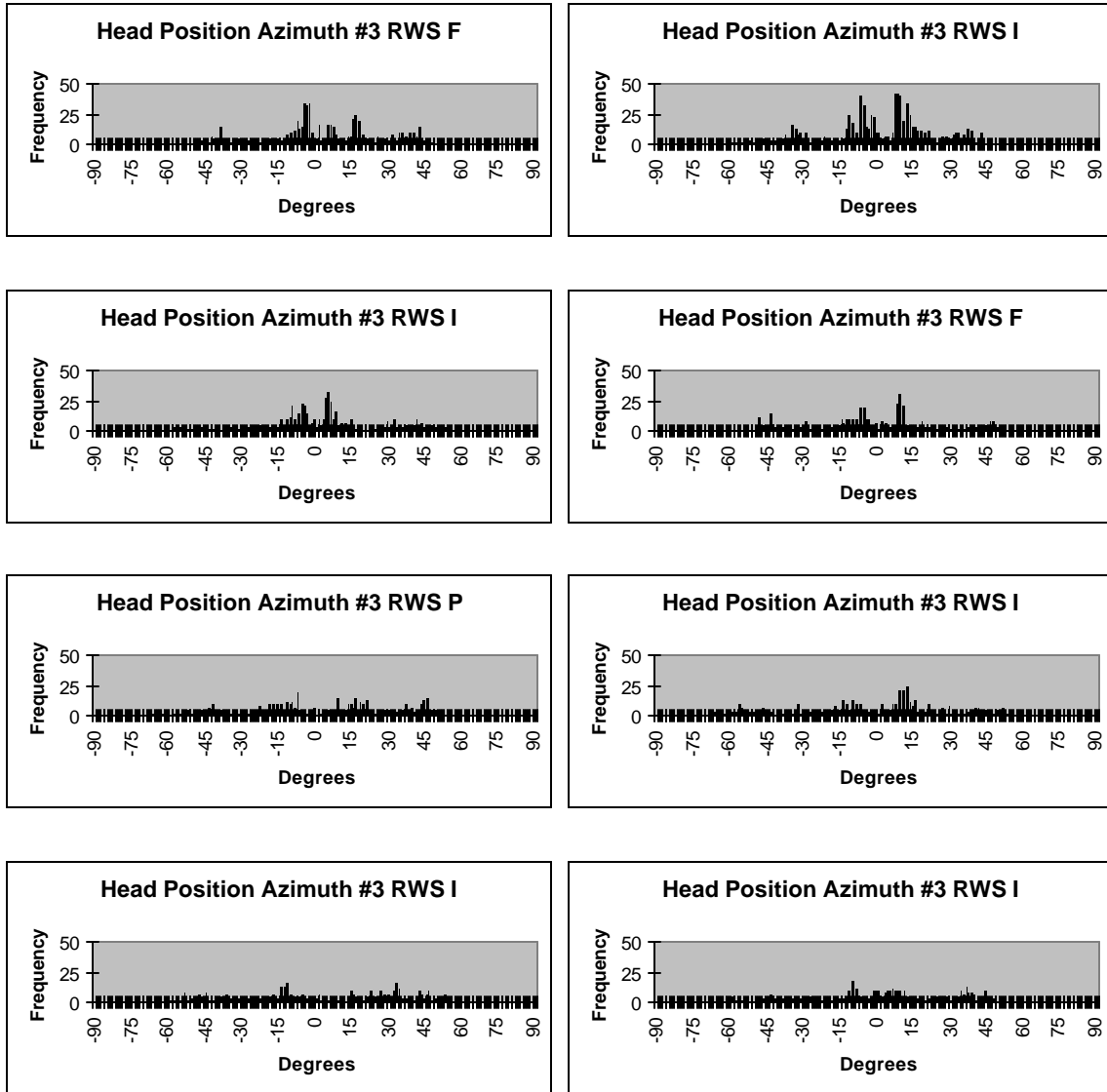


Figure B-12. Subject #3 RWS head position data.

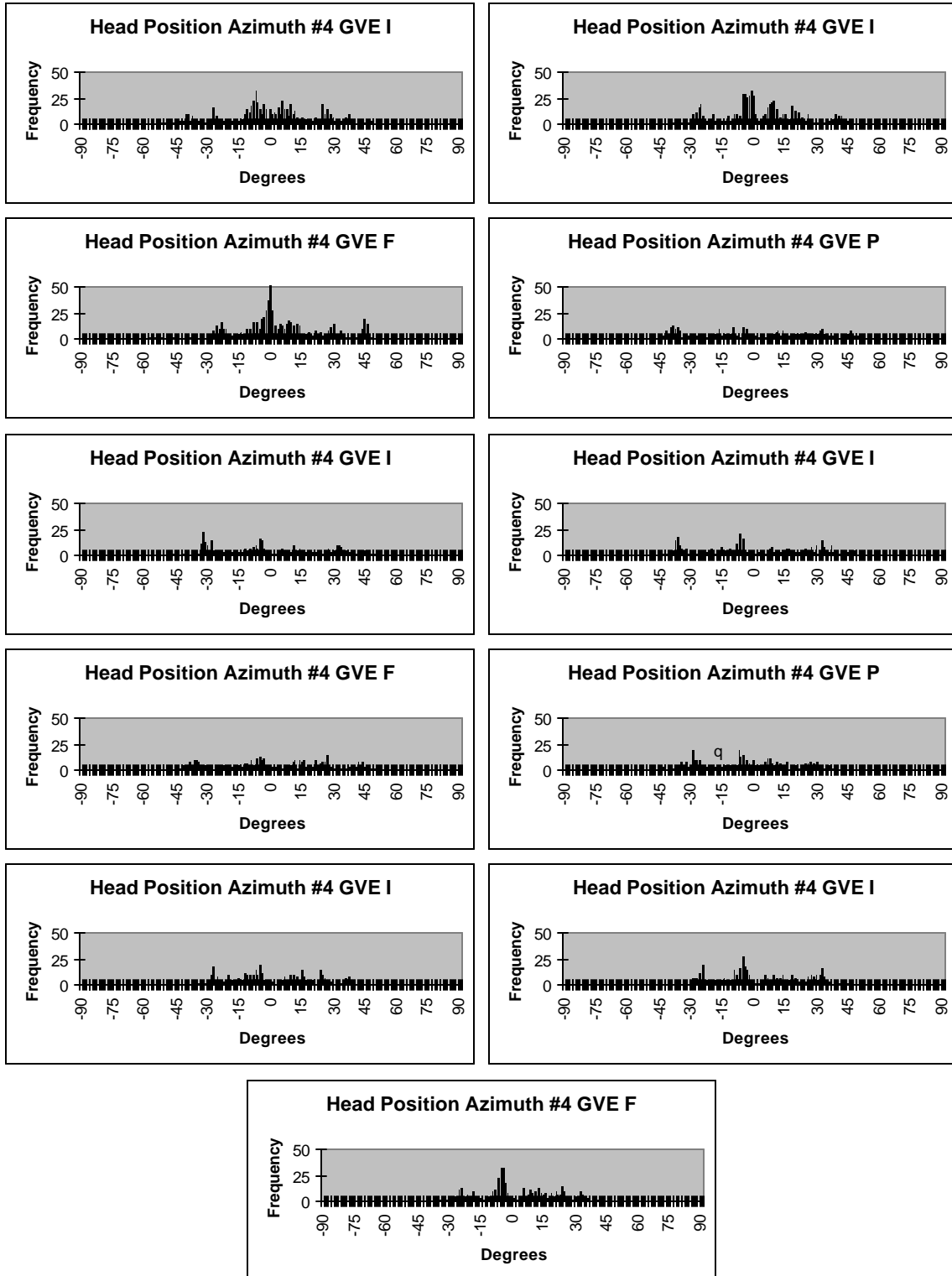


Figure B-13. Subject #4 GVE head position data.

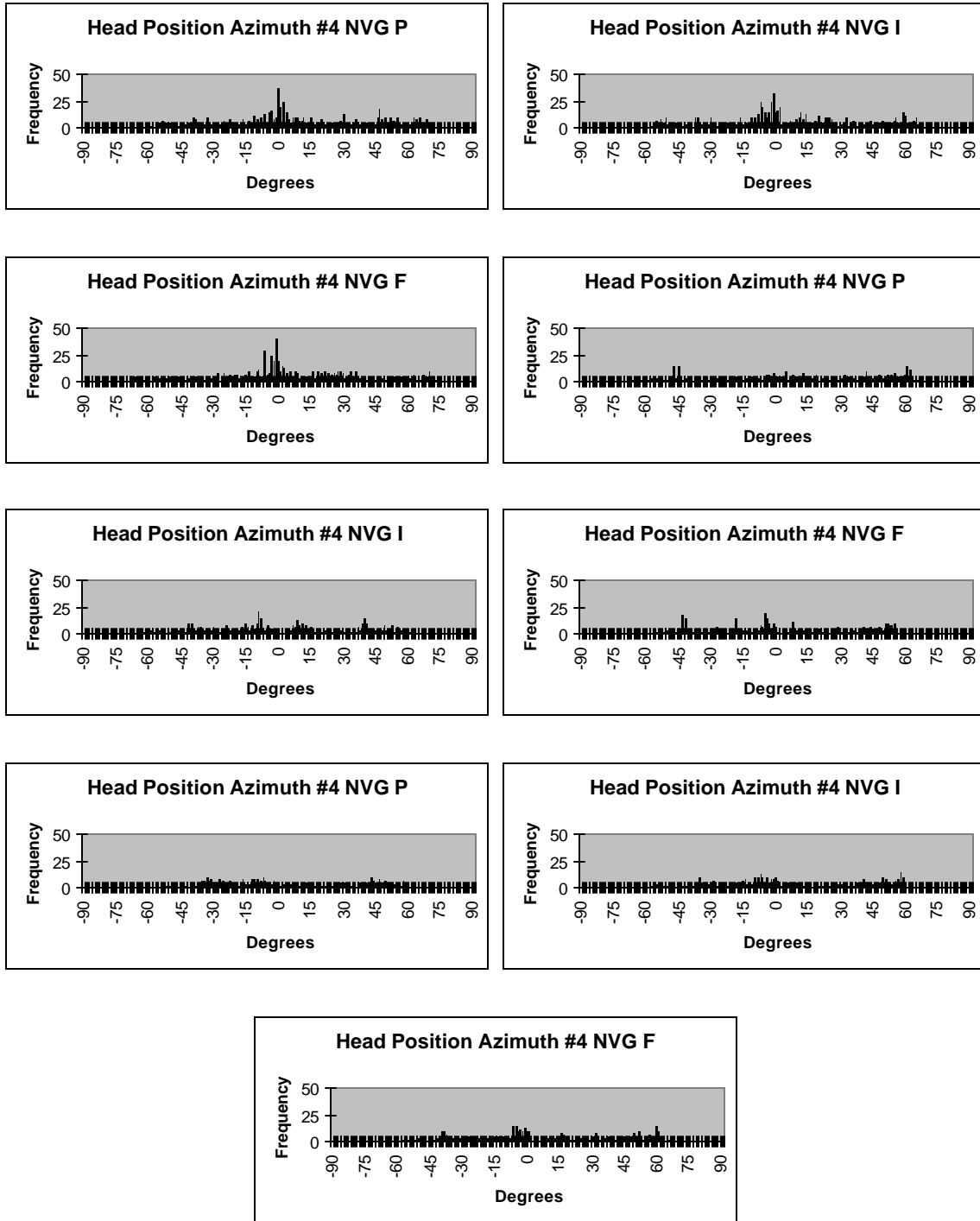


Figure B-14. Subject #4 NVG head position data.

Appendix C.

Graphical rationale for combining head motion data across LOA and run type.

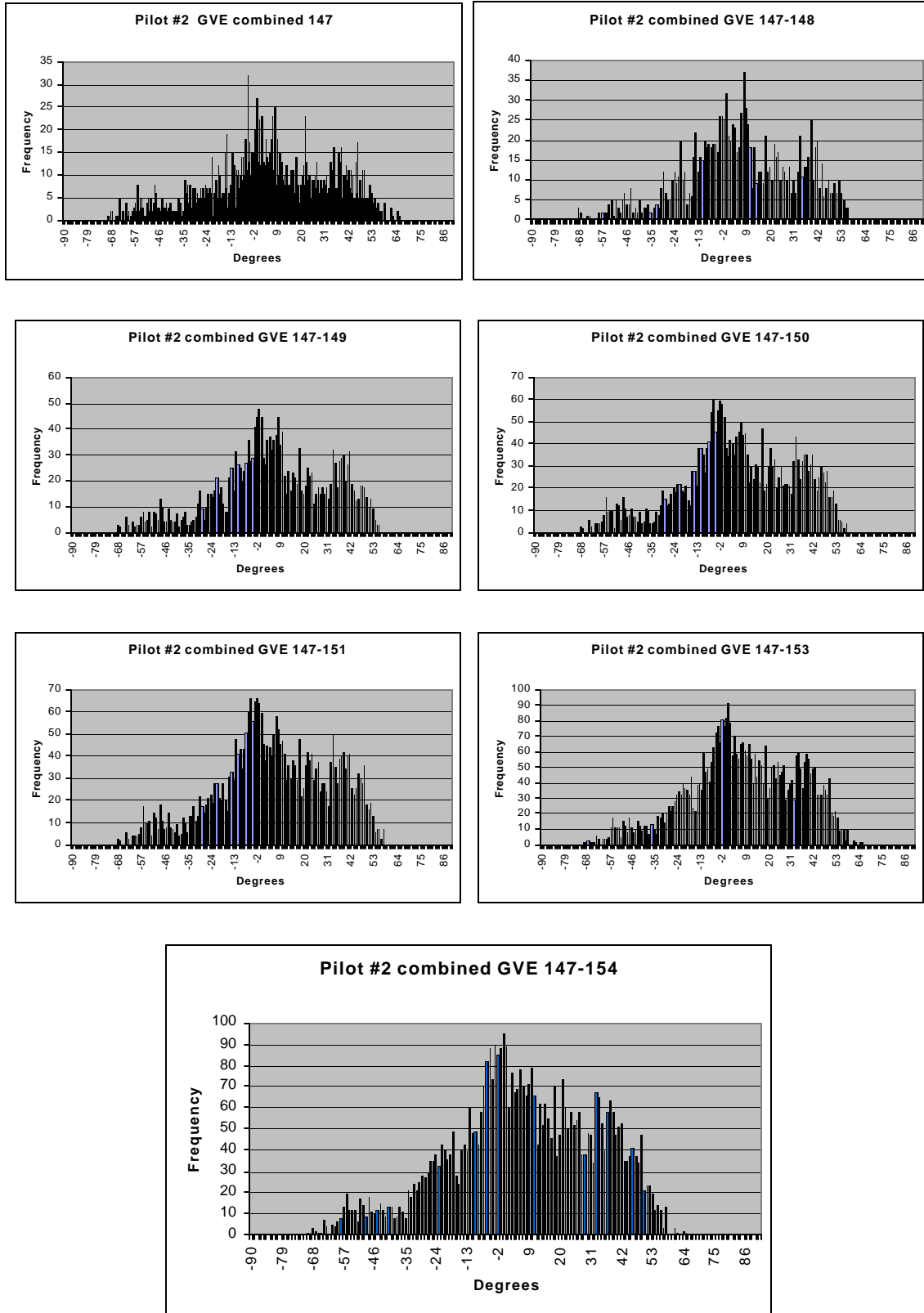


Figure C-1. Building the combined head motion distribution for GVE.

Appendix D.

Summary tables of azimuth position distributions by visual environment.

Table D-1.
Summary of moments and statistics for azimuth position, slalom course, GVE.
(azimuth values expressed in degrees)

Subject	Run	Time	Min	Max	Mean	Median	S.D.	IQR	Skew	Kurt
1	116	76.9	-65.8	51.4	-9.1	-12.8	26.5	-18.0 to 21.8	0.3	-0.1
1	117	75.7	-61.7	48.5	-7.3	-7.1	26.3	-10.8 to 16.9	0.1	0.0
1	118	76.9	-65.9	52.9	-8.2	-6.9	27.7	-13.6 to 20.8	0.2	-0.2
1	119	76.0	-63.3	45.7	-6.1	-3.7	24.9	-9.6 to 18.8	-0.2	0.1
1	128	45.2	-57.9	53.4	3.6	0.4	26.6	-7.9 to 24.6	-0.3	-0.5
1	129	48.1	-61.3	56.4	6.2	6.1	29.4	-12.6 to 33.4	-0.2	-0.9
1	130	48.6	-56.0	57.4	5.0	4.4	30.1	-10.5 to 28.5	-0.2	-0.7
1	131	43.8	-55.1	65.7	6.9	2.2	32.4	-13.9 to 37.0	-0.1	-1.0
1	132	45.6	-57.8	53.7	4.4	1.0	26.1	-8.8 to 24.2	-0.2	-0.5
1	133	49.8	-57.2	58.2	3.5	2.0	27.9	-12.2 to 25.6	-0.1	-0.7
1	134	51.1	-59.6	60.8	4.7	3.0	29.3	-8.3 to 29.8	-0.3	-0.5
1	135	52.9	-67.6	54.1	4.8	5.7	30.6	-8.4 to 29.9	-0.5	-0.4
Combined		690.6	-67.6	65.7	0.4	-1.8	28.8	-12.1 to 24.9	-0.1	-0.6
2	147	68.4	-68.3	55.9	6.5	6.1	24.4	-6.6 to 23.8	-0.3	0.1
2	148	65.1	-68.3	55.2	4.9	3.2	26.9	-14.0 to 26.5	-0.2	-0.6
2	149	71.7	-64.7	52.9	5.3	5.1	28.3	-9.6 to 29.8	-0.5	-0.3
2	150	73.9	-60.9	57.5	6.2	6.3	28.2	-9.9 to 27.4	-0.3	-0.5
2	151	47.0	-56.4	57.4	5.9	5.3	25.6	-12.8 to 26.0	-0.1	-0.8
2	152	52.2	-66.8	64.5	9.6	11.5	26.2	-8.9 to 31.3	-0.2	-0.5
2	153	51.7	-70.5	57.4	5.6	4.4	23.4	-7.6 to 24.9	-0.3	-0.3
2	154	50.4	-65.0	57.2	6.8	9.0	25.4	-6.3 to 24.1	-0.5	0.0
Combined		480.4	-70.5	64.5	6.3	6.0	26.3	-9.7 to 26.4	-0.3	-0.3
3	47	74.8	-38.0	61.1	15.1	18.0	26.8	-5.1 to 41.2	-0.3	-1.2
3	48	75.7	-38.3	55.0	13.4	16.0	25.0	-6.7 to 36.2	-0.2	-1.1
3	49	78.8	-39.1	57.3	12.4	13.7	27.4	-9.0 to 36.5	-0.2	-1.1
3	50	73.2	-41.2	55.6	12.0	11.7	26.1	-7.7 to 36.5	-0.2	-1.2
3	54	44.6	-30.0	60.6	16.6	19.0	23.9	-1.6 to 36.8	-0.2	-1.1
3	55	47.6	-33.6	53.3	14.5	16.0	24.0	-2.1 to 35.4	-0.3	-1.0
3	56	46.5	-33.3	56.0	14.7	17.8	23.7	-2.6 to 31.6	-0.2	-0.9
3	57	49.0	-34.3	54.8	17.7	20.7	24.1	1.7 to 39.4	-0.4	-0.8
3	64	50.6	-40.0	58.2	13.2	13.8	27.2	-9.4 to 38.2	-0.3	-1.2
3	65	46.8	-22.7	57.6	16.5	17.7	23.7	-3.1 to 36.9	0.0	-1.3
3	66	46.7	-31.6	54.5	13.9	10.9	25.7	-4.5 to 38.2	-0.1	-1.2
3	67	43.4	-28.7	54.8	17.2	23.1	25.0	-4.1 to 39.6	-0.2	-1.2
Combined		677.7	-41.2	61.1	14.5	16.2	25.5	-5.0 to 37.0	-0.2	-1.1
4	75	72.4	-54.3	48.7	-0.2	-0.4	21.1	-11.0 to 13.2	-0.1	-0.4
4	76	69.0	-38.6	46.2	2.6	-0.3	18.6	-7.2 to 14.1	0.2	-0.4
4	77	79.8	-57.0	48.7	4.7	0.3	20.6	-7.1 to 16.9	0.2	-0.1
4	81	42.0	-43.7	49.2	0.6	-3.5	28.5	-24.8 to 26.9	0.1	-1.3
4	82	42.6	-48.0	51.2	1.4	-4.6	25.8	-22.0 to 25.8	0.2	-1.2
4	83	46.0	-44.7	48.8	0.9	-5.3	26.5	-20.1 to 25.0	0.1	-1.1
4	84	45.0	-43.2	49.9	2.2	-0.7	25.6	-16.7 to 24.0	0.0	-1.1
4	92	44.4	-44.2	37.3	-2.4	-3.7	21.1	-20.1 to 13.4	0.0	-1.0
4	93	43.6	-34.1	39.9	0.8	-4.0	19.5	-13.7 to 15.9	0.2	-1.0
4	94	48.0	-29.6	48.5	2.5	-3.0	19.5	-10.1 to 18.9	0.2	-1.1
4	95	49.2	-36.6	43.9	2.0	-2.4	17.2	-8.3 to 15.2	0.1	0.7
Combined		582	-57.0	51.2	1.6	-1.0	22.1	-12.9 to 17.9	0.1	-0.7
All Subjects		2251.7	-70.5	65.7	6.4	5.2	26.3	-10.3 to 27.6	-0.2	-0.6

Table D-2.
Summary of moments and statistics for azimuth position, slalom course, NVG.
(azimuth values expressed in degrees, time in seconds)

Subject	Run	Time	Min	Max	Mean	Median	S.D.	IQR	Skew	Kurt
1	108	105.7	-65.3	53.6	2.2	-0.5	27.3	-18.6 to 25.4	0.1	-0.9
1	109	98.2	-64.4	54.3	-0.2	-3.3	30.5	-17.4 to 24.7	-0.1	-0.7
1	110	51.3	-65.8	59.5	2.3	-.08	28.8	-16.2 to 25.6	0.0	-0.7
1	111	51.7	-59.9	57.9	7.1	3.0	26.7	-10.1 to 28.6	-0.2	-0.6
1	112	51.1	-66.9	61.3	6.5	3.7	31.2	-12.0 to 31.7	-0.2	-0.6
1	121	54.0	-62.8	61.5	4.2	1.4	30.4	-15.0 to 28.1	-0.1	-0.7
1	123	55.2	-61.1	57.8	7.9	6.8	29.5	-9.0 to 32.7	-0.3	-0.6
Combined		467.2	-66.9	61.5	3.5	1.0	30.4	-15.3 to 28.3	-0.1	-0.7
2	171	80.0	-72.7	67.1	-2.6	-3.4	29.8	-19.5 to 18.9	-0.2	-0.2
2	172	80.9	-77.9	52.3	-1.5	-1.1	32.2	-16.1 to 24.6	-0.4	-0.4
2	173	103.2	-77.5	63.5	-1.2	-2.5	34.7	-15.4 to 20.7	-0.2	-0.4
2	177	70.6	-68.0	63.4	0.7	-2.9	31.0	-21.8 to 22.2	0.1	-0.7
2	178	63.0	-64.7	69.6	3.9	1.7	32.1	-15.1 to 27.5	-0.1	-0.6
2	179	54.3	-74.7	59.5	0.8	0.5	30.8	-18.8 to 22.1	-0.2	-0.6
Combined		452.0	-77.9	69.6	-0.3	-1.6	32.1	-18.2 to 22.3	-0.2	-0.4
3	51	71.8	-62.7	70.7	13.5	16.7	32.3	-9.9 to 42.1	-0.4	-0.9
3	52	73.9	-60.8	63.1	9.4	14.1	33.2	-18.7 to 38.7	-0.3	-1.1
3	53	68.2	-62.3	66.4	9.6	11.9	32.0	-12.1 to 36.8	-0.2	-0.9
3	58	50.5	-59.3	52.5	7.9	9.1	28.6	-9.4 to 30.9	-0.4	-0.7
3	59	51.9	-56.2	64.4	7.5	8.4	32.8	-15.4 to 32.7	-0.1	-1.0
3	60	52.6	-62.3	65.7	9.1	5.3	33.7	-16.4 to 39.2	-0.1	-1.0
3	68	53.6	-58.1	63.3	11.6	11.0	34.2	-16.1 to 42.8	-0.2	-1.2
3	69	53.8	-54.3	59.2	8.1	4.2	32.4	-20.7 to 41.5	0.0	-1.3
3	70	48.8	-64.6	67.2	11.9	14.0	35.0	-14.3 to 44.0	-0.1	-1.2
Combined		525.1	-64.6	70.6	10.0	11.0	32.7	-14.6 to 38.7	-0.2	-1.0
4	78	85.3	-61.4	70.4	7.7	2.6	33.8	-13.5 to 35.8	0.0	-0.8
4	79	81.9	-58.3	66.9	5.2	0.1	32.8	-13.3 to 26.6	0.1	-0.7
4	80	83.9	-68.3	72.0	3.0	-1.0	33.1	-15.7 to 25.8	0.1	-0.5
4	85	52.7	-68.6	67.2	4.4	4.1	38.7	-27.0 to 41.3	-0.1	-1.2
4	86	56.0	-65.0	60.2	1.4	-3.8	33.6	-24.1 to 30.6	0.0	-1.0
4	87	49.8	-55.2	58.9	2.6	-1.6	32.7	-25.7 to 31.6	0.0	-1.2
4	96	44.6	-54.3	58.4	4.8	0.4	30.4	-20.7 to 33.2	0.1	-1.2
4	97	47.0	-57.0	59.6	5.3	-1.3	32.8	-17.4 to 36.2	0.1	-1.1
4	98	46.1	-57.6	66.1	7.9	-0.3	33.1	-14.5 to 37.6	0.1	-1.1
Combined		547.3	-68.6	72.0	4.7	0.3	33.6	-18.6 to 32.7	0.0	-0.9
All Subjects		1856.1	-77.9	72.0	4.7	2.2	32.2	-15.7 to 30.4	-0.1	-0.8

Table D-3.

Summary of moments and statistics for azimuth position, slalom course, TIO.
(azimuth values expressed in degrees, time in seconds)

Subject	Run	Time	Min	Max	Mean	Median	S.D.	IQR	Skew	Kurt
1	138	85.7	-60.0	58.3	3.1	3.8	25.0	-5.7 to 19.6	-0.4	0.0
1	139	109.7	-60.9	61.1	6.5	1.8	28.2	-4.1 to 29.4	-0.2	-0.3
1	140	120.4	-72.2	53.3	5.0	3.5	30.1	-6.6 to 31.9	-0.5	-0.4
Combined		315.8	-72.2	61.1	5.0	2.8	28.2	-5.2 to 27.0	-0.4	-0.2
2	163	70.0	-54.3	50.1	1.9	-1.0	22.9	-10.4 to 18.0	-0.1	-0.3
2	164	82.5	-63.6	56.7	1.4	-2.9	26.1	-10.7 to 19.6	-0.0	-0.3
2	166	80.1	-58.3	52.1	-0.6	-0.9	25.0	-12.3 to 16.5	-0.4	-0.1
2	167	88.1	-67.9	63.3	2.0	0.7	27.3	-10.9 to 13.9	-0.1	0.0
Combined		320.7	-67.9	63.3	1.2	-1.0	25.5	-10.9 to 17.7	-0.1	-0.1
3	144	70.9	-63.1	57.5	4.3	4.0	28.4	-9.6 to 26.1	-0.3	-0.4
3	145	89.3	-55.2	58.1	1.5	1.0	26.6	-18.8 to 22.2	0.0	-0.8
3	146	97.9	-67.1	60.3	1.0	-3.2	27.4	-11.2 to 18.6	-0.2	-0.1
3	155	71.9	-68.4	54.7	-0.5	-2.9	28.9	-18.1 to 21.9	-0.2	-0.6
3	157	84.4	-57.3	50.7	0.5	0.2	234.0	-12.8 to 17.4	-0.3	-0.2
Combined		414.4	-68.4	60.3	1.3	-0.1	27.1	-13.4 to 20.1	-0.2	-0.4
4	None									
All Subjects		1059.9	-72.2	63.3	2.4	0.9	27.0	-10.9 to 21.3	-0.2	-0.3

Table D-4.
 Summary moments and statistics for azimuth position, slalom course, RWS.
 (azimuth values expressed in degrees, time in seconds)

Subject	Run	Time	Min	Max	Mean	Median	S.D.	IQR	Skew	Kurt
1	141	106.2	-58.9	57.8	7.3	3.8	26.6	-4.4 to 29.4	-0.3	-0.3
1	142	102.0	-61.4	49.9	2.5	0.2	22.2	-4.5 to 10.2	-0.1	0.7
1	143	120.0	-60.5	53.1	6.2	0.9	25.7	-3.9 to 26.1	-0.1	-0.1
Combined		328.2	-61.4	57.8	5.4	1.4	25.0	-4.3 to 24.5	-0.2	-0.0
2	168	83.2	-66.3	40.0	1.2	-2.9	24.2	-8.7 to 20.1	-0.4	-0.1
2	169	89.1	-51.1	54.3	5.1	1.9	25.9	-9.2 to 24.1	0.1	-0.7
2	170	101.1	-53.1	56.3	1.1	-2.7	21.6	-7.6 to 11.3	0.4	0.4
2	174	63.6	-49.4	61.1	2.5	-3.5	28.2	-15.3 to 26.8	0.2	-1.5
2	175	65.0	-66.2	42.8	0.0	-4.6	25.8	-10.1 to 18.3	-0.3	-0.5
2	176	63.8	-50.3	53.6	1.8	-3.9	26.0	-19.3 to 23.2	0.2	-0.9
Combined		465.8	-66.3	61.1	2.0	-2.6	25.1	-10.9 to 18.2	0.0	-0.4
3	158	71.2	-49.7	47.3	2.9	1.2	23.0	-8.8 to 17.8	-0.2	-0.5
3	159	94.8	-60.2	43.3	0.4	3.8	22.6	-10.7 to 13.9	-0.5	-0.2
3	161	61.2	-58.2	53.8	1.1	1.8	25.1	-10.0 to 12.9	-0.1	-0.1
3	162	55.3	-51.0	51.0	-0.6	-1.9	25.6	-14.5 to 12.9	0.0	-0.6
3	180	59.6	-66.6	50.5	2.4	7.7	30.9	-17.9 to 27.5	-0.3	-0.9
3	181	58.9	-67.7	53.1	-1.1	5.0	28.9	-17.5 to 15.9	-0.3	-0.5
3	182	52.9	-59.1	55.3	4.1	4.8	31.5	-18.1 to 32.5	-0.2	-1.1
3	183	43.9	-60.0	48.9	0.2	3.5	29.1	-20.2 to 23.0	-0.2	-0.9
Combined		497.8	-67.7	55.3	1.1	2.7	26.8	-13.7 to 19.0	-0.2	-0.5
4	None									
All Subjects		1291.8	-67.7	61.1	2.5	0.6	25.8	-10.2 to 19.6	-0.1	-0.4

Appendix E

Azimuth position box-plots.

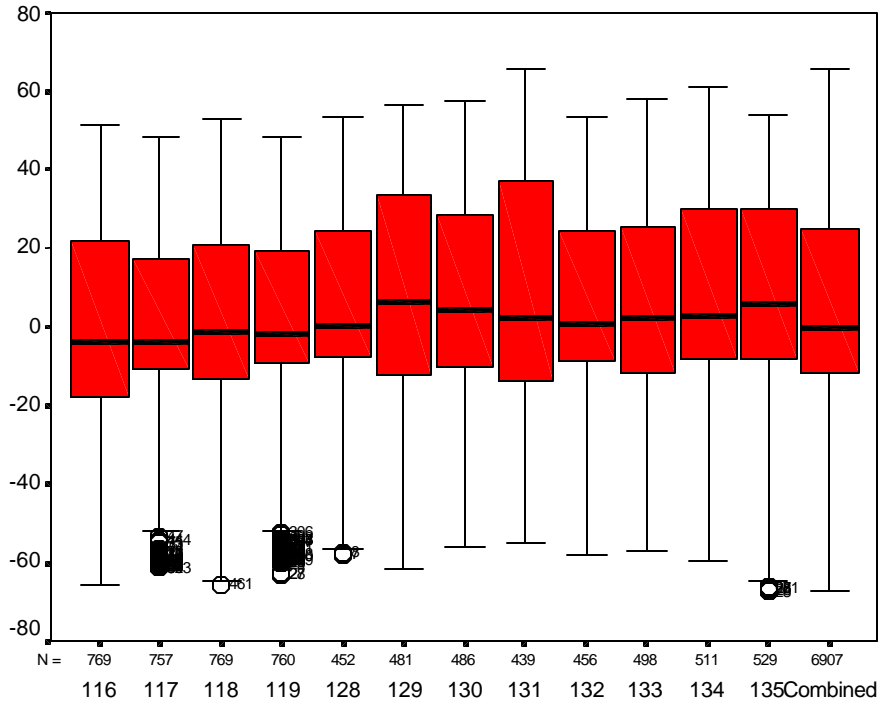


Figure E-1. Subject #1 GVE box plots.

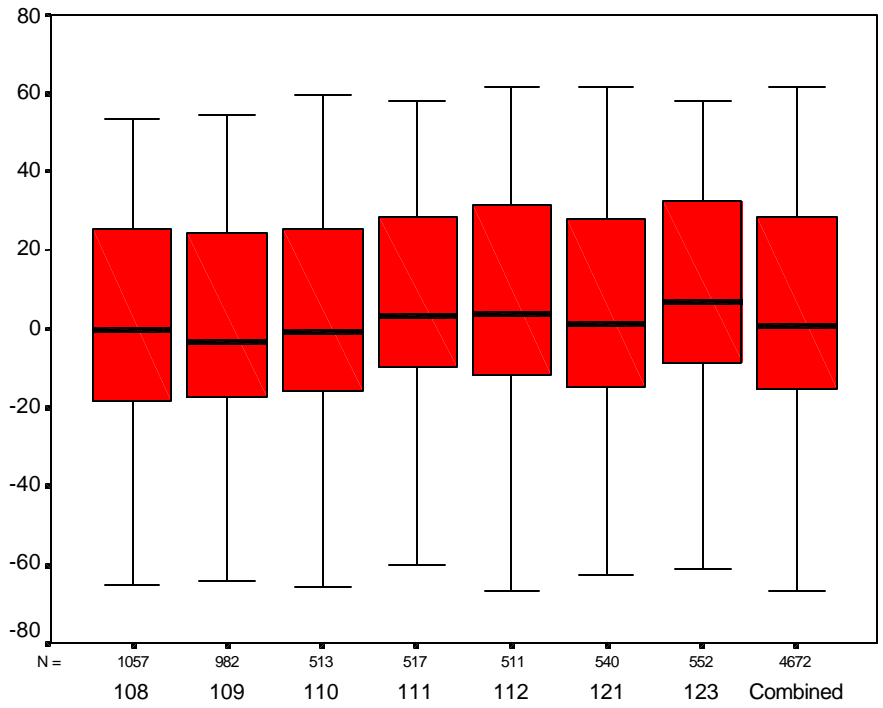


Figure E-2. Subject #1 NVG box plots.

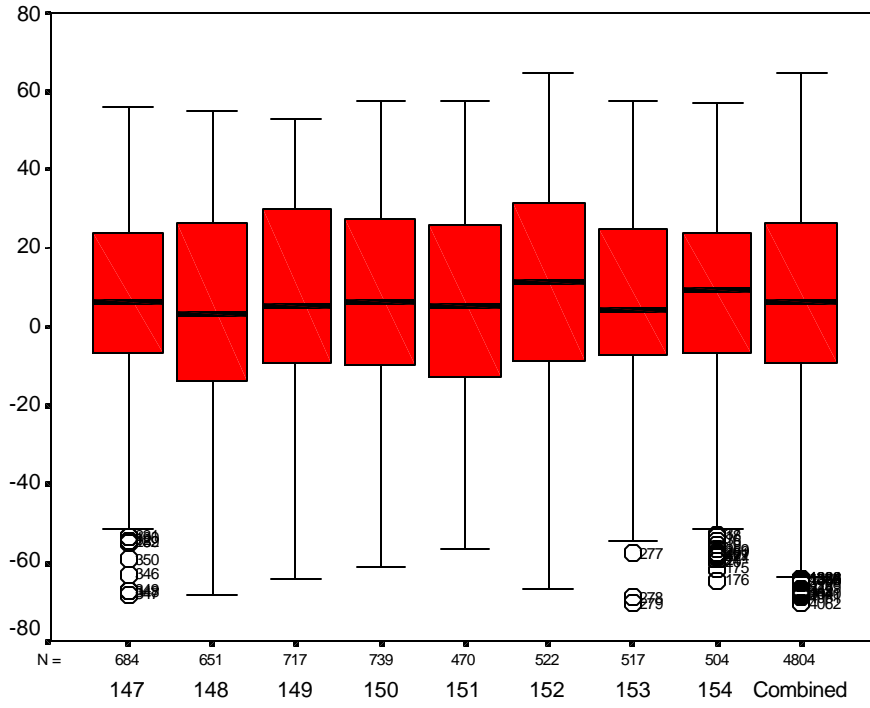


Figure E-5. Subject #2 GVE box plots.

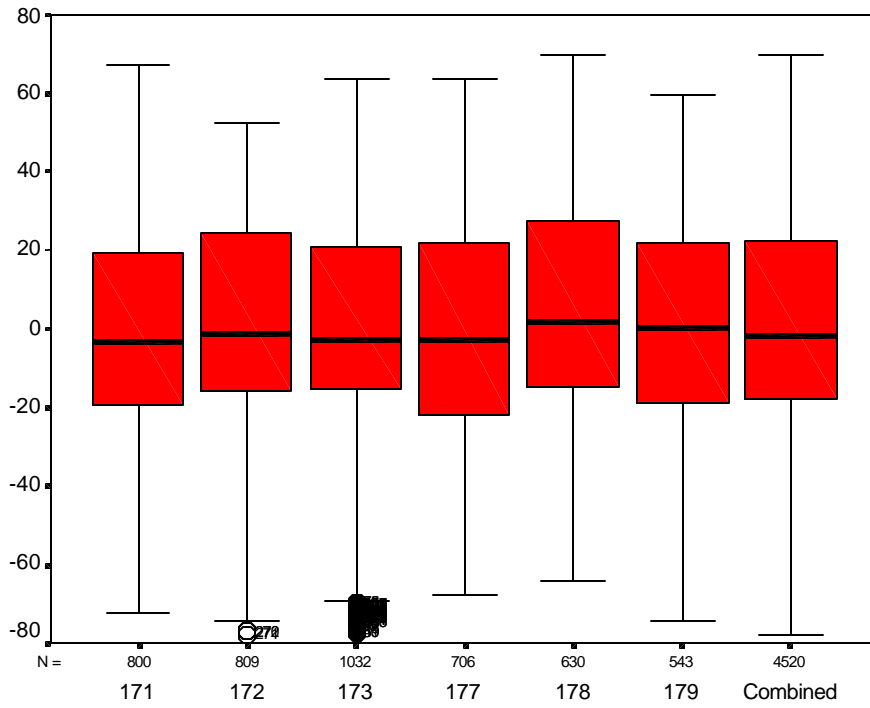


Figure E-6. Subject #2 NVG box plots.

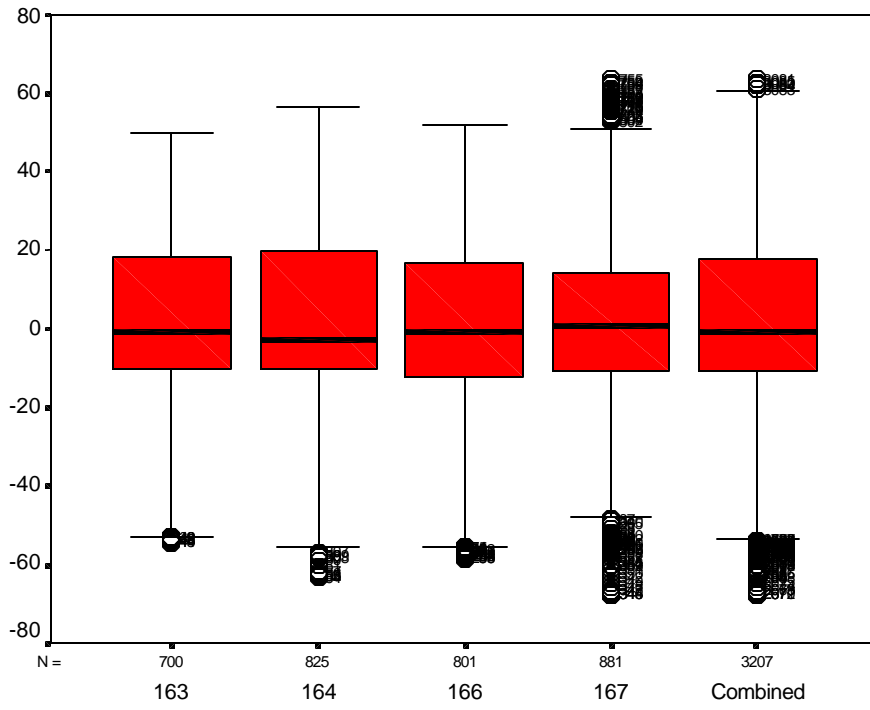


Figure E-7. Subject #2 TIO box plots.

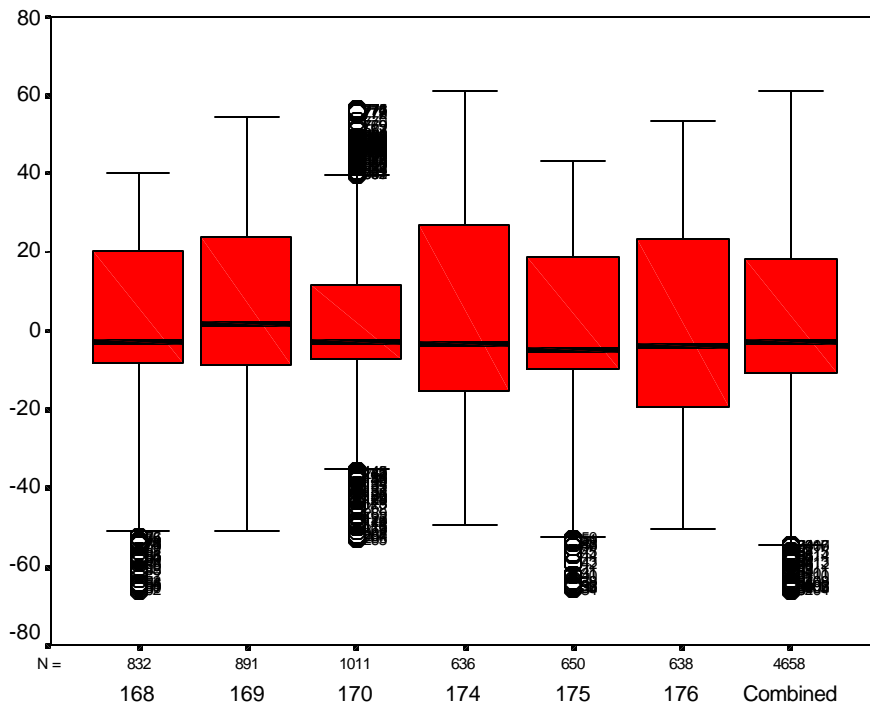


Figure E-8. Subject #2 RWS box plots.

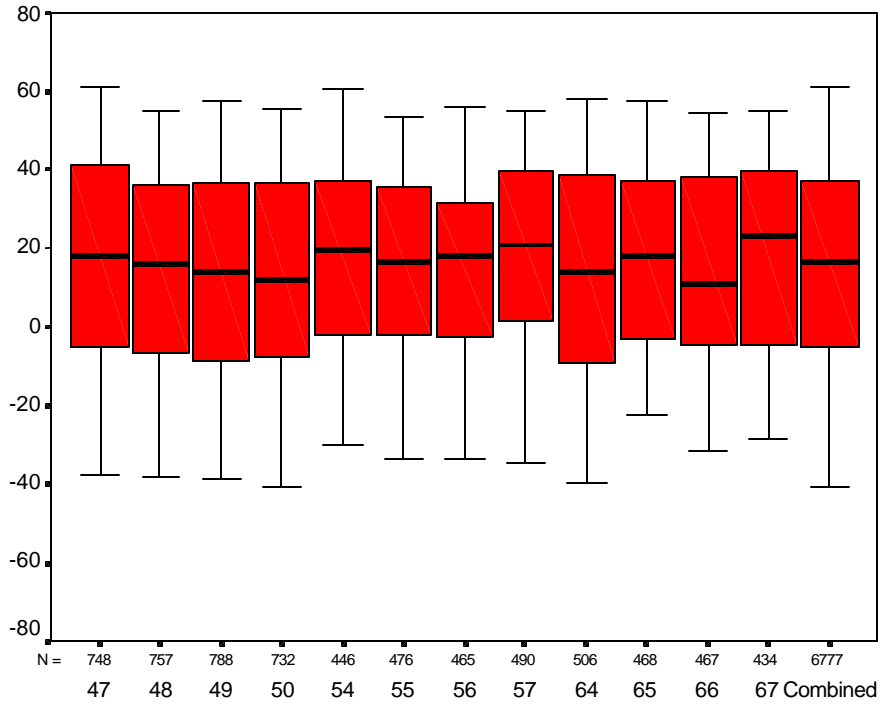


Figure E-9. Subject #3 GVE box plots.

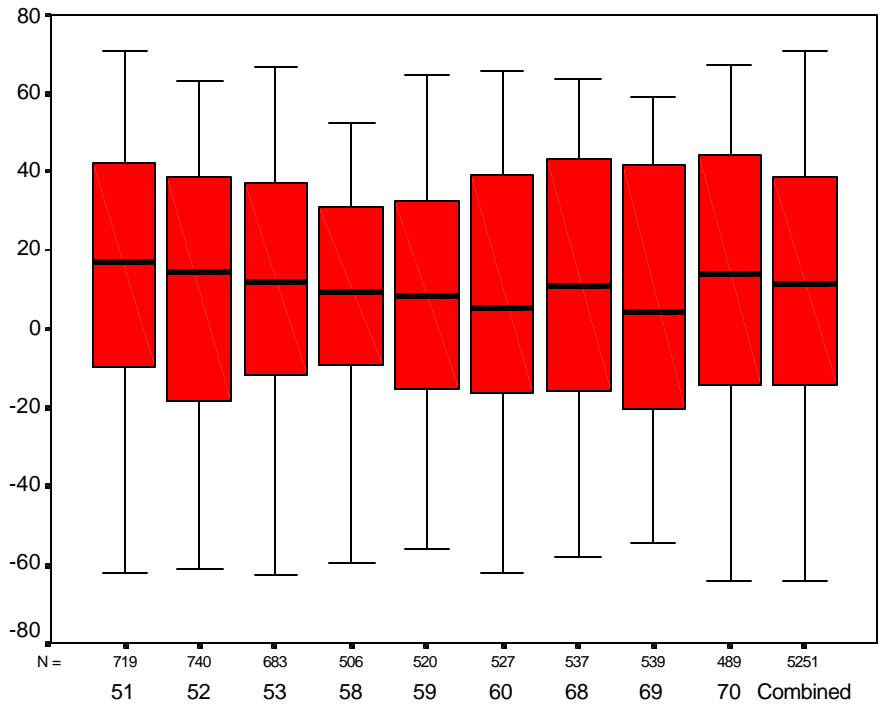


Figure E-10. Subject #3 NVG box plots.

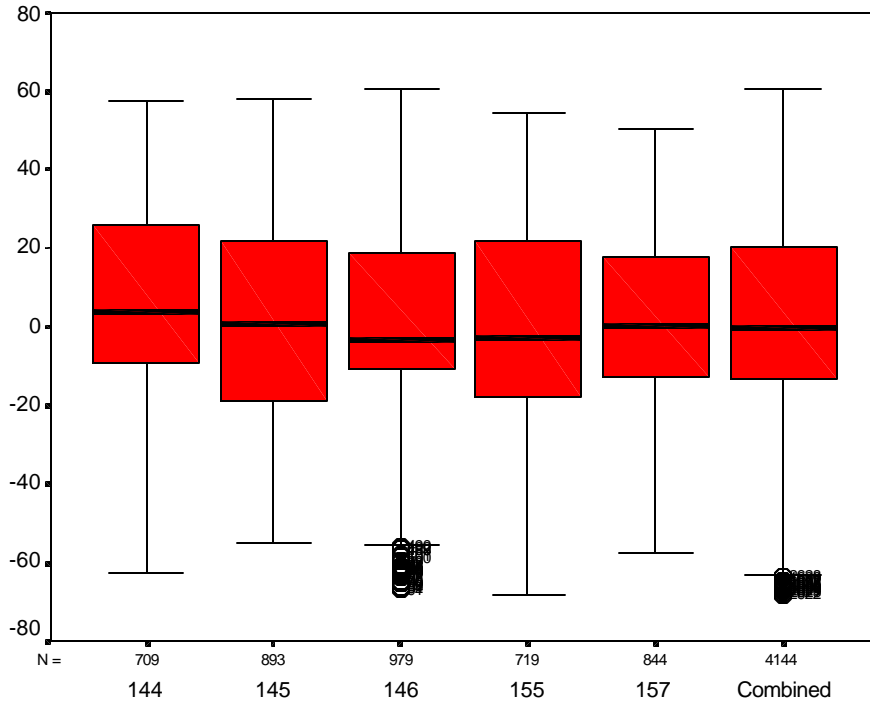


Figure E-11. Subject #3 TIO box plots.

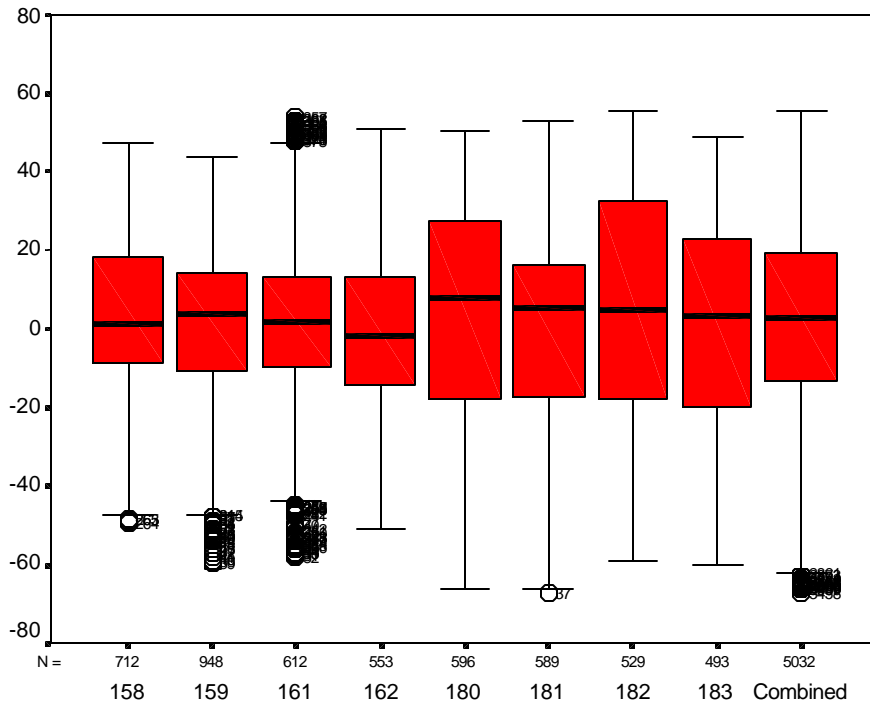


Figure E-12. Subject #3 RWS box plots.

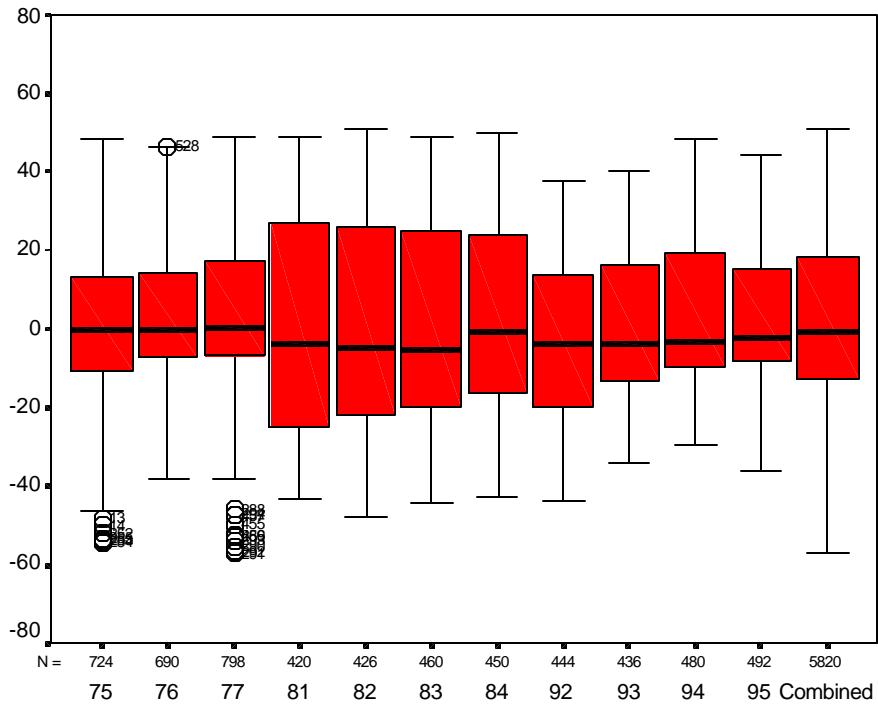


Figure E-13. Subject #4 GVE box plots.

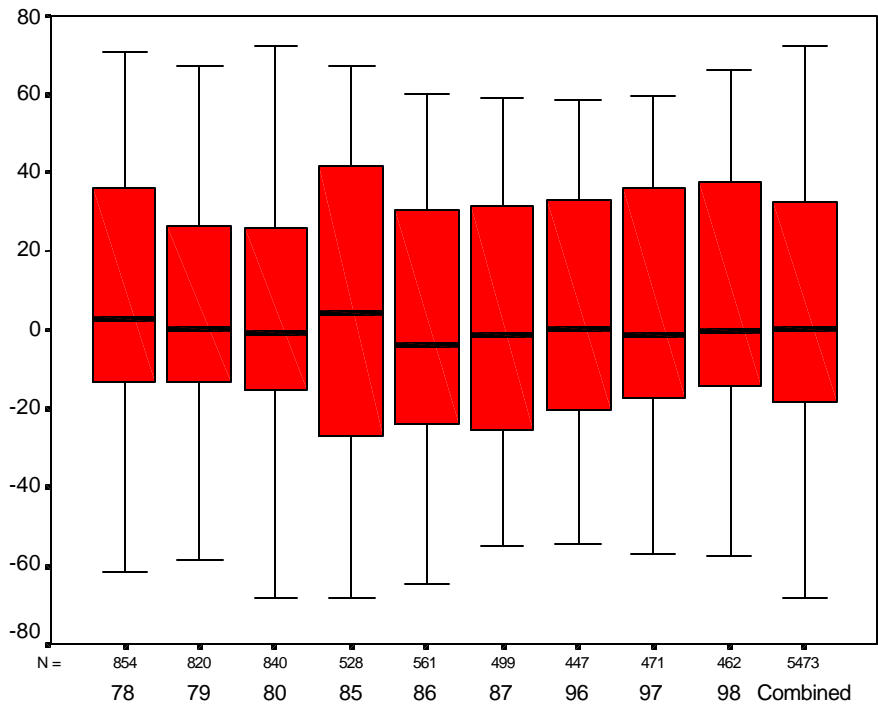


Figure E-14. Subject #4 NVG box plots.

Appendix F.

Azimuth position quantile curves for all subjects and visual environments.

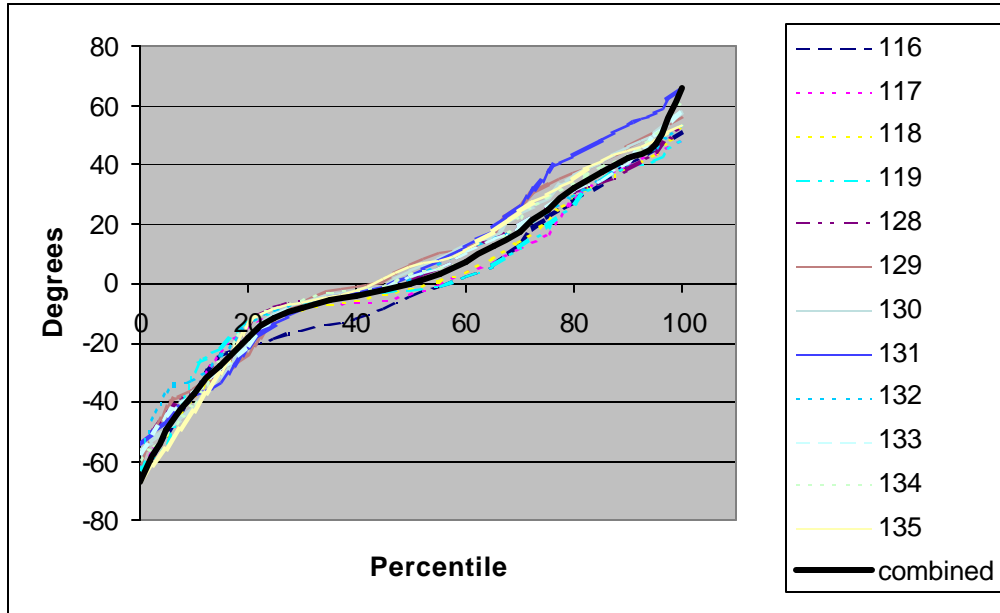


Figure F-1. Quantile curves for subject #1, GVE.

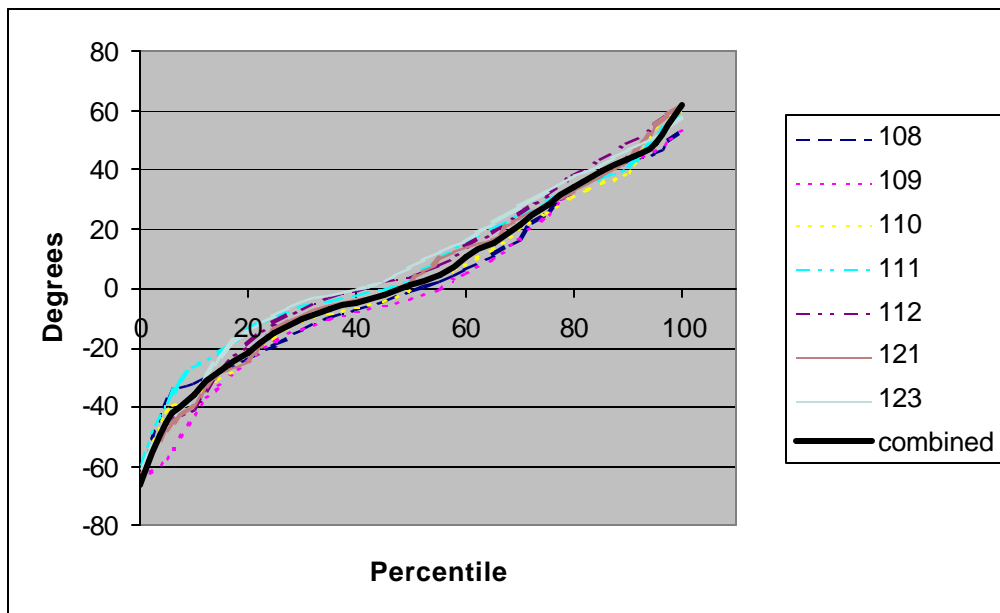


Figure F-2. Quantile curves for subject #1, NVG.

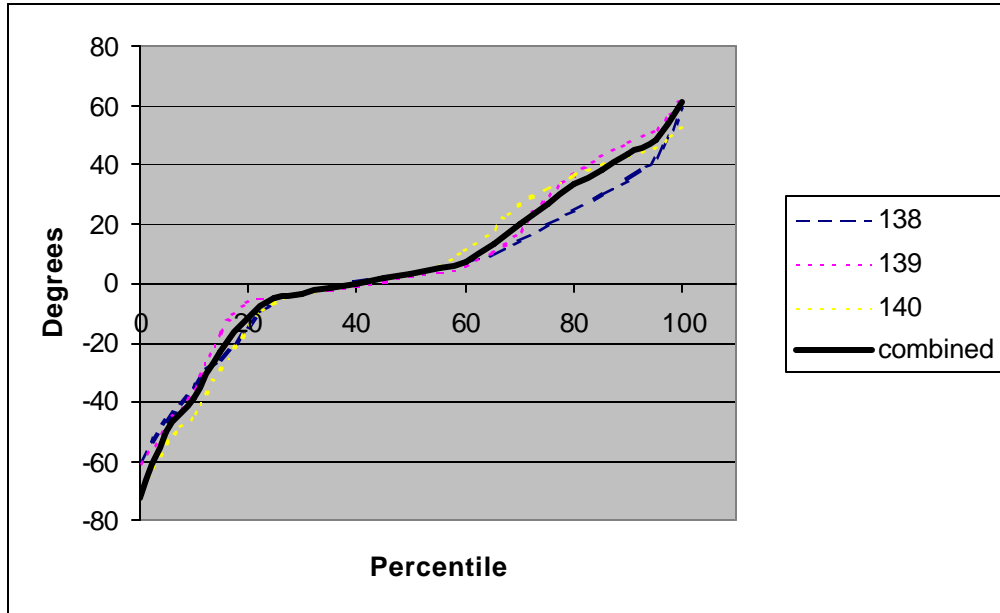


Figure F-3. Quantile curves for subject #1, TIO.

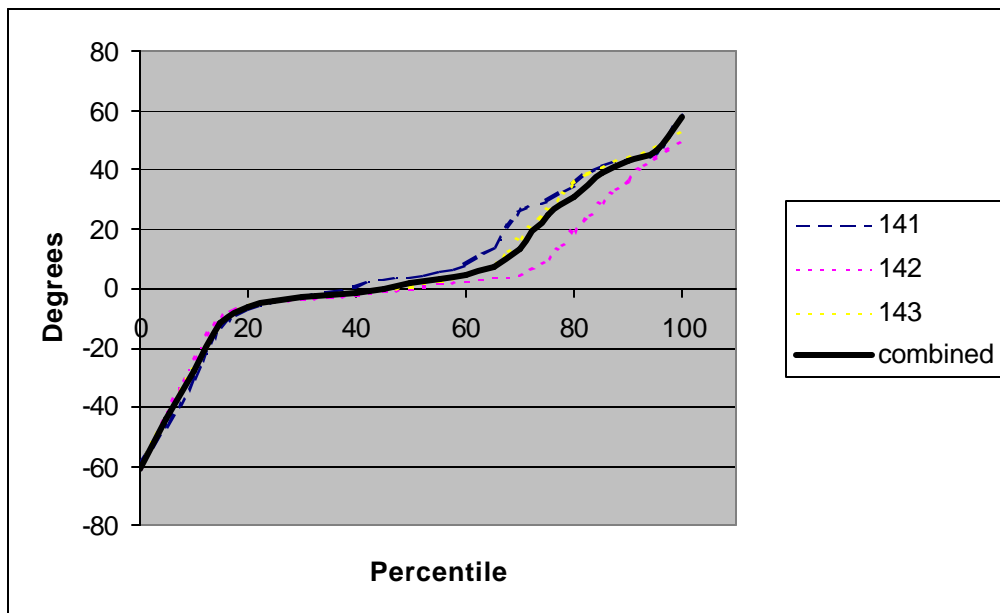


Figure F-4. Quantile curves for subject #1, RWS.

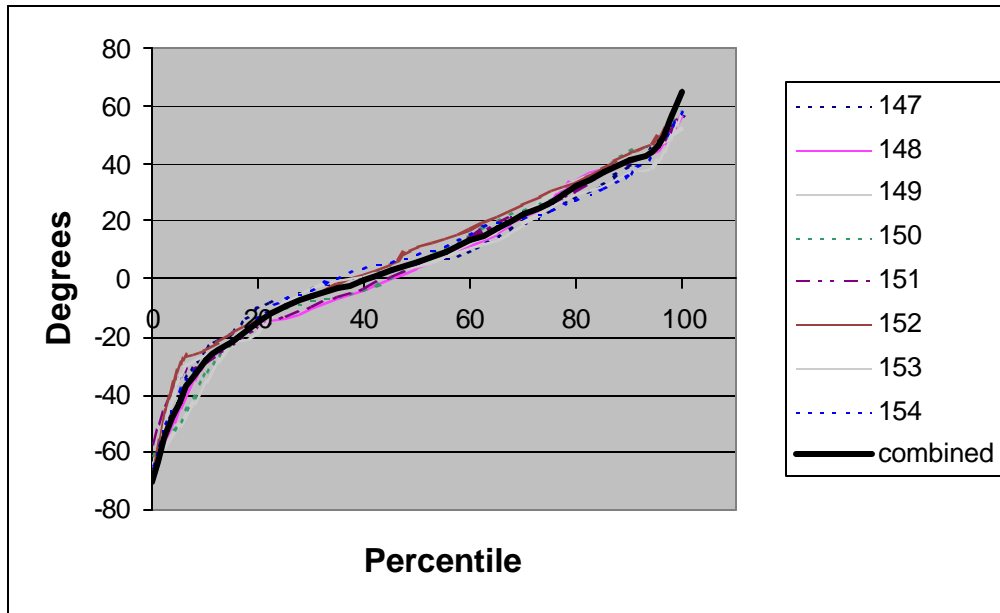


Figure F-5. Quantile curves for subject #2, GVE.

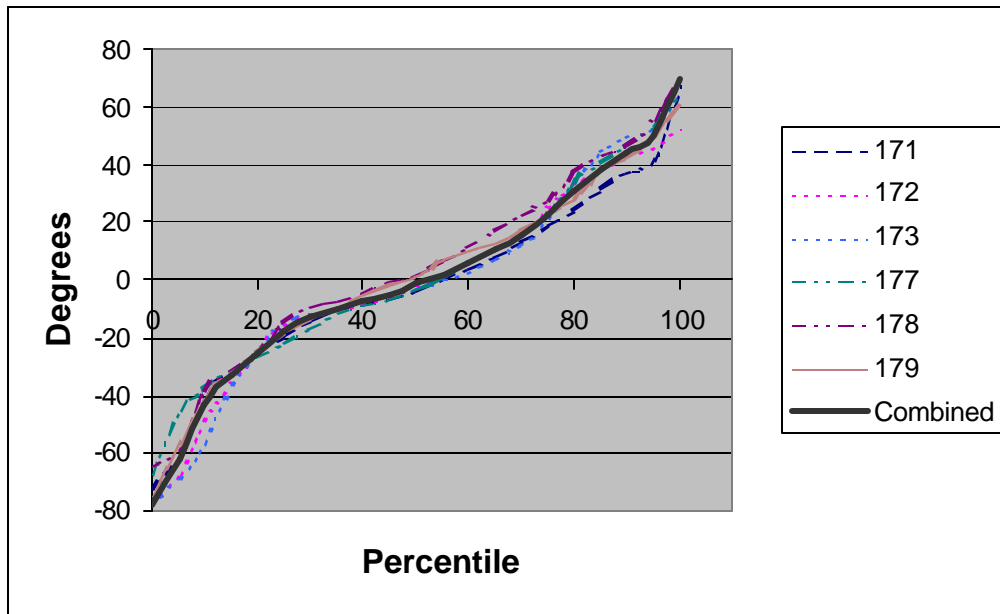


Figure F-6. Quantile curves for subject #2, NVG.

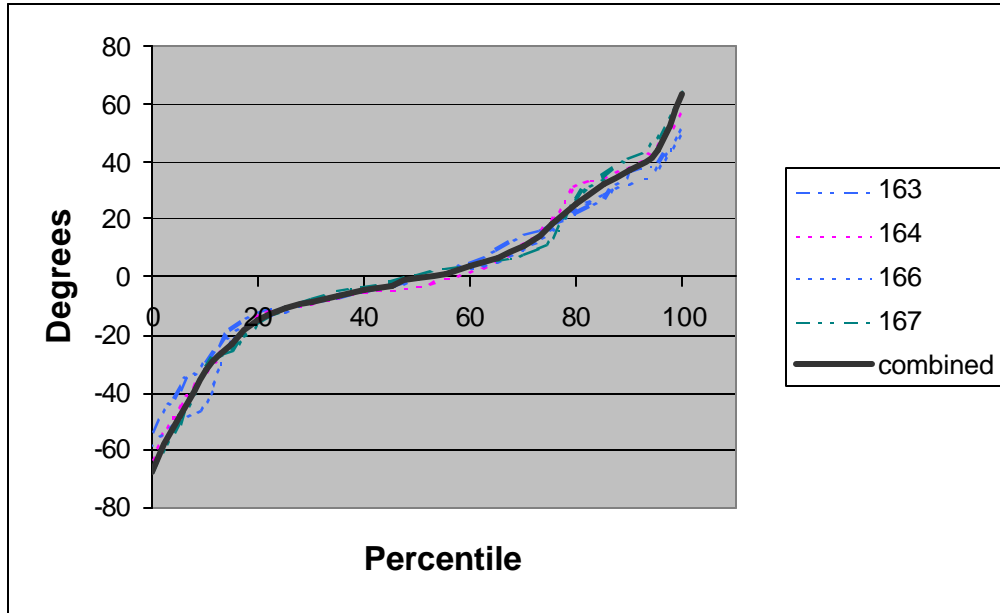


Figure F-7. Quantile curves for subject #2, TIO.

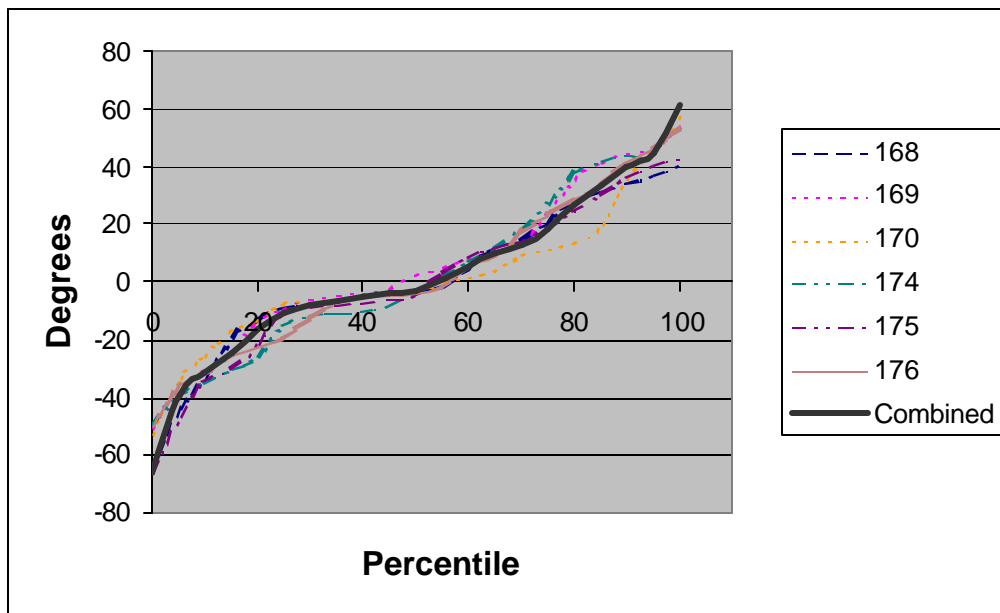


Figure F-8. Quantile curves for subject #2, RWS.

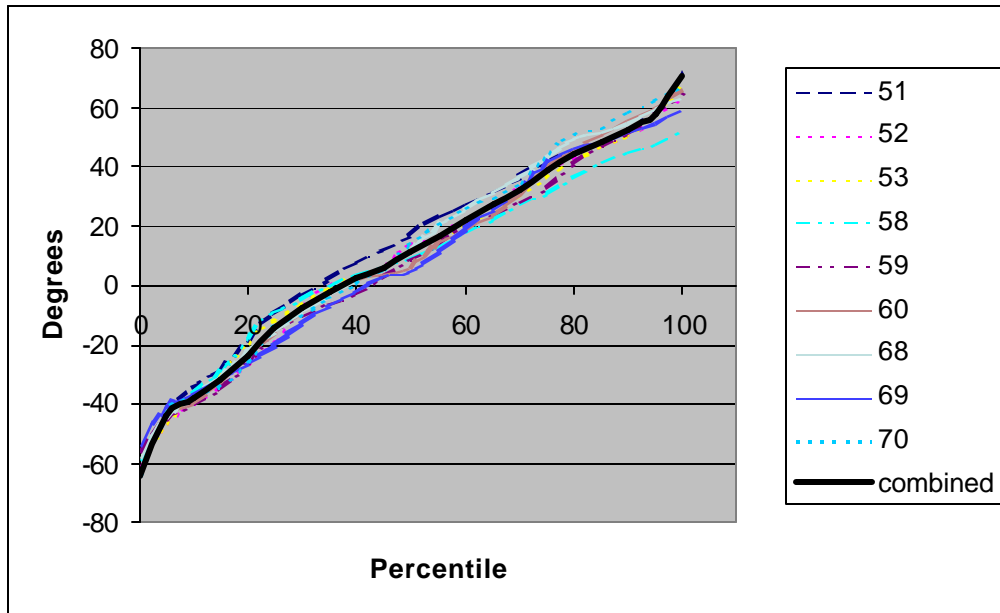


Figure F-9. Quantile curves for subject #3, GVE.

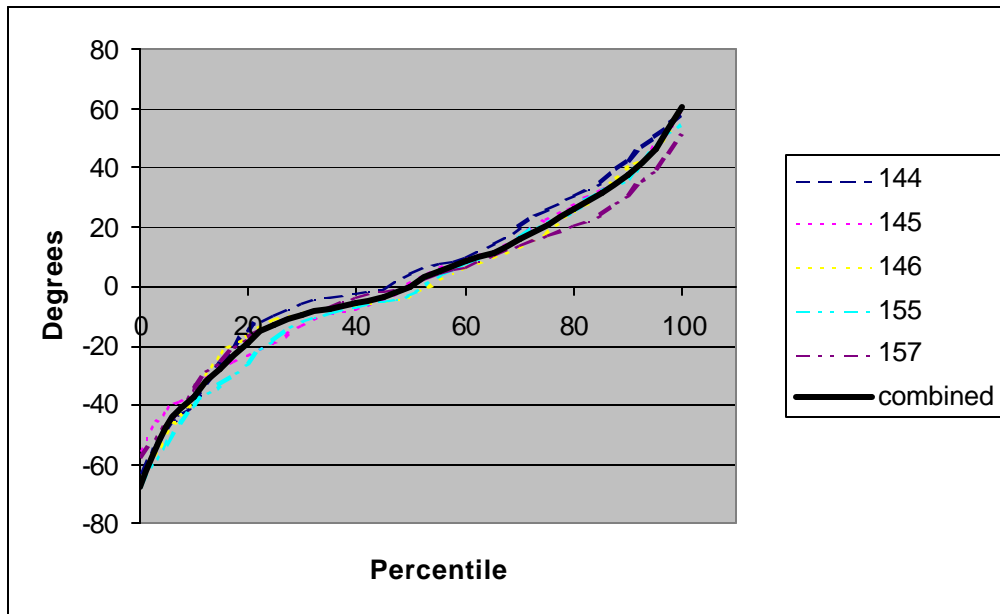


Figure F-10. Quantile curves for subject #3, NVG.

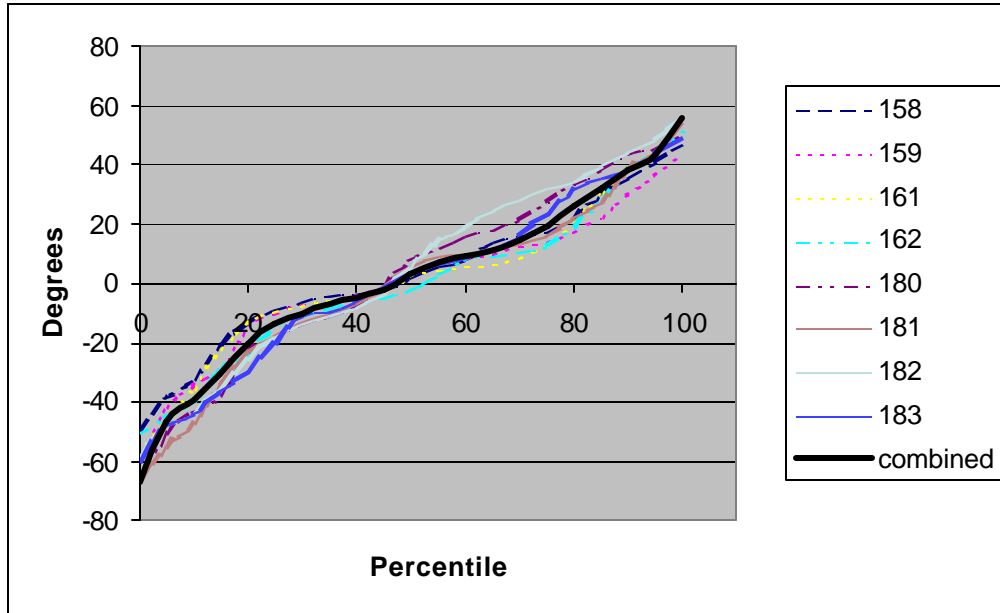


Figure F-11. Quantile curves for subject #3, TIO.

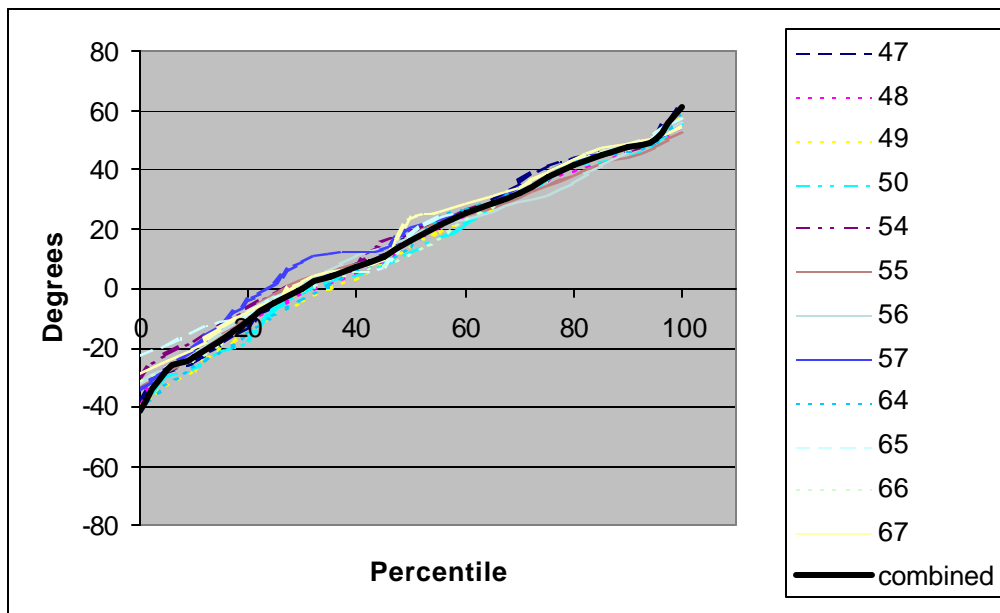


Figure F-12. Quantile curves for subject #3, RWS.

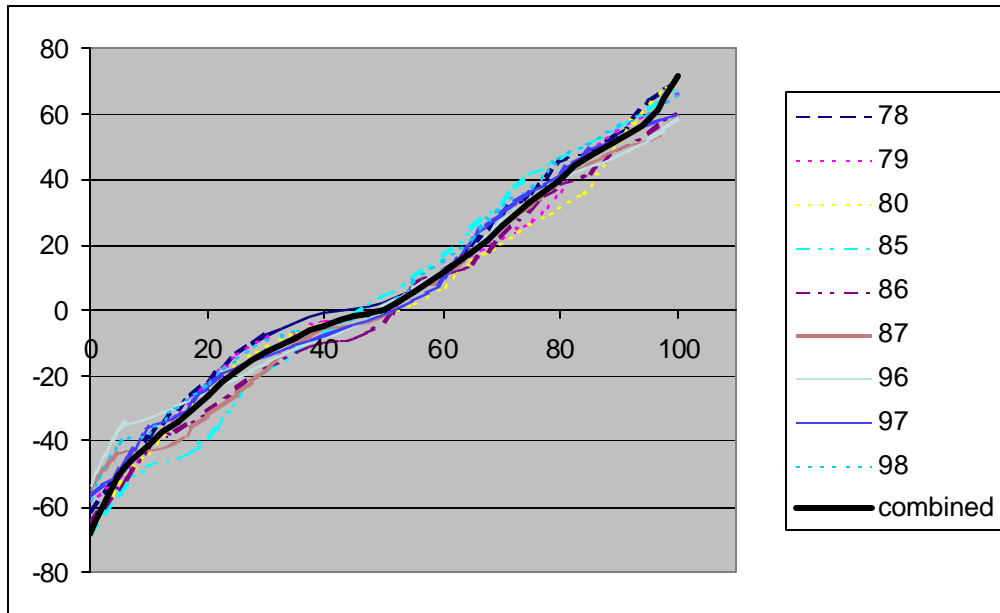


Figure F-13. Quantile curves for subject #4, GVE.

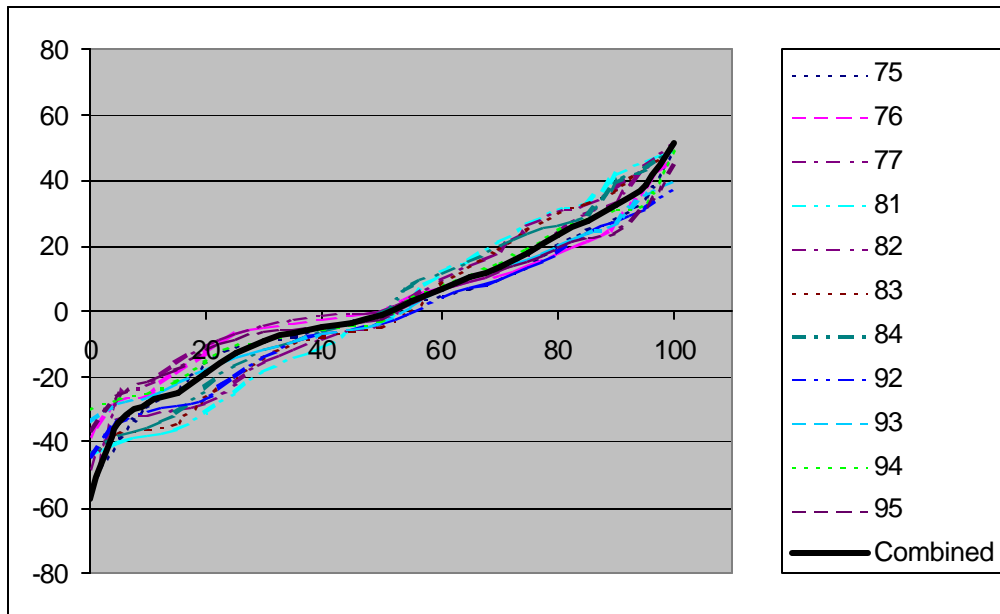


Figure F-14. Quantile curves for subject #4, NVG.

Appendix G.

Azimuth reversal summary tables.

Table G-1.
Summary statistics for azimuth reversals, slalom course, GVE.
(expressed in degrees)

Subject	Run	Time	# of Reversals	Rev/min
1	116	76.9	56	43.7
1	117	75.7	46	36.5
1	118	76.9	47	36.7
1	119	76.0	54	42.6
1	128	45.2	27	35.8
1	129	48.1	24	29.8
1	130	48.6	32	39.5
1	131	43.8	22	30.1
1	132	45.6	27	35.5
1	133	49.8	25	30.1
1	134	51.1	31	36.4
1	135	52.9	27	30.6
Combined		690.6	418	35.6
2	147	68.4	39	34.2
2	148	65.1	45	41.5
2	149	71.7	47	39.3
2	150	73.9	53	43.0
2	151	47.0	28	35.7
2	152	52.2	35	40.2
2	153	51.7	29	33.7
2	154	50.4	37	44.0
Combined		480.4	313	39.0
3	47	74.8	55	44.1
3	48	75.7	50	39.6
3	49	78.8	49	37.3
3	50	73.2	46	37.7
3	54	44.6	22	29.6
3	55	47.6	17	21.4
3	56	46.5	21	27.1
3	57	49.0	17	20.8
3	64	50.6	27	32.0
3	65	46.8	28	35.9
3	66	46.7	23	29.6
3	67	43.4	18	24.9
Combined		677.7	373	31.7
4	75	72.4	48	39.8
4	76	69.0	31	27.0
4	77	79.8	53	39.8
4	81	42.0	16	22.9
4	82	42.6	11	15.5
4	83	46.0	16	20.9
4	84	45.0	17	22.7
4	92	44.4	18	24.3
4	93	43.6	15	20.6
4	94	48.0	16	20.0
4	95	49.2	24	29.3
Combined		582	265	25.7
All Subjects		2430.7	1369	33.8

Table G-2.
 Summary statistics for azimuth reversals, slalom course, NVG.
 (expressed in degrees)

Subject	Run	Time	# of Reversals	Rev / min
1	108	105.7	77	43.7
1	109	98.2	72	44.0
1	110	51.3	27	31.6
1	111	51.7	38	44.1
1	112	51.1	31	36.4
1	121	54.0	26	28.9
1	123	55.2	39	42.4
Combined		467.2	310	38.7
2	171	80.0	55	41.3
2	172	80.9	50	37.1
2	173	103.2	66	38.4
2	177	70.6	46	39.1
2	178	63.0	35	33.3
2	179	54.3	31	34.3
Combined		452.0	283	37.3
3	51	71.8	55	46.0
3	52	73.9	56	45.5
3	53	68.2	47	41.3
3	58	50.5	28	33.3
3	59	51.9	31	35.8
3	60	52.6	33	37.6
3	68	53.6	42	47.0
3	69	53.8	38	42.4
3	70	48.8	38	46.7
Combined		525.1	368	41.7
4	78	95.3	55	34.6
4	79	81.9	52	38.1
4	80	83.9	57	40.8
4	85	52.7	28	31.9
4	86	56.0	33	35.4
4	87	49.8	26	31.3
4	96	44.6	21	28.3
4	97	47.0	23	29.4
4	98	46.1	16	20.8
Combined		557.3	311	32.3
All Subjects		2001.6	1272	38.1

Table G-3.
 Summary statistics for azimuth reversals, slalom course, TIO.
 (expressed in degrees)

Subject	Run	Time	# of Reversals	Rev /min
1	138	85.7	46	32.2
1	139	109.7	66	36.1
1	140	120.4	61	30.4
Combine d		315.8	173	32.9
2	163	70.0	38	32.6
2	164	82.5	46	33.5
2	166	80.1	34	25.5
2	167	88.1	39	26.6
Combine d		320.7	157	29.6
3	144	70.9	39	33.0
3	145	89.3	52	34.9
3	146	97.9	59	36.2
3	155	71.9	45	37.6
3	157	84.4	42	29.9
Combine d		414.4	237	34.3
4				
All Subjects		1050.9	567	32.4

Table G-4.
 Summary statistics for azimuth reversals, slalom course, RWS.
 (expressed in degrees)

Subject	Run	Time	# of Reversals	Rev /min
1	141	106.2	49	27.7
1	142	102.0	58	34.1
1	143	120.0	66	33.0
Combined		328.2	173	31.6
2	168	83.2	34	24.5
2	169	89.1	40	26.9
2	170	101.1	44	26.1
2	174	63.6	21	19.8
2	175	65.0	25	23.1
2	176	63.8	25	23.5
Combined		465.8	189	24.0
3	158	71.2	28	23.6
3	159	94.8	41	25.9
3	161	61.2	27	26.5
3	162	55.3	21	22.8
3	180	59.6	29	29.2
3	181	58.9	35	35.7
3	182	52.9	19	21.6
3	183	43.9	21	28.7
Combined		497.8	221	26.8
4	None			
All Subjects		1291.8	583	27.1

Appendix H.

Azimuth excursion distributions.

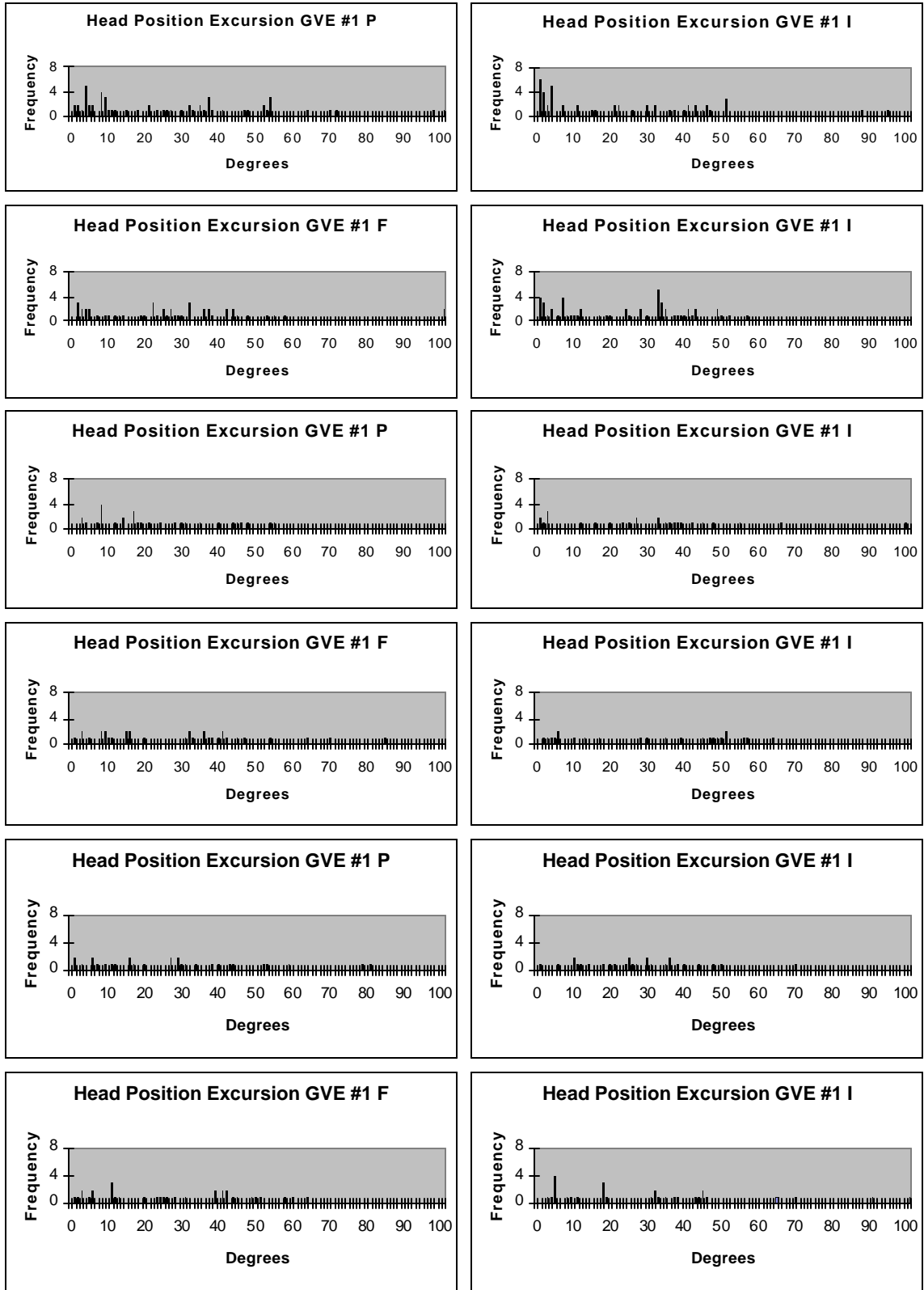


Figure H-1. Subject #1 GVE head position excursion histograms.

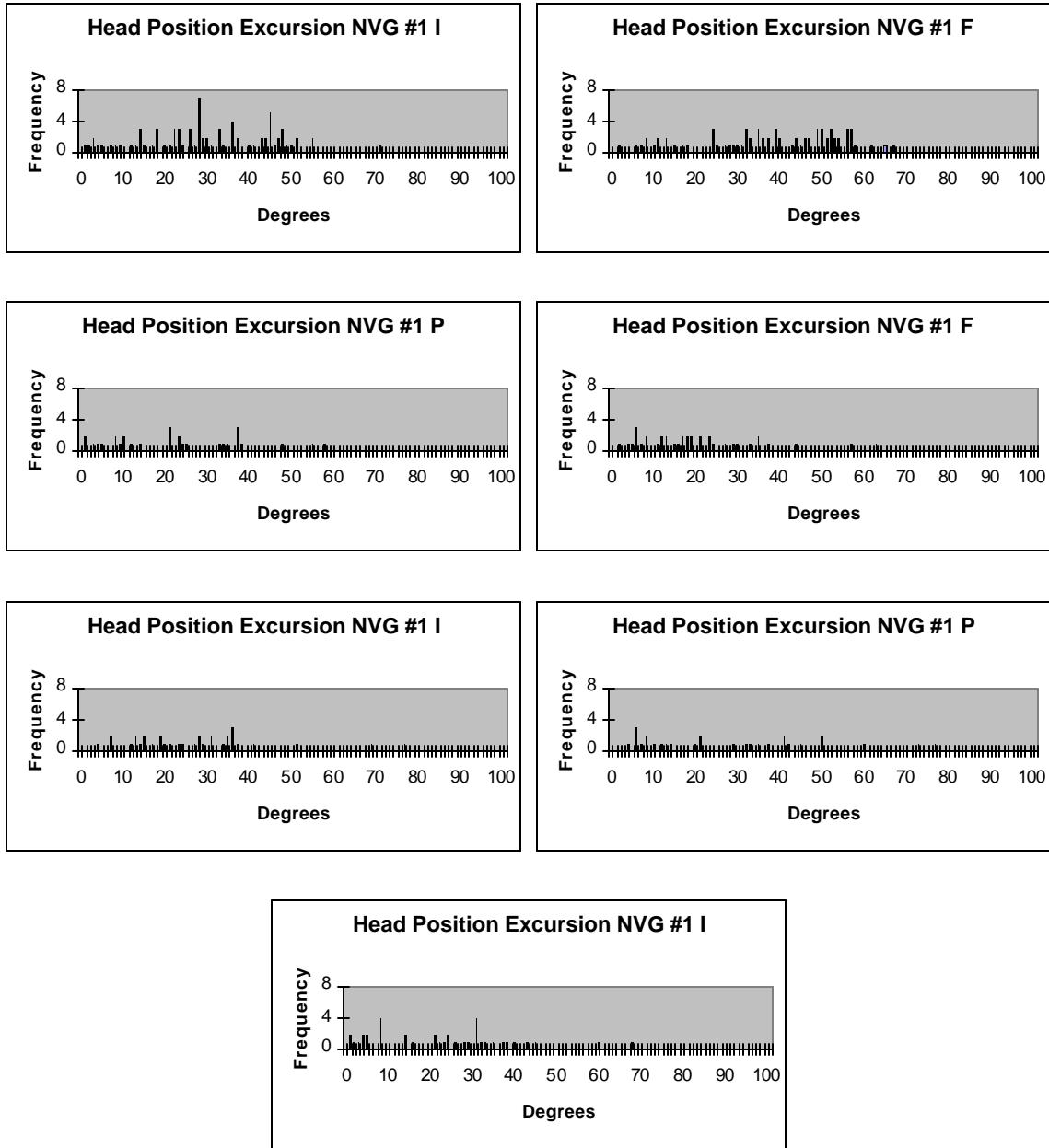


Figure H-2. Subject #1 NVG head position excursion histograms.

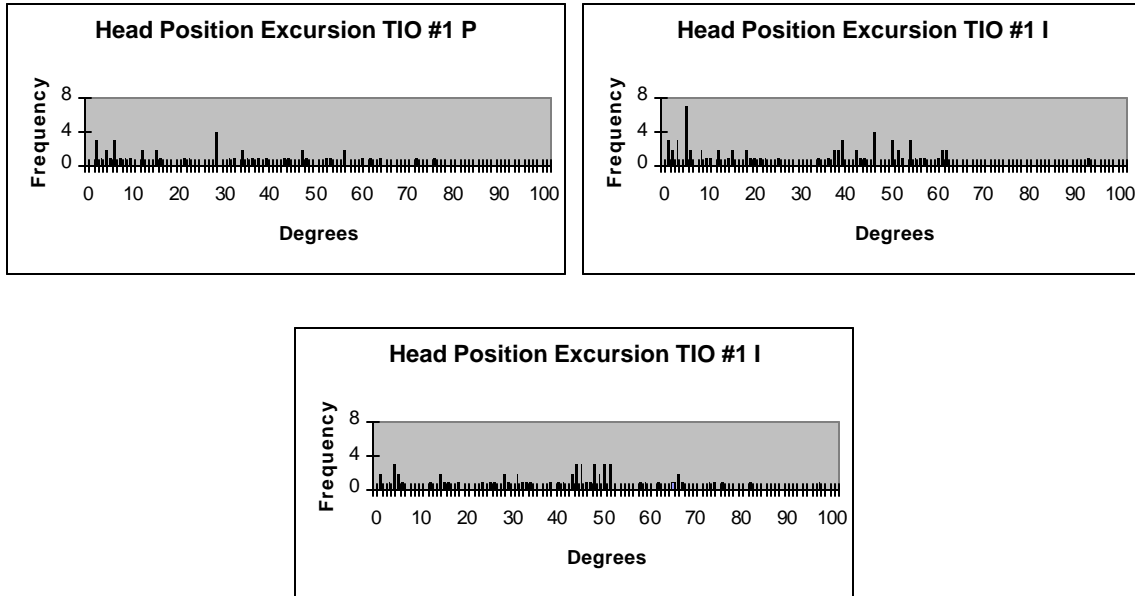


Figure H-3. Subject #1 TIO head position excursion histograms.

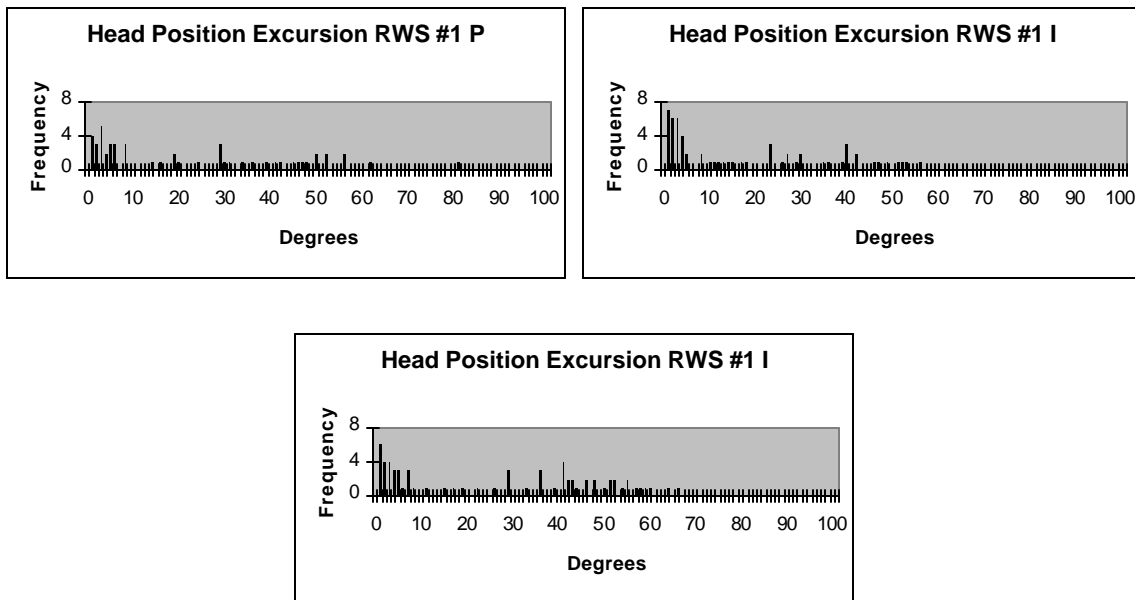


Figure H-4. Subject #1 RWS head position excursion histograms.

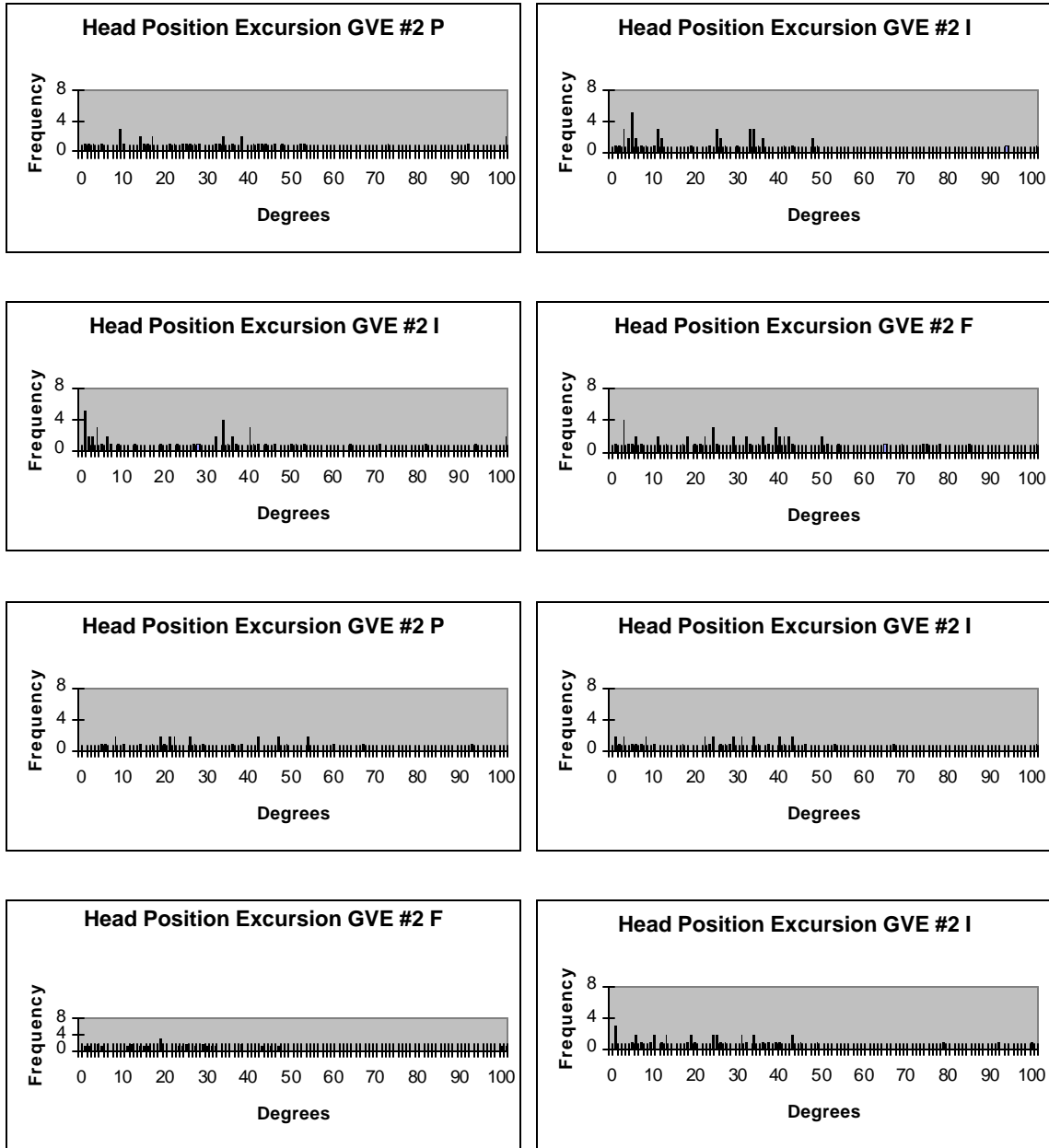


Figure H-5. Subject #2 GVE head position excursion histograms.

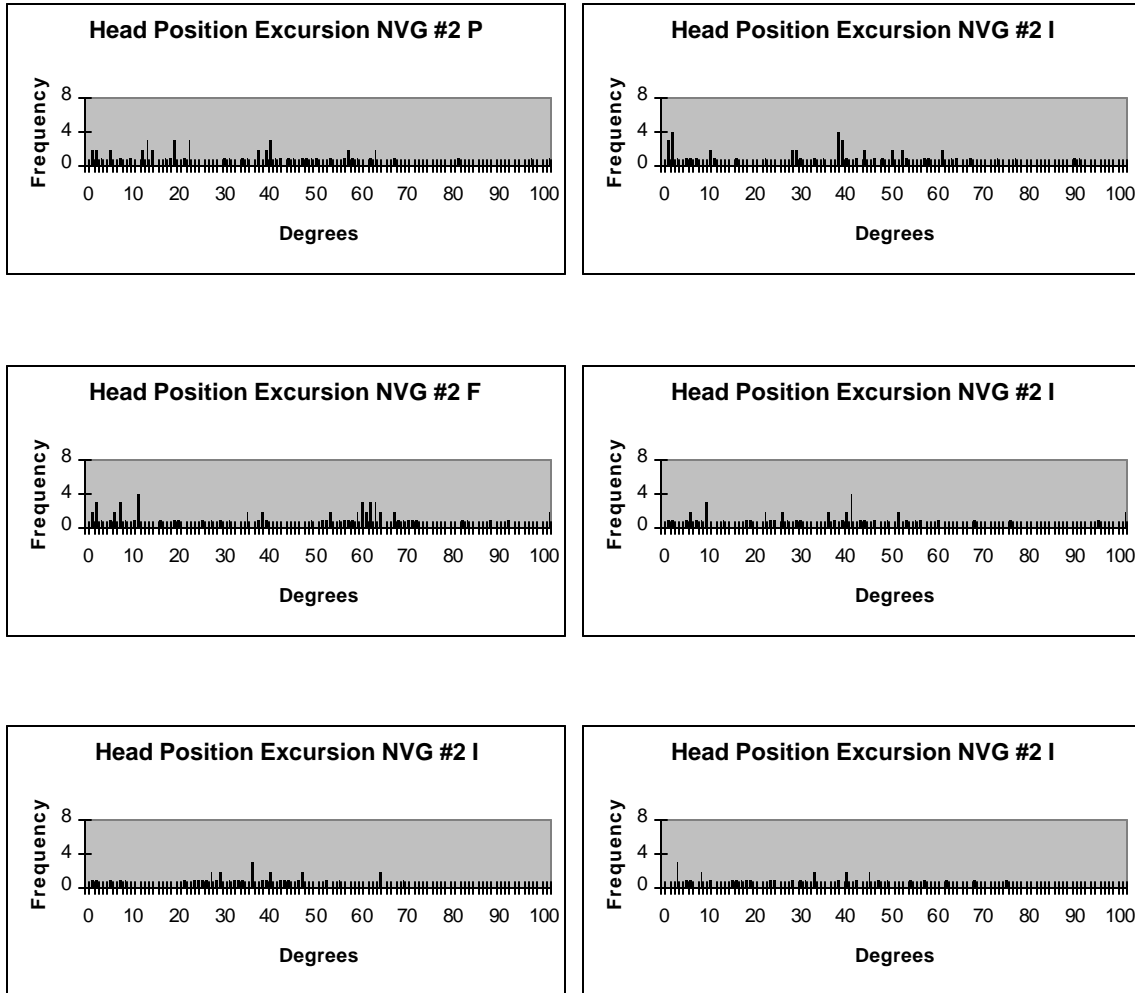


Figure H-6. Subject #2 NVG head position excursion histograms.

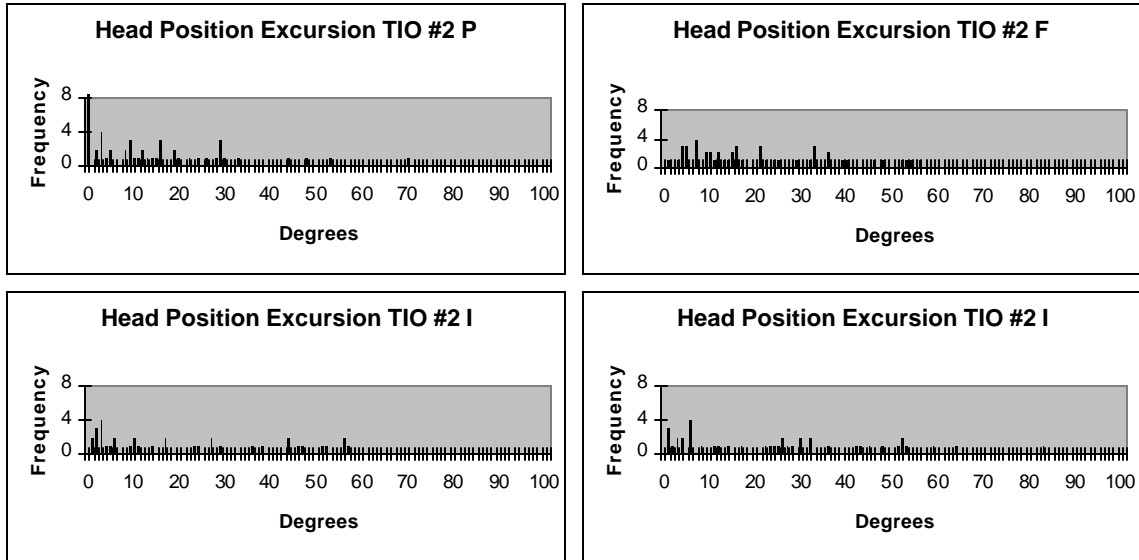


Figure H-7. Subject #2 TIO head position excursion histograms.

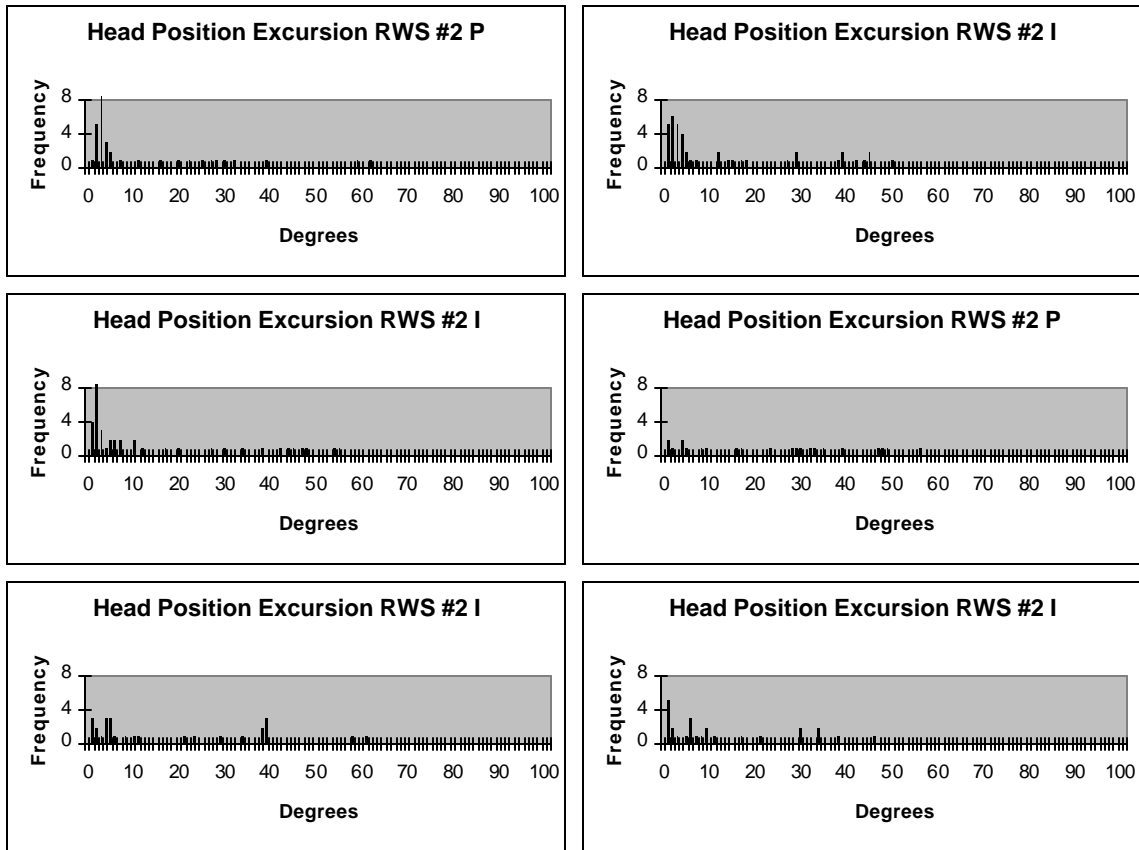


Figure H-8. Subject #2 RWS head position excursion histograms.

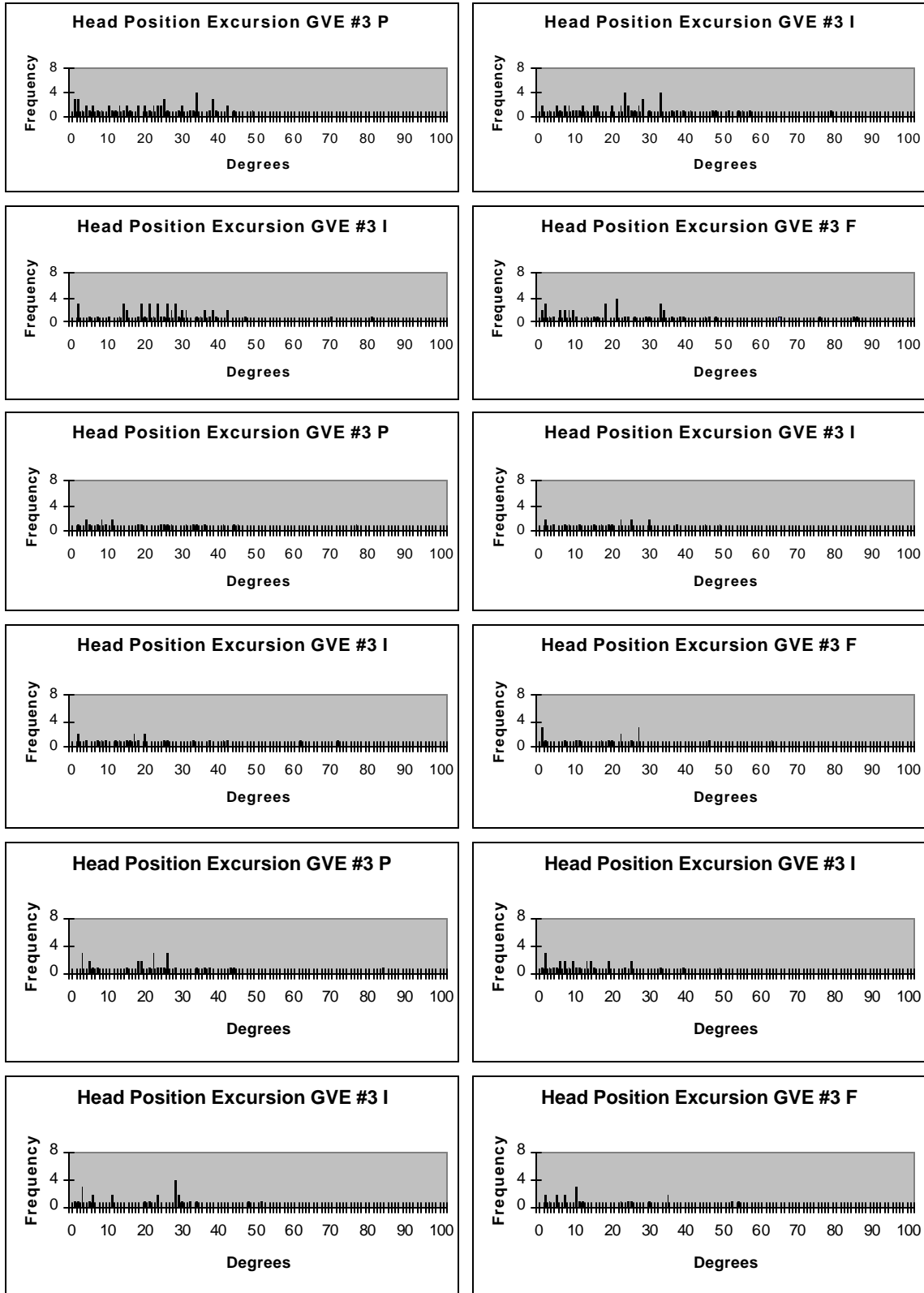


Figure H-9. Subject #3 GVE head position excursion histograms.

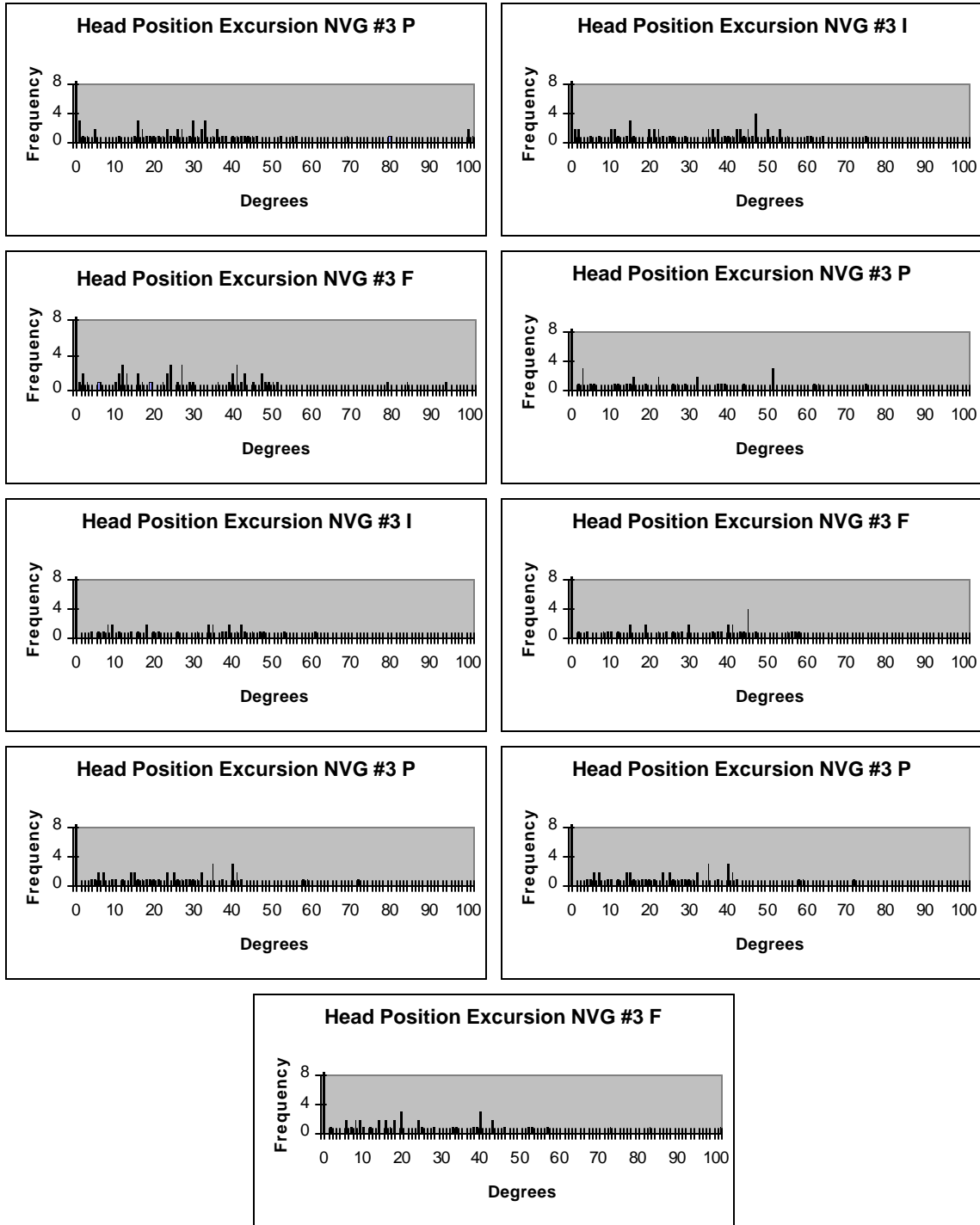


Figure H-10. Subject #3 NVG head position excursion histograms.

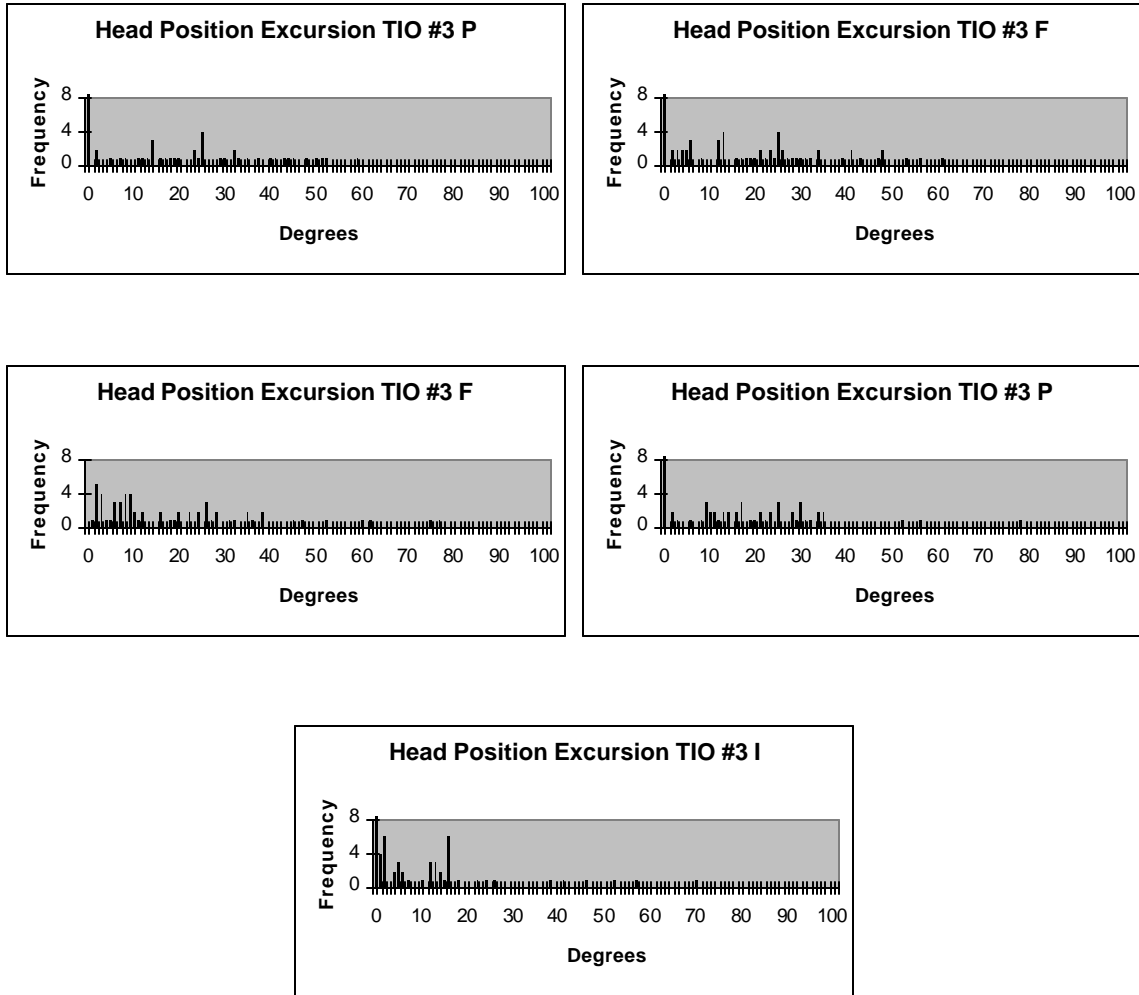


Figure H-11. Subject #3 TIO head position excursion histograms.

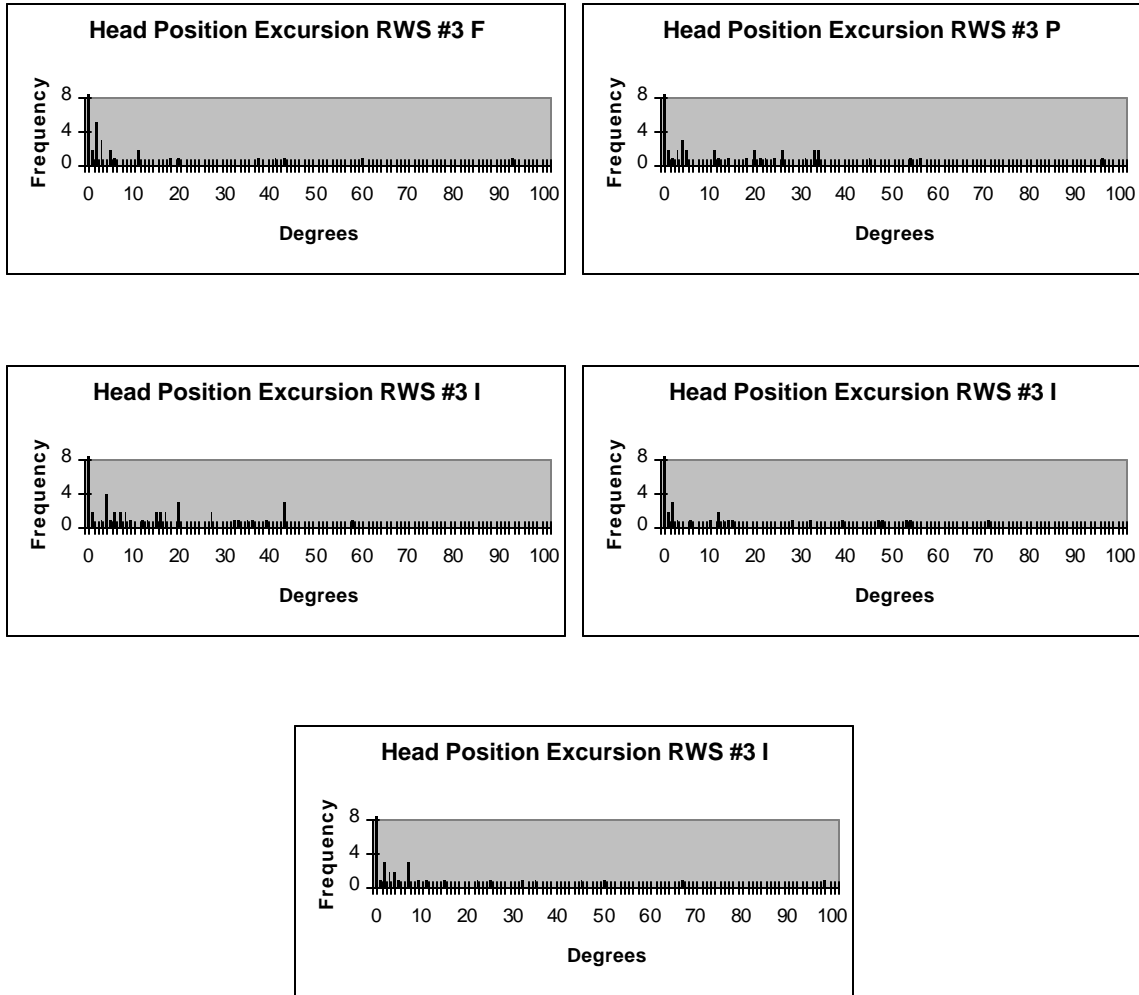


Figure H-12. Subject #3 RWS head position excursion histograms.

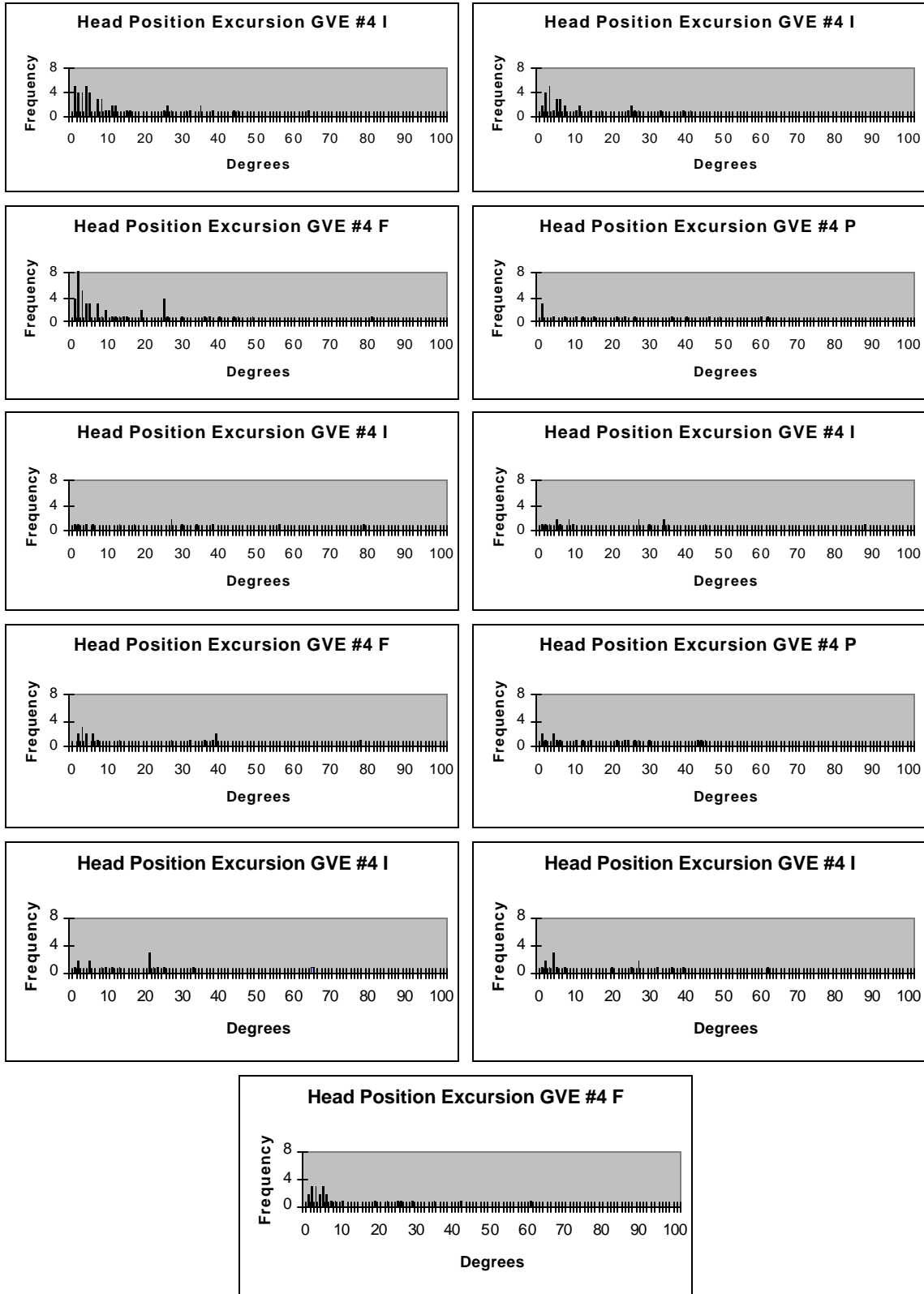


Figure H-13. Subject #4 GVE head position excursion histograms.

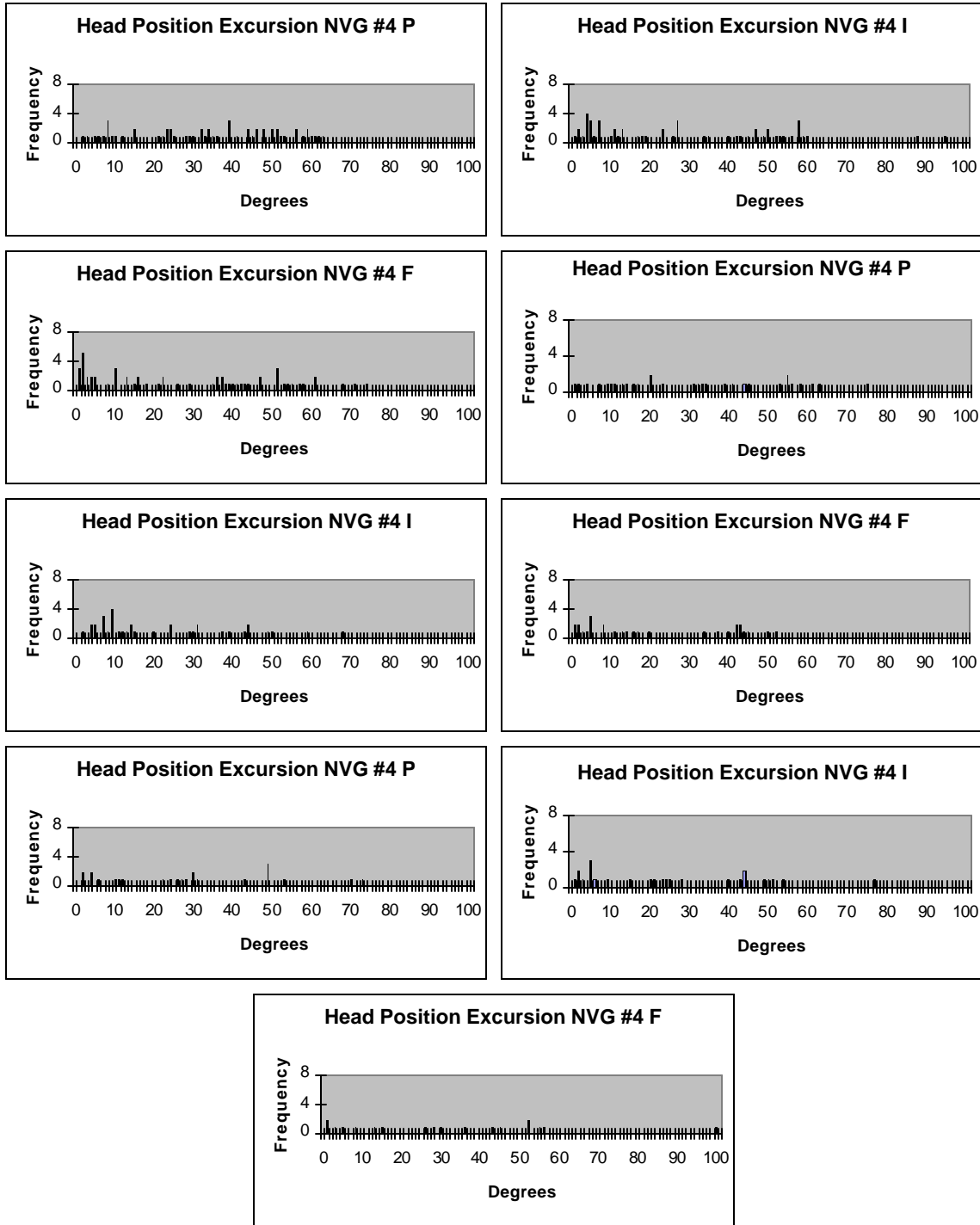


Figure H-14. Subject #4 NVG head position excursion histograms.

Appendix I.

Azimuth excursion summary tables.

Table I-1.
Summary statistics for azimuth excursions, slalom course, GVE.
(excursion values expressed in degrees)

Subject	Run	Time	# of Excursions	Exc/min	Min	Max	Mean	Median	S.D.	IQR
1	116	76.9	57	44.5	0.2	114.3	27.2	21.2	25.2	6.3 to 38.3
1	117	75.7	47	37.3	0.6	95.4	23.6	21.3	22.9	3.5 to 40.5
1	118	76.9	48	37.5	0.4	112.5	28.0	26.3	23.1	9.7 to 37.5
1	119	76.0	55	43.4	0.1	56.7	23.3	25.4	17.0	6.7 to 36.2
1	128	45.2	28	37.2	2.6	55.5	23.7	18.8	16.5	8.3 to 36.0
1	129	48.1	25	31.2	1.1	99.6	29.1	27.1	23.3	11.5 to 37.6
1	130	48.6	33	40.7	0.1	85.2	27.9	31.7	21.5	9.0 to 40.7
1	131	43.8	23	31.5	2.2	64.3	32.4	36.7	21.0	10.9 to 49.8
1	132	45.6	28	36.8	0.8	81.4	29.0	28.0	22.0	10.3 to 41.1
1	133	49.8	26	31.3	1.4	69.6	26.8	25.6	15.4	15.1 to 36.1
1	134	51.1	32	37.6	0.8	63.6	28.7	26.8	19.1	11.3 to 42.3
1	135	52.9	28	31.8	2.9	115.2	32.0	31.6	27.6	8.9 to 43.8
Combined		690.6	430	37.4	0.1	115.2	27.1	26.0	21.6	7.2 to 38.3
2	147	68.4	40	35.1	0.1	119.2	32.7	27.6	27.1	15.2 to 43.0
2	148	65.1	46	42.4	1.1	104.8	23.7	23.8	22.1	5.6 to 33.9
2	149	71.7	48	40.2	0.8	104.7	30.2	32.3	27.4	4.6 to 41.2
2	150	73.9	54	43.8	0.4	109.1	32.5	32.2	24.0	14.0 to 41.2
2	151	47.0	29	37.0	4.7	93.0	31.2	26.1	20.7	19.2 to 44.8
2	152	52.2	36	41.4	0.9	101.7	27.0	26.4	20.8	8.3 to 39.5
2	153	51.7	30	34.8	1.2	111.8	26.8	23.7	24.7	12.7 to 30.9
2	154	50.4	38	45.2	0.6	100.3	28.1	25.1	23.1	10.8 to 37.6
Combined		480.4	321	40.1	0.1	119.2	29.1	26.1	24.0	9.8 to 40.1
3	47	74.8	56	44.9	1.0	48.6	20.9	21.5	13.1	10.1 to 32.1
3	48	75.7	51	40.4	0.7	78.7	23.9	23.1	16.1	11.6 to 33.0
3	49	78.8	50	38.1	1.6	80.5	25.8	24.6	14.7	18.3 to 30.9
3	50	73.2	47	38.5	0.3	86.1	23.9	19.4	21.7	7.0 to 33.6
3	54	44.6	23	30.9	1.7	76.7	22.6	18.9	18.3	7.6 to 33.3
3	55	47.6	18	22.7	1.7	48.5	20.1	19.6	13.7	9.0 to 25.3
3	56	46.5	22	28.4	1.6	71.6	22.6	17.1	18.6	9.8 to 31.0
3	57	49.0	18	22.0	0.1	63.5	18.0	18.1	16.8	3.3 to 25.7
3	64	50.6	28	33.2	2.5	84.4	22.8	21.6	16.9	13.4 to 26.3
3	65	46.8	29	37.2	0.5	48.5	12.7	9.29	11.6	4.9 to 14.9
3	66	46.7	24	30.8	0.7	51.2	19.8	22.1	14.6	5.6 to 28.7
3	67	43.4	19	26.3	1.9	52.2	16.1	9.93	14.0	6.1 to 24.6
Combined		677.7	385	34.1	0.1	86.1	21.6	20.3	16.3	8.1 to 30.0
4	75	72.4	49	40.6	0.2	63.7	13.0	7.18	14.6	3.3 to 16.5
4	76	69.0	32	27.8	0.8	41.1	11.2	5.79	11.6	2.8 to 15.2
4	77	79.8	54	40.6	0.1	80.9	12.6	4.58	16.2	2.2 to 17.8
4	81	42.0	17	24.3	0.3	62.5	21.8	15.2	20.8	4.3 to 36.3
4	82	42.6	12	16.9	0.8	78.9	26.5	27.1	23.5	5.1 to 34.7
4	83	46.0	17	22.2	0.4	87.9	19.7	8.3	22.7	4.9 to 29.8
4	84	45.0	18	24.0	0.1	78.2	18.8	6.43	21.1	3.4 to 35.2
4	92	44.4	19	25.7	0.3	45.5	17.7	14.0	15.3	3.9 to 26.4
4	93	43.6	16	22.0	1.2	65.3	16.5	12.2	16.1	5.1 to 21.3
4	94	48.0	17	21.3	0.1	62.4	15.6	4.58	17.9	2.7 to 26.5
4	95	49.2	25	30.5	1.1	61.4	12.5	5.28	15.4	2.8 to 19.4
Combined		582	276	28.5	0.1	87.9	15.3	7.23	17.1	2.8 to 25.5
All Subjects		2430.7	1403	34.6	0.1	119.2	23.7	21.1	20.6	6.3 to 35.5

Table I-2.
Summary statistics for azimuth excursions, slalom course, NVG.
(expressed in degrees)

Subject	Run	Time	# of Excursions	Exc/min	Min	Max	Mean	Median	S.D.	IQR
1	108	105.7	78	44.3	0.3	70.8	29.9	28.5	15.1	20.6 to 43.8
1	109	98.2	73	44.6	0.1	67.1	36.8	39.1	16.9	25.2 to 50.8
1	110	51.3	28	32.7	1.2	57.6	22.1	21.5	16.2	9.0 to 34.1
1	111	51.7	39	45.3	2.3	63.5	20.2	17.7	14.1	9.6 to 25.5
1	112	51.1	32	37.6	3.6	76.6	27.1	25.4	16.3	15.0 to 34.9
1	121	54.0	27	30.0	4.2	76.8	28.2	21.3	21.1	9.1 to 41.1
1	123	55.2	40	43.5	0.3	68.2	23.0	23.3	16.7	7.8 to 32.0
Combined		467.2	317	40.7	0.1	76.8	28.3	27.8	17.2	13.9 to 40.2
2	171	80.0	56	42.0	0.9	101.4	34.1	34.8	24.0	13.7 to 49.5
2	172	80.9	51	37.8	0.7	91.4	36.5	38.1	24.1	13.2 to 52.1
2	173	103.2	67	39.0	1.3	121.4	43.7	53.0	29.2	11.4 to 62.7
2	177	70.6	47	39.9	0.3	113.7	35.7	36.5	26.0	16.4 to 47.4
2	178	63.0	36	34.3	1.5	69.5	34.0	34.8	16.6	25.9 to 43.7
2	179	54.3	32	35.4	2.8	75.1	30.9	30.7	19.9	15.7 to 44.5
Combined		452.0	289	38.4	0.3	121.4	36.6	36.9	24.7	15.8 to 53.2
3	51	71.8	56	46.8	0.7	104.4	32.1	29.2	23.3	17.5 to 38.9
3	52	73.9	57	46.3	0.5	75.2	31.2	34.9	18.7	15.0 to 46.2
3	53	68.2	48	42.2	0.5	94.5	29.9	26.5	20.7	12.9 to 41.3
3	58	50.5	29	34.5	1.6	75.0	27.2	22.4	20.4	11.7 to 38.7
3	59	51.9	32	37.0	4.2	61.0	28.6	33.9	16.2	13.0 to 41.2
3	60	52.6	34	38.8	1.6	58.5	31.5	33.4	16.2	19.1 to 43.8
3	68	53.6	43	48.1	4.6	72.4	26.4	25.1	15.2	14.7 to 35.1
3	69	53.8	39	43.5	1.2	78.0	26.5	25.6	16.3	15.4 to 39.2
3	70	48.8	39	48.0	1.8	106.4	28.7	20.0	22.6	12.8 to 40.1
Combined		525.1	375	42.8	0.5	106.4	29.4	26.8	19.2	15.0 to 40.9
4	78	95.3	56	35.3	0.1	63.2	33.3	34.0	18.8	19.5 to 49.6
4	79	81.9	53	38.8	0.01	95.1	27.6	22.6	24.0	6.0 to 47.1
4	80	83.9	58	41.5	0.1	74.5	27.8	23.8	22.4	4.9 to 46.0
4	85	52.7	29	33.0	1.2	75.2	32.0	32.5	21.4	13.1 to 53.2
4	86	56.0	34	36.4	1.6	67.9	22.7	14.2	18.1	8.3 to 35.3
4	87	49.8	27	32.5	0.7	50.1	20.6	14.4	17.6	5.0 to 40.7
4	96	44.6	22	29.6	2.0	73.5	27.7	26.8	21.3	10.2 to 39.9
4	97	47.0	24	30.6	1.5	76.6	24.9	21.9	21.0	5.1 to 43.0
4	98	46.1	17	22.1	0.8	100.2	30.5	27.9	26.4	8.4 to 45.0
Combined		557.3	320	34.5	0.1	100.2	27.9	25.3	21.3	7.8 to 44.5
All Subjects		2001.6	1301	39.0	0.1	121.4	30.4	28.6	20.9	11.7 to 43.9

Table I-3.
 Summary statistics for azimuth excursions, slalom course, TIO.
 (expressed in degrees)

Subject	Run	Time	# of Excursions	Exc/min	Min	Max	Mean	Median	S.D.	IQR
1	138	85.7	47	32.9	0.2	75.9	28.0	28.1	22.0	6.6 to 45.4
1	139	109.7	67	36.6	0.7	93.4	30.0	36.1	22.3	7.0 to 49.6
1	140	120.4	62	30.1	0.1	96.8	38.1	43.3	23.0	19.6 to 50.3
Combined		315.8	176	33.4	0.1	96.8	32.3	34.4	22.7	9.1 to 49.6
2	163	70.0	39	33.4	1.5	70.1	18.5	14.6	15.4	8.3 to 26.9
2	164	82.5	47	34.2	1.4	56.1	21.3	15.9	15.7	8.8 to 33.1
2	166	80.1	35	26.2	0.9	56.7	22.0	14.2	19.7	3.9 to 40.8
2	167	88.1	40	27.2	0.5	83.0	25.7	24.1	21.0	6.3 to 42.5
Combined		320.7	161	30.1	0.5	83.0	21.9	15.9	18.0	6.5 to 33.0
3	144	70.9	40	33.9	0.50	59.0	25.7	24.2	15.6	13.7 to 36.3
3	145	89.3	53	35.6	1.6	61.1	22.8	22.0	15.3	11.8 to 30.9
3	146	97.9	60	36.8	1.4	76.7	19.8	12.1	18.4	6.5 to 28.0
3	155	71.9	46	38.4	1.8	77.9	21.8	20.0	14.5	11.6 to 29.5
3	157	84.4	43	30.6	0.8	70.1	15.4	12.8	16.3	4.1 to 16.4
Combined		414.4	242	35.0	0.5	77.9	21.1	17.0	16.4	8.3 to 29.5
4	None									
All Subjects		1050.9	579	33.1	0.1	96.8	24.7	20.5	19.6	8.0 to 38.7

Table I-4.
Summary statistics for azimuth excursions, slalom course, RWS.
(expressed in degrees)

Subject	Run	Time	# of Excursions	Exc/min	Min	Max	Mean	Median	S.D.	IQR
1	141	106.2	50	28.2	1.1	81.4	23.1	17.2	21.4	3.8 to 41.6
1	142	102.0	59	34.7	0.2	56.5	18.1	10.6	17.8	2.7 to 32.7
1	143	120.0	67	33.5	0.1	65.5	26.7	28.6	22.1	3.5 to 46.1
Combined		328.2	176	32.2	0.1	81.4	22.8	16.4	20.8	3.1 to 41.6
2	168	83.2	35	25.2	0.3	62.4	12.6	4.0	16.2	2.6 to 21.1
2	169	89.1	41	27.6	0.4	49.5	14.2	4.6	16.2	2.4 to 27.2
2	170	101.1	45	26.7	0.03	55.2	12.9	3.4	17.4	1.9 to 16.8
2	174	63.6	22	20.8	0.3	56.0	21.4	20.1	17.6	4.5 to 32.7
2	175	65.0	26	24.0	0.7	60.8	18.7	8.9	18.8	4.0 to 36.8
2	176	63.8	26	24.5	0.2	46.4	12.5	6.6	14.0	1.4 to 20.2
Combined		465.8	195	25.1	0.03	62.4	14.8	5.4	16.8	2.2 to 27.8
3	158	71.2	29	24.4	0.2	85.1	16.9	7.19	18.4	2.5 to 18.5
3	159	94.8	42	26.6	0.1	57.1	11.8	5.2	14.9	1.4 to 15.7
3	161	61.2	28	27.5	0.2	63.8	15.4	6.5	18.4	2.7 to 18.0
3	162	55.3	22	23.9	0.4	92.7	16.4	3.8	24.1	2.4 to 19.2
3	180	59.6	30	30.2	0.6	96.1	21.7	18.8	21.0	4.4 to 32.4
3	181	58.9	36	36.7	0.8	57.6	18.0	15.0	14.8	6.0 to 27.9
3	182	52.9	20	22.7	1.0	71.2	20.5	12.4	20.8	3.0 to 33.5
3	183	43.9	22	30.1	1.0	98.4	20.5	7.9	25.4	3.5 to 30.6
Combined		497.8	229	27.6	0.1	98.4	16.8	8.3	19.3	2.7 to 26.1
4	None									
All Subjects		1291.8	600	27.9	0.1	98.4	17.9	8.2	19.2	2.6 to 32.0

Appendix J.

Azimuth excursion box-plots.

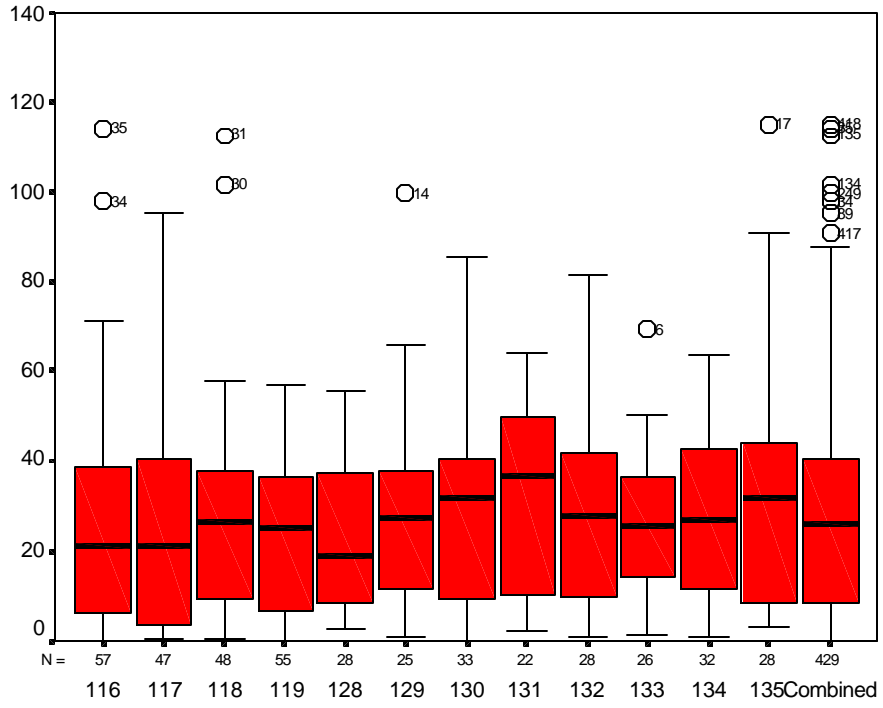


Figure J-1. Subject #1 GVE excursion box-plots.

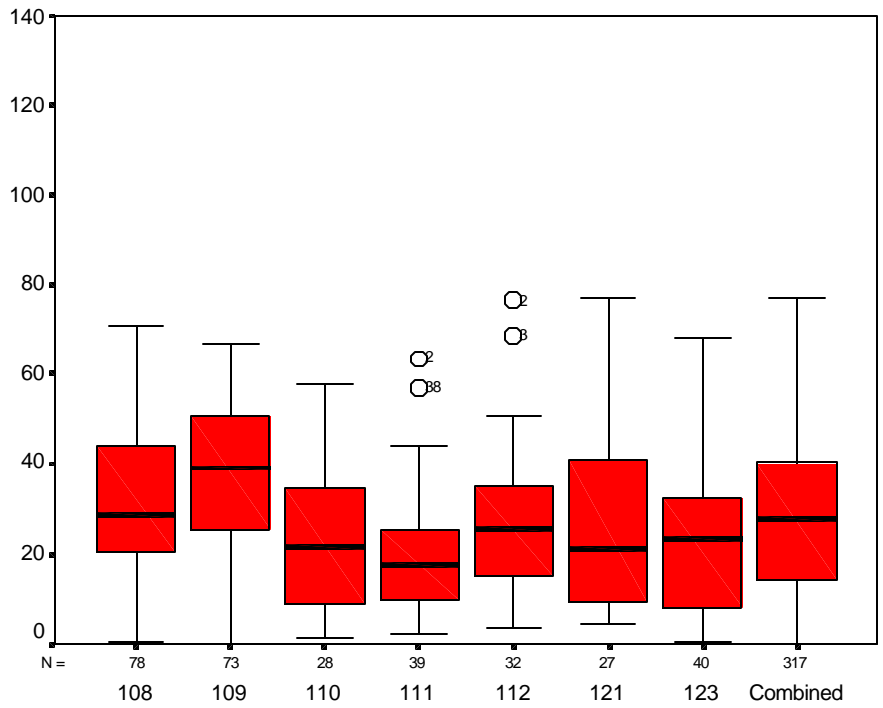


Figure J-2. Subject #1 NVG excursion box-plots.

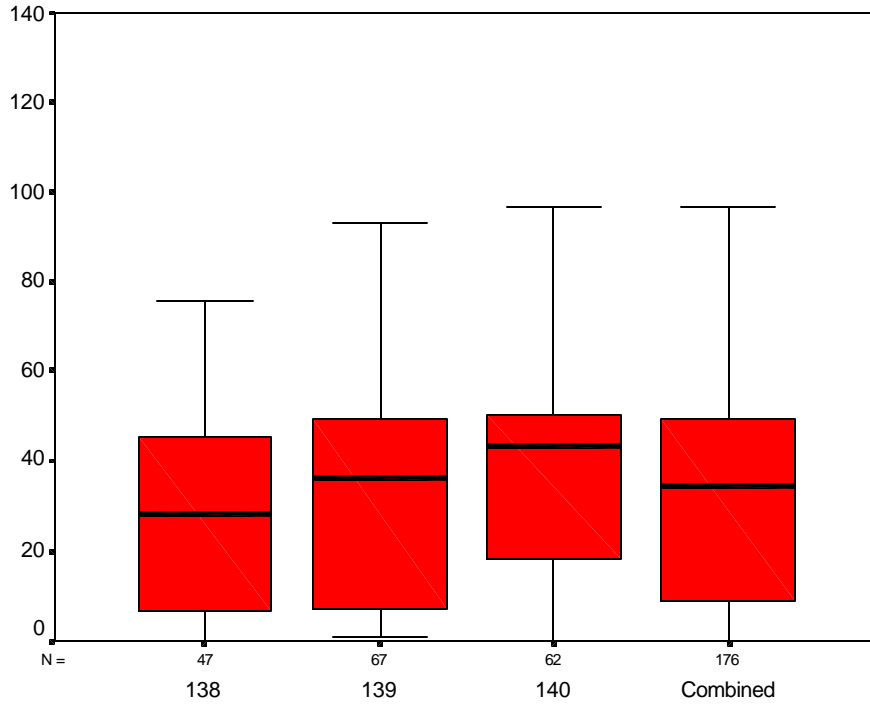


Figure J-3. Subject #1 TIO excursion box-plots.

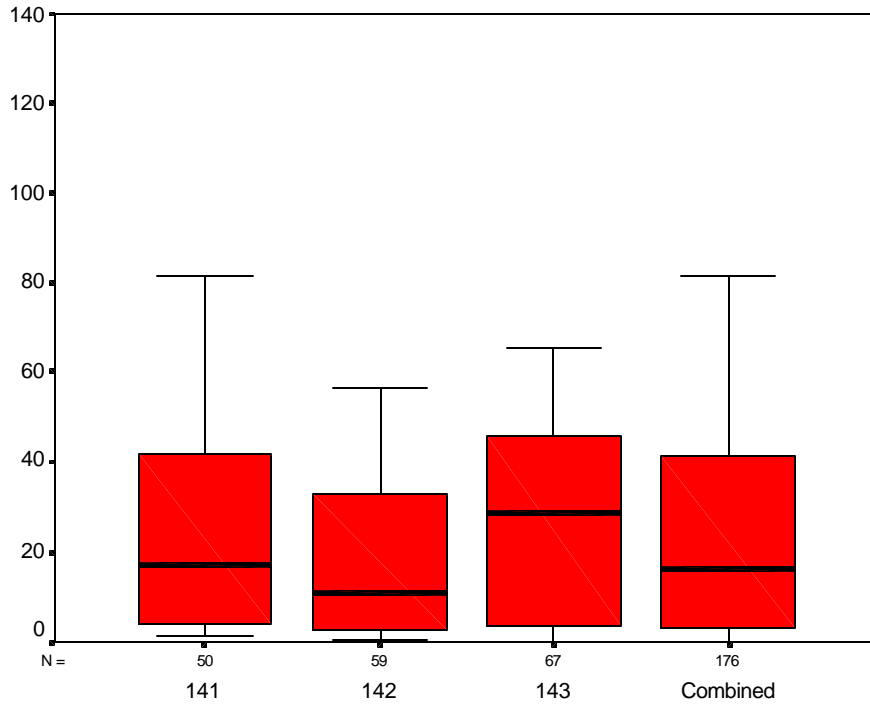


Figure J-4. Subject #1 RWS excursion box-plots.

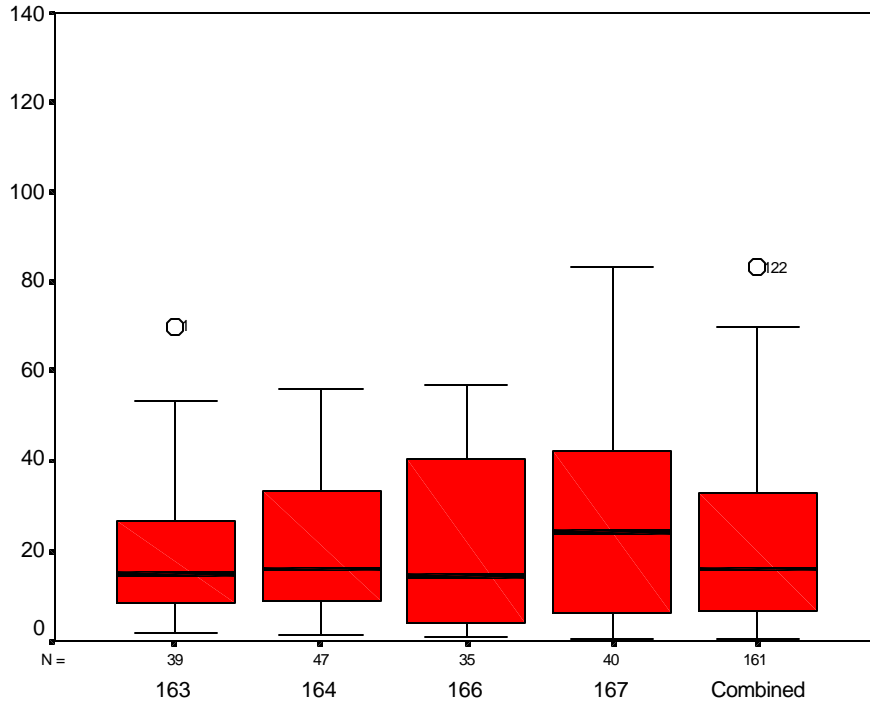


Figure J-7. Subject #2 TIO excursion box-plots.

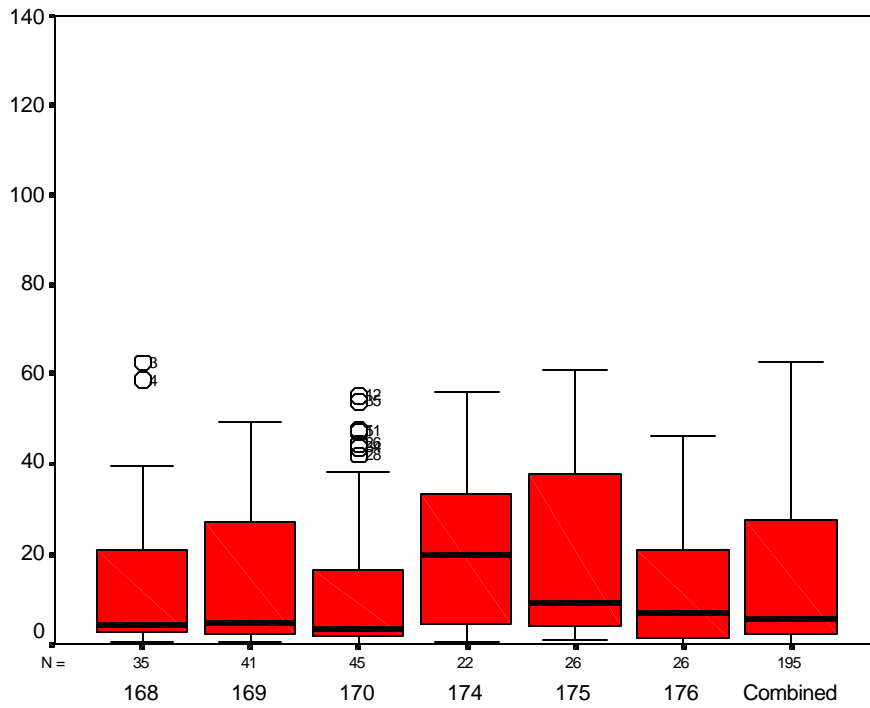


Figure J-8. Subject #2 RWS excursion box-plots.

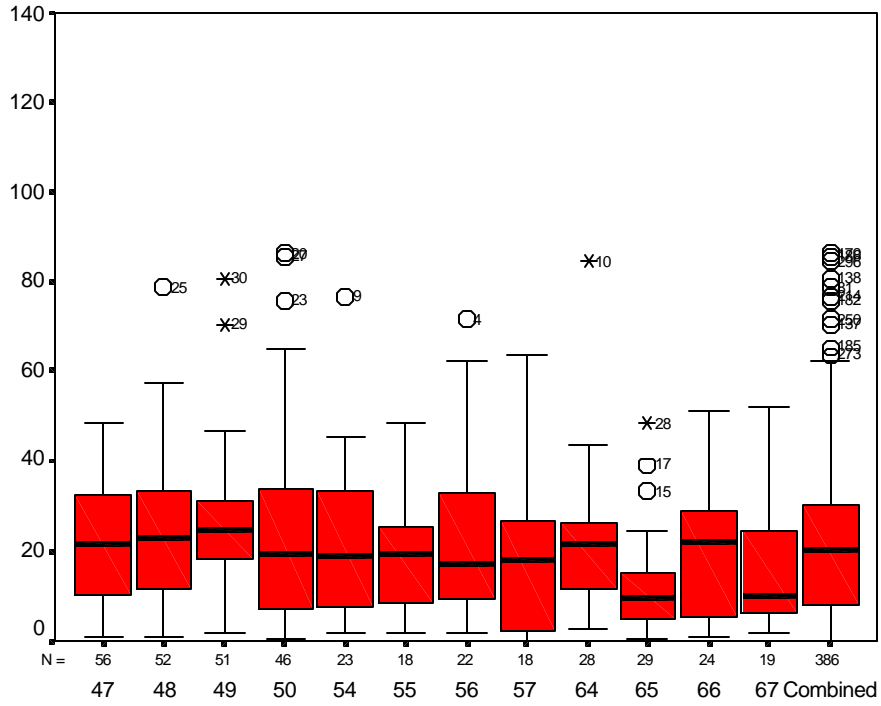


Figure J-9. Subject #3 GVE excursion box-plots.

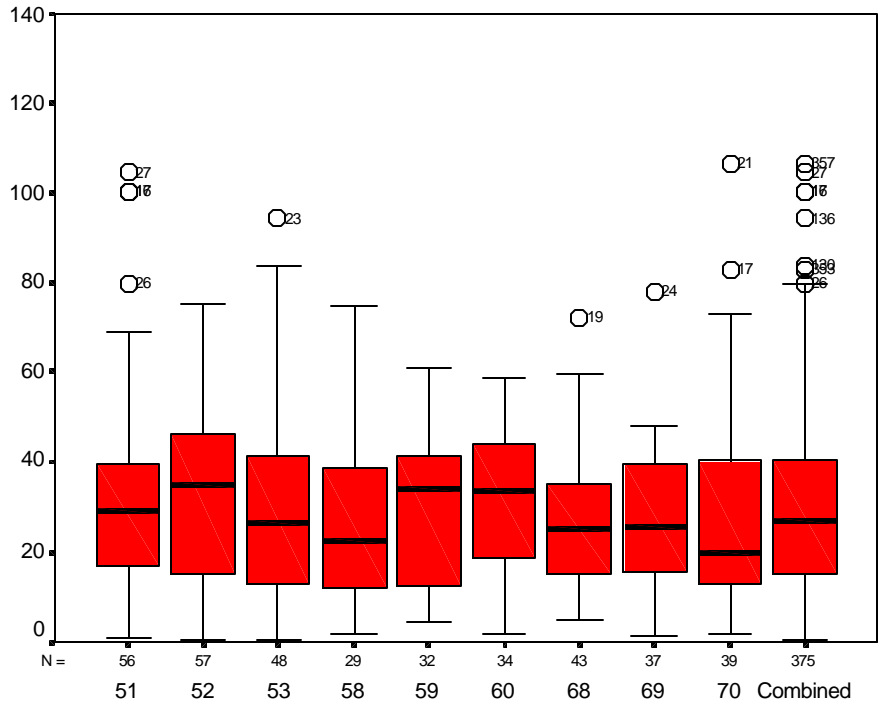


Figure J-10. Subject #3 NVG excursion box-plots.

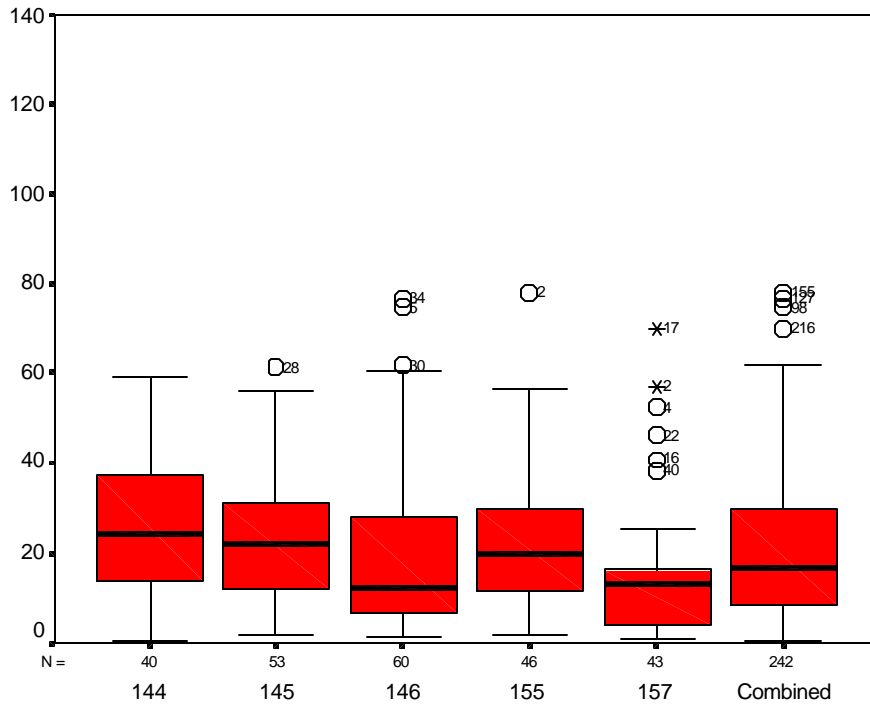


Figure J-11. Subject #3 TIO excursion box-plots.

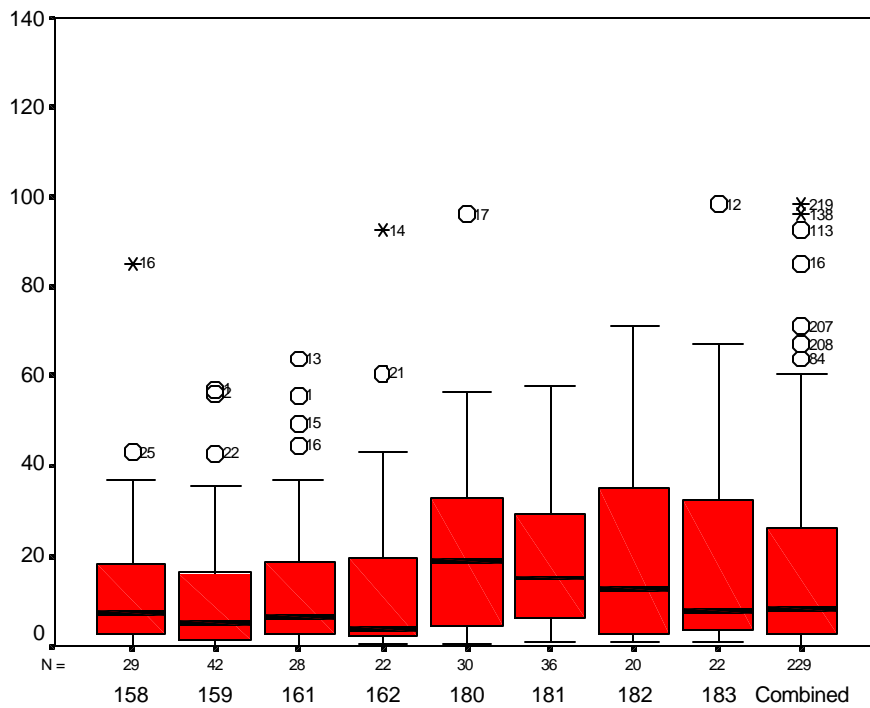


Figure J-12. Subject #3 RWS excursion box-plots.

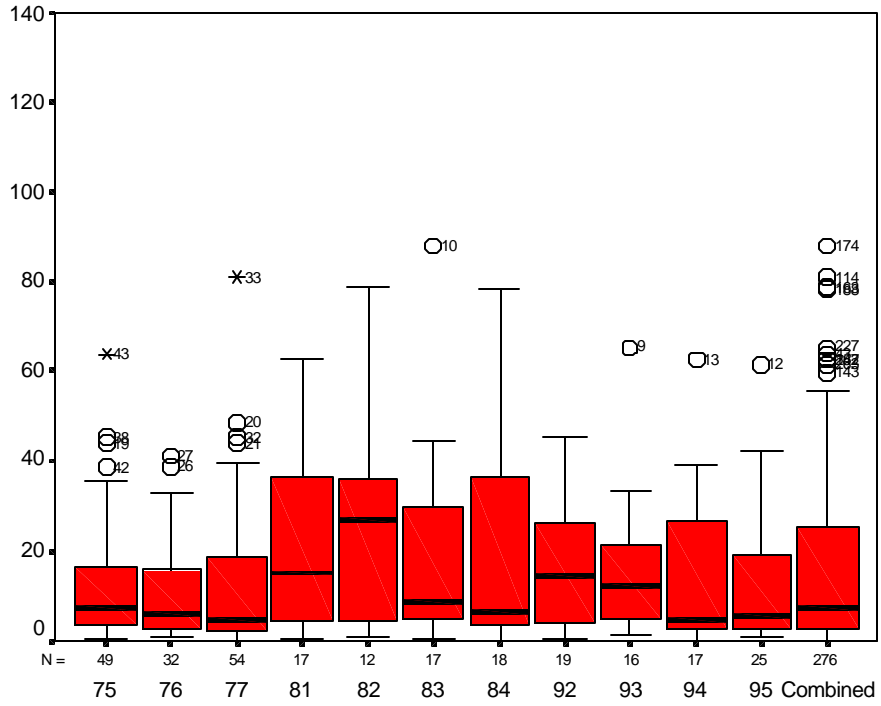


Figure J-13. Subject #4 GVE excursion box-plots.

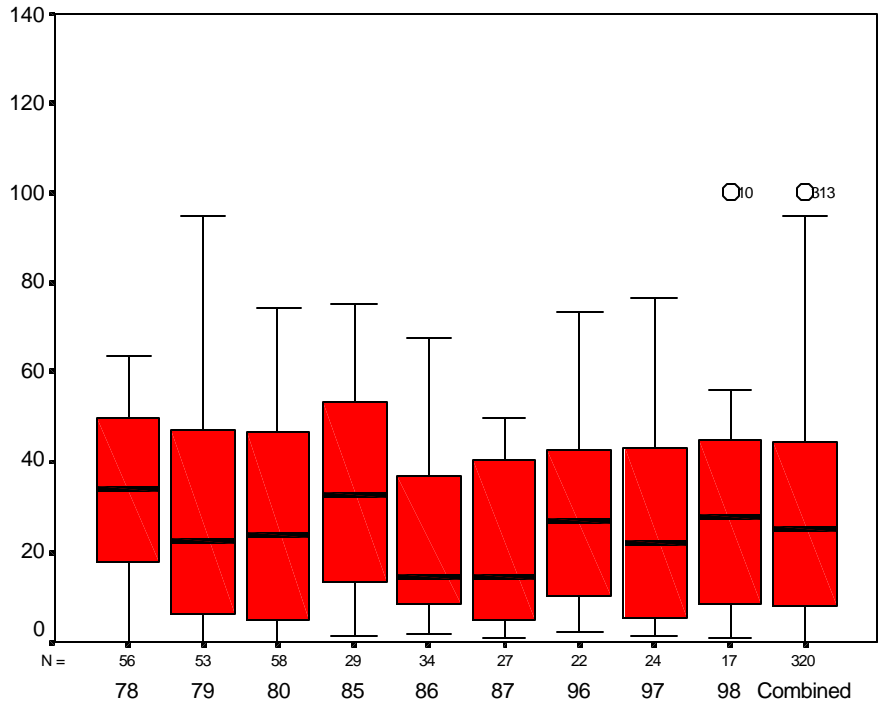


Figure J-14. Subject #4 NVG excursion box-plots.

Appendix K.

Azimuth velocity distributions.

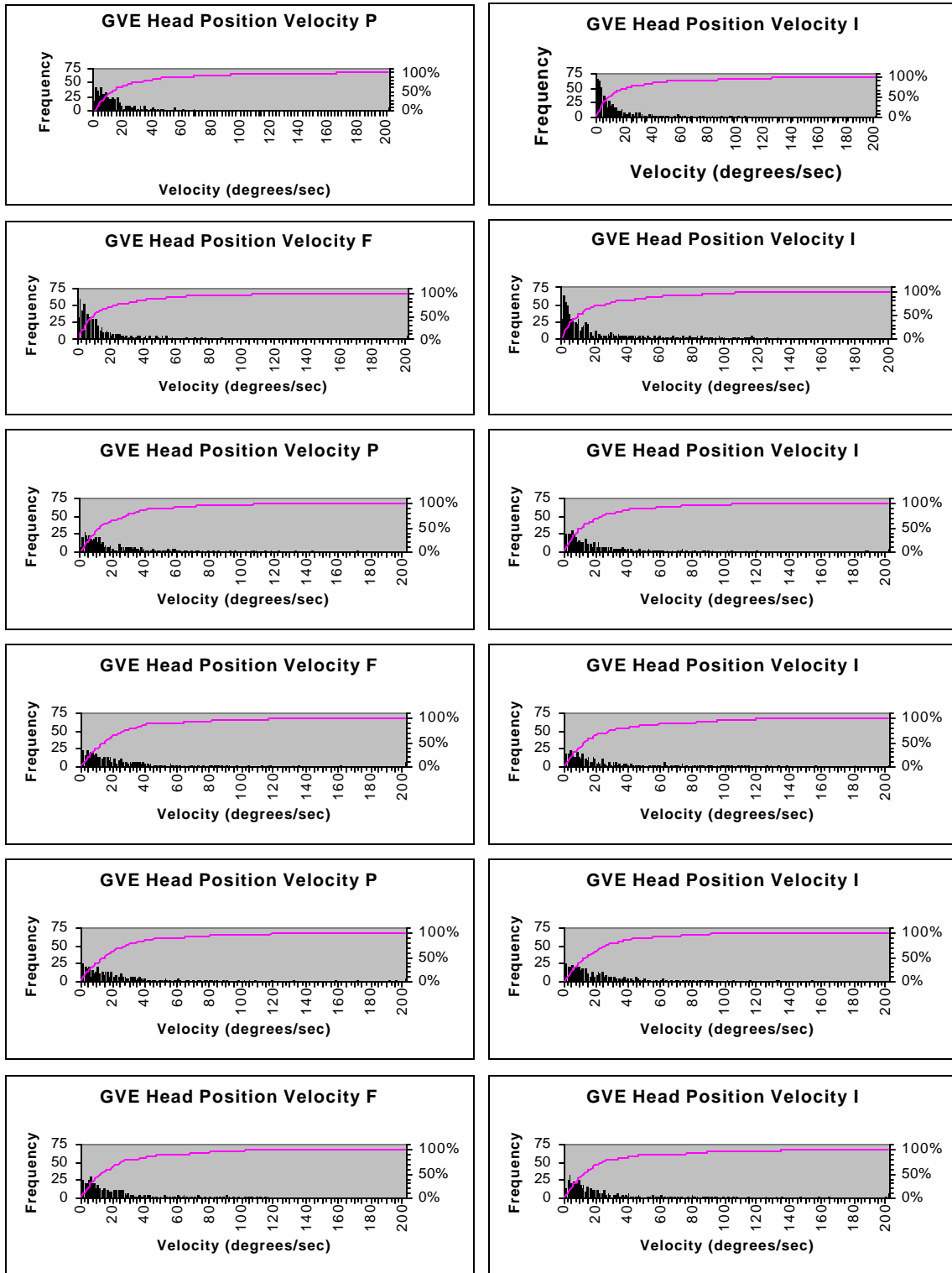


Figure K-1. Subject #1 GVE head velocity distributions with cumulative frequency curves.

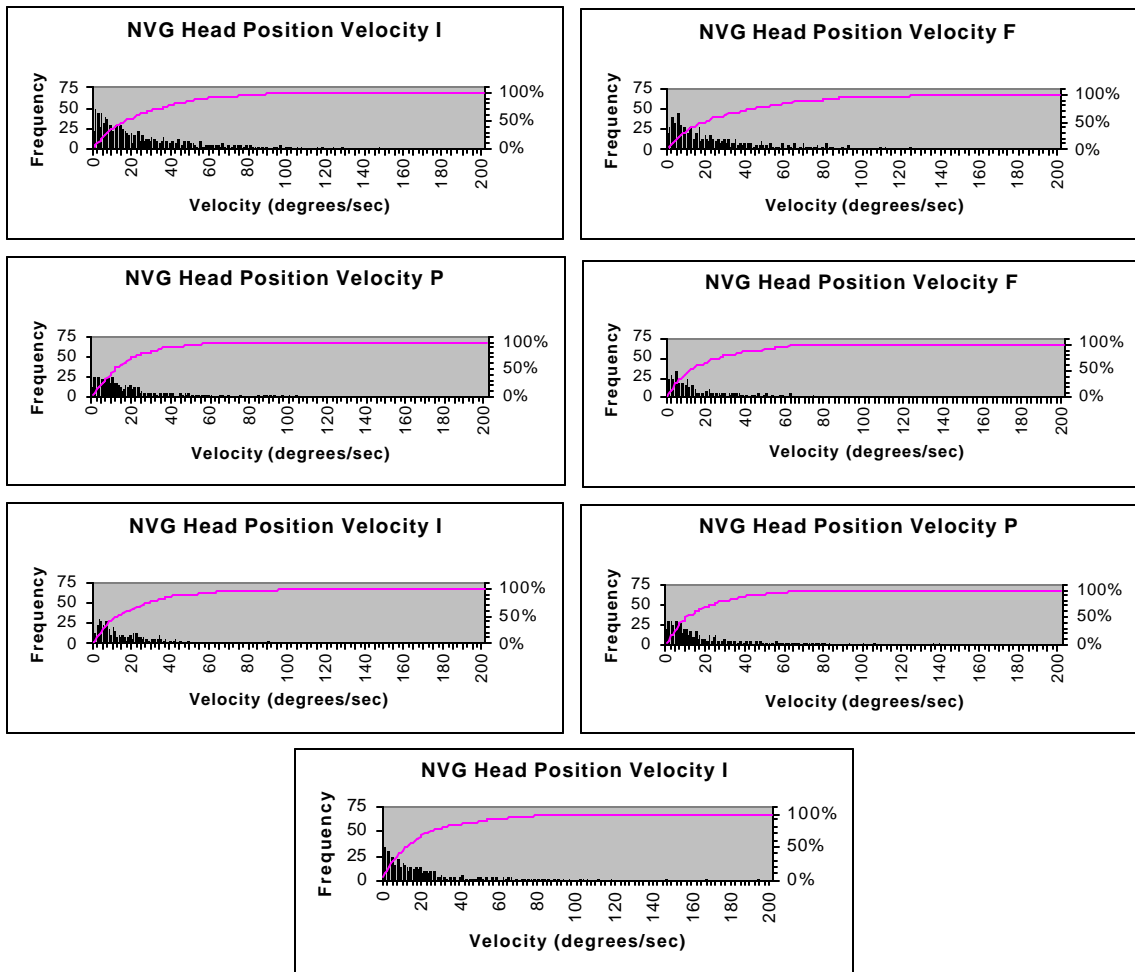


Figure K-2. Subject #1 NVG head velocity distributions with cumulative frequency curves.

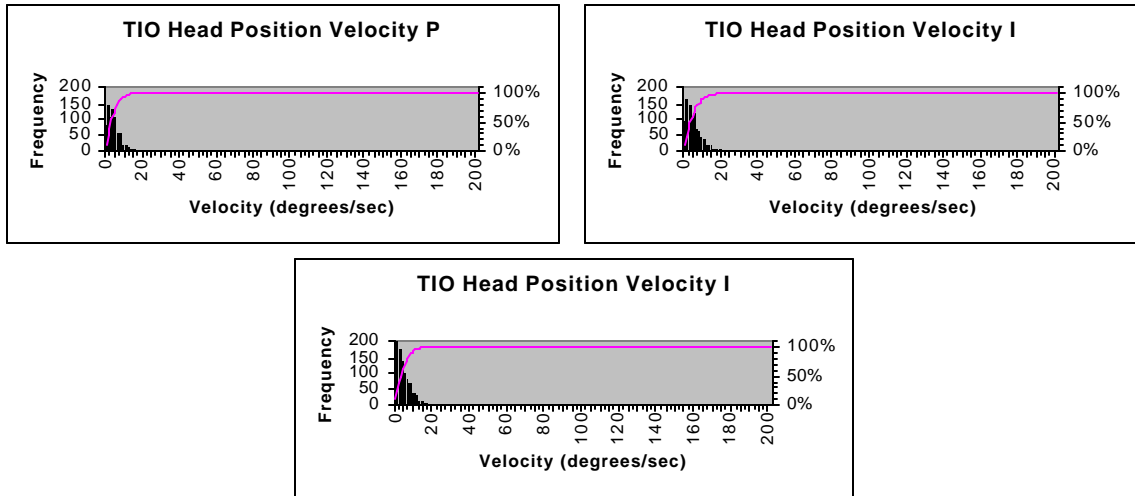


Figure K-3. Subject #1 TIO head velocity distributions with cumulative frequency curves.

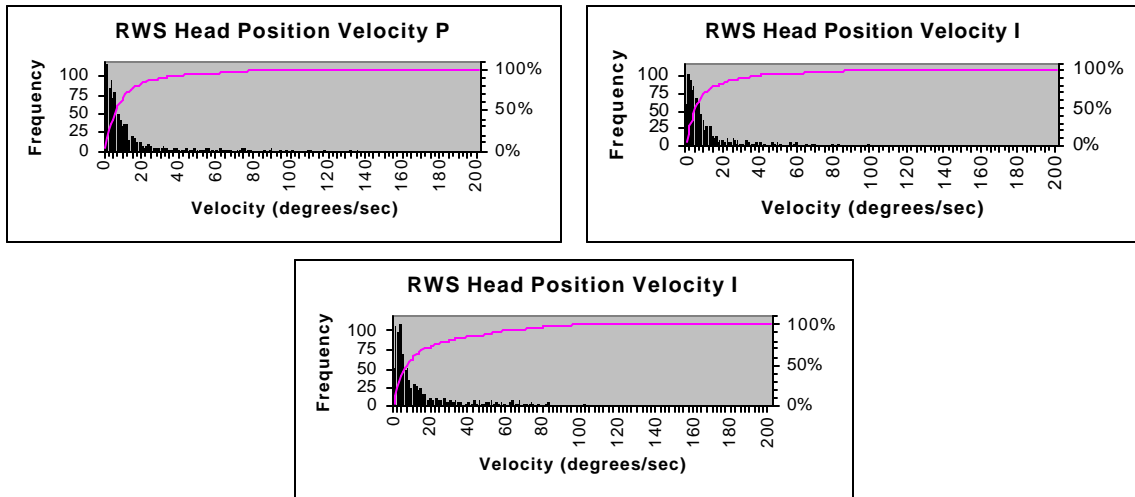


Figure K-4. Subject #1 RWS head velocity distributions with cumulative frequency curves.

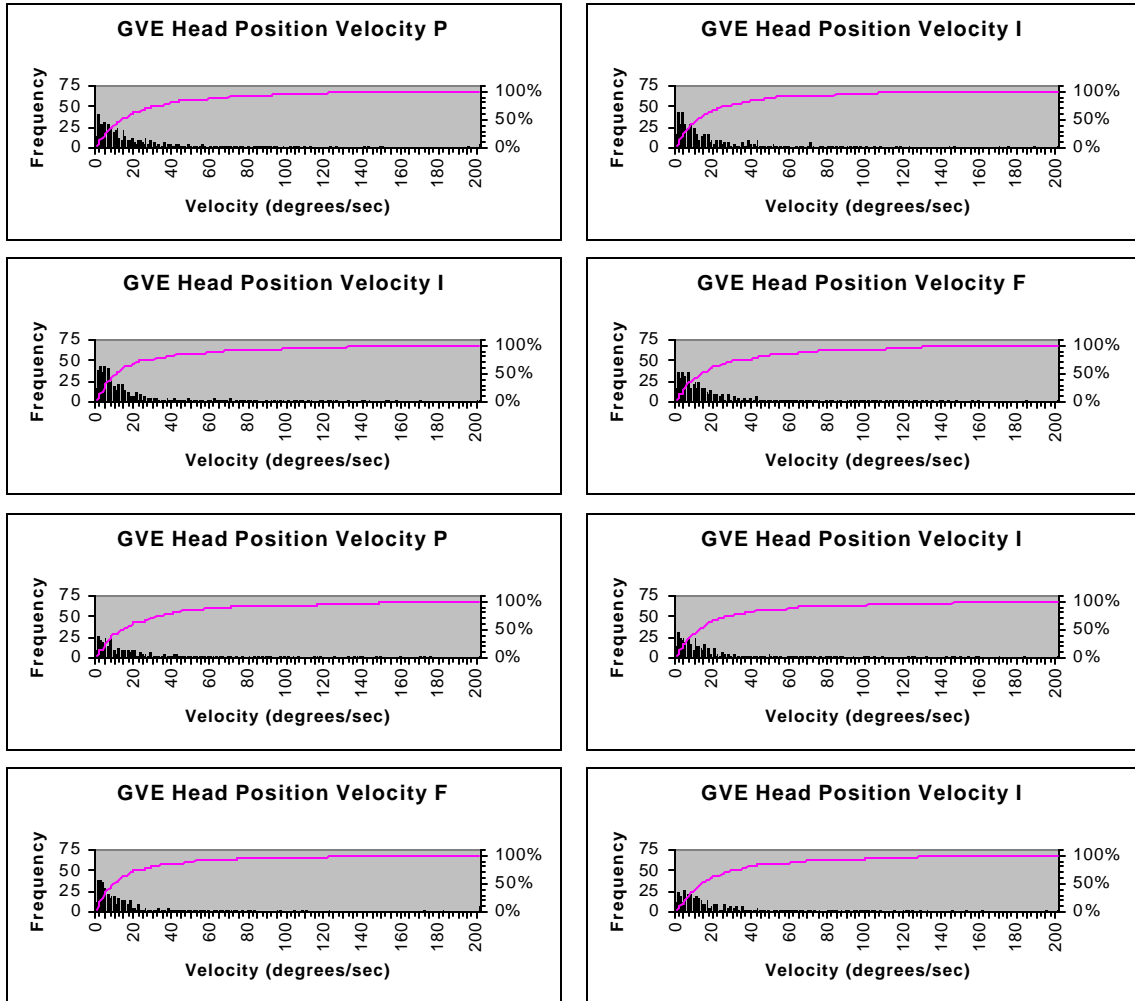


Figure K-5. Subject #2 GVE head velocity distributions with cumulative frequency curves.

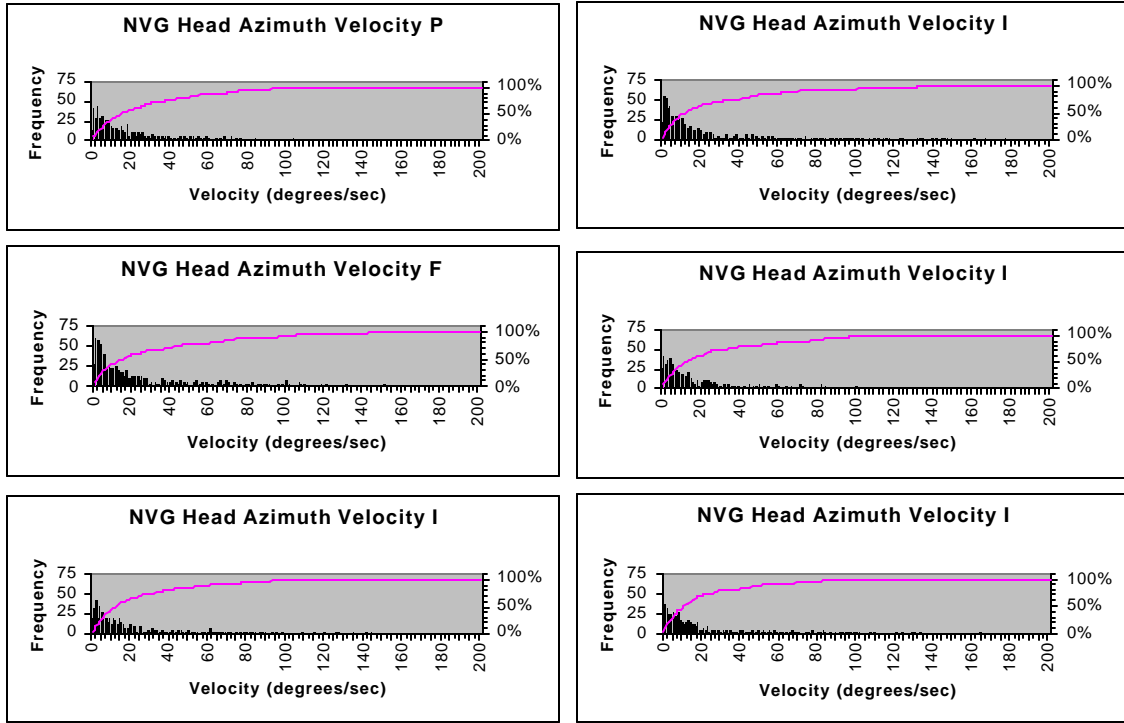


Figure K-6. Subject #2 NVG head velocity distributions with cumulative frequency curves.

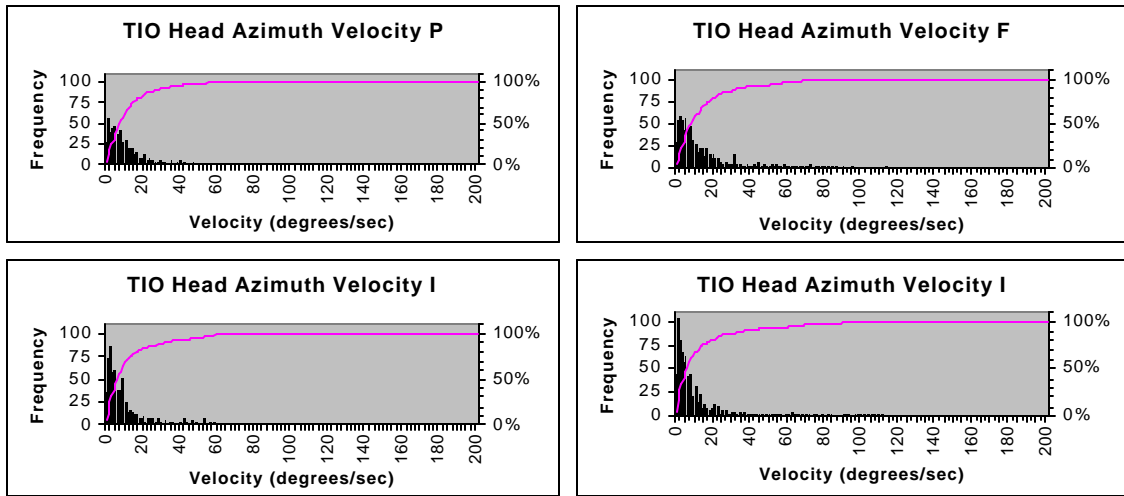


Figure K-7. Subject #2 TIO head velocity distributions with cumulative frequency curves.

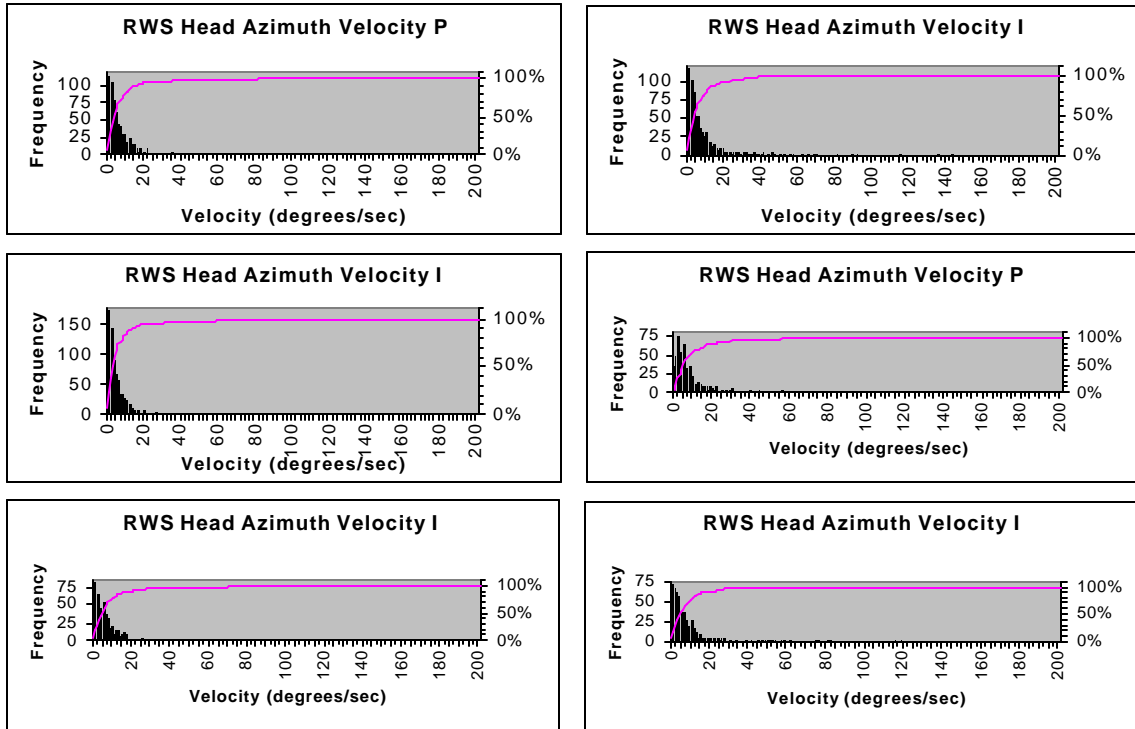


Figure K-8. Subject #2 RWS head velocity distributions with cumulative frequency curves.

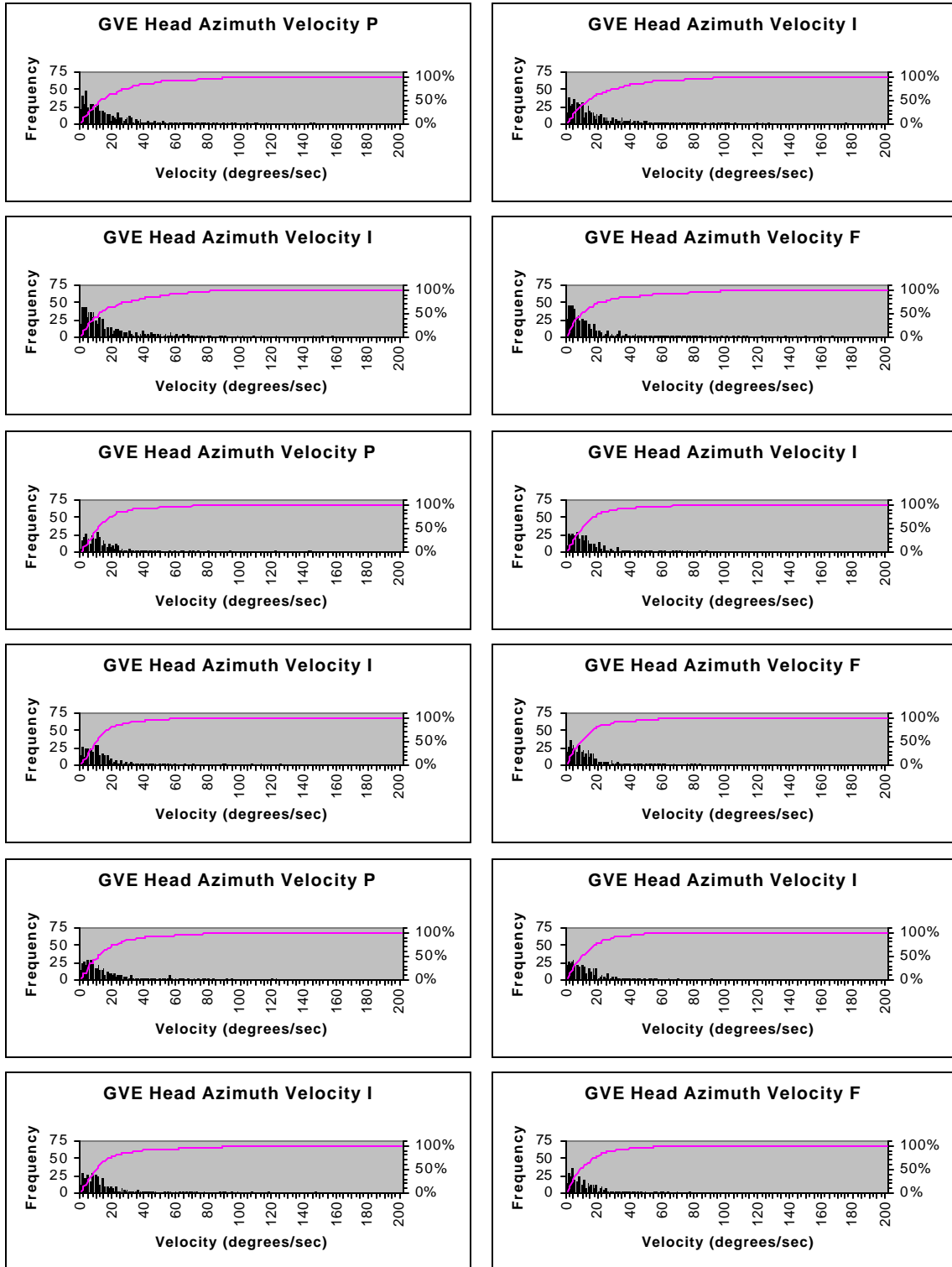


Figure K-9. Subject #3 GVE head velocity distributions with cumulative frequency curves.

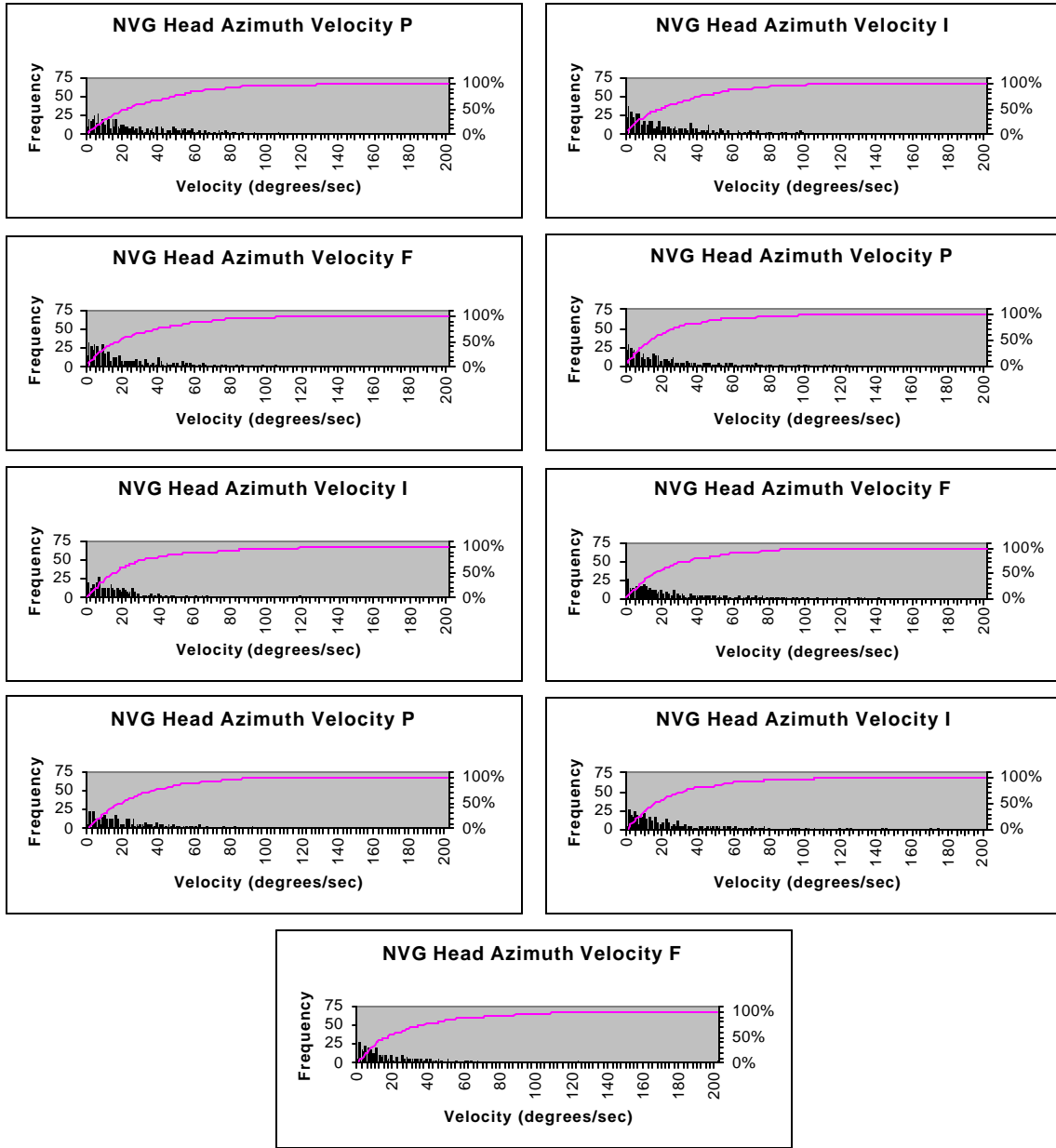


Figure K-10. Subject #3 NVG head velocity distributions with cumulative frequency curves.

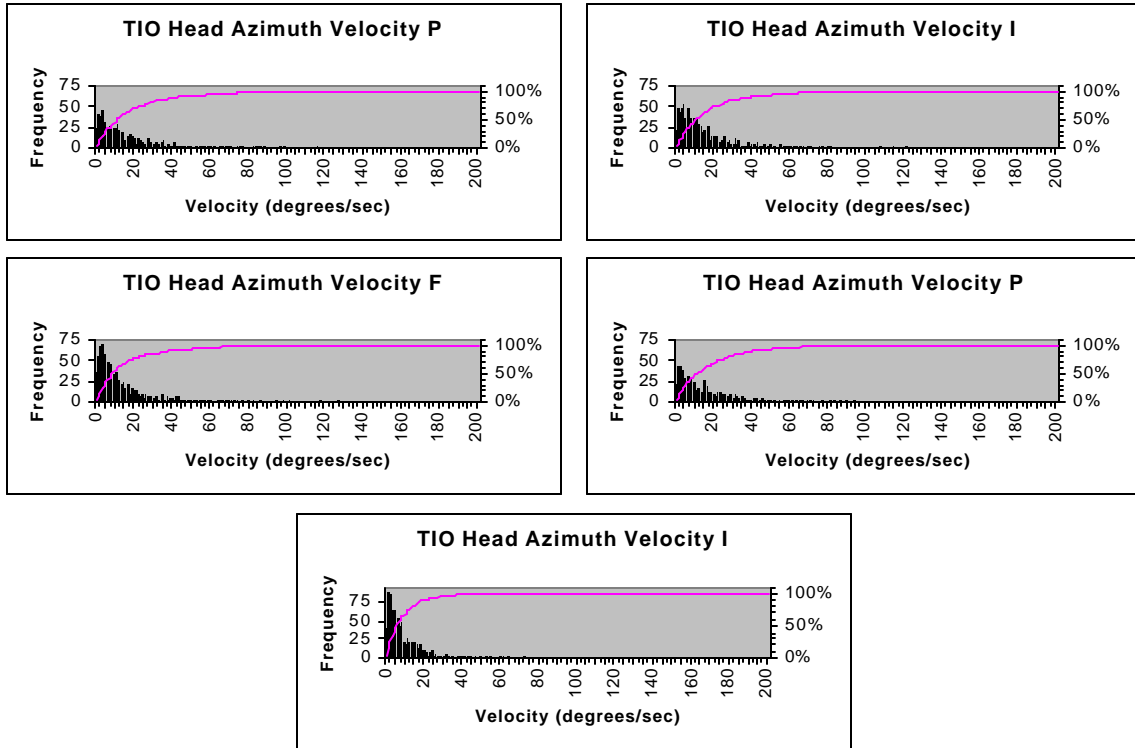


Figure K-11. Subject #3 TIO head velocity distributions with cumulative frequency curves.

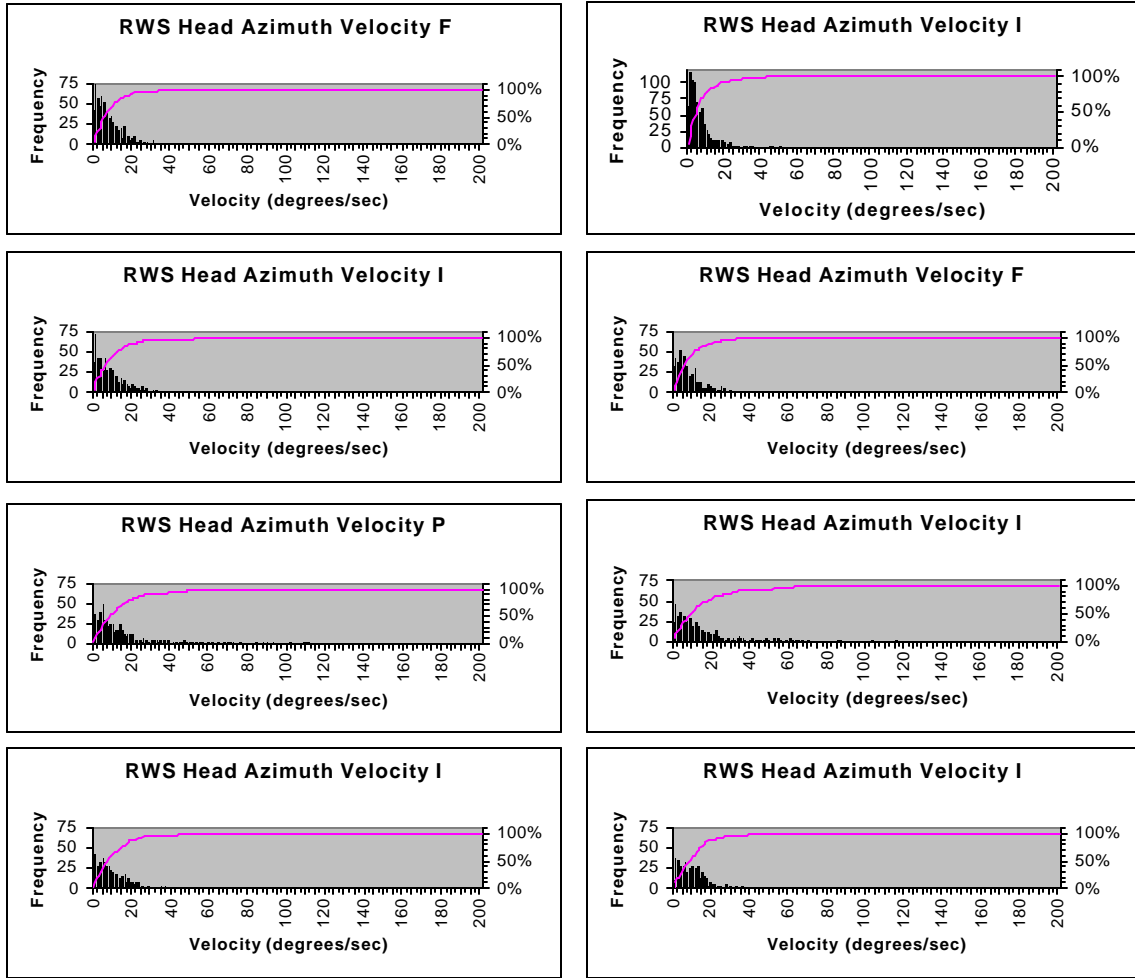


Figure K-12. Subject #3 RWS head velocity distributions with cumulative frequency curves.

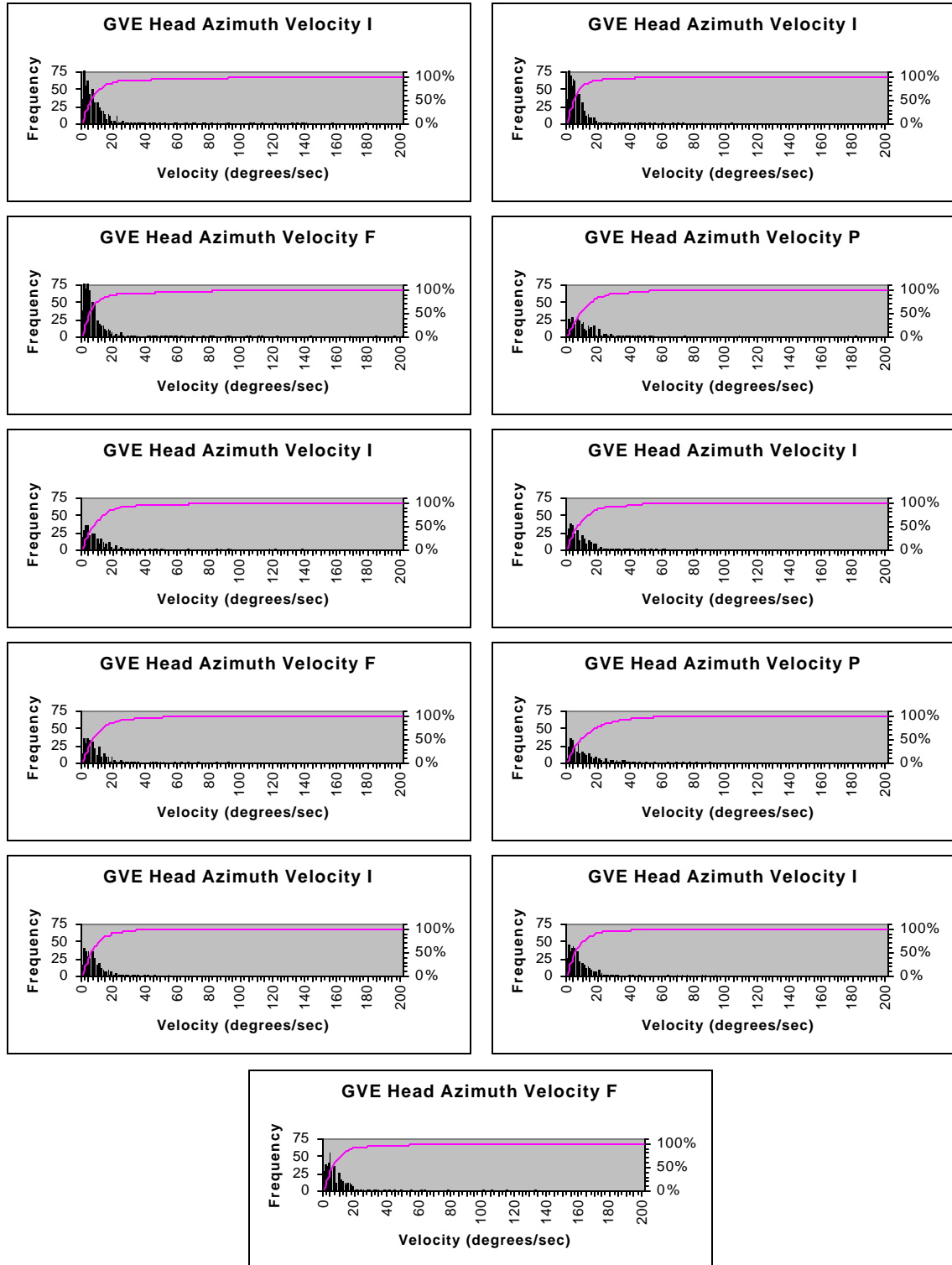


Figure K-13. Subject #4 GVE head velocity distributions with cumulative frequency curves.

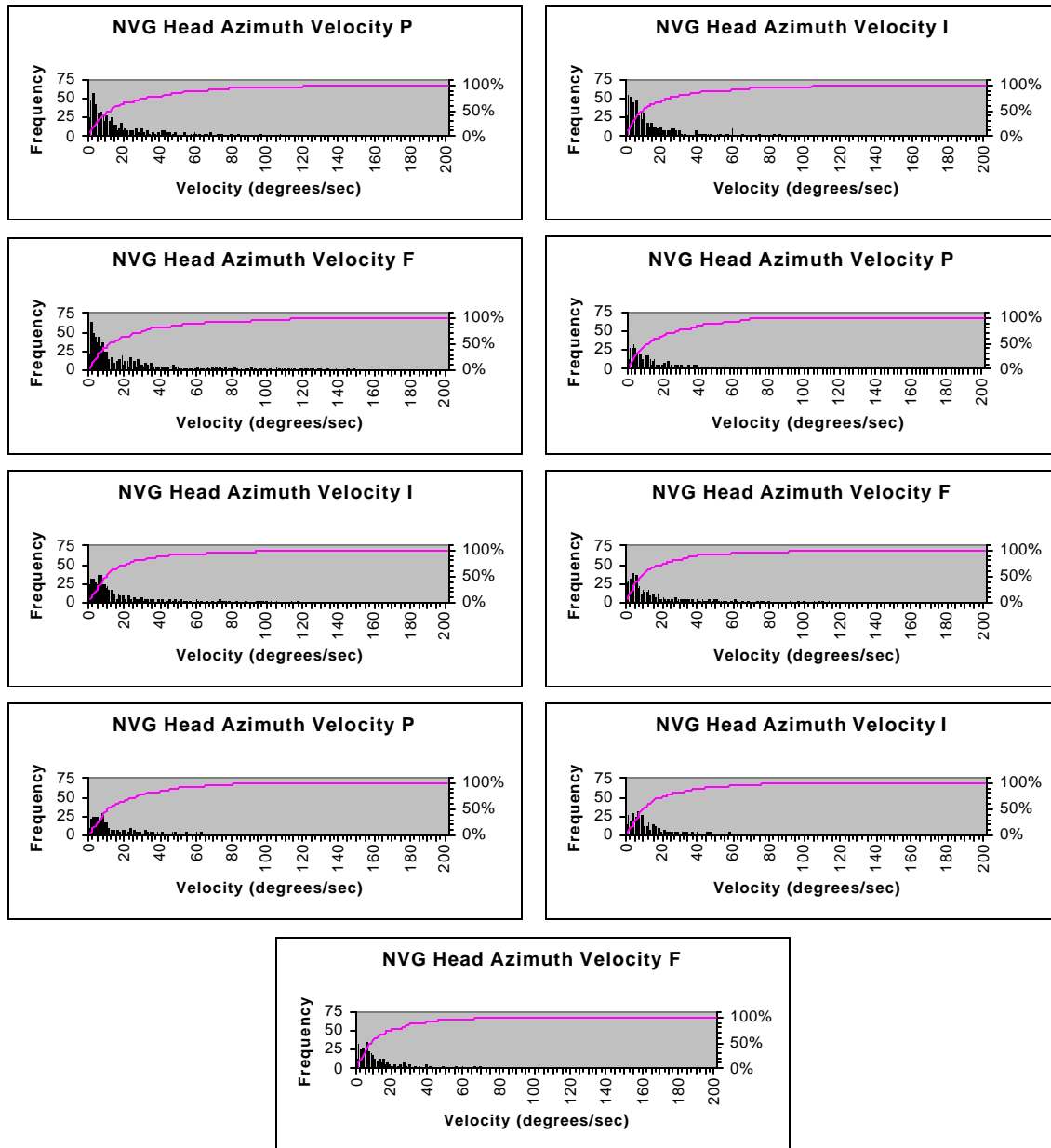


Figure K-14. Subject #4 NVG head velocity distributions with cumulative frequency curves.

Appendix L.

Azimuth velocity summary tables for combined distributions.

Table L-1.
Summary statistics for azimuth velocity, slalom course, GVE.
(velocity values expressed in degrees/sec, time in seconds)

Subject	Run	Time	Min	Max	Mean	Median	S.D.	Skewness	Kurtosis
1	116	76.9	0	297	24.3	12	34.8	3.5	16.0
1	117	75.7	0	350	20.3	9	33.1	4.7	32.1
1	118	76.9	0	344	20.6	9	33.4	4.8	33.8
1	119	76.0	0	132	20.8	10	26.1	1.9	3.2
1	128	45.2	0	171	20.5	11	24.1	2.5	8.1
1	129	48.1	0	300	20.5	11	31.6	4.8	30.7
1	130	48.6	0	312	23.4	14	33.3	4.6	28.8
1	131	43.8	0	202	24.3	13	30.1	2.3	6.5
1	132	45.6	0	267	23.3	15	31.7	3.9	20.7
1	133	49.8	0	154	20.4	14	21.7	2.3	7.3
1	134	51.1	0	116	20.1	12	23.6	1.9	3.4
1	135	52.9	0	320	23.4	12	34.6	4.0	21.5
Combined		690.6	0	350	21.8	12	30.5	3.9	24.0
2	147	68.4	0	332	25.6	14	34.4	3.4	18.6
2	148	65.1	0	362	22.0	11	31.0	4.4	33.0
2	149	71.7	0	320	23.6	11	33.7	3.2	15.5
2	150	73.9	0	221	27.2	13	33.9	2.1	4.7
2	151	47.0	0	298	27.7	14	37.7	2.9	11.6
2	152	52.2	0	348	24.8	12	35.2	3.6	19.7
2	153	51.7	0	339	21.1	9	36.8	4.9	30.7
2	154	50.4	0	288	26.2	14	33.7	2.9	11.9
Combined		480.4	0	362	24.8	12	34.4	3.4	17.5
3	47	74.8	0	144	20.7	13	22.4	2.0	4.9
3	48	75.7	0	88	21.8	13	23.7	2.2	7.3
3	49	78.8	0	125	20.8	12	22.7	1.9	4.9
3	50	73.2	0	83	19.2	10	25.2	2.5	7.4
3	54	44.6	0	122	15.7	11	17.1	3.5	18.2
3	55	47.6	0	91	13.8	10	14.0	2.3	6.3
3	56	46.5	0	147	14.0	10	14.9	3.3	16.5
3	57	49.0	0	77	13.1	9	13.6	2.2	6.0
3	64	50.6	0	122	17.1	11	18.7	2.3	6.7
3	65	46.8	0	91	13.3	10	12.5	1.8	4.9
3	66	46.7	0	191	16.2	10	19.5	2.8	9.7
3	67	43.4	0	88	12.9	9	12.6	1.8	4.2
Combined		677.7	0	191	17.3	11	19.8	2.6	9.3
4	75	72.4	0	178	11.6	6	20.2	4.6	25.0
4	76	69.0	0	103	7.6	5	10.4	4.6	29.7
4	77	79.8	0	215	11.2	5	21.7	5.5	37.4
4	81	42.0	0	181	12.8	9	16.5	5.8	50.4
4	82	42.6	0	138	11.5	7	15.7	4.3	24.7
4	83	46.0	0	81	10.6	7	11.4	2.3	6.6
4	84	45.0	0	92	10.8	7	12.3	3.1	13.0
4	92	44.4	0	89	13.7	9	13.9	2.0	5.4
4	93	43.6	0	54	8.6	6	8.1	1.9	4.8
4	94	48.0	0	93	8.6	6	10.9	4.3	25.1
4	95	49.2	0	133	9.3	6	13.4	5.0	34.0
Combined		582.0	0	215	10.5	6	15.3	5.3	42.2
All Subjects		2430.7	0	362	18.4	10	26.3	4.1	27.3

Table L-2.
 Summary statistics for azimuth velocity, slalom course, NVG.
 (velocity values expressed in degrees/sec, time in seconds)

Subject	Run	Time	Min	Max	Mean	Median	S.D.	Skewness	Kurtosis
1	108	105.7	0	147	24.4	16	23.2	1.4	2.1
1	109	98.2	0	170	30.9	19	31.4	1.4	1.7
1	110	51.3	0	104	17.7	12	18.0	2.1	5.3
1	111	51.7	0	123	19.0	11	19.9	1.8	3.6
1	112	51.1	0	175	22.0	13	25.0	2.4	7.7
1	121	54.0	0	139	18.2	11	20.1	2.2	6.4
1	123	55.2	0	194	20.6	12	24.4	2.5	9.1
Combined		467.2	0	194	23.0	14	24.8	1.9	4.7
2	171	80.0	0	171	27.1	15.5	27.1	1.8	3.4
2	172	80.9	0	177	25.6	12	25.6	1.9	3.7
2	173	103.2	0	179	32.4	15	32.4	1.5	1.5
2	177	70.6	0	205	26.5	13	26.5	2.1	5.1
2	178	63.0	0	144	22.0	13	22.0	1.9	3.9
2	179	54.3	0	164	21.2	11	21.2	2.1	4.7
Combined		452.0	0	205	26.5	13	31.9	1.9	3.6
3	51	71.8	0	233	33.2	22	32.6	1.7	4.0
3	52	73.9	0	131	28.4	19	27.6	1.2	0.8
3	53	68.2	0	147	27.1	17	27.8	1.5	2.0
3	58	50.5	0	123	21.0	14	22.5	1.8	3.6
3	59	51.9	0	140	26.7	16	29.5	1.8	2.8
3	60	52.6	0	140	25.8	16	26.6	1.7	2.7
3	68	53.6	0	148	27.1	19	26.1	1.6	2.8
3	69	53.8	0	174	24.5	15	25.9	2.2	6.3
3	70	48.8	0	247	29.1	15.5	36.3	2.6	9.0
Combined		525.1	0	247	27.3	17	28.8	1.9	5.0
4	78	95.3	0	171	24.3	12	29.5	1.9	3.8
4	79	81.9	0	175	20.1	9	26.2	2.2	5.5
4	80	83.9	0	148	22.7	12	27.8	2.0	3.7
4	85	52.7	0	126	20.8	11	22.8	1.7	3.2
4	86	56.0	0	117	16.9	9	20.4	2.2	5.4
4	87	49.8	0	113	15.6	8	19.4	2.4	6.8
4	96	44.6	0	108	19.2	10	20.6	1.7	2.7
4	97	47.0	0	130	16.6	9	19.1	2.3	6.2
4	98	46.1	0	125	15.1	8	17.0	2.1	6.0
Combined		557.3	0	175	19.7	10	24.2	2.2	5.5
All Subjects		2001.6	0	247	24.0	13	27.6	2.0	4.9

Table L-3.
 Summary statistics for azimuth velocity, slalom course, TIO.
 (velocity values expressed in degrees/sec, time in seconds)

Subject	Run	Time	Min	Max	Mean	Median	S.D.	Skewness	Kurtosis
1	138	85.7	0	45	4.0	3	3.7	3.2	23.7
1	139	109.7	0	34	4.7	4	4.3	2.0	6.9
1	140	120.4	0	26	4.3	3	3.6	1.4	2.7
Combined		315.8	0	45	4.3	3	3.9	2.1	9.6
2	163	70.0	0	103	11.8	8	13.4	2.8	10.8
2	164	82.5	0	113	14.5	8	17.1	2.3	5.7
2	166	80.1	0	84	11.8	7	14.8	2.2	4.5
2	167	88.1	0	111	13.5	6	19.7	2.6	7.2
Combined		320.7	0	113	13.0	7	16.6	2.6	7.6
3	144	70.9	0	116	17.3	11	18.2	1.8	3.7
3	145	89.3	0	121	16.1	11	16.4	2.0	5.8
3	146	97.9	0	127	14.6	9	16.7	2.3	7.2
3	155	71.9	0	94	16.8	11	16.5	1.6	2.7
3	157	84.4	0	72	9.0	6	9.6	2.3	7.6
Combined		414.4	0	127	16.0	9	16.0	2.1	5.9
4	None								
All Subjects		1059.9	0	127	11.0	6	14.5	2.8	9.9

Table L-4.
 Summary statistics for azimuth velocity, slalom course, RWS.
 (velocity values expressed in degrees/sec, time in seconds)

Subject	Run	Time	Min	Max	Mean	Median	S.D.	Skewness	Kurtosis
1	141	106.2	0	135	12.6	6	18.4	3.1	11.5
1	142	102.0	0	124	11.9	6	16.8	2.7	8.5
1	143	120.0	0	141	17.8	7	23.7	2.0	3.7
Combined		328.2	0	141	14.3	6	20.3	2.5	6.9
2	168	83.2	0	110	7.1	4	10.6	5.3	40.0
2	169	89.1	0	143	8.3	4	13.2	4.8	33.3
2	170	101.1	0	116	7.5	3	14.5	4.6	23.8
2	174	63.6	0	90	9.9	5	13.1	2.9	10.2
2	175	65.0	0	127	9.7	5	15.2	3.7	16.4
2	176	63.8	0	119	8.6	5	12.6	4.2	24.5
Combined		465.8	0	143	8.4	4	13.3	4.3	24.1
3	158	71.2	0	65	8.4	6	8.3	2.1	6.6
3	159	94.8	0	70	7.4	5	8.6	2.6	9.3
3	161	61.2	0	98	10.0	7	11.9	3.2	14.5
3	162	55.3	0	54	8.9	6	8.6	1.8	1.2
3	180	59.6	0	111	14.1	9	16.7	2.8	9.9
3	181	58.9	0	116	14.1	9	15.5	2.3	7.4
3	182	52.9	0	73	10.8	8	10.5	2.2	6.7
3	183	43.9	0	107	11.2	9	11.3	3.7	23.2
Combined		497.8	0	116	11.8	7	10.3	3.1	14.8
4	None								
All Subjects		1291.8	0	143	10.6	6	15.1	3.4	14.8

Appendix M.

Azimuth velocity box-plots.

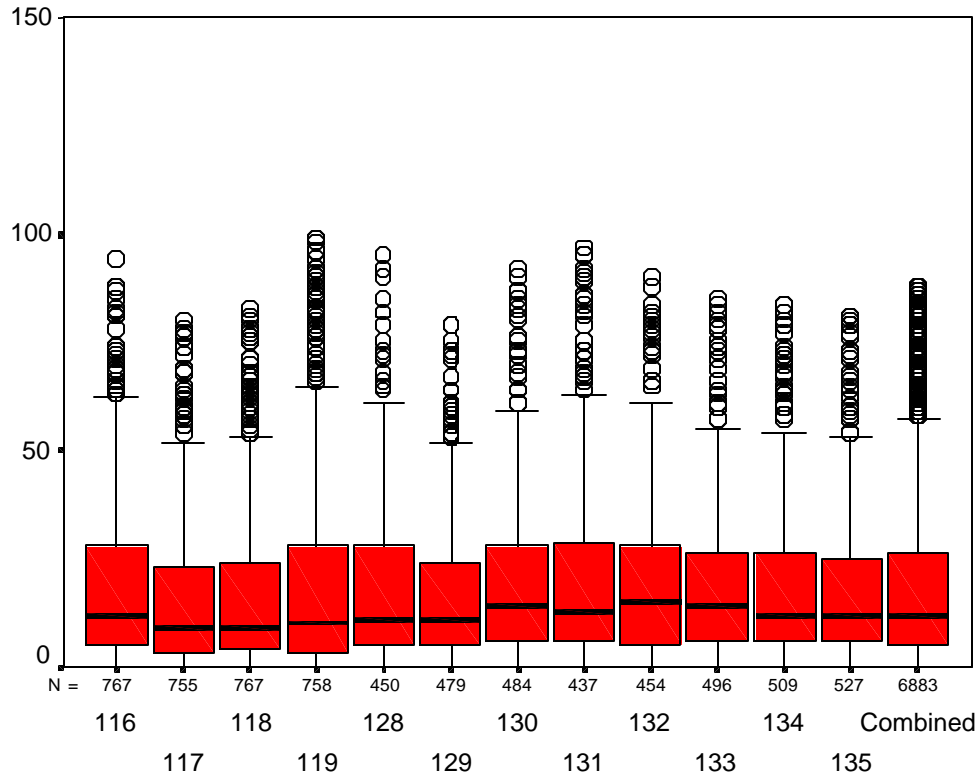


Figure M-1. Subject #1 GVE head velocity box-plots.

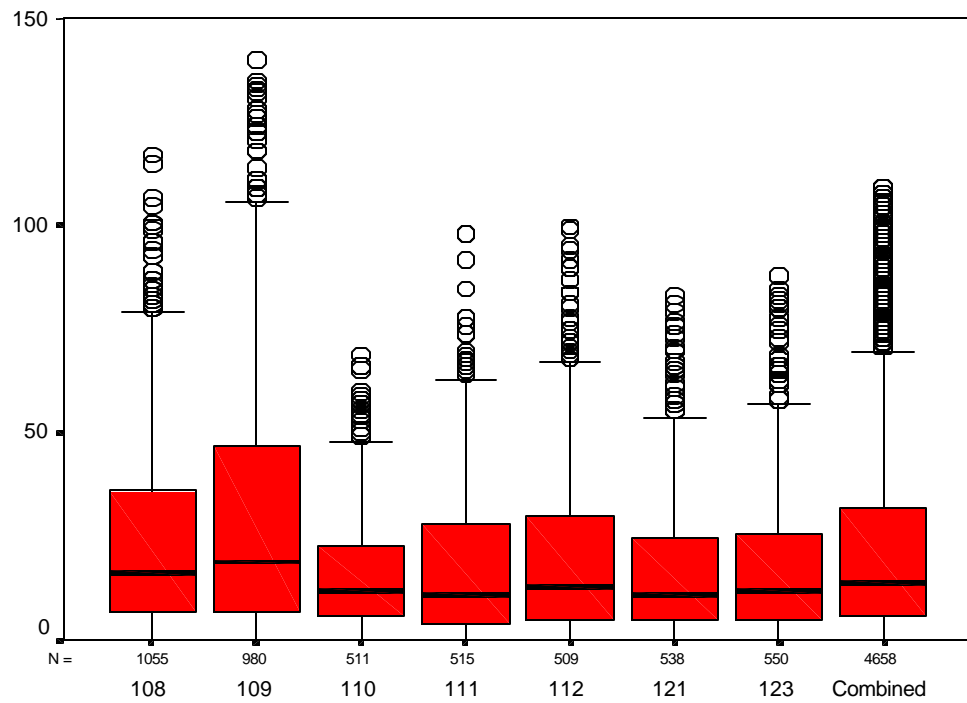


Figure M-2. Subject #1 NVG head velocity box-plots.

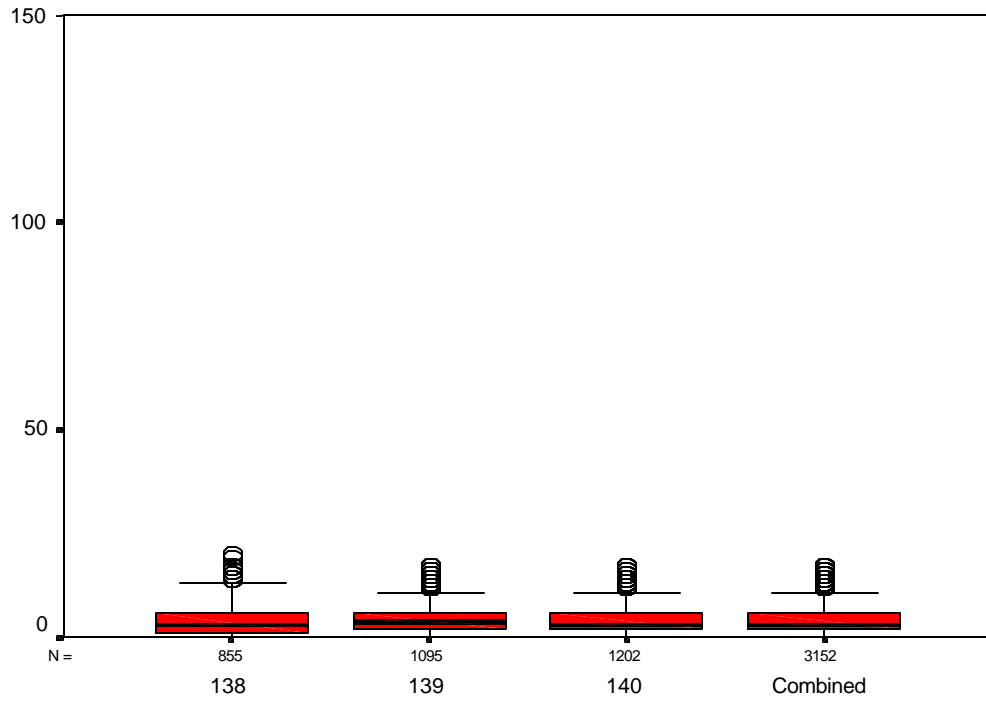


Figure M-3. Subject #1 TIO head velocity box-plots.

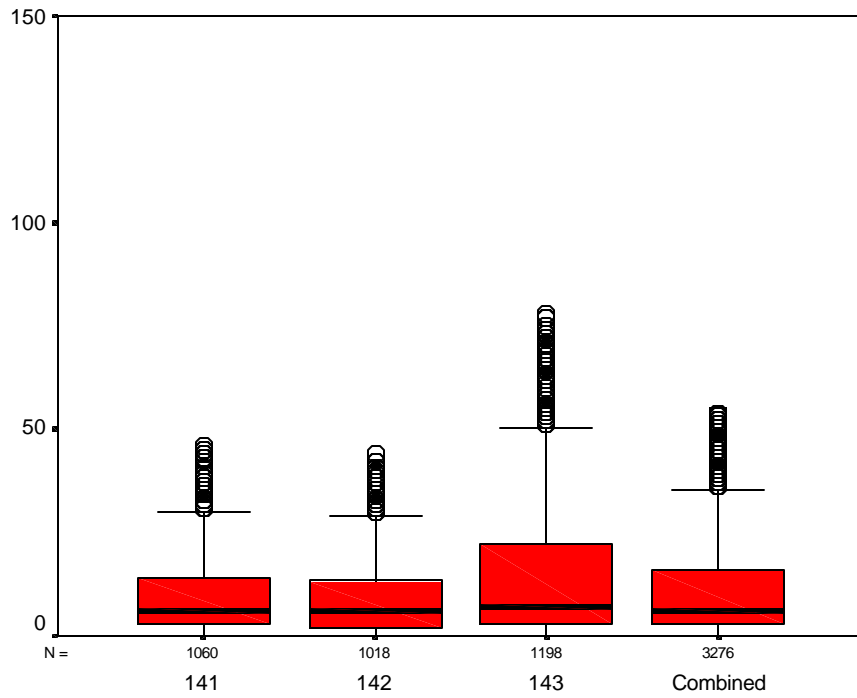


Figure M-4. Subject #1 RWS head velocity box-plots.

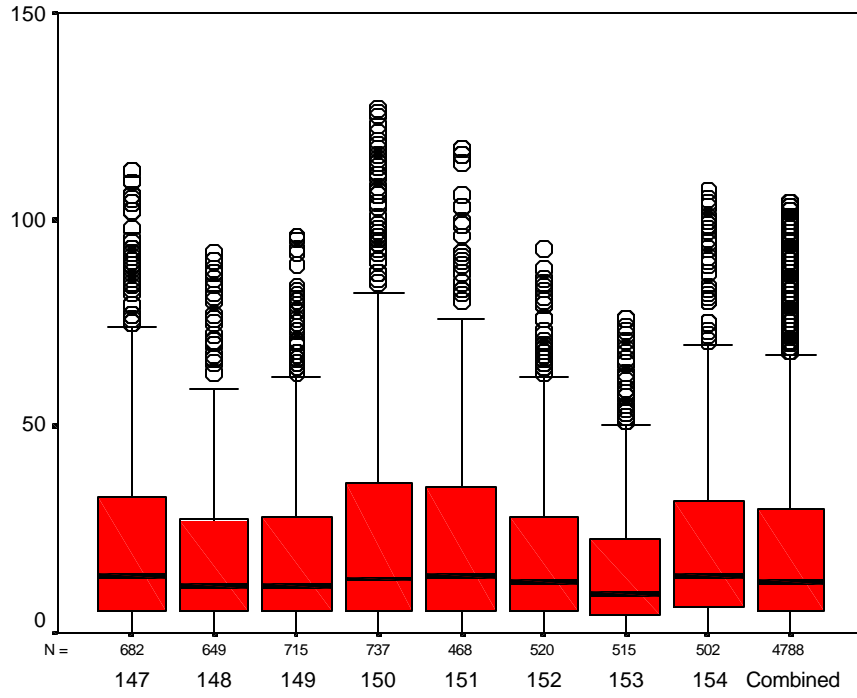


Figure M-5. Subject #2 GVE head velocity box-plots.

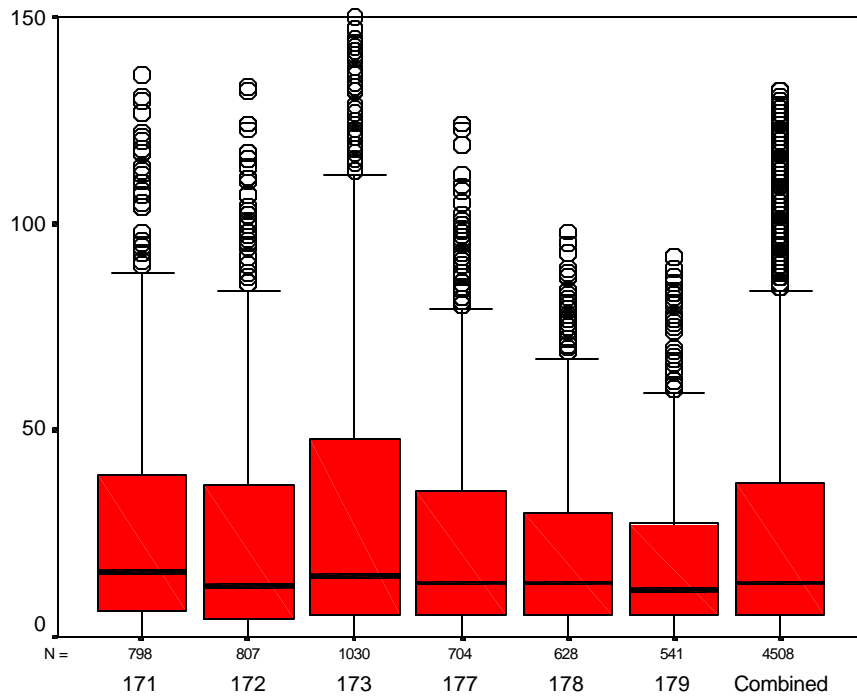


Figure M-6. Subject #2 NVG head velocity box-plots.

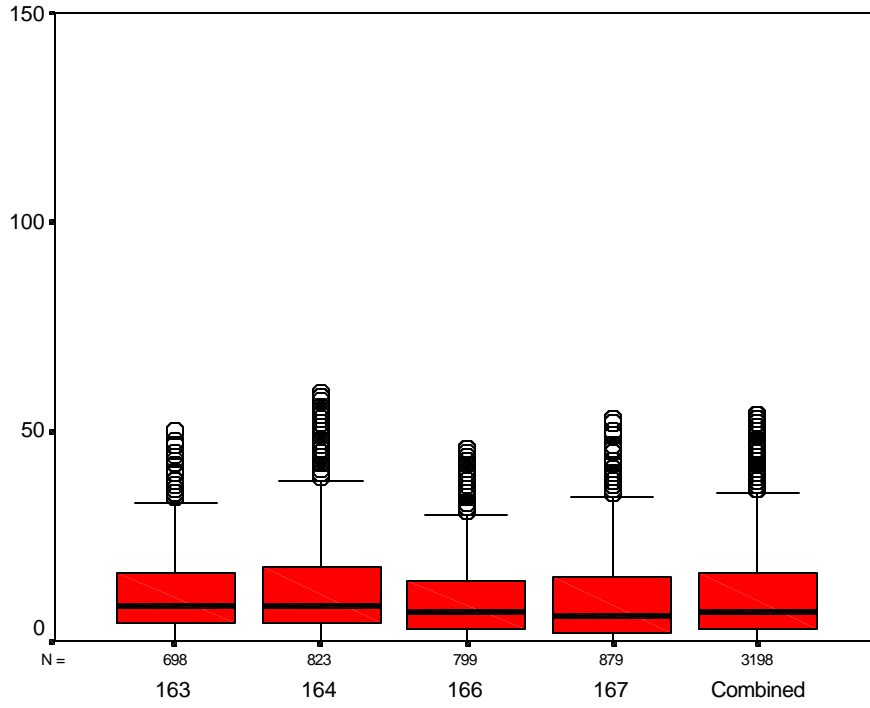


Figure M-7. Subject #2 TIO head velocity box-plots.

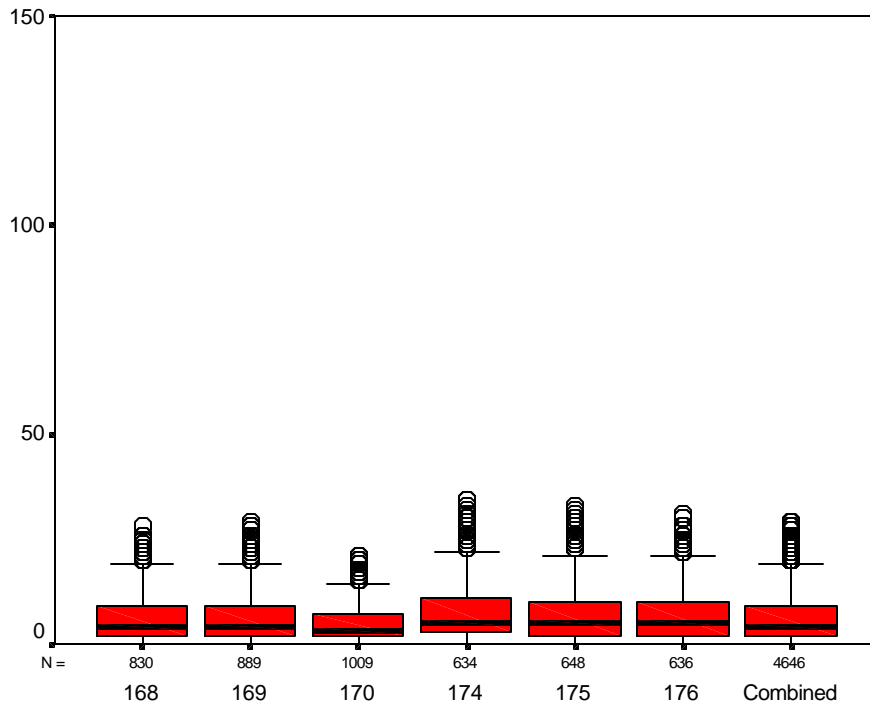


Figure M-8. Subject #2 RWS head velocity box-plots.

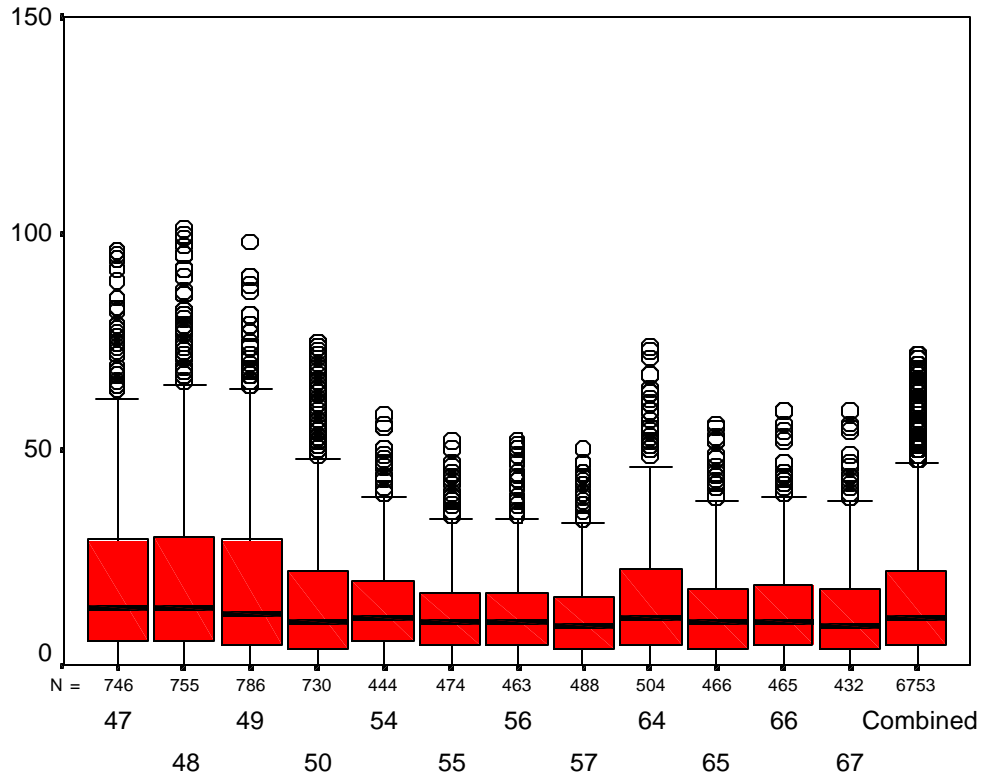


Figure M-9. Subject #3 GVE head velocity box-plots.

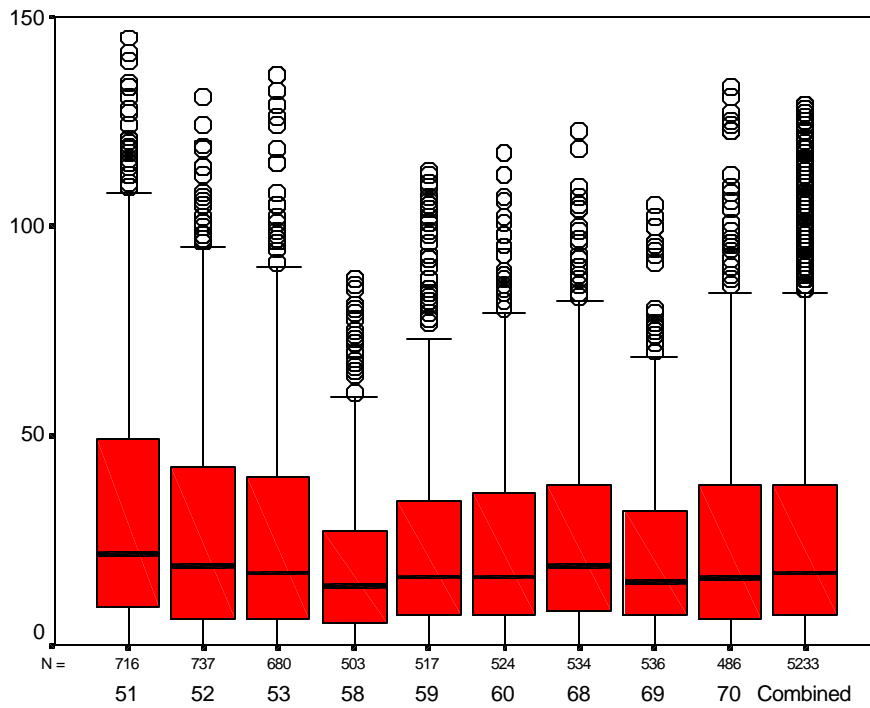


Figure M-10. Subject #3 NVG head velocity box-plots.

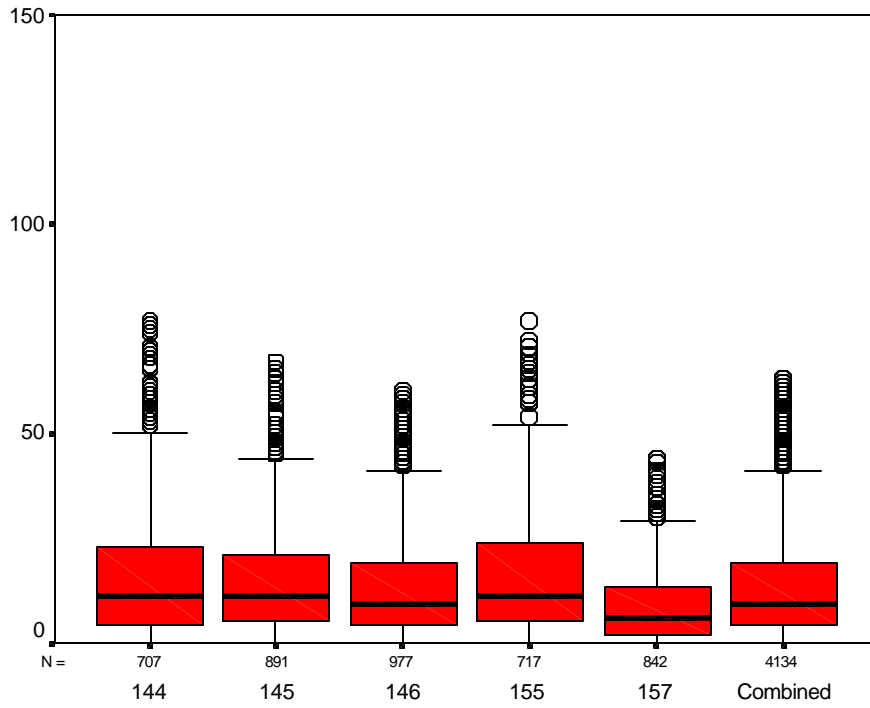


Figure M-11. Subject #3 TIO head velocity box-plots.

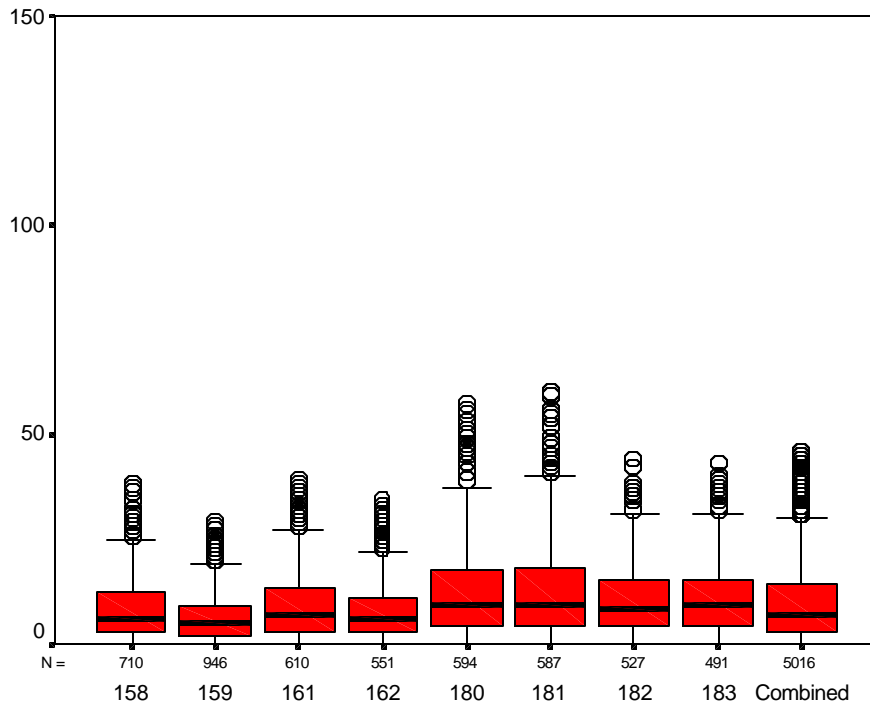


Figure M-12. Subject #3 RWS head velocity box-plots.

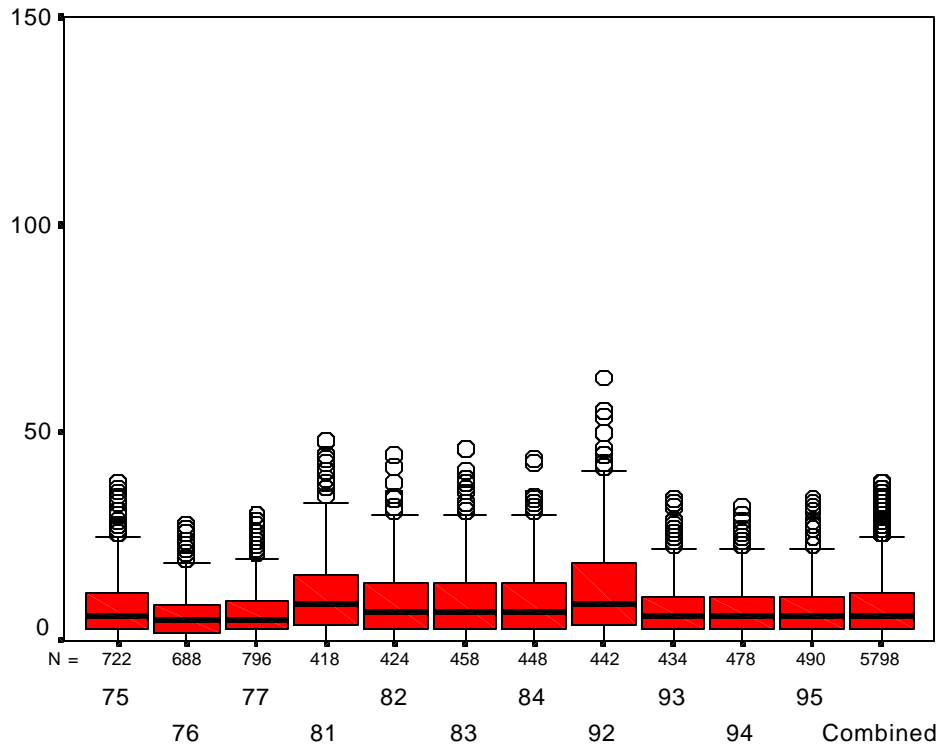


Figure M-13. Subject #4 GVE head velocity box-plots.

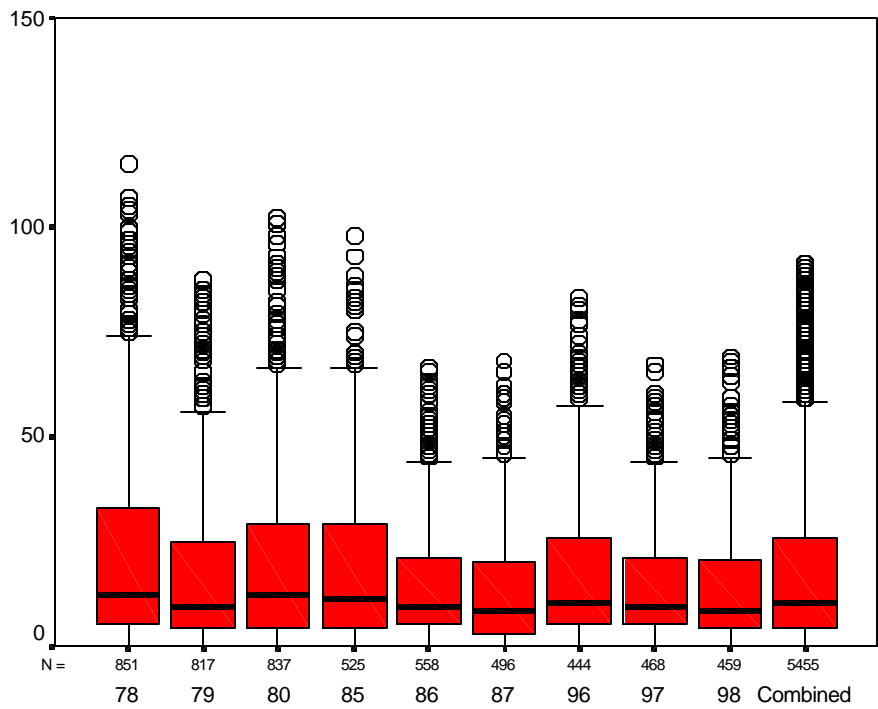


Figure M-14. Subject #4 NVG head velocity box-plots.